LONG-RANGE TRANSPORT OF POLLUTION TO EUROPE: ORIGINS, CHEMICAL AND TRANSPORT PATHWAYS, AND IMPACT ON TROPOSPHERIC COMPOSITION

THÈSE N^{O} 3561 (2006)

PRÉSENTÉE LE 26 JUIN 2006

À LA FACULTÉ ENVIRONNEMENT NATUREL, ARCHITECTURAL ET CONSTRUIT

Laboratoire de modélisation de la chimie atmosphérique

SECTION DES SCIENCES ET INGÉNIERIE DE L'ENVIRONNEMENT

ÉCOLE POLYTECHNIQUE FÉDÉRALE DE LAUSANNE

POUR L'OBTENTION DU GRADE DE DOCTEUR ÈS SCIENCES

PAR

Marion AUVRAY

ingénieur diplômée ENGEES,
DEA de chimie de la pollution atmosphérique et physique de l'environnement, Strasbourg, France
et de nationalité française

acceptée sur proposition du jury:

Prof. A. Buttler, président du jury
Prof. I. Bey, directrice de thèse
Dr K. Law, rapporteur
Dr M. Lawrence, rapporteur
Prof. H.van den Bergh, rapporteur

ÉCOLE POLYTECHNIQUE
FÉDÉRALE DE LAUSANNE

Lausanne, EPFL
2006

Abstract

Ozone (O_3) and aerosols are harmful to human health. Long-range transport sources contribute to the background levels upon which local pollution builds. The goal of this thesis is to describe and quantify the respective contribution of local and long-range transported sources to the O_3 and aerosol budget in the framework of European air quality management. This issue is examined using a global model of chemistry and transport, the GEOS-Chem model, constrained by several experimental datasets (e.g. trace gases and aerosol distributions, aerosol optical depth, particulate matter concentrations) taken from field experiments, ground-based sites and satellite.

The capabilities of the model to reproduce O_3 and aerosol patterns is first examined. The model reproduces well in general the distribution of O_3 and related species over the North Atlantic/Europe area. The simulation of particulate matter smaller than 2.5 μm ($PM_{2.5}$) and aerosol optical depth (AOD) over Europe is also satisfying in general, but this may reflect some compensating errors between individual components (e.g. underestimate of organic matter, and overestimate of sulphate and dust). Intercomparison between the GEOS-Chem and another global model (MOZECH) also reveals possible problems in the water vapour distribution associated with the processes which drive the vertical lifting of pollutant over continental boundary layers. Despite these (relative) deficiencies, the model provides anyway insights about the contribution of long-range transport on the O_3 and aerosol loads over Europe.

The impact of continental outflow on the O_3 chemical tendencies over oceanic regions is quantified. Net O_3 photochemical production in polluted air masses travelling over oceanic areas under the influence of continental outflow is enhanced all-year round compared to the background marine environment by 2 to 6 ppbv/day in the boundary layer and by 1 to 3 ppbv/day in the upper troposphere.

The origin of O_3 long-range sources and their impact on the European O_3 budget, as well as the role of changing emissions on this budget over the pasts decades is further investigated. Import of North American O_3 into Europe is mainly controlled by meteorological patterns and by photochemical production over the North Atlantic and thus reaches a maximum in summer. In addition, Asia contributes to long-range transported O_3 pollution by the Indian summer monsoon easterly winds during summer. During the monsoon period, convection is strong and associated NO_x lightning emissions also contribute to high O_3 levels, especially in the Mediterranean basin. North American

and Asian anthropogenic pollution contribute substantially to the annual O_3 burden (integrated over the whole tropospheric column) over Europe, accounting for 11% and 8%, respectively while the European contribution only accounts for 9%. The increase in Asian emissions from 1980 to 1997 have compensated the local reduction of O_3 precursors, especially in the free troposphere.

Finally, the aerosol load over Europe and the contribution of long and medium-range sources including anthropogenic and biomass burning pollution from North America and mineral dust from North Africa is examined. The model was used to interpret MODIS (Moderate Resolution Imaging Spectroradiometer) AOD and observations provided by the International Consortium for Atmospheric Research on Transport and Transformation (ICARTT) campaign over the North Atlantic and European area. Trans-Atlantic transport of aerosol is controlled by meteorological patterns and scavenging processes and reaches a maximum in spring. North American fluxes of aerosols reach Europe at lower altitudes than that of O_3 because a larger fraction of aerosols are scavenged in the venting from the boundary layer by frontal passages and deep convection. During high vegetation fire events in the boreal forest of Alaska and Canada, biomass burning pollution could also reach Europe at high altitudes, because a fraction of fire emissions are emitted directly in the free troposphere. Finally, the Saharan region also contributes significantly to the aerosol load over Europe. European sources contribute by 58% and 48% to the surface $PM_{2.5}$ and column AOD over Europe. The second main sources are the mineral dust which represent in average 20% of the surface $PM_{2.5}$ and AOD. In summer, North American anthropogenic and biomass burning emissions represent between 2 to 5% of the surface $PM_{2.5}$ and AOD. The $PM_{2.5}$ daily standard levels of the World Health organization (WHO) (10 $\mu g/m^3$) and of the U.S. Environmental Protection Agency (EPA) (65 $\mu g/m^3$) are often exceeded during dust outbreaks, especially in southern Europe.

Long-range transport of anthropogenic and natural pollution is thus an important issue which should be considered in the definition of air quality standards and regulation treaties.

Keywords: Ozone, aerosol, long-range transport, air quality, global modelling.

Résumé

L'ozone (O_3) et les aérosols sont néfastes pour la santé humaine. Les sources transportées sur de longues distances contribuent au niveau de fond, auquel s'ajoute la pollution locale. L'objectif de cette thèse est de décrire et de quantifier la contribution respective de ces sources locales et éloignées sur les budgets d'O_3 et d'aérosols dans le cadre de la maîtrise de la qualité de l'air. Ces travaux utilisent dans ce but un modèle de chimie-transport planétaire, GEOS-Chem, qui est confronté à plusieurs données expérimentales (distributions d'aérosols et de gaz, épaisseur optique des aérosols (AOD) ou concentration de la matière particulaire par exemple) résultant aussi bien de campagnes de mesures, d'observations satellitaires que de mesures depuis le sol.

Dans un premier temps, les capacités du modèle à reproduire les distributions d'aérosols et de gaz sont examinées. Le modèle simule en général correctement les distributions pour d'O_3 et ses précurseurs, au-dessus de l'Atlantique nord et de l'Europe. Les résultats pour les simulations de matière particulaire "fine" (inférieure à 2.5 μm, $PM_{2.5}$) et d'AOD en Europe montrent également un bon accord en général avec les observations, bien que cela puisse refléter une compensation des erreurs sur les contributions relatives des composés pris individuellement. Une inter-comparaison entre GEOS-Chem et un autre modèle global (MOZECH) révèle par ailleurs de possibles problèmes dans la distribution de la vapeur d'eau associée aux processus impliqués dans le transport vertical des polluants au-dessus de la couche limite continentale. Malgré ces déficiences relatives, le modèle fournit une information pertinente sur la contribution du transport à grande échelle sur les contenus en O_3 et en aérosols de l'atmosphère en Europe.

L'impact de l'export de la pollution nord américaine sur la production photochimique de l'O_3 au-dessus des régions océaniques est ainsi quantifiée. Dans les masses d'air polluées qui circulent au-dessus des régions océaniques sous l'influence de ces exports continentaux, la production photochimique nette de l'O_3 est augmentée de 2 à 6 ppbv/jour dans la couche limite et de 1 à 3 ppbv/jour dans la haute troposphère.

Ce travail a aussi permis de déterminer l'origine des sources d'O_3 éloignées et d'analyser leurs impacts sur le budget d'O_3 Européen, ainsi que de quantifier le rôle des changements des émissions qui ont eu lieu au cours des deux dernières décennies. L'import d'O_3 d'origine nord américaine est contrôlé par les variations saisonnières de la météorologie et de la production photochimique et atteint donc un maximum en

été. Des sources anthropiques venant d'Asie sont aussi transportées sur de longues distances et tout particulièrement en été par des vents d'est associés à la mousson indienne. Pendant cette période, les éclairs accompagnant les processus de convection émettent des NO_x qui contribuent à la production d'O_3, s'ajoutant aux fortes concentrations déjà présentes au niveau du bassin Méditerranéen. Les contributions anthropiques nord américaine et asiatique participent au budget d'O_3 sur l'Europe (intégrées sur la colonne troposphérique) à hauteur de 11 et 8% respectivement, alors que la participation anthropique européenne s'élève seulement à hauteur de 9%. L'augmentation des émissions anthropiques d'origine asiatique pendant les 20 dernières années a compensé (notamment dans la haute troposphère) les réductions locales des précurseurs d'O_3 menées en Europe.

Le contenu en aérosol sur l'Europe, ainsi que la part imputable au transport à longues et moyennes distances (pollution anthropique et celle liée aux feux de forêts d'Amérique du nord ainsi que les poussières désertiques venant d'Afrique du nord) est ensuite examiné. En particulier, le modèle a permis d'interpréter les observations MODIS (Moderate Resolution Imaging Spectroradiometer) et les mesures obtenues pendant la campagne de mesure ICARTT (International Consortium for Atmospheric Research on Transport and Transformation) au-dessus des régions Atlantique nord et Europe. Au dessus de l'Atlantique, le transport d'aérosol anthropique d'origine nord américaine est contrôlé par les conditions météorologiques, ainsi que par leur lessivage. Ce transport atteint donc un maximum au printemps. Comme une grande quantité d'aérosol est lessivée lors de l'export de la couche limite induit par les passages de front et la convection profonde, les flux d'aérosols nord américain atteignant l'Europe se situent à plus basse altitude que les flux d'O_3 de la même origine. Une partie des aérosols émise pendant les périodes de feux de forêt boréaux du Canada et de l'Alaska est directement injectée dans la haute troposphère, et de ce fait atteint l'Europe directement à hautes altitudes. Enfin, les poussières désertiques venant principalement du Sahara contribuent de manière significative au contenu en aérosol au-dessus de l'Europe. Les sources européennes ont un poids respectif de 58 et 48% par rapport aux $PM_{2.5}$ surfaciques et à la colonne d'AOD. Les poussières désertiques représentent la deuxième contribution principale qui s'élève à environ 20% des $PM_{2.5}$ surfacique et des AOD. En été, les sources nord américaine d'origine anthropique et liées aux feux de forêts contribuent entre 2 et 5 % aux $PM_{2.5}$ surfaciques et aux AOD. Les normes journalières définies par l'organisation mondiale de la santé (WHO) (10 $\mu g/m^3$) et par l'agence de protection environnementale des Etats-Unis (65 $\mu g/m^3$) est fréquemment dépassée pendant les épisodes de soulèvement de poussières désertiques, et ce notamment dans le sud de l'Europe.

L'impact du transport à longue distance, d'origine naturelle ou anthropique, est non négligeable. Il serait ainsi souhaitable qu'il soit pris en compte lors de la définition des normes régissant la qualité de l'air, ainsi que dans la mise en place de traités internationaux régulant les émissions de polluants.

Mots-Clés: Ozone, aérosol, transport à grande distance, qualité de l'air, modélisation globale.

Contents

List of Figures

List of Tables

List of Abbreviations and Symbols

ACE-Asia	Asian Pacific Regional Aerosol Characterization Experiment
ACSOE	Atmospheric Chemistry Studies in the Oceanic Environment
ADRIEX	Aerosol Direct Radiative Impact Experiment
AERONET	AErosol RObotic NETwork
AOD	Aerosol Optical Depth (τ)
ATSR	Along Track Scanning Radiometer
BC	Black carbon
BE	Background Environment
BNAm	North American biomass burning contribution
C_2H_6	Ethane
C_3H_8	Propane
CCB	Cold Conveyor Belt
CCC	Chemical Coordinating Centre
CDIAC	Carbon Dioxide Information Analysis Center
CH_3O_2	Methyl peroxy radical
CH_3O_2H	Methyl hydrogen peroxide
CH_4	Methane
CMDL	Climate Monitoring and Diagnostics Laboratory
CO	Carbon monoxide
CO_2	Carbon dioxide
CTM	Chemical transport model
DA	Dry Airstream
DEAD	Dust Emission And Deposition
DJF	December, January and February
DMS	Dimethyl sulfide $(CH_3)_2S$
EARLINET	European Aerosol Research LIdar NETwork
EC	European Community
ECMWF	European Centre for Medium-range Weather Forecasts
EEA	European Environment Agency
EMEP	European Monitoring and Evaluation Program
EoI	Exchange of Information
EOS	Earth Observing System
EPA	U.S. Environmental Protection Agency

ERA-40	ECMWF 40 year Re-Analysis
EXPORT	European eXport of Precursors and Ozone by long-Range Transport
GAW	Global Atmosphere Watch
GCM	General circulation model
GEIA	Global Emission Inventory Activity
GEOS	Goddard Earth Observing System
GMAO	Global Modeling and Assimilation Office
GOCART	Global Ozone Chemistry Aerosol Radiation and Transport
GOME	Global Ozone Monitoring Experiment
GR	Gas ratio
H_2O	Water
H_2O_2	Hydrogen peroxide
H_2SO_4	Sulfuric acid
HNO_2	Nitrous acid
HNO_3	Nitric acid
HNO_3^T	Sum of nitric acid (gas phase) plus nitrate
HNO_4	Peroxy nitric acid
HO_2	Hydroperoxy radical
hPa	Hectopascal (10^2 Pascal)
ICARTT	International Consortium for Atmospheric Research on Transport and Transformation
INTEX-NA	Intercontinental Transport Experiment - North America
ITCT2k4	Intercontinental Transport and Chemical Transformation
ITCZ	Intertropical Convergence Zone
ITOP	Intercontinental Transport of Ozone and Precursors
JJA	June, July and August
$j(O^1D)$	Photolysis frequency of ozone
$j(NO_2)$	Photolysis frequency of nitrogen dioxide
km	Kilometer (10^3 meter)
m^3	Cubic meter
μg	Microgram (10^{-6} gram)
μm	Micrometer (10^{-6} meter)
MAM	March, April and May
MINOS	Mediterranean Intensive Oxidant Study
MISR	Multi-angle Imaging SpectroRadiometer
MODIS	Moderate Resolution Imaging Spectroradiometer
MOZAIC	Measurement of Ozone by Airbus In-service Aircraft
MSLP	Mean Sea Level Pressure
N_2	Nitrogen
N_2O_5	Dinitrogen pentoxide
NABEL	National Air Pollution Monitoring Network
NaCl	Sodium chloride
NAm	North American anthropogenic contribution
NAO	North Atlantic Oscillation
NARE	North Atlantic Regional Experiment
NASA	National Aeronautics and Space Administration

NEAQS	New England Air Quality Study
NEI	National Emission Inventory
net P O_3	Ozone net production
NH_3	Ammonia
NH_4^+	Ammonium
NH_4NO_3	Ammonium nitrate
NH_x	Sum of ammonia (gas phase) plus ammonium aerosol
nm	Nanometer (10^{-9} meter)
NMHC	Non-methane hydrocarbons
NO	nitric oxide
NO_2	Nitrogen dioxide
NO_3	Nitrate radical
NO_3^-	Nitrate
NO_x	Nitrogen oxide
NO_y	Total reactive nitrogen oxides
NOAA	National Oceanic and Atmospheric Administration
$O(^1D)$	Excited state oxygen atom
O_2	Oxygen
O_3	Ozone
$O(^3P)$	Ground state oxygen atom
OC	Organic carbon
OECD	Organization for Economic Cooperation and Development
OH	Hydroxyl radical
PAN	Peroxyacetylnitrate $CH_3C(O)O_2NO_2$
PCF	Post Cold Front
PE	Polluted Environment
PEM-West	Pacific Exploratory Mission-West
PM	Particulate Matter
PM_{10}	Particulate Matter of diameter less than 10 μm
$PM_{2.5}$	Particulate Matter of diameter less than 2.5 μm
POM	Particulate organic matter
$ppbv$	Volume mixing ratio parts per billion (10^{-9})
$pptv$	Volume mixing ratio parts per trillion (10^{-12})
RETRO	REanalysis of the TROpospheric chemical composition over the past 40 years
RMS_c	Centered root mean square difference
S	Sulfur
SAEFL	Swiss Agency for Environment Forests and Landscape
SBUV	Solar Backscatter Ultraviolet
SO_2	Sulfur dioxide
SO_4^{2-}	Sulfate
SO_x	Sum of sulfur dioxide (gas phase) plus sulfate
SOA	Secondary Organic Aerosol
SON	September, October and November
Synoz	Synthetic ozone
Tg	Teragram (10^{12} gram)

TOMS	Total Ozone Mapping Spectrometer
TRACE-P	Transport and Chemical Evolution over the Pacific
UCT	Coordinated Universal Time
U.S.	United States
UV	Ultraviolet
VOC	Volatile Organic Carbon
WCB	Warm Conveyor Belt
WDCA	World Data Center for Aerosols
WHO	World Health organization
yr	year

Chapter 1

Introduction

Ozone (O_3) and aerosols (solid or liquid particles suspended in the atmosphere) are associated with major health effect problems, like respiratory irritation [e.g., *Pope et al.*, 2000; *WHO*, 2003]. Moreover, O_3 damages agricultural crop and natural ecosystems [e.g., *Mauzerall and Wang*, 2001]. The third Daughter Directive set in 2002 by the European community (2002/3/EC) defines the O_3 World Health Organization's [*WHO*, 2000] target values of 60 ppbv for an 8-hour daily average as the long-term objective. Over the U.S., the environmental protection agency [*EPA*, 2003] sets in 1997 a standard of 80 ppbv for an 8-hour daily average. However, recent epidemiological studies have shown positive association between O_3 levels and mortality and lead the WHO to decrease this quality guideline to 50 ppbv [*WHO*, 2005]. To identify damages on crop and forests, *EMEP* [2004] calculates the sum of the O_3 value above a fixed threshold (40 ppbv), which must not exceed 3000 ppbv h accumulated over 3 months for crop and 5000 ppbv h accumulated over 6 months for forests. Despite efforts to improve air quality over Europe, O_3 exceedances of the long-term objective for the protection of human health and of the thresholds for vegetation are observed in almost every European country [*EEA*, 2004; *EMEP*, 2004].

The first Daughter Directive set in 1999 by the European community (1999/30/EC) indicates limit values for particulate matter of diameter smaller than 10 μm (PM_{10}) fixed on an annual mean to 40 $\mu g/m^3$ for 2005 and 20 $\mu g/m^3$ for 2010. It also provides limitation for daily mean of 50 $\mu g/m^3$ that should not be exceeded more than 35 times per year in 2005 and more than 7 times per year in 2010. Although finer particles seem to be the more likely agent, the lack of measurements over Europe does not allow to set such standards [*Technical working group on particles*, 1997]. Over the U.S., standards are set for particulate matter of diameter smaller than 2.5 μm ($PM_{2.5}$). Such standards include an annual $PM_{2.5}$ level of 15 $\mu g/m^3$ and a 24-hour mean of 65 $\mu g/m^3$, although recently *EPA* [2006] proposes to decrease the 24-hour standard to 35 $\mu g/m^3$. *WHO* [2005] defines limitation levels for annual PM_{10} and $PM_{2.5}$ of 20 and

10 $\mu g/m^3$ respectively, as well as 24-hour mean of 50 and 25 $\mu g/m^3$. Although the European community PM_{10} annual standard is exceeded only at a few sites over Europe [*van Dingenen et al.*, 2004; *EMEP*, 2005], the EPA annual average $PM_{2.5}$ is exceeded at almost all European urban sites [*van Dingenen et al.*, 2004].

First recorded O_3 episodes over Los Angeles basin in the late 1940s and of smog episodes in London were initially thought to be of local origin. However, it was soon noticed that O_3 peaks appear in rural areas downwind of large cities rather than in the cities themselves, extending the scale of air pollution problem from local to regional [*NRC*, 1991]. In 1967, the Swedish scientist Svante Oden related acid deposition in Scandinavian lakes to sulphur emissions in continental Europe. A study from the Organization for Economic Cooperation and Development (OECD) involving eleven European countries confirm the fact that air pollution could cross political boundaries and affect foreign countries [*OECD*, 1977]. In response to these problems, environmental policy established the Convention on Long-range Transboundary Air Pollution (LRTAP), which was signed in 1979 by the European community, the U.S. and Canada. In the meantime, haze layers over the Arctic, first observed in the 1950s [*Mitchell*, 1956] became more severe in the 1970s [*Shaw*, 1975]. In mid 1980s, these layers were attributed to Eurasia [*Shaw*, 1995 and reference therein]. Long-range transport of dust is also observed as soon as the beginning of the 1980s [*Shaw*, 1980; *Prospero*, 1981]. However, at that time, observations of enhanced pollution level related to intercontinental transport were too sparse to be of significance relevance. It is only during the mid 1990s that it was demonstrated that long-range transport of pollutants could affect a continent downwind through episodic transport and increasing in the background (Figure 1.1) [e.g., *Parrish et al.*, 1993; *Wild and Akimoto*, 2001; *Holloway et al.*, 2003; *Akimoto*, 2003; *Keating et al.*, 2005].

Several large field studies have investigated trans-Pacific transport in great detail, as well as the impact of polluted Asian air masses over North America, both in term of O_3 and aerosols levels [e.g. *Jaffe et al.*, 1999; *Bernsten et al.*, 1999; *Yienger et al.*, 2000; *Fiore et al.*, 2002; *Parrish et al.*, 2004a and references therein; *Heald et al.*, 2006]. North western U.S. is more impacted by anthropogenic Asian plumes during springtime. Modelling studies indicate that anthropogenic Asian emissions impact the surface of the North western U.S. by around 5 ppbv for O_3 [*Bernsten et al.*, 1999; *Yienger et al.*, 2000; *Fiore et al.*, 2002; *Goldstein et al.*, 2004; *Hudman et al.*, 2004] and 0.16 $\mu g/m^3$ for sulfate aerosols [*Heald et al.*, 2006]. In addition, North America receive frequently dust outbreak from the Asian deserts [*McKendry et al.*, 2001; *Husar et al.*, 2001] and some biomass burning plumes from boreal Russian forest [*Bertschi et al., 2004*].

Evidences of episodic export of North American pollutants over the North Atlantic have been reported since the beginning of the 1990s [*Parrish et al.*, 1993]. The North Atlantic Regional Experiment (NARE) aircraft campaign in 1993 and 1997 was designed to estimate the contribution of anthropogenic continental sources over the North Atlantic [*Fehsenfeld et al.*, 1996 and references therein; *Cooper et al.*, 2001; *Stohl et al.*, 2002; *Li et al.*, 2004; *Parrish et al.*, 2004b]. Enhanced CO, O_3 and NO_y concentrations were found during North American polluted outflow events. Besides, in 1997, the

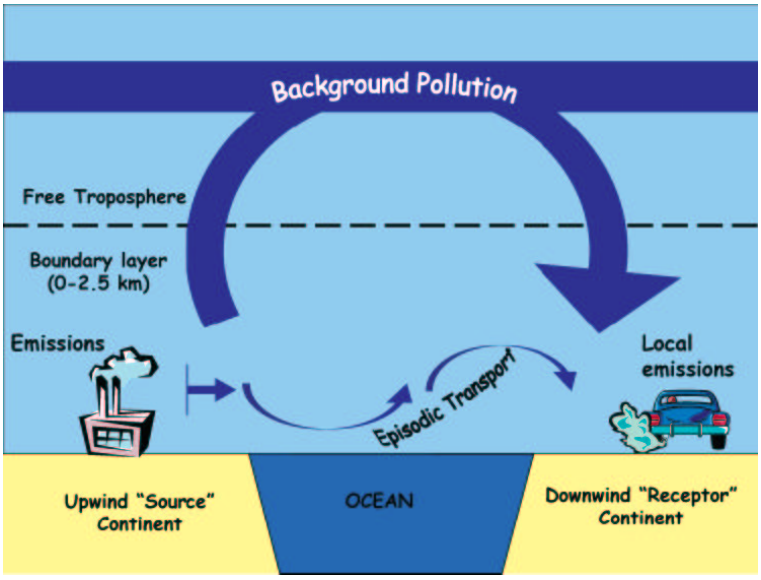

Figure 1.1: Schematic cartoon of long-range transport pollutants from the upwind "source" continent to the downwind "receptor" continent. Long-range transport occurs through episodic events or through increasing in the global background. Emissions from the upwind "source" may be transported into the boundary layer or mixed vertically in the free troposphere for rapid transport. Air pollutants received by the downwind "receptor" depends of the photochemical processing and deposition occurring during transport. From *Holloway et al.* [2003].

Atmospheric Chemistry Studies in the Oceanic Environment (ACSOE) aircraft campaign provides evidence of enhanced O_3 production over the remote North Atlantic associated with North American plumes [*Reeves et al.*, 2002]. More recently, in the summer 2004, the International Consortium for Atmospheric Research on Transport and Transformation (ICARTT) program was designed to provide insights on long-range transport using coordinated flights over North America, the North Atlantic and Europe. Such a wide program aims at improving our understanding of the factors controlling trans-Atlantic transport and more particularly to examine the factors determining air quality over North America, the remote regions of the North Atlantic and Europe.

In the meantime, despite few evidences of North American pollution at surface sites [*Derwent et al.*, 1998], observations at high Alpine site [*Huntrieser et al.*, 2005] and in the troposphere [*Stohl and Trickl*, 1999; *Naja et al.*, 2003] have recorded enhanced O_3 concentrations, which were attributed to North American pollution. Long-range transport of aerosols over Europe has been investigated more recently during biomass burning events originating from Canada [*Forster et al.*, 2001] or Russia [*Edwards et al.*, 2004, *Damoah et al.*, 2004] and subsequent enhancement in the free troposphere over Europe has been seen in lidar observations [*Forster et al.*, 2001; *Wandinger et al.*, 2002; *Mattis et al.*, 2003; *Damoah et al.*, 2004; *Müller et al.*, 2005]. In southern Europe, enhanced aerosols concentrations are also frequently associated with dust episodes [*Rodriguez et al.*, 2002; *Amiridis et al.*, 2005].

As pictured in Figure 1.1 [*Holloway et al.*, 2003], the long-range transport of pollu-

tion is not only seen in episodic events but also results in increases in the background pollution upon which regional pollution builds [*Prather et al.*, 2003]. On a global scale, observations have shown an increase in the O_3 background throughout the North hemisphere during the last century from a factor two to five, resulting from a global increase of anthropogenic emissions [*Marenco et al.*, 1994; *Vingarzan*, 2004]. Focusing on more specific regions like Europe for which regulations on O_3 precursors have been implemented over the last decades, the lack of decreasing O_3 trends at some European stations have lead some authors to question whether the long-range transported pollution could affect the mean levels of O_3 concentrations over Europe [e.g. *Brönnimann et al.*, 2000; 2002, *Simmonds et al.*, 2004; *Ordóñez et al.*, 2005]. Less attention has been paid to global aerosol background, but on a smaller scale, *van Dingenen et al.* [2004] showed that aerosol concentrations in cities are strongly affected by the regional aerosol background.

O_3 and aerosols, besides being of relevant importance for air quality problems are also linked to climate change in several ways. First, O_3 and black carbon (one of the constituents of aerosols) are light-absorbing components and together, they contribute to global warming in the same magnitude as CO_2 [*IPCC*, 2001]. On the other hand, other aerosol components like sulfate, nitrate and organic aerosols are light-scattering aerosol and as such, are expected to cool the atmosphere. *Jacob and Gilland* [2005] highlighted the fact that climate change could be impacted by air quality policies. For example, reducing SO_2 emissions (producing sulfate aerosol) for both amelioration of public health and ecosystems could warm the atmosphere. Second, air quality is heavily influenced by meteorological fluctuation like temperature, humidity, synoptic-scale circulation, mixing depth, and stagnation episodes [see *Mickley et al.*, 2004 and references therein]. The complex interplay between meteorology and chemistry makes difficult to assess clear tendencies in O_3 and aerosol distributions due to climate change. Several studies have shown that in a warming climate, O_3 pollution peaks would increase both in frequency and in duration [*Hogrefe et al.*, 2004]. Impact of climate change on $PM_{2.5}$ is more complex as even the effect of temperature alone is not well known [*Hogrefe et al.*, 2005]. Other parameters linked to climate change like enhancement of biomass burning, alteration in the hydrological cycle, the use of air conditioning, the effect of a raising temperature and light on natural emissions of isoprene and biogenic O_3 and $PM_{2.5}$ precursors need to be quantified in order to improve our understanding of interaction between climate and air quality [*Hogrefe et al.*, 2005].

Despite our lack of understanding in some areas of the atmospheric climate system, there is more and more scientific evidence that future hemispherical regulations for atmospheric pollutant should be implemented to account for their dual role in air quality and climate issues [*Holloway et al.*, 2003; *Keating et al.*, 2005]. The rapid economic growth of developing countries and their subsequent emission enhancement could offset the efforts of downwind industrialized countries to reduce their pollutant levels [*Jacob et al.*, 1999]. The increasing international contribution of developing countries and the impact of pollutants on health problems and climate change could thus motivate both developing and industrialized countries to decrease emissions globally [*Keating et al.*, 2005].

The implementation of adequate regulations requires a sound understanding of the fundamental processes that drive the global distributions of the key species mentioned above, namely tropospheric O_3 and aerosols. The main objective of this thesis is thus to get a better quantitative understanding of the processes involved in the long-range transport of O_3 and related species as well as aerosols. In particular, I examine in detail the long-range transport of pollution to Europe and attempt to quantify its impact on European tropospheric composition. For this purpose, I address the following questions:

- What are the processes controlling O_3 production over the Atlantic during long-range transport episodes?
- What are the processes controlling O_3 and aerosol transport over the Atlantic during long-range transport episodes?
- What are the O_3 and aerosol European budgets?
- How these budgets are influenced by long-range transport on a monthly and seasonal mean?
- How do specific long-range transport events influence the European troposphere?
- How changes in O_3 precursors emissions contribute to changes in background and total O_3 over Europe?
- How well global models represent the processes associated with long-range transport?

These questions were addressed using a global 3-D tropospheric chemistry transport model, the GEOS-Chem model [*Bey et al.*, 2001] together with a large set of data observations obtained during different fields studies, ground-based measurements of O_3 precursors, O_3 and aerosol concentrations and satellite and ground-based measurements of aerosol optical depth (AOD). Different versions of the model have been used during this thesis. Several aspects of the model, including O_3 and aerosol distribution, as well as O_3 chemical tendencies have been evaluated in detail with a focus on Europe and the North Atlantic regions.

Chapter 2 reviews the current understanding in terms of O_3 and aerosol chemistry and budget as well as precursor sources. It also provides a short summary of transport processes of air pollutants. Chapter 3 deals with the impact of continental outflow on O_3 chemical tendencies (Questions 1 and 2). A special focus is put on the North American outflow over the North Atlantic ocean but results are also presented for the Asian outflow over the Northwest Pacific ocean. In this chapter, we also use other tools not mentioned previously, including the MOZECH 3-D chemistry-climate model and several chemical box models used to simulate O_3 chemical terms. In Chapter 4 long-range transport of O_3 over Europe is examined in great detail (Questions 2 to 6). North American and Asian anthropogenic contributions to the O_3 budget are quantified and their transport pathways up to Europe are described. The change in

anthropogenic emissions from 1980 to 1997 is discussed in term of change in the O_3 background. Chapter 5 focuses on the aerosol long-range transport topic and intends to answer questions 3 to 5. This chapter is a little bit more "exploratory" than the other ones as successful aerosol simulation is more challenging. Main difficulties lie in the highly inhomogeneous distribution of aerosols which results from their short lifetimes (a few days). For instance, emissions and depositions are still largely unknown. Another matter of debate is also the chemistry of secondary organic aerosols. However, a thorough evaluation of the model provides a solid ground to identify long-range transport episodes of biomass burning and anthropogenic North American origin, as well as episodes of Saharan dust. Concluding remarks and recommendations for future research are given in Chapter 6.

References

Akimoto, H. (2003), Global air quality and pollution, *Science*, *302*, 1716–1719.

Amiridis, V., D. S. Balis, S. Kazadzis, A. Bais, E. Giannakaki, A. Papayannis, C. Zerefos (2005), Four-year aerosol observations with a Raman lidar at Thessaloniki, Greece, in the framework of European Aerosol Research Lidar Network (EARLINET), *J. Geophys. Res.*, *110*, D21203, doi:10.1029/2005JD006190.

Berntsen, T. K., S. Karlsdottir, and D. A. Jaffe (1999), Influence of Asian emissions on the composition of air reaching the North Western United States, *Geophys. Res. Lett.*, *26*, 2171–2174.

Bertschi, I. T., D. A. Jaffe, L. Jaeglé, H. U. Price, J. B. Dennison (2004), PHOBEA/ITCT 2002 airborne observations of transpacific transport of ozone, CO, volatile organic compounds, and aerosols to the northeast Pacific: Impacts of Asian anthropogenic and Siberian boreal fire emissions, *J. Geophys. Res.*, *109*, D23S12, doi:10.1029/2003JD004328.

Bey, I., D. J. Jacob, J. A. Logan, and R. M. Yantosca (2001), Asian chemical outflow to the Pacific in spring: Origins, pathways, and budgets, *J. Geophys. Res.*, *106*, 23097–23114.

Brönnimann, S., E. Schuepbach, P. Zanis, B. Buchmann, and H. Wanner (2000), A climatology of regional background ozone at different elevations in Switzerland (1992–1998), *Atmos. Environ.*, *34*, 5191–5198.

Brönnimann, S., B. Buchmann, and H. Wanner (2002), Trends in near-surface ozone concentrations in Switzerland: the 1990s, *Atmos. Environ.*, *36*, 2841–2852.

Cooper, O. R., J. L. Moody, D. D. Parrish, M. Trainer, T. B. Ryerson, J. S. Holloway, G. Hübler, F. C. Fehsenfeld, S. J. Oltmans, and M. J. Evans (2001), Trace gas signatures of the airstreams within North Atlantic cyclones: Case studies from the North Atlantic Regional Experiment (NARE'97) aircraft intensive, *J. Geophys. Res.*, *106*, 5437–5456.

Damoah, R., N. Spichtinger, C. Forster, P. James, I. Mattis, U. Wandinger, S. Beirle, T. Wagner, and A. Stohl (2004), Around the world in 17 days-Hemispheric-scale

transport of forest fire smoke from Russia in May 2003, *Atmos. Chem. Phys.*, *4*, 1311–1321.

Derwent, R. G., P. G. Simmonds, S. Seuring, and C. Dimmer (1998), Observation and interpretation of the seasonal cycles in the surface concentrations of ozone and carbon monoxide at Mace Head, Ireland from 1990 to 1994, *J. Atmos. Chem.*, *32*, 145–157.

Edwards, D. P., et al. (2004), Observations of carbon monoxide and aerosols from the Terra satellite: Northern Hemisphere variability, *J. Geophys. Res.*, *109*, D24202, doi:10.1029/2004JD004727.

EEA (2004), Air pollution by ozone in Europe in summer 2004 (http://reports.eea.eu.int/technical_report_2005_3/en/technical_3_2005.pdf), *EEA Technical Report n°3/2005*, European Environment Agency, Denmark.

EMEP (2004), EMEP assessment, part 1, European perspective, *EMEP report*, Norwegian Meteorological Institute, Norway. (Available at http://www.emep.int/index_assessment.html)

EMEP (2005), Transboundary particulate matter in Europe, *EMEP Status report 4/2005*, Norwegian Meteorological Institute and Norwegian Institute for Air research, Norway. (Available at http://www.nilu.no/projects/ccc/reports/emep4-2005.pdf)

EPA (2003), National Air Quality and Emissions Trends Report, 2003 special studies edition, *EPA 454/R-03-005*, Environmental Protection Agency. (Available at http://www.epa.gov/air/airtrends/aqtrnd03/toc.html)

EPA (2006), National Ambient Air Quality Standards for Particulate Matter; Proposed Rule, *40 CFR Part 50*, pp.90, Environmental Protection Agency. (Available at http://www.epa.gov/fedrgstr/EPA-AIR/2006/January/Day-17/a177.pdf)

Fehsenfeld, F. C., P. Daum, W. R. Leaitch, M. Trainer, D. D. Parrish, and G. Hübler (1996), Transport and processing of O_3 and O_3 precursors over the North Atlantic: An overview of the 1993 North Atlantic Regional Experiment (NARE) summer intensive, *J. Geophys. Res.*, *101*, 28877–28892.

Fiore, A. M., D. J. Jacob, I. Bey, R. M. Yantosca, B. D. Field, A. C. Fusco, and J. G. Wilkinson (2002), Background ozone over the United States in summer: Origin, trend, and contribution to pollution episodes, *J. Geophys. Res.*, *107*(D15), doi:10.1029/2001JD000982.

Forster, C., et al. (2001), Transport of boreal forest fire emissions from Canada to Europe, *J. Geophys. Res.*, *106*(D19), 22887-22906, 10.1029/2001JD900115.

Goldstein, A. H., D. B. Millet, M. McKay, L. Jaeglé, L. Horowitz, O. Cooper, R. Hudman, D. J. Jacob, S. Oltmans, A. Clarke (2004), Impact of Asian emissions on

observations at Trinidad Head, California, during ITCT 2K2, *J. Geophys. Res.*, *109*, D23S17, doi:10.1029/2003JD004406.

Heald, C. L., D. J. Jacob, R. J. Park, B. Alexander, T. D. Fairlie, R. M. Yantosca, D. A. Chu, Transpacific transport of Asian anthropogenic aerosols and its impact on surface air quality in the United States, *J. Geophys. Res.*, in press.

Hogrefe, C., B. Lynn, K. Civerolo, J.-Y. Ku, J. Rosenthal, C. Rosenzweig, R. Goldberg, S. Gaffin, K. Knowlton, P. L. Kinney (2004), Simulating changes in regional air pollution over the eastern United States due to changes in global and regional climate and emissions, *J. Geophys. Res.*, *109*, D22301, doi:10.1029/2004JD004690.

Hogrefe, C., R. Leung, L. Mickley, S. Hunt and D. Winner (2005), Considering climate in air quality management, *Environmental Manager*, pp. 35–39.

Holloway, T., A. Fiore, and M. G. Hastings (2003), Intercontinental Transport of air pollution: Will emerging science lead to a new hemispheric treaty?, *Environ. Sci. & Technol.*, *37*, 4535–4542.

Hudman, R. C., et al. (2004), Ozone production in transpacific Asian pollution plumes and implications for ozone air quality in California, *J. Geophys. Res.*, *109*, D23S10, doi:10.1029/2004JD004974.

Huntrieser, H., et al. (2005), Intercontinental air pollution transport from North America to Europe: Experimental evidence from airborne measurements and surface observations, *J. Geophys. Res.*, *110*, D01305, doi:10.1029/2004JD005045.

Husar, R. B., et al. (2001), Asian dust events of April 1998, *J. Geophys. Res.*, *106*(D16), 18317-18330, 10.1029/2000JD900788.

Intergovernmental Panel on Climate Change (IPCC) (2001), *Climate Change 2001: The Scientific Basis*, Edited by J.T. Houghton et al., Cambridge Univ. Press, New York.

Jacob, D. J., and A. B. Gilliland (2005), Modeling the impact of air pollution on global climate change, *Environmental Manager*, pp. 24–27.

Jacob, D. J., J. A. Logan, and P. P. Murti (1999), Effect of rising Asian emissions on surface ozone in the United States, *Geophys. Res. Lett.*, *26*, 2175–2178.

Jaffe, D., et al. (1999), Transport of Asian air pollution to North America, *Geophys. Res. Lett.*, *26*, 711–714.

Keating, T., J. West and D. Jaffe (2005), Air quality impacts of intercontinental transport, *Environmental Manager*, pp. 28–30.

Li, Q. B., D. J. Jacob, R. M. Yantosca, J. W. Munger, and D. D. Parrish (2004), Export of NO_y from the North American Boundary Layer: Reconciling Aircraft Observations and Global Model Budgets, *J. Geophys. Res.*, *109*, D02313, doi:10.1029/2003JD004086.

Marenco, A., H. Gouget, P. Nédélec, J.-P. Pagés, F. Karcher (1994), Evidence of a long-term increase in tropospheric ozone from Pic du Midi data series: Consequences: Positive radiative forcing, *J. Geophys. Res.*, *99*(D8), 16617–16632, 10.1029/94JD00021.

Mattis, I., A. Ansmann, U. Wandinger, D. Müller (2003), Unexpectedly high aerosol load in the free troposphere over central Europe in spring/summer 2003, *Geophys. Res. Lett.*, *30*(22), 2178, doi:10.1029/2003GL018442.

Mauzerall, D. L., and X. Wang (2001), Protecting agricultural crops from the effects of tropospheric ozone exposure: Reconciling science and standard setting in the United States, Europe, and Asia, *Ann. Rev. Energy & Environ.*, *26*, 237–268.

McKendry, I. G., J. P. Hacker, R. Stull, S. Sakiyama, D. Mignacca, K. Reid (2001), Long-range transport of Asian dust to the Lower Fraser Valley, British Columbia, Canada, *J. Geophys. Res.*, *106*(D16), 18361-18370, 10.1029/2000JD900359.

Mickley, L. J., D. J. Jacob, B. D. Field, D. Rind (2004), Effects of future climate change on regional air pollution episodes in the United States, *Geophys. Res. Lett.*, *31*, L24103, doi:10.1029/2004GL021216.

Mitchell, Jr J.M. (1956), Visual Range in the Polar Regions with Particular Reference to the Alaskan Arctic, *Atmos. Terr. Phys.*, pp 195–211.

Müller, D., I. Mattis, U. Wandinger, A. Ansmann, D. Althausen, A. Stohl (2005), Raman lidar observations of aged Siberian and Canadian forest fire smoke in the free troposphere over Germany in 2003: Microphysical particle characterization, *J. Geophys. Res.*, *110*, D17201, doi:10.1029/2004JD005756.

Naja, M., H. Akimoto, and J. Staehelin (2003), Ozone in background and photochemically aged air over central Europe: Analysis of long-term ozonesonde data from Hohenpeissenberg and Payerne, *J. Geophys. Res.*, *108*(D2), 4063, doi:10.1029/2002JD002477.

NRC (National Research council) (1991), *Committee on tropospheric ozone formation and measurement - Rethinking the ozone problem in urban and regional air pollution*, National Academy Press, Washington DC.

OECD (1977), *The OECD programme on long-range transport of air pollutants*, Measurements and findings, Paris.

Ordóñez, C., H. Mathis, M. Furger, S. Henne, C. Hüglin, J. Staehelin, A. S. and H. Prévôt (2005), Changes of daily surface ozone maxima in Switzerland in all seasons from 1992 to 2002 and discussion of summer 2003, *Atmos. Chem. Phys.*, *5*, 1187–1203.

Parrish, D. D., J. S. Holloway, M. Trainer, P. C . Murphy, G. L. Forbes, and F. C. Fehenseld (1993), Export of North American ozone pollution to the North Atlantic Ocean, *Science*, *259*, 1436-1439.

Parrish, D. D., Y. Kondo, O. R. Cooper, C. A. Brock, D. A. Jaffe, M. Trainer, T. Ogawa, G. Hübler, F. C. Fehsenfeld (2004a), Intercontinental Transport and Chemical Transformation 2002 (ITCT 2K2) and Pacific Exploration of Asian Continental Emission (PEACE) experiments: An overview of the 2002 winter and spring intensives, *J. Geophys. Res.*, *109*, D23S01, doi:10.1029/2004JD004980.

Parrish, D. D., et al. (2004b), Fraction and composition of NO_y transported in air masses lofted from the North American continental boundary layer, *J. Geophys. Res.*, *109*, D09302, doi:10.1029/2003JD004226.

Pope, C. A. (2000), Review: Epidemiological basis for particulate air pollution health standards, *Aerosol Science and Technology*, *32*, 4–14.

Prather, M., et al. (2003), Fresh air in the 21st century?, *Geophys. Res. Lett.*, *30*(2), 1100, doi:10.1029/2002GL016285.

Prospero, J. M. (1981), Eolian transport to the world ocean, The sea, C. Emiliani, Ed., Wiley interscience, 801–874.

Reeves, C. E., et al. (2002), Potential for photochemical ozone formation in the troposphere over the North Atlantic as derived from aircraft observations during ACSOE, *J. Geophys. Res.*, *107*(D23), 4707.

Rodriguez, S., X. Querol, A. Alastuey and E. Mantilla (2002), Origin of high summer PM_{10} and TSP concentrations at rural sites in Eastern Spain, *Atmos. Environ.*, *36*, 3101–3112.

Shaw, G. E. (1975), The vertical distribution of atmospheric aerosols at barrow, Alaska, *Tellus*, *27*, 39–49.

Shaw, G. E. (1980), Transport of Asian desert aerosol to the Hawaiian Islands, *J. Appl. Meteor.*, *19*, 1254–1259.

Shaw, G. E. (1995), The Artic haze phenomenon, *Bull. Am. Met. Soc.*, *76*, 2403–2413.

Simmonds, P. G., R. G. Derwent, A. L. Manning, G. Spain, Significant growth in surface ozone at Mace Head, Ireland, 1987–2003, *Atmos. Environ.*, *38*, 4769–4778, 2004.

Stohl, A., and T. Trickl (1999), A textbook example of long-range transport: Simultaneous observation of ozone maxima of stratospheric and North American origin in the free troposphere over Europe, *J. Geophys. Res.*, *104*, 30445–30462.

Stohl, A., M. Trainer, T. B. Ryerson, J. S. Holloway, and D. D. Parrish (2002), Export of NO_y from the North American boundary layer during 1996 and 1997 North Atlantic Regional Experiments, *J. Geophys. Res.*, *107*(D11), doi:10.1029/2001JD000519.

Technical working group on particles (1997), Ambient air pollution by particulate matter, *Particles position paper*, European commission, Europe. (Available at http://europa.eu.int/comm/environment/air/pdf/pp_pm.pdf)

van Dingenen, R. et al. (2004), A European aerosol phenomenology-1: physical characteristics of particulate matter at kerbside, urban, rural and background sites in Europe, *Atmos. Environ.*, *38*, 2561–2577.

Vingarzan, R. (2004), A review of surface ozone background levels and trends, *Atmos. Environ.*, *38*, 3431–3442.

Wandinger, U. et al. (2002), Optical and microphysical characterization of biomass-burning and industrial-pollution aerosols from multiwavelength lidar and aircraft measurements, *J. Geophys. Res.*, *107*(D21), doi:10.1029/2000JD000202.

WHO (2000), *WHO air quality guidelines for Europe - second edition*, pp288., World Health organisation, Copenhagen, Denmark. (Available at http://www.euro.who.int/document/e71922.pdf)

WHO (2003), Health aspects of air pollution with particulate matter, ozone and nitrogen dioxide, *EUR/03/5042688*, pp.98, World Health organisation, Bonn, Germany. (Available at http://www.euro.who.int/Document/E79097.pdf)

WHO (2005), WHO air quality guidelines global update 2005, *EUR/05/5046029*, pp.30, World Health organisation, Bonn, Germany. (Available at http://www.euro.who.int/Document/E87950.pdf)

Wild, O., and H. Akimoto (2001), Intercontinental transport of ozone and its precursors in a three-dimensional global CTM, *J. Geophys. Res.*, *106*, 27729–27744.

Yienger, J., M. Galanter, T. A. Holloway, M. J. Phadnis, S. K. Guttikunda, G. R. Carmichael, W. J. Moxim, and H. Levy II (2000), The episodic nature of air pollution transport from Asia to North America, *J. Geophys. Res.*, *105*, 26931–26946.

Chapter 2

Scientific Background

The atmosphere contains gases and solid or liquid particles suspended in the air. These latter are called aerosols. Among the gases, the most well known are nitrogen (N_2) and oxygen (O_2), which account respectively for 78 and 21% of the atmosphere content. The 1% left is mainly formed of argon and water vapour. Other gases are also present in the atmosphere at very low concentrations (i.e., so called trace gases). Despite their low concentrations, these trace gases as well as aerosols are of critical importance for several environmental issues (including air quality and climate change) and health problem aspects. This chapter provides a brief overview of the processes which contribute to shape the distributions of compounds relevant for this thesis, including ozone (O_3) and aerosols. The chapter also includes a brief description of atmospheric circulation relevant for the dispersion of pollutants.

2.1 Tropospheric ozone

The study of O_3 is motivated by its impact on health and ecosystems, as well as its potential to warm the atmosphere via its greenhouse gas properties. O_3 is a secondary pollutant, i.e. it is not directly emitted in the atmosphere, but is mainly produced by the oxidation of hydrocarbons and carbon monoxide (CO) in the presence of nitrogen oxides ($NO_x = NO + NO_2$). Hydrocarbons, CO, and NO_x are thus called O_3 precursors. This section reviews briefly our current understanding in terms of sources of O_3 precursors, photochemistry involved in O_3 production, and global O_3 budget.

2.1.1 Ozone precursor emissions

O_3 precursors include NO_x, CO, methane (CH_4) and non-methane hydrocarbons (NMHC), which all have both anthropogenic and natural sources.

NO_x are emitted preferentially as NO, which photochemically equilibrates with NO_2 within a few minutes. NO_x sources are mainly of anthropogenic origin and are concentrated in the North Hemisphere. A quantitative estimate of NO_x sources is still missing, especially for the natural sources (e.g. lightning and soil), despite the progress made over the past decades. Table 2.1 reports the main sources of NO_x as estimated in *IPCC* [2001]. Free tropospheric sources of NO_x (e.g. from the stratosphere, lightning, and aircraft) are smaller but have a significant impact on O_3 production because they are directly injected in a relatively clean region.

Natural	
Soils	5.6
Lightning	5.0
Stratosphere	<0.5
Anthropogenic	
Fossil and domestic fuel	33.0
Aircraft	0.7
Biomass Burning	7.1
Total	51.9

Table 2.1: NO_x emissions in Tg N/yr as estimated in *IPCC* [2001].

Oxidation of CH_4	800
Oxidation of biogenic	700
Oxidation of acetone	20
Oxidation of industrial NMHC	110
Oxidation of biomass NMHC	30
Vegetation	150
Ocean	50
Biomass burning	700
Fossil and domestic fuel	650
Total	2780

Table 2.2: CO emissions in Tg CO/yr as estimated in *IPCC* [2001].

More than half of CO emissions are produced from human activities, via incomplete combustion of fossil fuel and biomass burning and are thus again found preferentially in the North Hemisphere (Table 2.2). In addition, CO is produced by oxidation of CH_4 and isoprene. CO is the main sink for hydroxyl radicals ($OH^{\cdot}$), and as such controls $OH^{\cdot}$ concentrations in the remote troposphere. As $OH^{\cdot}$ determines the lifetime of most atmospheric trace gases, CO is important in regard to its effect on the oxidizing capacity of the atmosphere.

Natural NMHC emissions are higher than anthropogenic emissions by a factor 10 (Table 2.3). The largest NMHC source is isoprene. Global biogenic emission estimates now benefit from dynamic vegetation models [*Guenther et al.*,1995], allowing the dependencies of emissions on leaf area index, temperature, etc. but they remain still highly uncertain, because of the complexity of the processes involved. For example, emission rates of biogenic compounds are related to the tree species, as well as on temperature and light intensity. Biogenic NMHC are however important with respect to photochemical O_3 production. For instance, in some cases, high biogenic emissions limit the efficiency of abatement of anthropogenic NMHC [*McKeen et al.*, 1991].

Besides playing an important role in O_3 photochemistry, CH_4 is the most abundant greenhouse gas in the troposphere after carbon dioxide (CO_2) and water vapour (H_2O).

Natural	
Oceanic	6–36
Vegetation	1245
Microbial production	6
Anthropogenic	
Transportation	22
Stationary source fuel combustion	4
Industrial processes	17
Organic solvents	15
Biomass Burning, incineration	45
Total	$\sim$ 1273

Table 2.3: NMHC emissions in Tg C/yr, adapted from *Brasseur et al.* [1999].

Natural	
Wetlands and rice	225
Termites	20
Ocean	15
Hydrates	10
Anthropogenic	
Energy	110
Landfills	40
Ruminants	115
Waste treatment	25
Biomass Burning	40
Total	600

Table 2.4: CH_4 emissions in Tg CH_4/yr, adapted from *Lelieveld et al.* [1998].

It is also the most abundant organic trace gas. Sources of CH_4 include both natural and anthropogenic sources (Table 2.4). A recent cost-analysis study suggested that CH_4 anthropogenic emission controls could be efficient in decreasing both air pollutants (such as O_3) and greenhouse gases concentrations [*West and Fiore*, 2005].

The trends in tropospheric O_3 concentrations are largely tied to the changes in precursor emissions (Note that trends in stratosphere-troposphere exchange and in stratospheric O_3 are also likely to shape global O_3 trends). The increase in anthropogenic emissions since the pre-industrial period is thus largely responsible for the observed increase (ranging from a factor 2 to 5) in tropospheric O_3 throughout the troposphere [*Marenco et al.*, 1994; *Vingarzan*, 2004].

Past estimates of future changes in emissions predicted an additional large increase in anthropogenic emissions of developing countries (e.g. Asia, India) from the 1990s onward, as well as a relatively stabilisation of emissions from the developed world (e.g. North America, Europe) [*Van Aardenne et al.*, 1999; *IPCC*, 2001]. However, in the last few years, a number of national and international measures have been undertaken to limit air pollution in developing countries with regards to health concerns. It is thus likely that the increase in emissions will be less dramatic than previously thought [*Dentener et al., 2005*].

2.1.2 Ozone photochemistry

One of the major roles of O_3 is its capacity to oxidize the atmosphere by initiating the formation of $OH^{\cdot}$, which in turn, is responsible for the removing of several key atmospheric trace gases (including one of the major greenhouse gases, e.g. CH_4).

O_3 initiates the formation of $OH^{\cdot}$ through UV photolysis at wavelengths < 319 nm (R 2.1) in presence of water vapor (R 2.2). Only a small fraction of $O(^1D)$ reacts with

H_2O, as the main part of $O(^1D)$ is collisionally deactivated with a molecule M, like O_2 or N_2 (R 2.3) to rapidly reproduce O_3 (R 2.4).

R 2.1 $$O_3 + h\nu\,(\lambda < 319\,nm) \xrightarrow{J_{2.1}} O_2 + O(^1D)$$

R 2.2 $$O(^1D) + H_2O \xrightarrow{k_{2.2}} 2OH^{\cdot}$$

R 2.3 $$O(^1D) + M \xrightarrow{k_{2.3}} O(^3P) + M$$

R 2.4 $$O(^3P) + O_2 + M \xrightarrow{k_{2.4}} O_3 + M$$

NO reacts with O_3 to form NO_2 (R2.5). Photolysis of NO_2 takes then place during daytime to form NO and $O(^3P)$ (R 2.6) which regenerates O_3 via (R 2.4). Those three reactions R 2.5, R 2.6 and R 2.4 cycled very fast.

R 2.5 $$O_3 + NO \xrightarrow{k_{2.5}} NO_2 + O_2$$

R 2.6 $$NO_2 + h\nu\,(\lambda < 430\,nm) \xrightarrow{J_{2.6}} NO + O(^3P)$$

This equilibrium is perturbated in the presence of CO and hydrocarbons (CH_4 and NMHC). For example, CO is oxidized by $OH^{\cdot}$ and forms $HO_2^{\cdot}$. $HO_2^{\cdot}$ in turn reacts with NO (if a sufficient level of NO is available) to form NO_2 (R 2.7), and to regenerate $OH^{\cdot}$. O_3 is then produced through photolysis of NO_2 (R 2.6) and reaction R 2.4.

R 2.7 $$NO + HO_2^{\cdot} \xrightarrow{k_{2.7}} NO_2 + OH^{\cdot}$$

In the same manner, CH_4 and NMHC are oxidized by $OH^{\cdot}$ form peroxy radical $CH_3O_2^{\cdot}$ and $RO_2^{\cdot}$ (R=C_2H_5 or higher organic grouping), respectively. Those peroxy radicals in turn can react with NO if a sufficient level of NO is available (R 2.8 and R 2.9). Photolysis of NO_2 (R 2.6) followed by reaction R 2.4 produces O_3.

R 2.8 $$NO + CH_3O_2^{\cdot} \xrightarrow{k_{2.8}} NO_2 + CH_3O^{\cdot}$$

R 2.9 $$NO + RO_2^{\cdot} \xrightarrow{k_{2.9}} NO_2 + RO^{\cdot}$$

$CH_3O^{\cdot}$ ($RO^{\cdot}$) further reacts with O_2 and form $HO_2^{\cdot}$ and formaldehyde HCHO (aldehyde RCHO). Again, $HO_2^{\cdot}$ reacts with NO if a sufficient level of NO is available (R 2.7). As NO_2 is formed by the reactions of NO with peroxy radicals ($HO_2^{\cdot}$, $CH_3O_2^{\cdot}$ and $RO_2^{\cdot}$) without O_3 being destroyed, the reactions R 2.7, R 2.8 and R 2.9 are the limiting steps that provide an additional source of NO_2 (and thus O_3).

Besides producing O_3 through the hydrocarbon oxidation chains, $OH^{\cdot}$ radicals serve also as a sink for O_3 (R 2.10).

R 2.10 $\mathrm{O_3 + OH^{\cdot} \xrightarrow{k_{2.10}} O_2 + HO_2^{\cdot}}$

An additional sink for O_3 is via reaction with $HO_2^{\cdot}$ (R 2.11).

R 2.11 $\mathrm{O_3 + HO_2^{\cdot} \xrightarrow{k_{2.11}} 2O_2 + OH^{\cdot}}$

This O_3-NO_x-NMHC cycle (Reactions R 2.1–2.2, R 2.4–2.11) is illustrated in Figure 2.1. Each color corresponds to a production or loss pathway for O_3. For simplicity, termination reactions of the radical cycle are not included. Such reactions include peroxy radical $HO_2^{\cdot}$ self-reaction, reaction of NO_2 with $OH^{\cdot}$ radicals and reactions between $HO_2^{\cdot}$ and $RO_2^{\cdot}$ radicals (R 2.12, R 2.13 and R 2.14). Nitric acid (HNO_3) is then removed principally by deposition from the troposphere.

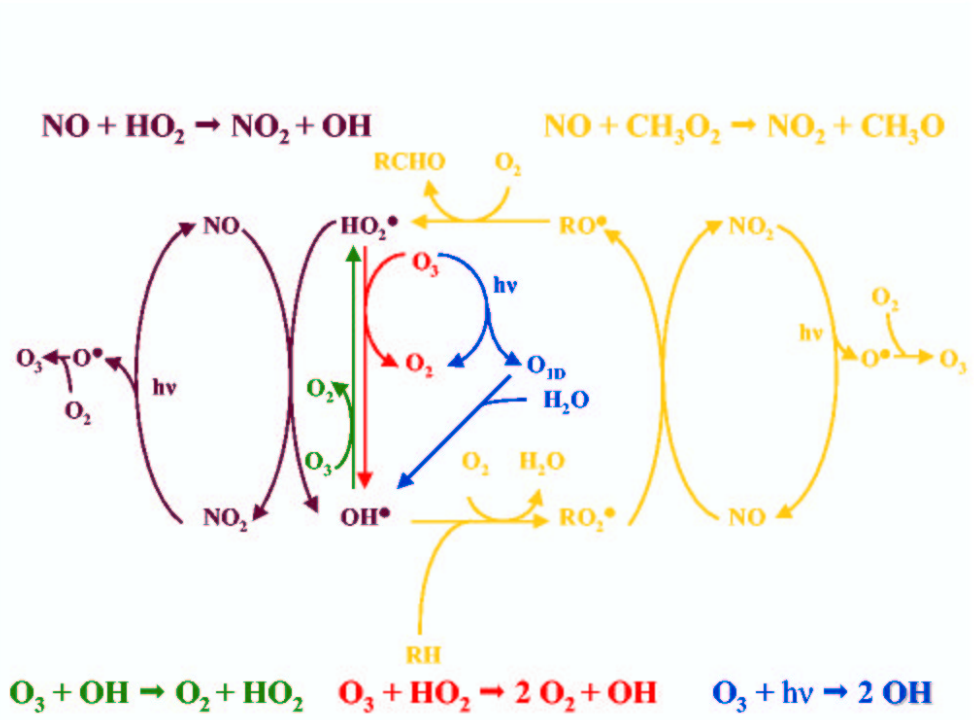

Figure 2.1: Schematic O_3-NO_x-NMHC cycle. Each color indicates a production or loss pathway for O_3.

R 2.12 $\mathrm{HO_2^{\cdot} + HO_2^{\cdot} \xrightarrow{k_{2.12}} H_2O_2 + O_2}$

R 2.13 $\mathrm{NO_2 + OH^{\cdot} + M \xrightarrow{k_{2.13}} HNO_3 + M}$

R 2.14 $\mathrm{HO_2^{\cdot} + RO_2^{\cdot} \xrightarrow{k_{2.14}} ROOH + O_2}$

Because the cycling between O_3, NO and NO_2 is very fast, the limiting steps in the production of O_3 are reactions R 2.7, R 2.8 and R 2.9. The production and loss rates can thus be written as follows (Equation 2.1 and 2.2, respectively).

$$P_{O_3} = k_{2.7}[NO][HO_2^{\cdot}] + k_{2.8}[NO][CH_3O_2^{\cdot}] + k_{2.9}[NO][RO_2^{\cdot}] \quad (2.1)$$

$$L_{O_3} = k_{2.2}[O(^1D)][H_2O] + k_{2.10}[O_3][OH^{\cdot}] + k_{2.11}[O_3][HO_2^{\cdot}] \quad (2.2)$$

The NO_x concentration is the main factor that determines whether the hydrocarbon oxidation chains lead to a production or loss of O_3. For small NO concentrations (smaller than about 10 to 30 pptv), O_3 is destroyed by photolysis (R 2.1) and reaction with $HO_2^{\cdot}$ and $OH^{\cdot}$ (R 2.10, R 2.11). However, if sufficient concentration of NO is available, the reaction of peroxy radicals with NO to form NO_2 (reactions R 2.7, R 2.8, R 2.9), and thus O_3 via reaction R 2.4, induces a production of O_3 that exceeds the destruction of O_3 by photolysis and by reaction with $HO_2^{\cdot}$ and $OH^{\cdot}$. For these situations, a net production of O_3 occurs.

Because of the relatively short lifetime of NO_x (e.g. a few days [*Munger et al.*, 1998; *Penner et al.*, 1998]), net O_3 production occurs mainly in the regions with elevated concentrations of O_3 precursors, e.g., in the boundary layer of urban and industrialized regions, as well as in the boundary layer of regions with vegetation fires. However, NO_x can also be released from nitrogen reservoir species in the free troposphere. One of the most important reservoir species is peroxyacetylnitrate (PAN). PAN is produced from oxidation of carbonyl compounds in the presence of NO_x. PAN can be transported over long distances and decompose to release NO_x far from its source regions. Observations gathered during several aircraft campaigns conducted over remote oceanic areas have indicated that net chemical O_3 production is also taking place over regions far away from primary sources of precursors. In particular it has been shown that net O_3 production occurs in polluted air masses exported from continental (polluted) regions while travelling over long distances [*Davis et al.*, 1996, 2003; *Crawford et al.*, 1997; *Reeves et al.*, 2002]. Chapter 3 of the present thesis investigates in detail O_3 production in long-range transported plumes over the North Atlantic and the Northwest Pacific regions.

Due to the complexity of O_3 photochemistry, the reduction of NO_x or NMHC emissions does not provide a linear answer on the O_3 concentrations. For example, the impact of concomitant NO_x and NMHC emission reductions may differ from the sum of the impact of individual emission reduction of each compound. A decrease in NO_x emissions generally leads to a decrease in $OH^{\cdot}$ and O_3 concentrations because of a slower cycling of the hydrocarbon oxidation chain (except for high NO_x levels). However, as the main sink of NO_x is the reaction between NO_2 and $OH^{\cdot}$, those lower $OH^{\cdot}$ levels enhanced the NO_x lifetime. Because of this negative feedback, *Kunhikrishnan and Lawrence* [2004] showed that the lower troposphere over the Indian ocean is only weakly sensitive to the enhanced continental NO_x emissions. On the other hand, a decrease in CO emissions leads to an increase in $OH^{\cdot}$ concentrations, that in turn decreases CO lifetime. This positive feedback also affects CH_4 concentrations [*Prather*, 1996]. This

non-linear chemistry makes difficult the quantitative estimate of the role of emission reduction strategies.

One goal of the thesis is to estimate the contribution of different geopolitical regions to the O_3 burden. These estimates are usually obtained by model sensitivity simulations in which anthropogenic emissions for a given region are turned off. In chapter 4 of this thesis, we quantify the effect on non-linearity on our results (i.e., the respective contributions of different regions to the European O_3 burden). In that particular case, the effect of non-linearity is relatively small, which is probably due to different compensating effects (e.g., enhanced NO_x lifetime and reduced CO lifetime as explained above).

2.1.3 Ozone budget

Sources of O_3 in the troposphere include transport from the stratosphere and in-situ photochemical production induced by hydrocarbon oxidation in presence of NO_x, as described above. The O_3 budget is closed by dry deposition as well as by O_3 chemical destruction through water vapour, and hydroxyl ($OH^{\cdot}$) and hydroperoxy ($HO_2^{\cdot}$) radicals. Before the 1970s, stratosphere was considered as the predominant source of O_3 [e.g., *Junge*, 1962; *Danielsen*, 1968]. O_3 photochemical production was originally thought to be a rather special process occurring only in the Los Angeles basin [*Haagen-Smit et al.*, 1953]. The importance of tropospheric photochemistry as a source of O_3 was established in the 1970s [e.g., *Levy, 1971*; *Chameides and Walker*, 1973; *Crutzen*, 1974]. The relative contribution of in-situ production and stratospheric input to the global O_3 sources is still a question of debate for the scientific community as further discussed in the following.

O_3 burden is difficult to estimate on a global scale, as O_3 concentrations are highly variable in the troposphere, reflecting the rapid O_3 chemical turnover. O_3 budget terms are even more difficult to quantify. Global chemical transport three-dimensional models (CTM) are useful tools to improve our knowledge of global chemical budgets. Such models integrate the different processes that drive the compounds distributions, including emissions, chemistry, transport and deposition. The dependence of species concentrations to those processes is mathematically expressed through the continuity equation, which is a statement of mass conservation (Equation 2.3), with dC_i/dt is the variation of the concentration of individual species in function of the time.

$$dC_i/dt = emissions + transport + chemical\ processes + deposition \qquad (2.3)$$

A number of global CTMs have been developed over the past two decades [*Law et al.*, 1998; 2000; *Lawrence et al.*, 1999, *Wild and Prather* 2000; *Horowitz*, 2003; *Hauglustaine et al.*, 2004]. They share the same theoretical foundations but differ in many ways including resolution, driving meteorology fields, transport algorithms, chemical schemes, and emission inventories. Two different CTMs will be used in this thesis, including the GEOS-Chem model, which is driven by offline meteorological parameters

provided by the NASA Goddard Earth Observing System (GEOS) (Chapter 3 to 5) and the MOZECH model which is embedded into a general circulation model (GCM) (Chapter 3).

The validity of CTMs to reproduce for example O_3 is assessed by careful comparison of the simulated field with field data, including ground-based O_3 measurements at the surface, O_3 soundings, in-situ aircraft measurements and satellite observations. Most of the global models available in the literature are now capable of reproducing mean seasonal variations by about 10 to 20 ppbv [*IPCC*, 2001; *Stevenson, et al.*, 2006]. However, because of the complexity of the various processes that contribute to O_3 production and destruction, it is often difficult to unravel which processes may be responsible for model errors. Use (and inter-comparison exercise) of several global models is thus a way to increase the robustness of results and to quantify levels of uncertainty. Such a study [*Stevenson et al.*, 2006] involving an ensemble of 26 state-of-the-art atmospheric chemistry models (including the GEOS-Chem and MOZECH models) recently estimated the O_3 budget (Table 2.5). The budget results in a net O_3 photochemical production of 442 Tg/yr and a stratospheric input of 552 Tg/yr more or less balanced by a deposition of 1003 Tg/yr. Stratospheric input and photochemical production are now believed to account for about 10 and 90% to the O_3 sources, respectively [*Stevenson et al.*, 2006].

Sources (Tg O_3.yr^{-1})	
Chemical production	5110 $\pm$ 606
Stratospheric input	552 $\pm$ 168
Sinks (Tg O_3.yr^{-1})	
Chemical loss	4668 $\pm$ 727
Deposition	1003 $\pm$ 200
Burden (Tg O_3)	344 $\pm$ 39
Lifetime (days)	22.2 $\pm$ 2.2

Table 2.5: O_3 budget from *Stevenson et al.* [2006] obtained by an ensemble of 26 state-of-the-art atmospheric chemistry model.

2.2 Aerosols

Similarly to O_3, aerosols play a key role in the Earth climate system and are of primary importance for air quality issues. Elevated aerosol concentrations at the surface have been associated with respiratory damage as well as excess mortality and morbidity [*Pope et al.*, 2000; *Wallace*, 2000]. The particles directly absorb and scatter the solar and terrestrial radiation [*Charlson et al.*, 1992]. Aerosols also act as cloud condensation nuclei (CCN) and therefore indirectly influence the cloud albedo, cloud lifetime and thus precipitation rates [*Twomey*, 1974; *Albrecht*, 1989; Pincus and Baker, 1994]. Radiative forcing, which is the imbalance between incoming solar radiation and outgoing terrestrial radiation at the top of atmosphere, depends strongly on the aerosol type. For example,

black carbon is a light-absorbing aerosol and thus contributes to global warming, while sulfate, nitrate, ammonium and organic aerosols are light-scattering aerosols and thus contribute to global cooling. However, uncertainties in the magnitude of radiative forcing for each aerosol types are large, as shown in Figure 2.2 [e.g., *Hansen and Sato*, 2001; *Boucher and Haywood*, 2001; *IPCC*, 2001]. In particular, the sign of the direct forcing for mineral dust remains unknown [e.g., *Sokolik et al.*, 2001]. Besides, the uncertainties concerning the indirect effect are at present the largest in the climatic system and can potentially be of the same order of magnitude - but of the opposite sign - as the warming due to greenhouse gases [*IPCC*, 2001]. Finally, most of the aerosols modify atmospheric chemistry through heterogeneous reactions and photolysis rates [e.g., *Martin et al.*, 2003 and reference therein, *Dentener et al.*, 1996]. Fine aerosols, which are mainly issued from anthropogenic origin, are expected to have a larger impact on the atmosphere because of their higher scattering efficiency and their longer lifetime [*IPCC*, 2001]. In addition, relatively to health concerns, fine particles are believed to be the more likely agent, rather than the coarse particles. All these effects have motivated the study of the aerosol budget over Europe (Chapter 5).

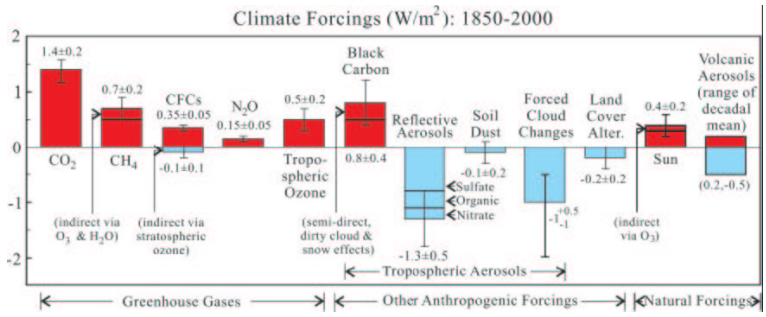

Figure 2.2: Estimation of the radiative forcing for each external climatic agents from the pre-industrial period (1850) to present (2000) [*Hansen and Sato*, 2001].

2.2.1 Aerosol sources and sinks and production mechanism

Aerosols are present in the atmosphere over a wide range of size. The coarse fraction ranges from 1 to 10 μm in radius. The fine fraction includes the accumulation mode, ranging from 0.01 to 1 μm and the nucleation mode ranging from 10^{-3} to 10^{-2} μm. Aerosols in the nucleation mode are mainly produced by clustering of gas molecules. They grow rapidly to the accumulation mode by condensation of gases and coagulation. Therefore, no distinction is made between these two modes for the rest of this study. The fine particle fraction includes carbonaceous compounds and ionic species, like sulfate (SO_4^{2-}), nitrate (NO_3^-) and ammonium (NH_4^+). Coarse particles are mainly formed of dust and sea-salt particles. Aerosols can be either emitted directly into the atmosphere (primary aerosols), or formed from gaseous precursors (secondary aerosols). They can combine to form mixed particles. Once in the troposphere, aerosols are removed by dry and wet deposition, as well as by sedimentation. Coarse particles are mainly removed by sedimentation. Fine particles are mainly removed by scavenging by

cloud droplets and subsequent rainout or by direct scavenging by raindrops. Aerosol lifetimes vary widely, depending of their size. Coarse aerosols are removed first and have a shorter lifetime (minutes to days), while fine aerosols have a lifetime ranging from days to weeks [*Seinfeld and Pandis*, 1998].

The two main precursors of sulfate aerosols are sulfur dioxide (SO_2) from anthropogenic sources and volcanoes, and dimethyl sulfide (DMS) from biogenic sources (especially from oceanic phytoplankton) (Table 2.6). In the Northern Hemisphere, sulfate is predominantly of anthropogenic origin (73%) [*IPCC*, 2001], and is thus a good indicator of human activities. Ammonium comes from ammonia, which is mainly emitted during bacterial metabolism of animals, through agriculture, biomass burning and oceans (Table 2.7). In the Northern hemisphere, about 80% of ammonia sources are anthropogenic [*Bouwman et al.*, 1997] and mainly reflect agricultural activities. Ammonia preferentially combines with sulfate to form ammonium sulfate. If ammonia is in excess, it then combines with HNO_3 to form ammonium nitrate, which is the predominant source of nitrate aerosols.

SO_2 (Tg S.yr^{-1})	
Fossil fuel and industry (1985)	76
Aircraft (1992)	0.06
Biomass burning (1990)	2.2
Volcanoes	9.3
DMS (as Tg S.yr^{-1})	
Oceans	24
Land biota and soils	1.0

Table 2.6: SO_2 and DMS emissions from *IPCC* [2001].

NH_3 (Tg N.yr^{-1})	
Domestic animals (1990)	21.6
Agriculture (1990)	12.6
Humans (1990)	2.6
Biomass burning (1990)	5.7
Fossil fuel and industry (1990)	0.3
Natural Soils (1990)	2.4
Wild animals	0.1
Oceans	8.2

Table 2.7: NH_3 emissions from *IPCC* [2001].

Carbonaceous aerosols consist of elemental carbon (also called black carbon, BC) and a variety of organic compound (also called POM which stands for particulate organic matter). BC results from incomplete combustion of fossil fuel and biomass burning (Table 2.8). POM is either emitted directly through incomplete combustion of biomass burning to form primary organic carbon (referred as OC) or is formed from oxidation of biogenic and anthropogenic volatile organic compound and is then referred to as secondary organic aerosol (SOA) (Table 2.8).

Dust is mainly emitted from aeolian erosion occurring in arid and semi-arid areas. This natural source may be influenced by human induced changes of land use and land cover. Dust is one of the largest contributors to the global aerosol loading. Global current dust emissions range from 1000 to 2150 Tg/yr [*Zender et al.*, 2004]. Dust consists of the minerals and organic material making up soil. Their effects on the Earth radiative budget depend strongly on the composition and size of the particle, and other dust properties. As all those properties vary both in time and space, uncertainties remain in the sign and magnitude of radiative forcing on a global and even regional scale [*Sokolik et al.*, 2001]. Dust also impacts terrestrial and ocean biogeochemistry when

Organic matter (Tg.yr^{-1})	
Biomass burning	54
Fossil Fuel	28
Biogenic	56
Black carbon (Tg.yr^{-1})	
Biomass burning	5.7
Fossil fuel	6.6
Aircraft	0.006

Table 2.8: Emission estimates of carbonaceous compounds from *IPCC* [2001].

deposited onto the ground or ocean [e.g., *Chadwick et al.*, 1999]. Dust emissions occur when surface winds exceed a threshold velocity, which is mainly function of surface roughness, grain size, soil moisture and vegetation cover. The particle size determines the lifetime of dust, as well as their motion. There are three major types of grain motion. Finer particles are transported directly through turbulent eddies, what is called suspension. Particles ranging from 60 to 200 μm are transported to very short distance through direct mobilization (at a height less than 1 m) by the wind before being carried downwind back to the surface (saltation process). The larger particles roll and creep along the surface (creeping process). However, most of the particles are not directly mobilized by the wind because of cohesive forces. Laboratory and wind field tunnel studies have shown that dust is preferentially mobilized by ejection of clay and silt particles resulting of the bombardment of saltating particles. This process is referred to as sandblasting.

Sea-salt particles form when winds and waves force air bubbles to burst at the sea surface. They consist mainly of water and sodium chloride (NaCl) and to a lesser extent of magnesium. Sea-salt particles are emitted primarily in the coarse mode, but a part is also found in the fine mode. Their size range from 0.05 to 10 μm diameter. Sea-salt emissions are estimate to range between 1000 to 6000 Tg/yr [*Gong et al.*, 1998; *IPCC*, 2001].

Two different quantities are usually used to describe the radiative perturbation and the health effects of aerosols. Aerosol optical depth (AOD), which is a measure of how much light aerosols prevent from passing through a column of atmosphere is directly linked to the radiative perturbation. The number and mass of aerosol concentrations, often represented through measurements of particulate matter (PM) are used to assess air quality and health issues. Mass loading per unit area (M) and AOD (τ) are related to each other through the relation $\tau = 3QM/(4\rho r_e)$ where ρ is the particle density, r_e the effective radius and Q the extinction coefficient calculating from the Mie-scattering theory. The variables τ and Q are wavelength dependent.

2.2.2 Specific difficulties related to the aerosol study

Since the 1990s, aerosol modules have been implemented into several GCM to understand the sulfur cycle [e.g., *Rasch et al.*, 2000 and references therein] and its impact on climate. However, such models generally represent multiyear values averaged over large area, that make difficult to represent daily and yearly variability. Aerosol modules have been only recently implemented into CTM with the aim to improve our knowledge of aerosol dynamical processes like nucleation, condensation, evaporation and coagulation and to quantify the aerosol impact on the environment. Sulfate-ammonium-nitrate modules were first introduced [*Chin et al.*, 2000 and references therein, *Boucher and Pham*, 2002; *Park et al.*, 2004], followed by dust [*Ginoux et al.*, 2001; *Zender et al.*, 2003] and carbonaceous modules including secondary organic aerosol [*Chung and Seinfeld*, 2002; *Park et al.*, 2003; *Reddy and Boucher*, 2004], and more recently sea-salt particles [*Gong et al.*, 1998; *Alexander et al.*, 2005].

Although CTMs have been extensively tested against trace gases observations, evaluation of aerosol components (optical properties and concentrations) is largely incomplete, partly due to a lack of measurements. For instance, although several satellites [*Kaufman et al.*, 1997; *Tanré et al.*, 1997; *Herman et al.*, 1997; *Husar et al.*, 1997] and ground-based sunphotometer [*Holben*, 1998] retrieved total column AOD, only little information on vertical profiles is available. As the altitude of the aerosol layer could also affect the magnitude of the direct radiative forcing [*Hansen et al.*, 1997], it is essential to have information on the vertical distribution of aerosols and to know if models simulate correctly aerosol profiles. Ongoing efforts are done to measure aerosol properties during field campaign, which provide information at selected altitudes. Besides, development of lidar network such the European Aerosol Research LIdar NETwork (EARLINET) could feed model with vertical information and give insights in long-range transported aerosol layers. Ground-based aerosol concentrations are also available, but remain very sparse and difficult to interpret because of inhomogeneous techniques of measurements.

Simulating aerosol field is thus more challenging than simulating trace gases concentrations. Moreover, mechanisms conducive to the formation of secondary aerosols is still a matter of debate, as the role of isoprene for initiating SOA formation is not evident at the moment [*Pandis et al.*, 1991; *Claeys et al.*, 2004a; 2004b; *Kroll et al.*, 2005]. In addition deposition and scavenging of aerosol are highly sensitive to clouds and rain, which are poorly simulated variables. Finally, emissions inventories are still uncertain. These are the reasons why we provide a thorough evaluation of the GEOS-Chem model capabilities over Europe (Chapter 5).

2.3 Transport of Tropospheric Air Pollution

2.3.1 General circulation

Large-scale atmospheric circulation patterns are first driven by the uneven distribution of radiative heating in the Earth system, resulting in a mean meridional flow. Secondly, atmospheric circulation is driven by the conservation of the angular momentum (tendency for the Earth's atmosphere to move with the Earth around its axis of rotation). Heat and momentum could be transported vertically or horizontally. Vertical motions reflect a balance between the vertical pressure gradient pushing air upward and the force of gravity pulling it downward. Horizontal motions depend of the horizontal pressure gradient, the Coriolis force and near the surface of the force of friction.

Only a small component of trace gases is redistributed through the meridional circulation. The major part is transported through quasi-zonal flow, which is perturbated by orographic features and surface temperature, as well as synoptic systems. In the boundary layer, extending approximately from the ground up to 1 km, the effect of surface is more important than in the free troposphere (extending from 1 km to 12 km). Efficient mixing processes occur in the boundary layer, transporting air masses upward and downward.

2.3.2 Long-range transport of air pollution

Major pathways for long-range transport of pollutants are depicted in Figure 2.3. Main pathways occur in the free troposphere. At high altitudes, transport is faster and temperature lower than at lower altitudes, leading to an increase in chemical lifetime of pollutants. Polluted air masses injected in the free troposphere are thus believed to have more impact on the downwind continent. Vertical uplifting of polluted air masses from the boundary layer to the free troposphere occurs through deep convection, orographic lifting (especially important for Asian export [e.g., *Liu et al.*, 2003]) as well as uplifting associated with cyclones.

Deep convection is driven by thermally turbulent mixing and is often associated with thunderstorms and lightning. In summer, strong heating at the surface causes moist, hot air to rise. Rising air cools, causing water to condense, which release latent heat that reinforces the rising motion. Deep convection injects thus air quickly into the mid and upper troposphere (and can extend up to the tropopause) where higher wind speeds can rapidly transport the pollutants downwind. In GEOS-Chem, deep convection is computed using the GEOS convective, entrainment, and detrainment mass fluxes as described by *Allen et al.* [1996a, 1996b]. Over Asia, deep convection occurs preferentially in the southeast in spring and over central China in summer [*Bey et al.*, 2001; *Liang et al.*, 2003]; while over the U.S., it occurs preferentially over the central and south-eastern U.S. [*Thompson et al.*, 1994; *Li et al.*, 2005]. Finally, over Europe, this process is more important in summer over Germany and the Ural mountains in Russia [*Duncan and Bey*, 2004].

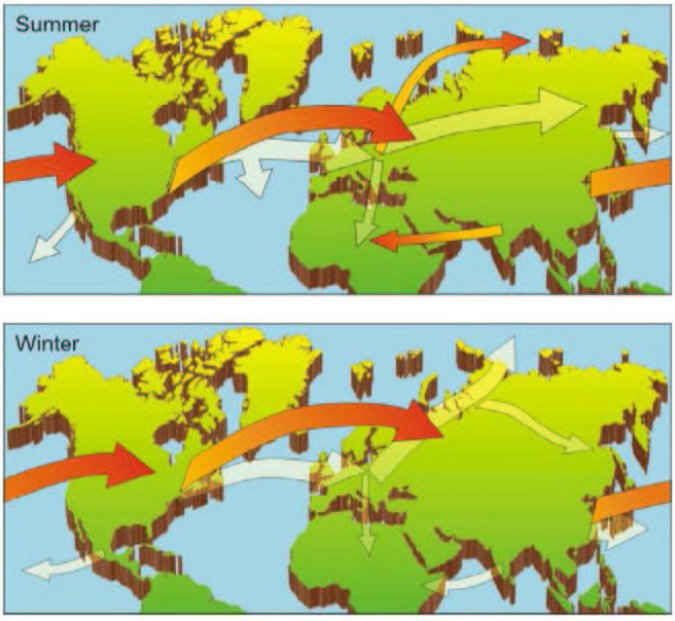

Figure 2.3: Schematic illustration of the pathways of intercontinental transport in the Northern Hemisphere. The orange arrows illustrate transport in the middle and upper troposphere, whereas the light shaded arrows illustrate lower-level transport. The arrows' widths qualitatively indicate how much pollution is transported along the respective pathways. From *Forster et al.,* [2005].

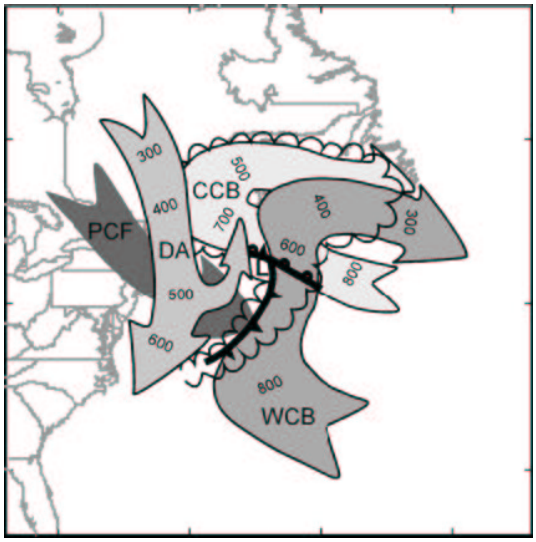

Figure 2.4: Schematic diagram of mid-latitude cyclone showing the different air masses: the warm (WCB), cold conveyor belt (CCB), dry airstream (DA), and post-cold-front airstream (PCF). The center of the cyclone is indicated (L) and the scalloped lines indicate the edges of the comma cloud formed by the airstreams. The numbers on the WCB and CCB indicate the pressure at the top of these airstreams, while the numbers on the DA indicate the pressure at the bottom of this airstream. From *Cooper et al.* [2002].

A typical cyclone is composed of four major airstreams: the warm conveyor belt (WCB), the cold conveyor belt (CCB), the dry airstream (DA) and the post cold front airstream (PCF) (see Figure 2.4) [*Cooper et al.*, 2002]. In general, those airstreams move along sloping isentropic surfaces. If the air mass is not saturated, a constant potential temperature characterizes the isentropic surfaces [*Cooper et al.*, 2001]. The different airstreams are typically of the order of a few kilometers across and of 1 km in depth [*Eckhardt et al.*, 2004 and references therein]. In such cyclones, WCB (a rising air mass ahead of a cold front, located on the eastern side of the cyclone) is the most important airstream for injection of air into the free troposphere and subsequent direct long-range transport. *Esler et al.*, 2003 report that WCBs generally extend from 50 to 250 km and could ascent by 3 to 8 km per day. WCBs originate preferentially from the eastern seaboard of Asia and North America [*Stohl*, 2001]. They occur all-year round, but with a lower frequency in summer [*Eckhardt et al.*, 2004]. Once transported in the free troposphere, pollutants are transported rapidly across the oceans. In the free troposphere, transpacific transport is mainly controlled by the semi permanent Pacific high and Aeulian low, while transatlantic transport is mainly controlled by the semi permanent Bermuda-Azores high and Icelandic low. Global models such as GEOS-Chem represent the location and timing of cyclones correctly, but because of their coarse resolution, they are not able to distinguish in great detail the different airstreams.

It has also been recently demonstrated that in summer, Europe, in addition to the westerly flow from North America, receives easterly winds from the Indian monsoon in Asia [*Lelieveld et al.*, 2002]. During the summer monsoon, pollution is uplifted during deep convective events over Asia. The two upper tropospheric anticyclones that are located over Tibet and over north Arabia move back and forth and thus result in a large elongated anticyclone on a monthly period. On the south side of this large anticyclone, tropical easterly jets inject the uplifted Asian pollution up to northeast Africa and to the Mediterranean basin [*Lawrence*, 2004]. During the Mediterranean Intensive Oxidant Study (MINOS) aircraft campaign, measurements of trace gases associated with back trajectories [*Traub et al.*, 2003] and modeling studies [*Lawrence et al.*, 2003; *Scheeren et al.*, 2003; *Roelofs et al.*, 2003] have shown that the Mediterranean free troposphere is highly impacted by these processes.

In addition to these high altitudes export pathways, pollutants could be also exported directly in the oceanic boundary layer from Asia toward North America [*Carmichael et al.*, 1998; *Liu et al.*, 2003 and *Liang et al.*, 2004] and from North America toward Europe [*Li et al.*, 2002; 2005]. European pollution export occurs mainly at low altitudes toward Asia through westerly winds, toward North Africa and toward the Arctic in winter [*Wild and Akimoto*, 2001; *Duncan and Bey*, 2004].

Chapter 3 and 4 describe in detail the transport pathways that contribute to import into Europe.

References

Albrecht, B. A. (1989), Aerosols, cloud microphysics, and fractional cloudiness, *Science*, *245*,1227–1230.

Alexander, B., R. J. Park, D. J. Jacob, Q. B. Li, R. M. Yantosca, J. Savarino, C. C. W. Lee, M. H. Thiemens (2005), Sulfate formation in sea-salt aerosols: Constraints from oxygen isotopes, *J. Geophys. Res.*, *110*, D10307, doi:10.1029/2004JD005659.

Allen, D. J., R. B. Rood, A. M. Thompson, R. D. Hudson (1996a), Three-dimensional ^{222}Rn calculations using assimilated meteorological data and a convective mixing algorithm, *J. Geophys. Res.*, *101*(D3), 6871–6882, 10.1029/95JD03408.

Allen, D. J., P. Kasibhatla, A. M. Thompson, R. B. Rood, B. G. Doddridge, K. E. Pickering, R. D. Hudson, S.-J. Lin (1996b), Transport-induced interannual variability of carbon monoxide determined using a chemistry and transport model, *J. Geophys. Res.*, *101*(D22), 28655-28670, 10.1029/96JD02984.

Bey, I., D. J. Jacob, J. A. Logan, R. M. Yantosca (2001), Asian chemical outflow to the Pacific in spring: Origins, pathways, and budgets, *J. Geophys. Res.*, *106*(D19), 23097–23114, 10.1029/2001JD000806.

Boucher, O., and J. Haywood (2001), On summing the components of radiative forcing of climate change, *Climate Dyn.*, *18*, 297–302.

Boucher, O. and M. Pham (2002), History of sulfate aerosol radiative forcings, *Geophys. Res. Lett.*, *29* (9), doi:10.1029/2001GL014048.

Bouwman, A. F., D. S. Lee, W. A. H. Asman, F. J. Dentener, K. W. VanderHoek, and J. G. J. Olivier (1997), A global high-resolution emission inventory for ammonia, *Global Biogeochem. Cycles*, 11(4), 561–587.

Brasseur, G. J., J. Orlando and G. Tyndall (1999), *Atmospheric chemistry and global change*, Oxford University Press, New-York, USA.

Carmichael, G. R., I. Uno, M. J. Phadnis, Y. Zhang, Y. Sunwoo (1998), Tropospheric ozone production and transport in the springtime in east Asia, *J. Geophys. Res.*, *103*(D9), 10649–10672, 10.1029/97JD03740.

Chadwick, O. A., L. A. Derry, P. M. Vitousek, B. J. Huebert, and L. O. Hedin (1999), Changing sources of nutrients during four million years of ecosystem development, *Nature*, *397*, 491–496.

Chameides, W. L. and J. C. G. Walker (1973), Photochemical theory of tropospheric ozone, *J. Geophys. Res.*, *78*, 8751–8760.

Charlson, R. J., S. E. Schwartz, J. M. Hales, R. D Cess, J. A. Coakley, J. E. Hansen, D. J. Hofmann (1992), Climate forcing by anthropogenic aerosols, *Science*, *255*, 423–430.

Chin, M., R. B. Rood, S.-J. Lin, J.-F. Müller, A. M. Thompson (2000), Atmospheric sulfur cycle simulated in the global model GOCART: Model description and global properties, *J. Geophys. Res.*, *105*(D20), 24671–24688, 10.1029/2000JD900384.

Chung, S. H., and J. H. Seinfeld (2002), Global distribution and climate forcing of carbonaceous aerosols, *J. Geophys. Res.*, *107* (D19), 4407, doi:10.1029/2001JD001397.

Claeys, M. et al. (2004b), Formation of secondary organic aerosols through photooxidation of isoprene, *Science*, *303*, 1173–1176.

Claeys, M., W. Wang, A. C. Ion, I. Kourtchev, A. Gelencsér and W. Maenhaut (2004a), Formation of secondary organic aerosols from isoprene and its gas-phase oxidation products through reaction with hydrogen peroxide, *Atmos. Environ.*, *38*, 4093–4098.

Cooper, O. R., J. L. Moody, D. D. Parrish, M. Trainer, T. B. Ryerson, J. S. Holloway, G. Hübler, F. C. Fehsenfeld, and M. J. Evans (2002), Trace gas composition of midlatitude cyclones over the western North Atlantic Ocean: A conceptual model, *J. Geophys. Res.*, *107* (D7), doi:10.1029/2001JD000901.

Cooper, O. R., J. L. Moody, D. D. Parrish, M. Trainer, T. B. Ryerson, J. S. Holloway, G. Hübler, F. C. Fehsenfeld, S. J. Oltmans, M. J. Evans (2001), Trace gas signatures of the airstreams within North Atlantic cyclones: Case studies from the North Atlantic Regional Experiment (NARE'97) aircraft intensive, *J. Geophys. Res.*, *106*(D6), 5437–5456, 10.1029/2000JD900574.

Crawford, J., et al. (1997), An assessment of ozone photochemistry in the extratropical western North Pacific: impact of continental outflow during the late winter/early spring, *J. Geophys. Res.*, *102*(D23), 28469–28488, 10.1029/97JD02600.

Crutzen, P. J. (1974), Photochemical reactions initiated by and influencing ozone in the unpolluted tropospheric air, *Tellus*, *26*, 47–57.

Danielsen, E. F. (1968), Stratospheric-tropospheric exchange based on radioactivity ozone and potential vorticity, *J. Atmos. Sci.*, *25* , 502–518.

Davis, D. D., et al. (1996), Assessment of ozone photochemistry in the western North Pacific as inferred from PEM-West A observations during the fall 1991, *J. Geophys. Res.*, *101*(D1), 2111–2134, 10.1029/95JD02755.

Davis, D. D., et al. (2003), An assessment of western North Pacific ozone photochemistry based on springtime observations from NASA's PEM-West B (1994) and TRACE-P (2001) field studies, *J. Geophys. Res.*, *108* (D21), 8829, doi:10.1029/2002JD003232.

Dentener, F. J., G. R. Carmichael, Y. Zhang, J. Lelieveld, and P. J. Crutzen (1996), Role of mineral aerosol as a reactive surface in the global troposphere, *J. Geophys. Res.*, *101*(D17), 22,869–22,889.

Dentener, F. J., D. Stevenson, J. Cofala, R. Mechler, M. Amann, P. Bergamaschi, F. Raes, R. Derwent (2005), The impact of air pollutant and methane emission controls on tropospheric ozone and radiative forcing: CTM calculations for the period 1990–2030, *Atmos. Chem. Phys.*, *5*, 1731–1755.

Duncan, B. N., I. Bey (2004), A modeling study of the export pathways of pollution from Europe: Seasonal and interannual variations (1987–1997), *J. Geophys. Res.*, *109*, D08301, doi:10.1029/2003JD004079.

Eckhardt, S., A. Stohl, H. Wernli, P. James, C. Forster, and N. Spichtinger (2004), A 15-year climatology of warm conveyor belt, *J. Climate*, *17*, 218–237.

Esler, J. G., P. H. Haynes, K. S. Law, H. Barjat, K. Dewey, J. Kent, S. Schmitgen, and N. Brough (2003), Transport and mixing between airmasses in cold frontal regions during Dynamics and Chemistry of Frontal Zones (DCFZ), *J. Geophys. Res.*, *108* (D4), 4142, doi:10.1029/2001JD001494.

Fehsenfeld, F. C., P. Daum, W. R. Leaitch, M. Trainer, D. D. Parrish, G. Hübler (1996), Transport and processing of O_3 and O_3 precursors over the North Atlantic: An overview of the 1993 North Atlantic Regional Experiment (NARE) summer intensive, *J. Geophys. Res.*, *101*(D22), 28877–28892, 10.1029/96JD01113.

Forster, C., A. Stohl, P. Wind and A. Benedictow (2005), Intercontinental air pollution transport, *Transboundary Acidification, Eutrophication and Ground Level Ozone in Europe in 2003*, EMEP Report 1/2005, pp. 127–153, Norwegian Meteorological Institute, Norway. (Available at http://www.emep.int/publ/reports/2005/status_report1.pdf)

Ginoux, P., M. Chin, I. Tegen, J. M. Prospero, B. Holben, O. Dubovik, S.-J. Lin (2001), Sources and distributions of dust aerosols simulated with the GOCART model, *J. Geophys. Res.*, *106*(D17), 20255–20274, 10.1029/2000JD000053.

Gong, S. L., L. A. Barrie, J.-P. Blanchet, and L. Spacek (1998), *Modelizing size-distributed sea-salt aerosols in the atmosphere: An application using Canadian climate models*, Plenum Press, New-York.

Guenther, A., et al. (1995), A global model of natural volatile organic compound emissions, *J. Geophys. Res.*, *100*(D5), 8873–8892, 10.1029/94JD02950.

Haagen-Smit, A. J., C. E. Bradley, M. M. Fox (1953), Ozone formation in photochemical oxidation of organic substances, *Industrial Engineering Chemistry*, *45*, 2086–2089.

Hansen, J. E., and M. Sato (2001), Trends of measured climate forcing agents, *Proc. Natl. Acad. Sci.*, *98*, 14778–14783.

Hansen, J., M. Sato, R. Ruedy (1997), Radiative forcing and climate response, *J. Geophys. Res.*, *102*(D6), 6831–6864, 10.1029/96JD03436.

Hauglustaine, D. A., F. Hourdin, L. Jourdain, M.-A. Filiberti, S. Walters, J.-F. Lamarque, E. A. Holland (2004), Interactive chemistry in the Laboratoire de Météorologie Dynamique general circulation model: Description and background tropospheric chemistry evaluation, *J. Geophys. Res.*, *109*, D04314, doi:10.1029/2003JD003957.

Herman, J. R., P. K. Bhartia, O. Torres, C. Hsu, C. Seftor, E. Celarier (1997), Global distribution of UV-absorbing aerosols from Nimbus 7/TOMS data, *J. Geophys. Res.*, *102*(D14), 16911–16922, 10.1029/96JD03680.

Holben, B. N. , et al. (1998), AERONET - A federated instrument network and data archive for aerosol characterization, *Rem. Sens. Environ.*, *66*, 1–16.

Horowitz, L. W., et al. (2003), A global simulation of tropospheric ozone and related tracers: Description and evaluation of MOZART, version 2, *J. Geophys. Res.*, *108* (D24), 4784, doi:10.1029/2002JD002853.

Husar, R. B., J. M. Prospero, L. L. Stowe (1997), Characterization of tropospheric aerosols over the oceans with the NOAA advanced very high resolution radiometer optical thickness operational product, *J. Geophys. Res.*, *102*(D14), 16889–16910, 10.1029/96JD04009.

Intergovernmental Panel on Climate Change (IPCC) (2001), *Climate Change 2001: The Scientific Basis*, edited by J. T. Houghton et al., Cambridge Univ. Press, New York.

Junge, C. E. (1962), Global ozone budget and exchange between stratosphere and troposphere, *Tellus*, *14*, 363–377.

Kaufman, Y. J., D. Tanré, L. A. Remer, E. F. Vermote, A. Chu, B. N. Holben (1997), Operational remote sensing of tropospheric aerosol over land from EOS moderate resolution imaging spectroradiometer, *J. Geophys. Res.*, *102*(D14), 17051–17068, 10.1029/96JD03988.

Kroll, J. H., N. L. Ng, S. M. Murphy, R. C. Flagan, J. H. Seinfeld (2005), Secondary organic aerosol formation from isoprene photooxidation under high-NO_x conditions, *Geophys. Res. Lett.*, *32*, L18808, doi:10.1029/2005GL023637.

Kunhikrishnan, T., M. G. Lawrence (2004), Sensitivity of NO_x over the Indian Ocean to emissions from the surrounding continents and nonlinearities in atmospheric chemistry responses, *Geophys. Res. Lett.*, *31*, L15109, doi:10.1029/2004GL020210.

Law, K. S., P. H. Plantevin, D. E. Shallcross, H. L. Rogers, J. A. Pyle, C. Grouhel, V. Thouret, A. Marenco (1998), Evaluation of modeled O_3 using Measurement of Ozone by Airbus In-Service Aircraft (MOZAIC) data, *J. Geophys. Res.*, *103*(D19), 25721–25737, 10.1029/98JD01482.

Law, K. S., P.-H. Plantevin, V. Thouret, A. Marenco, W. A. H. Asman, M. Lawrence, P. J. Crutzen, J.-F. Muller, D. A. Hauglustaine, M. Kanakidou (2000), Comparison between global chemistry transport model results and Measurement of Ozone and Water Vapor by Airbus In-Service Aircraft (MOZAIC) data, *J. Geophys. Res.*, *105*(D1), 1503–1526, 10.1029/1999JD900474.

Lawrence, M. G. (2004), Export of air pollution from southern Asia and its large-scale effects, in *Inter-continental transport of air pollution*, edited by A. Stohl, pp. 131–172.

Lawrence, M. G., P. J. Crutzen, P. J. Rasch, B. E. Eaton, N. M. Mahowald (1999), A model for studies of tropospheric photochemistry: Description, global distributions, and evaluation, *J. Geophys. Res.*, *104*(D21), 26245–26278, 10.1029/1999JD900425.

Lawrence, M. G. et al. (2003), Global chemical weather forecasts for field campaign planning: predictions and observations of large-scale features during MINOS, CONTRACE, and INDOEX, *Atmos. Chem Phys.*, *3*, 267–289.

Lelieveld, J., P. Crutzen and F. J. Dentener (1998), Changing concentration, lifetime and climate forcing of atmospheric methane, *Tellus*, *50B*, 128–150.

Lelieveld, J., et al. (2002), Global air pollution crossroads over the Mediterranean, *Science*, *298*, 794–799.

Levy, H. (1971), Normal atmosphere: large radical and formaldehyde concentrations predicted, *Science*, *173*, 141–143.

Li, Q. B., et al. (2002), Transatlantic transport of pollution and its effects on surface ozone in Europe and North America, *J. Geophys. Res.*, *107* (D13), doi:10.1029/2001JD001422.

Li, Q. B. , D. J. Jacob, R. Park, Y. Wang, C. L. Heald, R. Hudman, R. M. Yantosca, R. V. Martin, M. Evans (2005), North American pollution outflow and the trapping of convectively lifted pollution by upper-level anticyclone, *J. Geophys. Res.*, *110*, D10301, doi:10.1029/2004JD005039.

Liang, Q., L. Jaeglé, D. A. Jaffe, P. Weiss-Penzias, A. Heckman, J. A. Snow (2004), Long-range transport of Asian pollution to the northeast Pacific: Seasonal variations and transport pathways of carbon monoxide, *J. Geophys. Res.*, *109*, D23S07, doi:10.1029/2003JD004402.

Liu, H., D. J. Jacob, I. Bey, R. M. Yantosca, B. N. Duncan, G. W. Sachse (2003), Transport pathways for Asian pollution outflow over the Pacific: Interannual and seasonal variations, *J. Geophys. Res.*, *108* (D20), 8786, doi:10.1029/2002JD003102.

Marenco, A., H. Gouget, P. Nédélec, J.-P. Pagés, F. Karcher (1994), Evidence of a long-term increase in tropospheric ozone from Pic du Midi data series: Consequences: Positive radiative forcing, *J. Geophys. Res.*, *99*(D8), 16617–16632, 10.1029/94JD00021.

Martin, R. V., D. J. Jacob, R. M. Yantosca, M. Chin, and P. Ginoux (2003), Global and regional decreases in tropospheric oxidants from photochemical effects of aerosols, *J. Geophys. Res.*, *108*(D3), 4097, doi:10.1029/2002JD002622.

McKeen, S. A., E.-Y. Hsie and S. C. Liu (1991), A study of the dependence of rural ozone on ozone precursors in the eastern United States, *J. Geophys. Res.*, *96*, 15,377–15,394.

Munger, J. W., S.-M. Fan, P. S. Bakwin, M. L. Goulden, A. H. Goldstein, A. S. Colman, S. C. Wofsy (1998), Regional budgets for nitrogen oxides from continental sources: Variations of rates for oxidation and deposition with season and distance from source regions, *J. Geophys. Res.*, *103*(D7), 8355–8368, 10.1029/98JD00168.

Pandis, S. N., Paulson, S. E., Seinfeld, J. H., Flagan, R. C., (1991) Aerosol formation in the photooxidation of isoprene and β-pinene, *Atmos. Environ.*, *25A*, (5/6), 997–1008.

Park, R. J., D. J. Jacob, B. D. Field, R. M. Yantosca, M. Chin (2004), Natural and transboundary pollution influences on sulfate-nitrate-ammonium aerosols in the United States: Implications for policy, *J. Geophys. Res.*, *109*, D15204, doi:10.1029/2003JD004473.

Park, R. J., D. J. Jacob, M. Chin, R. V. Martin (2003), Sources of carbonaceous aerosols over the United States and implications for natural visibility, *J. Geophys. Res.*, *108* (D12), 4355, doi:10.1029/2002JD003190.

Penner, J. E., D. J. Bergmann, J. J. Walton, D. Kinnison, M. J. Prather, D. Rotman, C. Price, K. E. Pickering, S. L. Baughcum (1998), An evaluation of upper troposphere NO_x with two models, *J. Geophys. Res.*, *103*(D17), 22097–22114, 10.1029/98JD01565.

Pincus, R., and M. Baker (1994), Precipitation, solar absorption, and albedo susceptibility in marine boundary layer clouds, *Nature*, *372*, 250–252.

Pope, C.A., (2000), Review: Epidemiological basis for particulate air pollution health standards, *Aerosol Science and Technology*, *32*, 4–14.

Prather, M. J., (1996), Time scales in atmospheric chemistry: Theory, GWPs for CH_4 and CO, and runaway growth, *Geophys. Res. Lett.*, *23*(19), 2597–2600, 10.1029/96GL02371.

Rasch, P. J., M. C. Barth, J. T. Kiehl, S. E. Schwartz, C. M. Benkovitz (2000), A description of the global sulfur cycle and its controlling processes in the National Center for Atmospheric Research Community Climate Model, Version 3, *J. Geophys. Res.*, *105*(D1), 1367–1386, 10.1029/1999JD900777.

Reddy, M. S., O. Boucher (2004), A study of the global cycle of carbonaceous aerosols in the LMDZT general circulation model, *J. Geophys. Res.*, *109*, D14202, doi:10.1029/2003JD004048.

Reeves, C. E., et al. (2002), Potential for photochemical ozone formation in the troposphere over the North Atlantic as derived from aircraft observations during ACSOE, *J. Geophys. Res.*, *107* (D23), 4707.

Roelofs, G.-J., B. Scheeren, J. Heland, H. Ziereis and J. Lelieveld (2003), A model study of ozone in the eastern Mediterranean free troposphere during MINOS (August 2001), *Atmos. Chem. Phys.*, *3*, 1199–1210.

Scheeren, H. A., et al. (2003), The impact of monsoon outflow from India and Southeast Asia in the upper troposphere over the eastern Mediterranean, *Atmos. Chem. Phys.*, *3*, 1589–1608.

Seinfeld, J. and S. Pandis (1998), *Atmospheric chemistry and physics*, John Wiley and Sons, Inc., New York.

Sokolik, I. N., D. M. Winker, G. Bergametti, D. A. Gillette, G. Carmichael, Y. J. Kaufman, L. Gomes, L. Schuetz, J. E. Penner (2001), Introduction to special section: Outstanding problems in quantifying the radiative impacts of mineral dust, *J. Geophys. Res.*, *106*(D16), 18015–18028, 10.1029/2000JD900498.

Stevenson, D. S. et al. (2006), Multi-model ensemble simulations of present-day and near-future tropospheric ozone, *J. Geophys. Res.*, in press.

Stohl, A., A 1-year Lagrangian "climatology" of airstreams in the Northern Hemisphere troposphere and lowermost stratosphere, *J. Geophys. Res.*, *106*(D7), 7263–7280, 10.1029/2000JD900570T.

Tanré, D., Y. J. Kaufman, M. Herman, S. Mattoo (1997), Remote sensing of aerosol properties over oceans using the MODIS/EOS spectral radiances, *J. Geophys. Res.*, *102*(D14), 16971–16988, 10.1029/96JD03437.

Thompson, A. M. Jr., D. J. Jacob, J. R. Scala, W.-K. Tao, D. P. McNamara, J. Simpson (1994), Convective transport over the central United States and its role in regional CO and ozone budgets, *J. Geophys. Res.*, *99*(D9), 18703–18712, 10.1029/94JD01244.

Traub, M., et al. (2003), Chemical characteristics assigned to trajectory clusters during the MINOS campaign, *Atmos. Chem. Phys.*, *3*, 459–468.

Twomey, S. (1974), Pollution and planetary albedo, *Atmos. Environ.*, *8*, 1251–1256.

van Aardenne, J. A., G. R. Carmichael, H. Levy, D. Streets, and L. Hordijk (1999), Anthropogenic NO_x emissions in Asia in the period 1990–2020, *Atmos. Environ.*, *33*, 633–646.

Vingarzan, R. (2004), A review of surface ozone background levels and trends, *Atmos. Environ.*, *38*, 3431–3442.

Wallace, L. (2000), Correlations of personnal exposure to particles with outdoor air measurements: a review of recent studies, *Aerosol Science and Technology*, *32*, 15–25.

West, J. J. and A. Fiore (2005), Management of tropospheric ozone by reducing methane emissions, *Environ. Sci. Technol.*, *39*(13), 4685–4691.

Wild, O., H. Akimoto (2001), Intercontinental transport of ozone and its precursors in a three-dimensional global CTM, *J. Geophys. Res.*, *106*(D21), 27729–27744, 10.1029/2000JD000123.

Wild, O., M. J. Prather (2000), Excitation of the primary tropospheric chemical mode in a global three-dimensional model, *J. Geophys. Res.*, *105*(D20), 24647–24660, 10.1029/2000JD900399.

Zender, C. S., H. Bian, D. Newman (2003), Mineral Dust Entrainment and Deposition (DEAD) model: Description and 1990s dust climatology, *J. Geophys. Res.*, *108* (D14), 4416, doi:10.1029/2002JD002775.

Zender, C. S., R. Miller, and I. Tegen (2004), Quantifying Mineral Dust Mass Budgets: Terminology, Constraints, and Current Estimates, *Eos Trans. AGU*, *85*(48), 509–512.

Chapter 3

Impact of plumes on ozone chemical tendencies

Submitted for publication: Auvray, M., I. Bey, E. Llull, M.G. Schultz, S. Rast (2006), A model investigation of tropospheric ozone chemical tendencies in long-range transported pollution plumes, Journal of Geophysical Research.

Abstract

The impact of continental outflow on the ozone chemical tendencies (e.g. production and loss rates) is quantified in the North Atlantic and Northwest Pacific regions using the GEOS-Chem and the MOZECH global models of chemistry and transport. The ozone tendencies simulated by the global models are compared to box model simulations constrained by observations in different regions and seasons. The impact of different chemical mechanisms and environmental parameters on the ozone tendencies is investigated in a series of sensitivity experiments. The two global models generally capture the seasonal and regional variations of the ozone chemical tendencies. The largest discrepancies are seen in the lower troposphere of the eastern North Atlantic during the ACSOE campaign, and are attributed to differences between chemical schemes and too strong NO_x concentrations in the global models. Plume and background environments are differentiated using criteria based on simulated daily CO concentrations. The continental outflow impacts ozone chemical tendencies over the entire column in North Atlantic and Northwest Pacific at all seasons. According to the models, net ozone production is enhanced by 2 to 6 ppbv/day in the boundary layer and by 1 to 3 ppbv/day in the upper troposphere, whereas the effect of pollution ranges from -1 ppbv/day to $+1$ ppbv/day in the middle troposphere (3–7 km), depending on the model used. The different responses of the two models are associated with the water vapour distribution

with respect to pollution transport processes. In particular, GEOS-Chem tends to transport pollution in a drier sector of cyclones than MOZECH.

3.1 Introduction

In many regions of the world, ozone (O_3) concentrations are close to or even above the thresholds for plant damage or health effects [e.g, *EMEP*, 2004]. Elevated O_3 concentrations are associated with photochemical episodes which were initially thought to be local and regional scale problems. These issues have now to be considered on a hemispheric and even global scale as more and more scientific evidence is showing that transport of pollution can take place over long distances, e.g. across the Atlantic ocean [*Parrish et al.*, 1993; *Fehsenfeld et al.*, 1996; *Collins et al.*, 2000; *Li et al., 2002a*; *Wild and Akimoto*, 2001; *Trickl et al.*, 2003; *Auvray and Bey*, 2005] and the Pacific ocean [*Jaffe et al.*, 1999; 2003; *Bernsten et al.*, 1999; *Yienger et al.*, 2000; *Fiore et al.*, 2002]. An important question is to quantify the relative contributions of long-range transport and of local/regional pollution to the exceedances of air quality standards set by environmental agencies.

Enhanced O_3 concentrations together with elevated carbon monoxide (CO) or nitrogen-containing compounds associated with long-range transport of pollution have been observed in the free troposphere over the North Atlantic in several cases [e.g., *Parrish et al.*, 1993; *Fehsenfeld et al.*, 1996]. Enhanced O_3 concentrations have been also reported at alpine sites [*Huntrieser et al.*, 2005] and in the lower troposphere of Europe [*Stohl and Trickl*, 1999; *Naja et al.*, 2003; *Trickl et al.*, 2003], but there is rarely a significant O_3 increase at surface stations associated with the arrival of such plumes over Europe [*Derwent et al.*, 1998]. *Guerova et al.* [2006] reported, for example, that long-range transport events from North America to Europe in summertime mainly occur during periods of unstable weather conditions and therefore do not coincide, in general, with the highest surface O_3 concentrations which are observed and simulated during stagnant sunny conditions. However, it has been suggested that long-range transported pollution affects substantially the mean levels of O_3 concentrations [e.g. *Brönnimann et al.*, 2000; 2002, *Fiore et al.*, 2002; *Simmonds et al.*, 2004; *Ordóñez et al.*, 2005].

While net photochemical formation of O_3 typically occurs near the source regions of precursor emissions, aircraft observations gathered over oceanic areas like the Northwest Pacific have indicated that it can also take place over remote regions during long-range transport [e.g., *Davis et al.*, 1996, 2003; *Crawford et al.*, 1997; *Olson et al.*, 2001; *DiNunno et al.*, 2003; *Kondo et al.*, 2004; *Wild et al.*, 2004]. Similar results have been reported for the North Atlantic ocean [*Wild et al.*, 1996; *Reeves et al.*, 2002]. It has been postulated that the continental outflow of O_3 and its precursors from the source regions into the remote atmosphere can lead to perturbations of the chemical environment in these regions, thereby affecting the production and loss rates of O_3 and thus influencing its chemical lifetime [e.g. *Schultz et al.*, 1998; *Honrath et al.*, 2004]. *Wild et al.* [2004] suggested that the impact of photochemical processes associated with such export events could have a substantial impact on O_3 levels on a global

scale. Even though O_3 chemical tendencies (e.g. production and loss rates) have been discussed in several case studies with detailed analysis of aircraft observations, the overall contribution of the chemical perturbation due to long-range transport in remote areas to the global O_3 budget remains poorly quantified.

The main objective of this paper is to examine how the O_3 tendencies over remote marine environments is modified by continental outflow. To this end we analysed the characteristics of background and plume conditions over several oceanic regions using two global three-dimensional (3-D) chemistry transport models. Section 3.2 describes the two models and the simulations used in this study. In section 3.3, we examine to what extent the models are capable of reproducing the O_3 production and loss rates resulting from detailed analyses of aircraft observations. We then discuss the discrepancies with respect to some aspects in the chemical mechanisms used in different studies. Section 3.4 first describes our choice of background and plume conditions. The impact of continental pollution outflow from North America into the North Atlantic ocean in spring and summer is then discussed as well as for the other seasons. The Northwest Pacific region is described in section 3.5. Summary and conclusions are provided in section 3.6.

3.2 Model Description and Simulation Set-up

The two three-dimensional models used in this study are the chemistry transport model GEOS-Chem [*Bey et al.*, 2001a] and the chemistry-climate model MOZECH [Rast et al., Sensitivity of a chemistry climate model to changes in emissions and the driving meteorology, manuscript in preparation, henceforth cited as *Rast et al.*, 2006]. A recent inter-comparison between an ensemble of global chemistry transport models has shown that there are still significant differences in the simulated concentrations of trace gases and the global tropospheric budget of O_3, even when the models use similar emission inventories for anthropogenic and biomass burning sources and are run for the same meteorological year [*Stevenson et al.*, 2006]. *Stevenson et al.* [2006] noted that the best agreement with observations is obtained with an average of all the model results. In this study, we choose to employ two global models which include different physical parameterisations, transport algorithms, chemical schemes, and emission inventories. This allows us to explore the sensitivity of our results to different modeling tools and thus enhance the robustness of our results. Both models participated in the study of *Stevenson et al.* [2006] and they represent two rather different members of the ensemble. For example, the MOZECH model tends to have above-average O_3 concentrations. GEOS-Chem on the other hand generally agrees well with the mean model, as well as with the observations, but tends to underestimate O_3 concentrations in the free troposphere of the northern mid-latitudes. In the present work, simulations were performed for the years 1997 and 2000, thereby taking into account variations in emissions and meteorology (GEOS-Chem) or only meteorological variations (MOZECH). In the following we briefly describe the main features of the two models.

3.2.1 GEOS-Chem

The GEOS-Chem model [*Bey et al.*, 2001a], version 7–02 (http://www.as-harvard.edu/chemistry/trop/geos/), is driven by assimilated meteorological fields from the Goddard Earth Observing System (GEOS) of the NASA Global Modeling and Assimilation Office (GMAO). For this study, the model was run in a horizontal resolution of 2° of latitude by 2.5° of longitude. The meteorological fields for the simulation of the years 1997 and 2000 are provided on 26 vertical levels up to 0.1 hPa and on 30 vertical levels up to 0.01 hPa, respectively. Advection and convection are computed every 15 minutes. Advection is computed with a flux form semi-Lagrangian method [*Lin and Rood*, 1996], and convection used the GEOS convective, entertainment and detrainment mass fluxes [*Allen et al.*, 1996a; 1996b]. A full mixing is assumed within the boundary layer. The model transports 24 tracers and includes more than 80 species and 300 chemical reactions based on *Horowitz et al.* [1998] to describe the O_x-NO_x-VOC photochemistry. Heterogeneous reactions on aerosols are taken into account as described in *Jacob* [2000] and *Martin et al.* [2003]. Aerosol fields are provided by the Global Ozone Chemistry Aerosol Radiation and Transport (GOCART) model [*Chin et al.*, 2002]. Photolysis frequencies are calculated with the FAST-J algorithm [*Wild et al.*, 2000].

The inventory of anthropogenic emissions is similar to *Bey at al.* [2001a] except for the replacement of the European emissions with EMEP expert emissions following *Auvray and Bey* [2005]. To improve the emission estimates for specific years, the inventory is scaled using CO_2 emission trends as described in *Bey et al.* [2001a]. NO_x ship emissions follow the EDGAR3.2 database and accounts for 3.1 Tg N/yr as described in *Dentener et al.* [2005]. NO_x anthropogenic sources are spread in the first two levels of the model, and other anthropogenic sources in the first level. Biomass burning emissions are from *Duncan et al.* [2003] with interannual variability being estimated from Along Track Scanning Radiometer (ATSR) firecounts. NO_x emissions from lightning are determined from cloud top height following the parameterization of *Price and Rind* [1992] as implemented by *Wang et al.* [1998a] with vertical profiles from *Pickering et al.* [1998], and account for about 6 Tg N/yr.

Above the tropopause (diagnosed with a 2 K km^{-1} lapse rate), a simplified chemical representation is used, including production and loss of NO_y, CO and formaldehyde. Monthly mean production rates for NO_y are provided by the 2-D model of *Schneider et al.* [2000], along with NO_x/HNO_3 concentration ratios used to partition NO_y. This simplified stratospheric chemistry provides a source of NO_y to the troposphere. Transport of O_3 from the stratosphere is parameterized using the Synoz method (synthetic ozone) proposed by *McLinden et al.* [2000], leading to an O_3 cross-tropopause flux of about 550 Tg/yr.

3.2.2 MOZECH

The "MOZART in ECHAM" (MOZECH) model is a newly developed fully coupled chemistry-climate model on the basis of the ECHAM5 general circulation model [*Roeck-*

ner et al., 2003] and the MOZART2 chemistry scheme including its numerical solver [*Horowitz et al.*, 2003]. For the purpose of this study the model is relaxed towards 6-hourly European Centre for Medium-Range Weather Forecasts (ECMWF) meteorological fields of surface pressure, temperature, vorticity, and divergence with time constants of 24h, 24h, 6h, and 48h, respectively. The resolution is T42L31, corresponding to a horizontal grid of about $2.8^\circ \times 2.8^\circ$ with 31 vertical levels from the surface to 10 hPa. Convection in ECHAM5 is parameterised according to *Tiedtke* [1989] and *Nordeng* [1994], and boundary layer mixing according to Monin-Obukhov [*Roeckner et al.*, 2003]. Further details on the physical and dynamical equations of ECHAM5 can be found in *Roeckner et al.* [2003]. 63 species and 168 reactions are considered to describe the O_x-NO_x-VOC chemistry. Hydrolysis of N_2O_5 on sulfate aerosols is taken into account using climatological fields of sulfate aerosols from MOZART2 [*Horowitz et al.*, 2003]. Photolysis frequencies are computed based on a pre-compiled multidimensional lookup table for zenith angle, total O_3 column, temperature, and surface albedo. An empirical cloud correction is applied as described in *Horowitz et al.* [2003].

Anthropogenic emissions (including those from international ship traffic) are adapted from the model intercomparison experiment described by *Dentener et al.* [2005] and *Stevenson et al.* [2006] and are representative for the year 2000. Biomass burning emissions are prescribed as 5-year mean monthly averages from 1997–2001 following *van der Werf et al.* [2003]. The production of NO_x from lightning is linked to the convective mass flux as described in *Grewe et al.* [2001] and are distributed following a C-shaped vertical profile. The annual source strength of lightning is of 3.3 Tg N/yr.

Stratospheric NO_x, HNO_3, and CO concentrations are supplied from simulations of the 3-D MOZART3 model. These concentrations are fixed at the topmost two model levels (pressures of 30 hPa and lower). At other model levels above the tropopause, the simulated concentrations are relaxed towards these values with a relaxation time of 10 days. Stratospheric O_3 concentrations in MOZECH are prescribed as monthly zonal mean climatologies derived from observations [*Logan*, 1999; *Randel et al.*, 1998]. The net influx of O_3 from the stratosphere, diagnosed as residual term in the global tropospheric O_3 budget, is 660 Tg/yr.

3.3 O_3 Chemical Terms: Model Inter-comparison and Sensitivity Analysis

In this section, we evaluate results from the two 3-D models using trace gas observations and O_3 tendencies from different aircraft field experiments. As direct measurements of the O_3 production and loss rates are not available, we have to rely on box model calculations which are constrained by observed concentrations [e.g. *Davis et al.*, 1996; 2003; *Jacob et al.*, 1996; *Crawford et al.*, 1997; *Jaeglé et al.*, 1998; *Schultz et al.*, 1999; *Reeves et al.*, 2002]. In order to obtain realistic concentrations for species or quantities not directly observed, the box models are typically run in a diurnal steady state mode, i.e. the diurnal cycle of chemical reactions is repeated until a dynamic

equilibrium has been reached. The results from such calculations can then be tested with independent observations such as NO/NO_2 ratio (e.g. *Schultz et al.*, 1999) or OH concentrations (e.g. *Wild et al.*, 2004). While good agreement was reported for some studies, significant discrepancies were found in others, which could not always be reconciled (e.g. *Wild et al.*, 2004). Nevertheless, O_3 production and loss rates obtained from those box models can provide interesting insights on the capability of the global models. Note however that 3-D models are superior to box models if the observed trace gases concentrations are reproduced because they give a complete picture of air mass transport and history.

In the present work, we used observations and box model results provided by several aircraft experiments that were mainly dedicated to the sampling of continental outflow over oceanic regions. These include ACSOE (eastern North Atlantic ocean, April and September 1997, section 3.3.1), EXPORT (continental Europe, summer 2000, section 3.3.2), PEM-West A (North Pacific ocean, fall 1991, section 3.3.3), and TRACE-P (North Pacific ocean, spring 2001, section 3.3.3). We limit the direct comparison of observed and simulated trace gas concentrations to those campaigns for which we performed dedicated model simulations (ACSOE in 1997 and EXPORT in 2000). We then compare photochemical O_3 tendencies derived from various box models constrained by trace gas observations to those obtained in our 3-D models for all campaigns. In addition, we perform a sensitivity study with the photochemical box model chem1d [*Jacob et al.*, 1996; *Jaeglé et al.*, 1998; *Schultz et al.*, 1999] to quantify the uncertainties in O_3 tendencies due to various parameters. This allows us to better interpret differences between the O_3 chemical tendencies estimated by the box models and those calculated in the global models.

3.3.1 Eastern North Atlantic Ocean (ACSOE, Spring and Summer 1997)

The ACSOE aircraft campaign took place in April (three flights) and September (five flights) 1997 to investigate the O_3 photochemistry over the North Atlantic ocean [*Reeves et al.*, 2002; *Penkett et al.*, 2004]. While O_3 net production was generally found to be negative in the marine boundary layer and lower troposphere, *Reeves et al.* [2002] noticed a few cases with a positive net O_3 production (further referred to as netP O_3), which appeared to be associated either with recent ship emissions or with long-range transport of pollution from North America.

Comparison to observed trace gases

The top two rows of Figure 3.1 compare the median vertical profiles of different trace gas concentrations observed during ACSOE in April and September 1997 with the results from the GEOS-Chem and MOZECH models. CO concentrations were only measured in September, when they exhibit an almost height-independent profile and are well reproduced by the models. In the lower troposphere the observed CO levels are

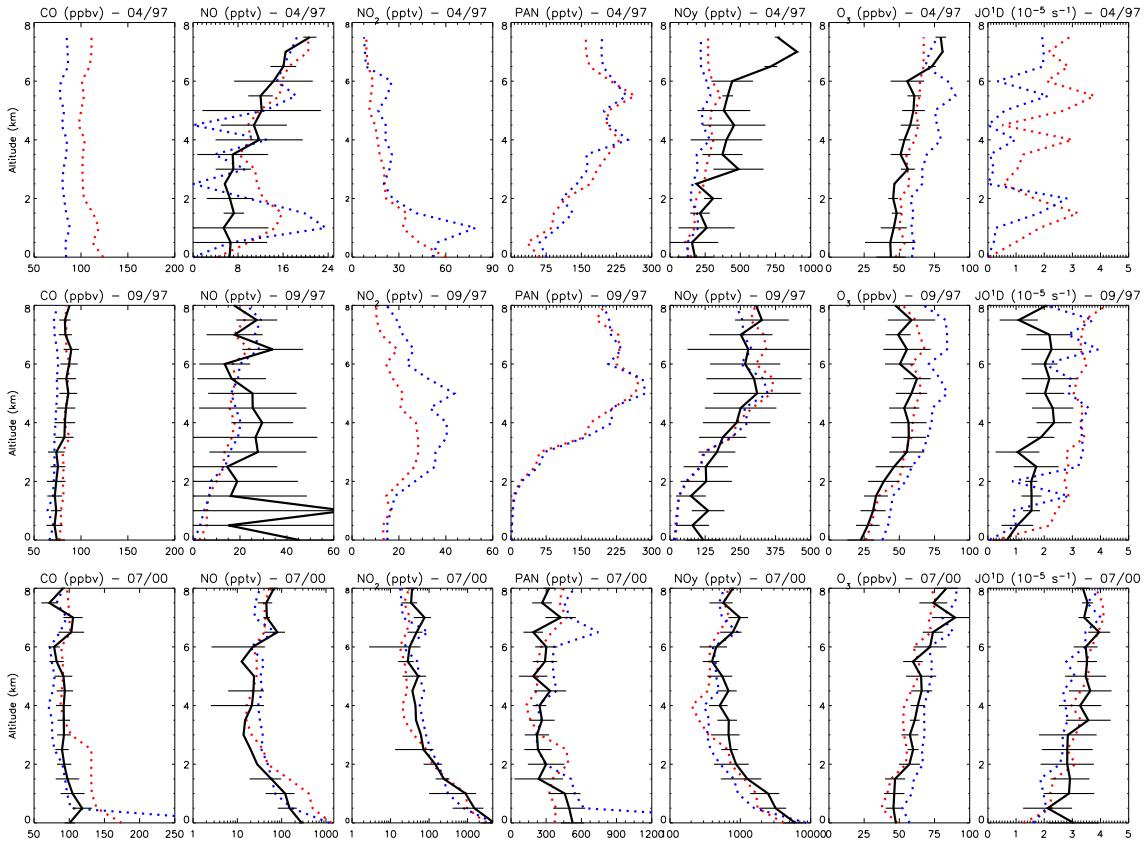

Figure 3.1: Observed (solid line) vertical profiles of the five minute median CO, NO, NO_2, PAN, NO_y, O_3, and J(O^1D) binned over 500 metres for the ACSOE (top two rows) and the EXPORT (bottom row) campaigns. GEOS-Chem results (dotted red line) are sampled along the flight tracks at the time and location of the flights. MOZECH results (dotted blue line) are sampled every five minutes following the flight tracks, using model outputs every three hours. The horizontal bars show the observed standard deviations which reflect the variability found over the course of the three flights in April 1997, five flights in September 1997 and six flights in July-August 2000. CO, NO_2, PAN observations are not available for April 1997 and NO_2, PAN observations are not available for September 1997. For GEOS-Chem and MOZECH, NO_y correspond to the sum of NO_x and PAN (see details in the text, section 3.3.1). Logarithmic scale is used for NO, NO_2 and NO_y for EXPORT.

closer to the MOZECH results, whereas GEOS-Chem performs better in the middle and upper troposphere. MOZECH CO concentrations are always lower than those simulated by GEOS-Chem, which may reflect excessive OH concentrations in MOZECH, and this is more pronounced in April than in September. In April, both models reproduce the NO concentrations in the upper troposphere, while there are some differences at lower altitudes. Below 3 km, GEOS-Chem overestimates NO by about 6 pptv (80 %) while MOZECH exhibits excessive variability in the vertical profile and also tends to overestimate NO concentrations. In contrast, in September, the two models tend to underestimate NO below 5 km. These discrepancies in the lower troposphere may be due to the representation of the NO_x emissions from ships in the global models. As emissions are smoothed out over the model grid boxes, the models tend to overestimate NO_x concentrations in clean regions (i.e. in April), while they tend to underestimate the elevated NO_x concentrations observed in September, which are due to individual ship plumes as reported by *Reeves et al.* [2002]. As measurements of NO_2 and PAN were not made in ACSOE, we can only compare the two models with each other. The simulated PAN concentrations generally agree well, whereas the differences are larger for NO_2. Here, MOZECH always simulates higher NO_2 concentrations than GEOS-Chem, implying higher levels of NO_x and a smaller NO/NO_2 ratio. This is consistent with the higher O_3 concentrations simulated by MOZECH (see below). As described in *Bauguitte [2000]* and *Penkett et al.* [2004], the NO_y observations do not include soluble species (e.g. HNO_3), but consist predominantly of NO_x and PAN. The simulated (NO_x + PAN) vertical profiles of the two models are again rather close to each other, and they generally agree well with the measurements. Exceptions are a significant underestimate of NO_y in the upper troposphere in April, and the underestimate in the boundary layer in September, which could again be explained by local ship emissions. The shape of the vertical O_3 profile is reproduced well by both models, but MOZECH overestimates O_3 by about 15 ppbv (30%) throughout the tropospheric column (except for altitudes above 6 km in April). The photolysis frequency of O_3 ($j(O^1D)$) was only measured in September, and it appears that both models are overestimating $j(O^1D)$ by almost a factor of two during that season. In April, GEOS-Chem and MOZECH O_3 photolysis rates exhibit a large variability below 5 km, which is consistent with the finding of *Reeves et al.* [2002] who derived $j(O^1D)$ from observed $j(NO_2)$.

Comparison to box model O_3 chemical tendencies

Figure 3.2 (a-b) shows the comparison between the O_3 chemical tendencies from photochemical box model calculations reported by *Reeves et al.* [2002] with the 3-D model results for the April ACSOE flights. The box model used in *Reeves et al.* [2002] was constrained by observed temperature, pressure, NO_2 photolysis frequency, and observed concentrations of O_3, NO, H_2O, CO, H_2O_2, and CH_3OOH. CO concentrations were set to 133 ppbv (which is reasonably close to the GEOS-Chem values, but about a factor of two higher than MOZECH), while HCHO and CH_4 were set to 300 pptv and 1800 ppbv, respectively [*Reeves et al.*, 2002]. *Reeves et al.* [2002] found that the O_3 loss rates (median of the three April flights) decrease with altitude (reflecting drier air aloft)

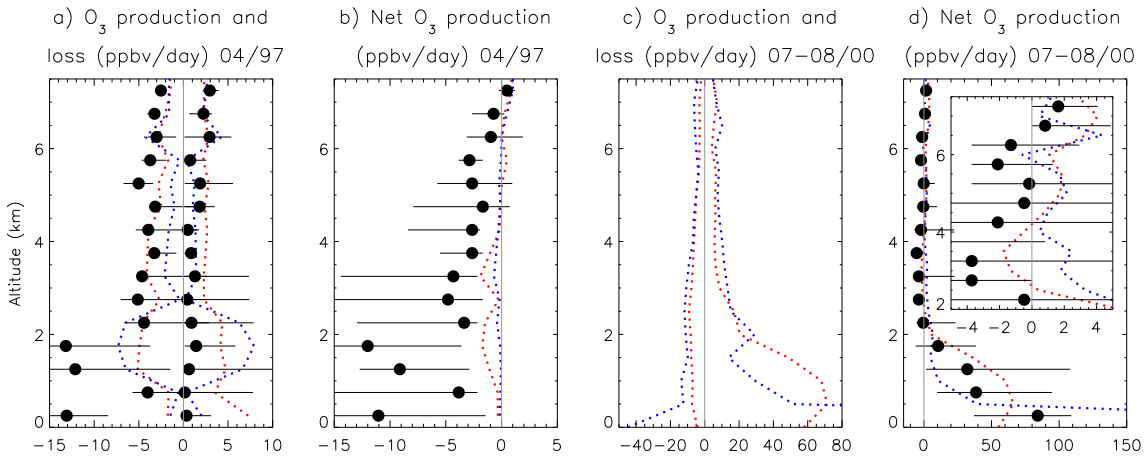

Figure 3.2: Vertical profiles of the median O_3 loss (negative value), production (positive value) rates, and net O_3 production binned over 500 metres altitude for (a-b) the ACSOE flights in April 1997 [*Reeves et al.*, 2002] and (c-d) the EXPORT flights in the summer 2000 [*Reeves et al.*, 2003] (in black). GEOS-Chem results (red dotted line) are sampled along the flight tracks at the time and location of the flights. MOZECH results (blue dotted line) are sampled every five minutes following the flight tracks, using model outputs every three hours. Horizontal bars represent observed 10^{th} and 90^{th} percentile. Units are in ppbv/day.

while O_3 production rates increase with altitude (reflecting higher NO concentrations in the upper troposphere). In their calculation, the crossover from negative to positive netP occurs at about 7 km altitude.

We find substantial differences between the box model results of *Reeves et al.* [2002] and our global model calculations (Figure 3.2a). Above 3 km, MOZECH captures the O_3 production rates rather well, but yields O_3 loss rates which are about a factor of two lower than the box model. In contrast, GEOS-Chem reproduces well the O_3 loss rates between 3 and 5 km altitude, but overestimates the production rates by 20%. In the lower troposphere, both 3-D models exhibit substantially lower loss rates than the box model, but yield higher production rates, partly because the two global models overestimate observed NO. A deeper analysis of the GEOS-Chem and the box model results reveals that discrepancies in the O_3 production rates are due to both higher $NO+HO_2$ and $NO+CH_3O_2$ reaction rates in GEOS-Chem while discrepancies in the O_3 loss rates in the lower troposphere are mainly associated with O_3 photolysis (see Figure 3.1 in the supplementary online material (SOM - section 3.7). As a consequence of these discrepancies, the 3D models both show a much smaller (i.e., less negative) netP O_3 than the box model (Figure 3.2b).

Apart from differences in the trace gas distributions simulated by the various models (see section 3.3.1), there are also a few key reactions, which are parameterised in different ways and can have a significant impact on the results, as further discussed in section 3.3.1 In addition, *Reeves et al.* [2002] do not consider heterogeneous chemistry on aerosols, whereas the chemical schemes of GEOS-Chem and MOZECH include the

uptake of N_2O_5 and washout of HNO_3 and other soluble species. GEOS-Chem also considers the heterogeneous uptake of HO_2, which can have a significant effect on the radical chemistry [*Martin et al.*, 2003; *Tie et al.*, 2005]. Differences in the non-methane hydrocarbon (NMHC) chemistry should be of little relevance, because NMHC concentrations are typically low over the remote ocean.

Sensitivity analysis of O_3 chemical tendencies

In order to better understand the outcome of the comparison between the global and the box models, we performed a series of sensitivity experiments with the box model chem1d [*Jacob et al.*, 1996; *Jaeglé et al.*, 1998; *Schultz et al.*, 1999]. The box model was constrained with outputs from the GEOS-Chem model (temperature, pressure, NO_2 and O_3 photolysis frequencies, and concentrations of O_3, NO_x and related compounds ($NO + NO_2 + NO_3 + 2N_2O_5 + HNO_2 + HNO_4$), HNO_3, H_2O, CO, H_2O_2, CH_3OOH, CH_2O, C_2H_6, C_3H_8, and acetone). We ran two test cases representative of a plume and a clean environment over the North Atlantic ocean in September 1997. The chem1d results are compared with GEOS-Chem in Figure 3.3 (1^{st} row). The agreement is remarkably good, although the O_3 production rates in GEOS-Chem are slightly lower than in the chem1d box model in the polluted case. This could be due to the use of a simplified peroxy radical chemistry in the global model and to the absence of HNO_3 deposition in the box model, the photolysis of HNO_3 being an additional NO_x source.

One experiment was conducted with the chem1d box model to explore the sensitivity of the O_3 chemical tendencies to some key reactions of the chemical mechanism. For example, we used the reaction rates of *DeMore et al.* [1997] and *Sander et al.* [2000] for the reactions O^1D with H_2O and O^1D with N_2 (used in *Reeves et al.*, [2002] and also in MOZECH) instead of those from *Dunlea and Ravishankara* [2004] and *Ravishankara et al.* [2002] (used in GEOS-Chem). We find that O_3 production and loss change by about 9% and 19%, respectively, in average over the column (Figure 3.3, 2^{nd} row), indicating the importance of using similar reaction rates when interpreting differences between model results.

Additional tests were performed with the chem1d box model to investigate the sensitivity of O_3 chemical tendencies to various parameters. The parameters we explored either differ between the 3-D model results and the inputs used in the box model calculations by *Reeves et al.* [2002] (see section 3.3.1) or differ between the two global models and between polluted and background environment as discussed below (see section 3.4). A decrease of a factor 2 in the photolysis rate $j(O^1D)$, corresponding to the discrepancy between observed and simulated values, reduces the loss and production rates by about 35% and 23%, respectively, which tends to increase the netP O_3 (Figure 3.3, 3^{rd} row). A similar effect is obtained when the water vapour concentration is decreased by a factor 2 (Figure 3.3, 4^{th} row). As will be shown below, water vapour concentrations in polluted air masses are distinctly different between the two global models. If the NO_x concentrations are increased by a factor 2 (see for instance differences between observed and simulated NO_x during ACSOE for September 1997), the O_3 loss rates remain almost unaffected, whereas the production rates are enhanced

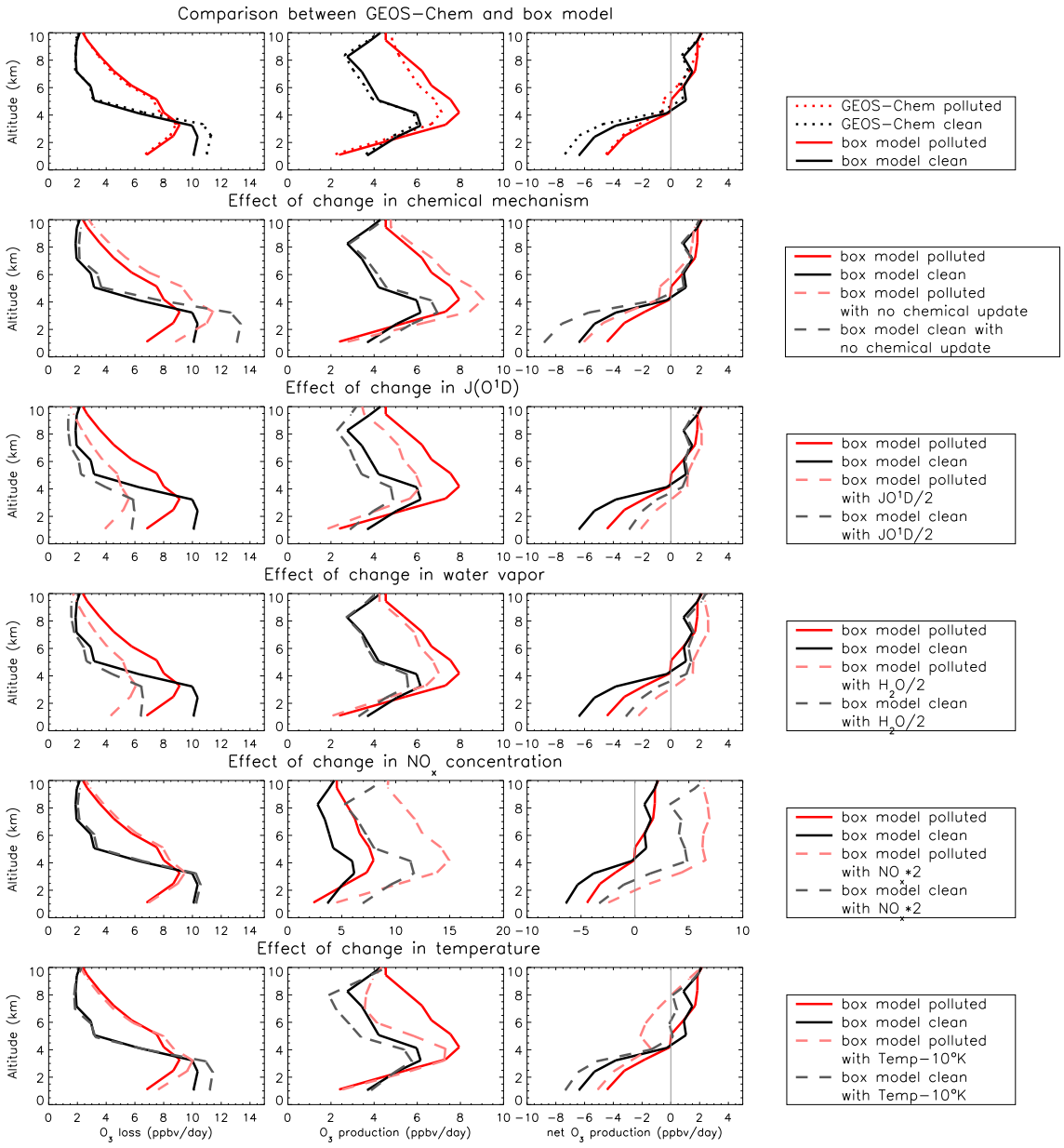

Figure 3.3: Top row: vertical profiles of O_3 loss, O_3 production and net O_3 production (ppbv/day) as calculated by chem1d (full line) and GEOS-Chem (dotted line) for a polluted (red line) and clean case (black line). Subsequent rows: different tests are shown to explore the sensitivity of chemical tendencies to various parameters (dashed lines).

almost linearly, increasing thus the netP O_3 by a similar factor (Figure 3.3, 5^{th} row). Finally, a decrease of the temperature by 10 K over the whole tropospheric column, corresponding to the maximum difference between the background and polluted environments found in GEOS-Chem (see section 3.4) was tested. This leads to a column average change of about 5% and -9% for O_3 loss and production rates, respectively, thus causing a decrease of the netP O_3 (Figure 3.3, 6^{th} row).

3.3.2 Continental Europe (EXPORT, Summer 2000)

The EXPORT campaign took place in July and August 2000 over central and eastern Europe to investigate the fate of the European pollution [e.g., *Purvis et al.*, 2003]. Median profiles of observed CO, NO, NO_2, PAN, NO_y, and O_3 concentrations as well as J(O^1D) photolysis frequencies [*Brough et al.*, 2003; *Gerbig et al.*, 1999] are shown in the bottom row of Figure 3.1 for the six flights of the C-130 British aircraft. Much higher levels of primary pollutants are typically observed in the boundary layer compared to the measurements of the ACSOE campaigns, reflecting the proximity of sources. The 3-D models are able to reproduce the profile shapes of all components rather well. However, neither models agree well with observation in the boundary layer, and a more careful quantitative analysis reveals differences of up to a factor of four for boundary layer NO concentrations. MOZECH tends to yield lower NO and CO concentrations in the boundary layer than GEOS-Chem, but it shows rather high levels of precursors in the lowest model layer, which likely reflects differences in the schemes used for boundary layer mixing in the two models. The observed vertical O_3 profile resembles that of the April 1997 ACSOE campaign and falls between the results from the two models. Here GEOS-Chem tends to underestimate O_3 by about 10 ppbv especially in the middle troposphere while it is the opposite for MOZECH. The j(O^1D) profile is well represented by both models with maximum errors of about 20%.

The vertical profile of the net O_3 production rates is qualitatively similar between the box model of *Reeves et al.* [2003] and the two 3-D models (Figure 3.2d). Below 2 km altitude, the netP O_3 is much higher than in the oceanic boundary layer. Except for the lowest model layer, MOZECH generally yields lower netP O_3 than the box model, whereas GEOS-Chem exhibits higher values. The shape of the three netP O_3 profiles remains rather similar above 2 km, but the two 3D models predict a neutral to slightly positive net O_3 tendency, while the median box model results show an O_3 loss of up to 5 ppbv/day above 4 km altitude. O_3 production and loss rates were not reported individually by *Reeves et al.* [2003]. The 3-D models agree reasonably well with each other in the free troposphere while they differ by up to a factor 2 in the boundary layer and especially at the surface (Figure 3.2c).

3.3.3 North Pacific Ocean (Pem-West A, Summer/Fall 1991 and TRACE-P, Spring 2001)

The PEM-West A and TRACE-P campaigns took place over the North Pacific rim in fall 1991 and spring 2001, respectively. Both campaigns reveal that the region north of 20°N is highly impacted by outflow of anthropogenic pollution from East Asia especially in spring when the outflow is at a maximum, while the southern latitudes are more influenced by tropical/equatorial air masses [e.g., *Davis et al.*, 1996; *Crawford et al.*, 1997; *Jacob et al.*, 2003]. As we do not have detailed output from the 3-D models available for the years of the PEM-West A and TRACE-P campaigns, we restrict the evaluation of our results for the North Pacific to a comparison of simulated O_3 production and loss terms and netP O_3 with results from *Davis et al.*, [1996; 2003] (note that we used in fact results from an updated version of the box model which include a newer radiative transfer code and chemical scheme [*J. Crawford*, personal communication, 2005]). Global model results are presented for the years 1997 and 2000. Because of the different meteorological conditions and the changes in precursor emissions (and thus outflow concentrations), we do no expect perfect agreement between the box model and the two global models, but the profile shape and the magnitude of the terms can nevertheless provide insight into potential model biases. More detailed evaluations of GEOS-Chem over the North Pacific ocean are reported elsewhere [*Bey et al.*, 2001b; *Liu et al.*, 2002; *Heald et al.*, 2003; *Hudman et al.*, 2004; *Heald et al.*, 2004]. Generally, GEOS-Chem reproduces well the observed latitudinal and vertical gradients associated with continental outflow onto the North Pacific [*Bey et al.*, 2001b, *Hudman et al.*, 2004] but the stratospheric contribution to O_3 in the free troposphere appears to be underestimated in spring over the North Pacific [*Hudman et al.*, 2004].

Figure 3.4 shows that the 3-D models can reproduce many features of the vertical profiles of the O_3 tendencies for the two campaigns. The box model (as well as the 3-D models) calculates higher production rates in the northern part than in the southern part of the regions, indicating a stronger influence of continental outflow north of 20°N especially in spring. Both the production and loss rates appear to be higher during TRACE-P than during PEM-West A, especially in the boundary layer, reflecting the increasing photochemical activity in spring (as well as changes in O_3 precursor emissions over a decade, at least in the box model). Of particular interest is the small positive netP O_3, which is calculated by the box model over the entire column in the region and season more strongly affected by the continental outflow (e.g. in spring north of 25°N) [*Crawford et al.*, 1997; *Davis et al.*, 2003]. This is relatively well reproduced by GEOS-Chem. MOZECH however tends to have stronger O_3 loss rates over the Pacific that are likely associated with higher O_3 concentrations, and this leads to net O_3 destruction in that particular case.

3.3.4 Summary of the Model Intercomparison

The two global models generally capture the seasonal and regional variations of O_3 chemical tendencies derived from different box models constrained with observations.

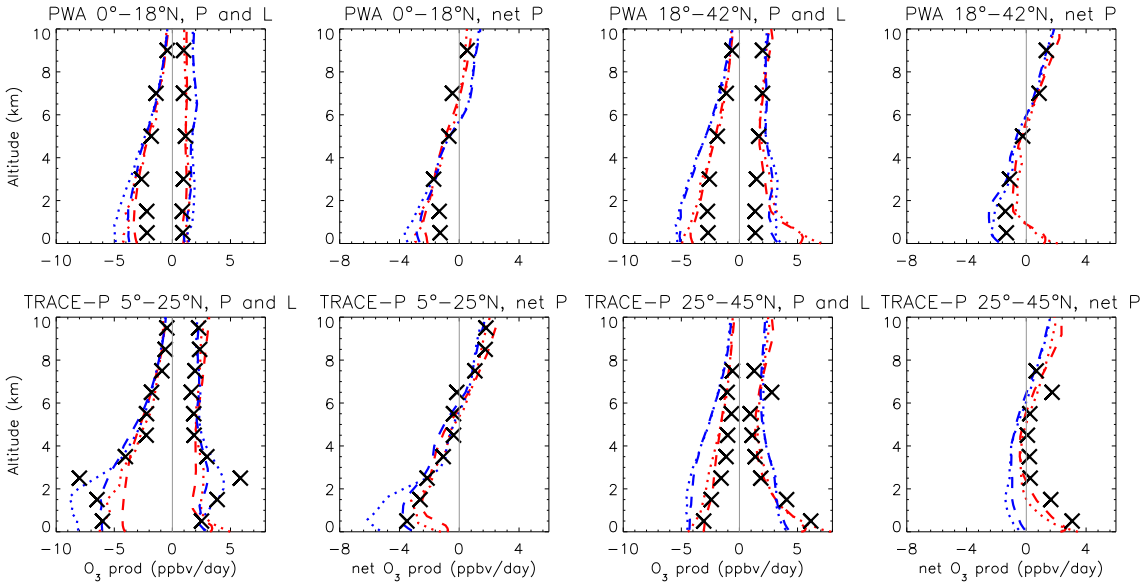

Figure 3.4: Vertical profiles of O_3 production and loss rate and net O_3 production rate in ppbv/day for the PEM-WEST A (first row) and TRACE-P (second row) campaigns. Black crosses : box model calculations for PEM-WEST A (PWA) and TRACE-P (J. Crawford, personal communication, 2005). Colored lines: GEOS-Chem (red) and MOZECH (blue) O_3 tendencies averaged over the southern (0-18°N) and northern (18-42°N) parts of the PEM-WEST A region (September-October) and over the southern (5-25°N) and northern (25-45°N) parts of the TRACE-P region (March-April). Model results are shown for two different meteorological years, 1997 (dotted lines) and 2000 (dashed lines).

Vertical profiles of the chemical tendencies are also well reproduced. In particular, over the oceans, global and box models find a shift from negative netP O_3 in the lower troposphere to positive netP O_3 in the middle/upper troposphere, even though the shift may occur at slightly different altitudes. Note, however, that a quantitative agreement between the global models and the box model could not always be reached. The largest discrepancies are seen in the lower troposphere of the eastern North Atlantic during the ACSOE campaign. We suggest that these discrepancies are mainly due to differences between i) the chemical schemes used in the models (as discussed in section 3.3.1) and ii) the NO_x concentrations observed during the campaign (and thus used in the box model) and those simulated in the global models.

3.4 O_3 Chemical Terms in Polluted and Background Environment Over the North Atlantic

This section examines how plumes transported over the North Atlantic ocean affect O_3 tendencies in the free troposphere. We differentiate between the polluted environment (PE) and the background environment (BE) using daily averaged CO concentrations of ocean grid boxes within the North Atlantic ocean (see region in Figure 3.5). CO is emitted by incomplete combustion and is thus representative of both anthropogenic and biomass burning pollution. With a lifetime of about 2 months, CO is a good tracer of long-range transported plumes of various origins. BE is defined on each model level as the subset of grid box values for which the daily CO concentrations are lower than the regional monthly median CO concentration. PE is defined as the subset of grid boxes in the same region for which daily CO concentrations exceed the regional monthly median CO concentration plus one standard deviation. The choice of these criteria is somewhat arbitrary. However, sensitivity studies using different criteria (e.g. BE restricted to all grid box values for which CO is smaller than the median minus one standard deviation) yielded only little changes in the results which are negligible compared to the model uncertainties and the differences between the two models. The BE and PE statistics are computed separately for the two models. As the plumes are expected to chemically evolved as they are travelling, we first examined how the chemical tendencies differ between PE and BE in different longitudinal slices (60°W, 40°W, and 20°W) along the north eastward path followed by most of the pollution plumes exported from the North American continent [e.g. *Trickl et al.*, 2003] (Figure 3.5). This test showed that considering an average over the entire oceanic region (rather than examining individual slices) also provides a reasonable picture of the O_3 tendencies and chemical behaviors in the two environments (see Figures 3.10 and 3.11 in the SOM). We thus discuss the seasonal variations of PE versus BE using various diagnosed quantities averaged over the entire oceanic region.

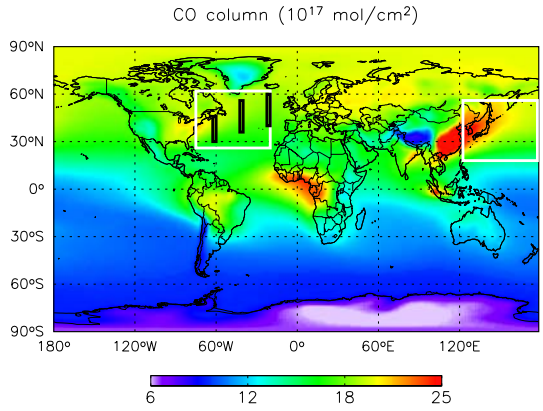

Figure 3.5: Geographical locations of the study regions described in this paper superimposed onto the annual mean GEOS-Chem CO column (10^{17} mole/cm^2) integrated from the surface up to 180 mbar. North Atlantic region: 26–62°N, 75–20°W. Northwest Pacific region: 18–56°N, 122.5–177.5°E. The three black lines over the North Atlantic ocean show the locations of the slices examined in section 3.4.

3.4.1 Spring

Figure 3.6a shows vertical profiles of CO, NO_x, and O_3 concentrations in April 1997 for BE and PE conditions averaged over the North Atlantic area (see Figure 3.5 for the region and note that a land mask is applied so that only oceanic boxes are considered). As previously mentioned (section 3.3), there are some substantial differences in the PE and BE trace gas concentrations between the two models. CO concentrations are in general lower in MOZECH than in GEOS-Chem while in contrast, MOZECH predicts in general higher O_3 concentrations than GEOS-Chem. The BE NO_x concentrations in the upper troposphere (above 8 km) are larger in MOZECH than in GEOS-Chem. As the lightning sources in GEOS-Chem are twice that in MOZECH, this is most probably due to different parameterisations used for representing the stratospheric flux of NO_y species (see section 3.2).

Despite these differences, similar differences in the CO concentrations between the two environments (further referred to as $\Delta CO = CO_{PE}$-CO_{BE}) are seen for both models over the entire column. This mainly reflects the various pathways which contribute to pollution export out of the U.S. boundary layer. (Note that pollution exported from the Asian continent is relatively well mixed over the North Atlantic, therefore its contribution likely falls in the BE rather than in the PE.) Major pathways for North American pollution export are associated with mid-latitude cyclones and in particular i) rising air masses ahead of cold fronts (warm conveyor belt, WCB) which transport pollution at a large altitude range and ii) low level air stream behind cold fronts (post cold front, PCF) [e.g. *Stohl and Trickl*, 1999; *Cooper et al.*, 2001, 2002a, 2002b; *Stohl*, 2001; *Li et al.*, 2002a; *Trickl et al.*, 2003]. Transport in the cyclones occurs all year round, but is particularly important in spring, fall and winter [*Stohl*, 2001].

ΔO_3 and ΔNO_x are positive in the lower and middle troposphere. ΔO_3 (for the two

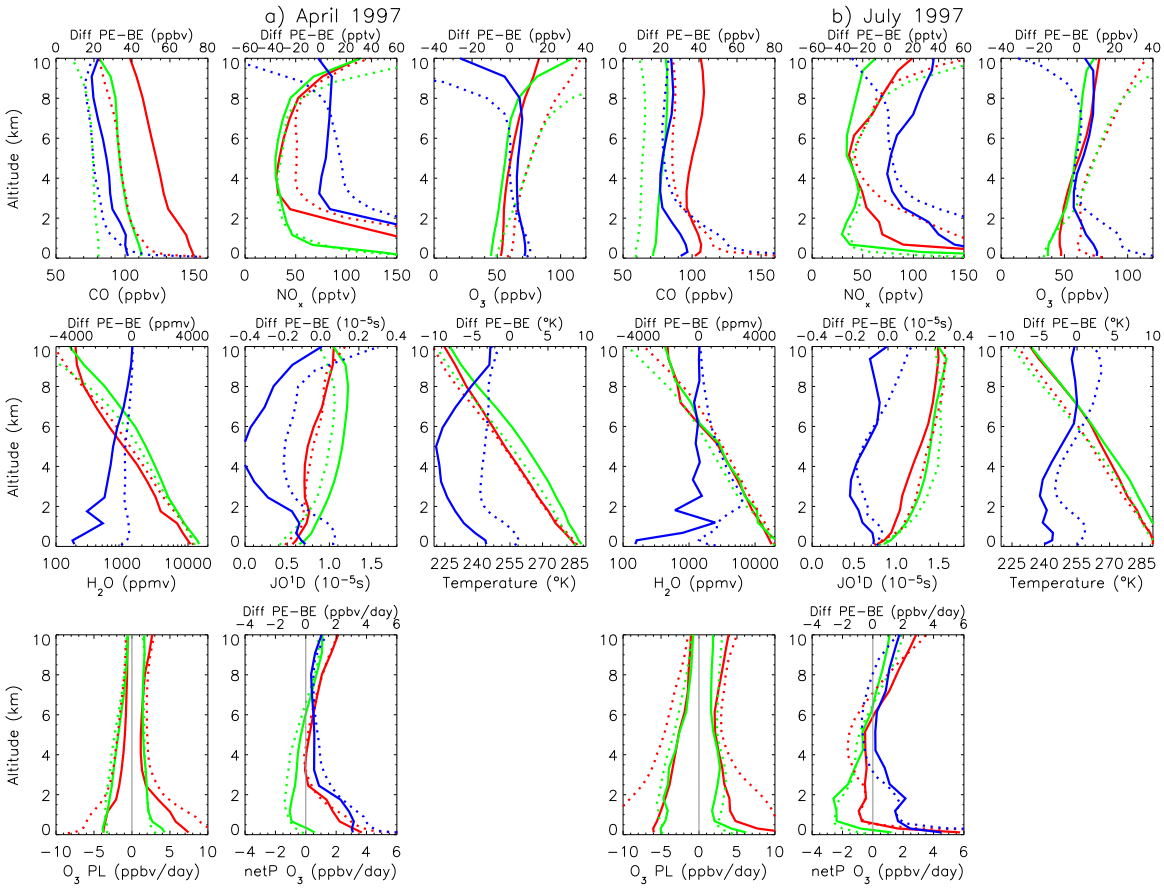

Figure 3.6: Simulated vertical profiles of CO (ppbv), NO_x (pptv), O_3 (ppbv), H_2O (ppmv), O_3 photolysis rate (10^{-5}s), temperature (K), and O_3 chemical tendencies (ppbv/day), for April (left 8 panels) and July (right 8 panels) 1997 over the North Atlantic ocean. Green line: background environment (BE). Red line: plume environment (PE) (definitions in the text). Blue line: difference between the plume and the background environments (x-axis for the difference between the two environments is given at the top of each panel). Full line: GEOS-Chem. Dotted line: MOZECH.

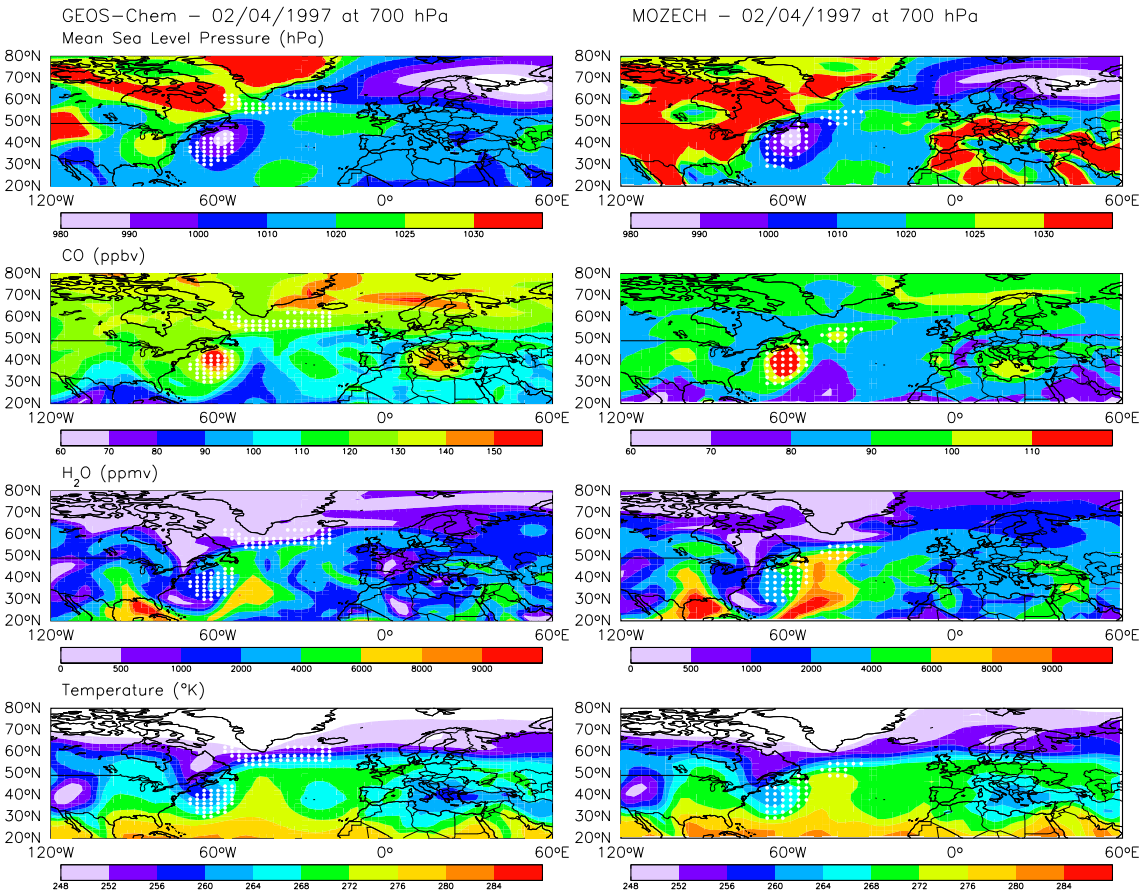

Figure 3.7: Mean sea level surface pressure (hPa), CO concentrations (ppbv), H_2O concentrations (ppmv) and temperature (°K) at 700 hPa for the 2^{nd} of April 1997 simulated with GEOS-Chem (first column) and MOZECH (second column). White dots indicate the grid boxes identified as plumes (as defined in section 3.4) at 700 hPa. Note that the scales are different for CO.

models above 6 km) and ΔNO_x (for MOZECH above 8 km) become negative, reflecting an increase in stratospheric contribution with altitude. Stratospheric intrusions are generally associated with low CO concentrations and are therefore included in the BE class. We find an O_3 production efficiency per unit CO decomposed ($\Delta O_3/\Delta CO$) of about 0.22 and 0.25 ppbv/ppbv near the surface at 60°W, in GEOS-Chem and MOZECH respectively. This is in good agreement with the value given by *Parrish et al.* [1998] for Sable Island in spring (0.19).

Figure 3.6a also shows the vertical profile of water vapour concentrations, temperature and O_3 photolysis rates in BE and PE. GEOS-Chem predicts that PE is characterized by drier conditions than the surrounding background while in MOZECH, PE shows higher or similar water vapour levels than BE. This is especially seen at 60°W close to the region of export (Figure 3.10 of the SOM). A detailed analysis of daily scenes of surface pressure, water vapour, temperature fields, and plume location indicates that the two models tend to simulate similar transport episode occurrence and compare

rather well in terms of plume locations, as illustrated in Figure 3.7. In spring these episodes are frequently associated with transient cyclones, as expected. We find however that GEOS-Chem tends to transport the pollution in a drier sector of the cyclones, in comparison to MOZECH (Figure 3.7). These significantly different behaviors of the two models may reflect the use of different advection, convection and boundary layer mixing schemes in the two models with some substantial consequences on the pollution re-distribution with respect to export processes. However this also may be related to the way water vapour transport is taken into account in the two models. While GEOS-Chem only interpolates between assimilated H_2O fields (updated every 6 hours), the GCM MOZECH includes a full parameterisation of the hydrological cycle and advects water with the same routine as the chemical tracers. Both models indicate that PE is colder than BE, but the difference in temperature between the two environments is much larger in GEOS-Chem (up to 10 K) than in MOZECH (up to 5 K). Both models also predict enhanced presence of clouds in PE (not shown), which reduces the $j(O^1D)$ in PE by up to 30% and 20% in GEOS-Chem and MOZECH, respectively.

The differences in terms of the respective distributions of water vapour and trace gases have important implications for the O_3 chemical tendencies. O_3 loss is higher in PE than in BE in the boundary layer in MOZECH. This reflects higher O_3 concentrations and slightly higher O_3 photolysis rates in PE. On the contrary, in GEOS-Chem, O_3 loss is lower in PE than in BE throughout the column, as the effect of enhanced O_3 in PE is counter-balanced by the lower water vapour concentrations, temperature and O_3 photolysis rates in PE (see also discussion in section 3.3.1 and Figure 3.3). In both model, O_3 production is enhanced in PE because of higher NO_x concentrations.

Despite these different behaviors, both models predict a positive ΔnetP O_3 over the entire column, indicating the strong impact of long-range transport on chemical tendencies. The ΔnetP O_3 reaches about 2–3 ppbv/day. A positive ΔnetP O_3 is more clearly seen in the boundary layer and in the upper troposphere where the ΔNO_x is higher.

As a consequence, the O_3 lifetime (i.e. the ratio of O_3 mass divided by O_3 loss) is affected by long-range transport in different ways in the two models. MOZECH predicts a small decrease of O_3 lifetime in PE (of 6 days on seasonal and regional average), while GEOS-Chem estimates an increase of 10 days on seasonal and regional average (27 days in the BE against 37 days in the PE). The largest increase in O_3 lifetime in GEOS-Chem is found in the middle and upper troposphere (38 days in BE against 62 days in PE), where O_3 has the greater impact on radiative budget.

3.4.2 Summertime and Other Seasons

Figure 3.6b shows the impact of long-range transport on O_3 chemical tendencies over the North Atlantic in summer. The impact of pollution export is also seen over the entire column as in spring. Pollution export out off the North American boundary layer in summer is governed by i) cyclones (although they are less frequent in that season [*Stohl*, 2001]), (ii) low level zonal flows occurring between the well established Azores

high and transient cyclones [e.g. *Guerova et al.*, 2006], and (iii) deep convection, which occurs predominantly over central and south-eastern U.S. and injects air directly at high altitudes (8 km and above) [e.g. *Thompson et al.*, 1994; *Horowitz et al.*, 1998; *Li et al.* 2002a; 2005]. The large enhancement seen in ΔCO in the lowest 3 km likely reflects these low level outflow events while the slight "bump" seen in ΔCO at around 8 km (especially at 60°W, see Figure 3.11 of the SOM) is likely associated with deep convection. Effect of deep convection is more clearly seen in the ΔNO_x profiles (especially in GEOS-Chem) and is consistent with the findings of *Choi et al.* [2005] who reported evidence for simultaneous enhancements of NO_x and CO over the western North Atlantic ocean associated with convective transport and lightning. Sensitivity tests without lightning performed with GEOS-Chem indicated that lightning NOx contribute more importantly to PE than BE. This is also true in MOZECH but to a lesser extent, as the global lightning NO_x emissions are lower by a factor of two than in GEOS-Chem.

Similarly to what was found for the spring season, the two models predict different patterns in BE and PE, especially in the ΔNO_x vertical profiles. In addition to the possible reasons discussed in section 3.4.2, differences in the parameterisation of lightning sources could explain some of the differences seen in the PE and BE NO_x in the upper troposphere. In addition, the meteorological winds used in GEOS-Chem in the present work may suffer from excessive deep convection over the Caribbean and western North Atlantic [*Li et al.*, 2002b].

GEOS-Chem predicts an O_3 production efficiency per unit CO decomposed ($\Delta O_3/\Delta$CO) of about 0.25 ppbv/ppbv at the surface at 60°W, which is comparable to the value of *Parrish et al.* [1998] at Sable Island in July (0.27) while MOZECH tends to overestimate this value (0.41).

Substantial differences are also found between the water vapour profiles of the two models. As indicated in section 3.4.1, GEOS-Chem predicts drier air masses in PE (although this effect is limited to the first kilometer) while MOZECH predicts enhanced water vapour in PE. Figure 3.12 of the SOM illustrates an event of low level transport occurring at the periphery of the Azores High. This event is clearly seen in the two models, however the plumes tend to be located in more humid air masses in the case of MOZECH.

Again, these differences in water vapour concentrations largely drive the differences in ΔnetP O_3 found between the two models. Because of the larger O_3 concentrations and water vapour levels in PE, MOZECH predicts a much higher O_3 loss in PE than in BE. This outweighs the enhanced O_3 production in PE (associated with elevated NO_x concentrations), inducing a negative ΔnetP O_3 in the middle troposphere. In contrast, the O_3 loss rates in PE and BE are similar in GEOS-Chem (as the increase in O_3 concentrations is balanced by drier and colder air masses in plumes), and the increase in O_3 production associated with the ΔNO_x induces a positive ΔnetP O_3 over the entire column. The ΔnetP O_3 is at a maximum in the boundary layer and reaches up to 2–6 ppbv/day depending on the model.

Finally, Figure 3.8 (first row) shows the netP O_3 for PE and BE for all seasons

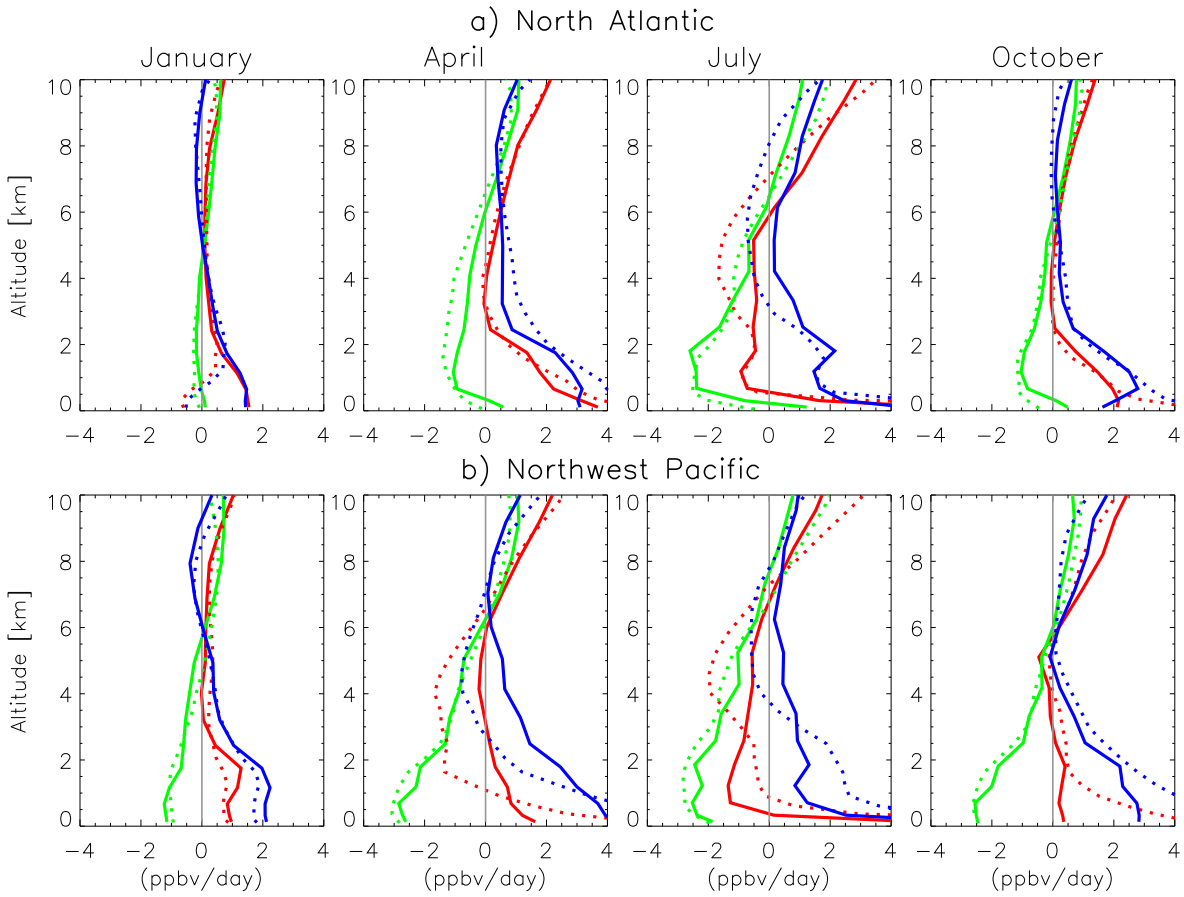

Figure 3.8: Simulated vertical profiles of net O_3 production (ppbv/day), for January, April, July, and October 1997 over the North Atlantic ocean and the Northwest Pacific ocean. Green line: background environment. Red line: plume environment. Blue line: difference between the plume and the background environment (x-axis for the difference between the two environments is given at the top of each figure). Full line: GEOS-Chem. Dotted line: MOZECH.

over the North Atlantic. The ΔnetP O_3 in fall resembles that in spring and only little additional O_3 formation is seen in winter, as expected.

3.5 Chemical Terms in the Northwest Pacific Region

The ΔnetP O_3 over the Northwest Pacific is shown in Figure 3.8 (second row). Continental outflow from Asia towards the Pacific ocean occurs all year round with a maximum in spring [*Liu et al.*, 2003; *Liang et al.*, 2004]. Similarly to the North Atlantic, mid-latitude cyclones [*Carmichael et al.*, 1998; *Yienger et al.*, 2000; *Stohl*, 2001; *Hannan et al.*, 2003] and convection [*Folkins et al.*, 1997; *Newell et al.*, 1997; *Bey et al.*, 2001b] are the two main mechanisms for export over the Pacific ocean. The outflow is especially strong in spring as biomass burning pollution from Southeast Asia adds to the anthropogenic pollution and transport is most vigorous. The Northwest Pacific

exhibits similar patterns as the North Atlantic for the key species concentrations (see for example NO_x concentrations in Figure 3.13 in the SOM) and for the ΔNetP O_3 (Figure 3.8), except that the ΔNetP O_3 is in general slightly higher over the Pacific. As before, the two models differ. GEOS-Chem predicts positive ΔnetP O_3 (up to 4 ppbv/day) over the entire column in both spring and summer, while MOZECH finds large positive ΔnetP O_3 up to 6 ppbv/day in the boundary layer but a negative value of 1 ppbv/day in the middle troposphere. As discussed above, these differences between the two models are likely related to the relative distributions of water vapour and trace gases in plumes. MOZECH predicts a positive ΔH_2O in spring, while GEOS-Chem predicts drier air masses in polluted environments (Figure 3.13 of the SOM).

3.6 Conclusion

This paper quantifies the perturbation in O_3 chemical tendencies associated with continental outflow over the North Atlantic and Northwest Pacific oceans as seen in two global models, namely GEOS-Chem and MOZECH. The global models are first evaluated by comparing their results to observations-derived O_3 production and loss rates provided by several box models in various environments. Thereafter, the impact of continental pollution outflow on the O_3 chemical production and loss terms over oceanic regions were investigated using CO concentration statistics as an indicator of plume locations. The two environments (i.e. polluted and background) were characterized in the two models in terms of tracer concentrations, water vapour content, temperature, and O_3 tendencies over the North Atlantic and the Northwest Pacific at different seasons.

Some substantial differences were found between the box model of *Reeves et al.* [2002] and the global models (especially over the eastern Atlantic ocean), and between the two global models. A sensitivity analysis suggests that these discrepancies mainly result from different reaction rates used, whereas an analysis of individual episodes also suggests an important impact of the water vapour transport and distribution. Both models generally reproduce the seasonal and regional variations of O_3 chemical tendencies. For example, they capture the shift from negative to positive netP O_3 reported in the middle/upper troposphere in most of the cases and GEOS-Chem also reproduces the positive netP O_3 calculated in the entire column over the Pacific ocean in spring associated with high continental outflow of both anthropogenic and biomass burning. MOZECH generally tends to have stronger O_3 loss rates than GEOS-Chem, and this leads to a decrease of the netP O_3 in the middle troposphere over the Northern Pacific in contrast to the photochemical box model results. Additional observation-based O_3 tendencies (and in particular those of the individual chemical pathways) would be useful to better evaluate global O_3-related chemical tendencies.

The impact of long-range transported plumes on the O_3 chemical tendencies is seen over the entire tropospheric column in both regions and in all seasons. GEOS-Chem predicts an enhancement of the netP O_3 in plumes over the entire column, which reaches a maximum of 3–4 ppbv/day in the boundary layer and up to 2 ppbv/day in

the upper troposphere. MOZECH predicts in general a larger effect (up to 6 ppbv/day) in the boundary layer. In the middle troposphere netP O_3 in MOZECH is reduced in the plume environment. Note however that the apparent agreement of the two models in the prediction of a positive ΔnetP O_3 may reflect, to some extent, the effect of compensating processes. For example, the positive ΔnetP O_3 in MOZECH mainly results from enhanced NO_x concentrations in PE (which increase O_3 production and thus netP O_3 in PE), while in GEOS-Chem, this mainly results from decreased water vapour and temperature in PE (which both increase netP O_3 in PE, see also discussion in section 3.3.1 and Figure 3.3).

These differences between the polluted and background environments reflect changes in various processes which contribute to O_3 photochemistry. In particular, O_3 production is enhanced when NO_x concentrations are higher, and O_3 loss will be reduced (enhanced) if water vapour is reduced (enhanced) in the plumes. Differences in the water vapour concentration fields in the two models with respect to the transport processes lead to significant differences in the photochemical tendencies. For example, over the North Atlantic in spring, GEOS-Chem tends to transport the pollution in a drier sector of the cyclones than MOZECH. We suggest that these discrepancies reflect differences between the two models in transport schemes (e.g., boundary layer mixing, convective mixing, advection) and in water vapour transport. Differences between the two models are also caused by the representation of lightning. The differing water vapour and NO_x distributions in the two models result in different O_3 lifetime in background and polluted environments. At that stage, further investigation is needed to quantify the chemical tendencies in individual long-range transport events. This could be based for example on observations gathered during Lagrangian aircraft experiments such as those performed in the frame of the International Consortium for Atmospheric Research on Transport and Transformation (ICARTT) program.

Results were discussed in detail for the year 1997 but similar results are found for the year 2000 (see Figures 3.14 to 3.16 in the SOM). *Parrish et al.* [2004] suggested that the chemical environment over the North Pacific changed significantly over the last 20 years and is now characterized by a less efficient O_3 destruction. Further studies are needed to quantify the change in netP O_3 due to the changes in anthropogenic emissions and to quantify the impacts of climate change (e.g. changes in water vapour levels and temperature).

Our criterion to determine the spatial and temporal distribution of plumes is based on elevated CO concentrations, which can be indicative of anthropogenic or biomass burning events. It would be interesting to investigate whether the photochemical perturbation caused by plumes associated with biomass pollution differs from those with a more anthropogenic signature. Finally, the work presented here should be extended to also consider the impact of aerosols on the O_3 chemical tendencies. For example, *Price et al.* [2004] have shown that long-range transport events can be associated with large aerosol loadings thus reducing the UV radiation and inducing a negative O_3/CO ratio in some cases. In the simulations used in our work, aerosols were only accounted for on a climatological basis, i.e. they were not transported along with the trace gases. Note also that, because aerosols are highly soluble, a better understanding of the discrep-

ancies in terms of water vapour content in the plumes between the two models would be especially crucial to ensure a quantitative simulation of the export and subsequent long-range transport of aerosols.

Acknowledgements

The GEOS-Chem model is managed by the Atmospheric Chemistry Modeling Group at Harvard University with support from the NASA Atmospheric Chemistry Modeling and Analysis Program. IB and MA wish to thank Claires Reeves for providing us with valuable information about her work and James Crawford for sending us updated box model results. IB and MA are grateful to Johannes Staehelin for commenting on an earlier version of that work conducted by Eric Llull and wish to thank Daniel Jacob for helpful discussions. SR and MGS acknowledge funding from the EU under contract EVK2-CT-2002-00170 (RETRO) and helpful discussions with Johann Feichter and Stefan Kinne. Comments from two anonymous reviewers led to significant improvements in the manuscript, and are greatly appreciated.

3.7 Supplementary online material

Supplementary online material (SOM) to the paper, A model investigation of tropospheric ozone chemical tendencies in long-range transported pollution plumes, M. Auvray, I. Bey, E. Llull, M.G. Schultz, S. Rast.

3.7.1 Loss and production rates during the ACSOE campaign simulated by GEOS-Chem (Complement to section 3.3.1)

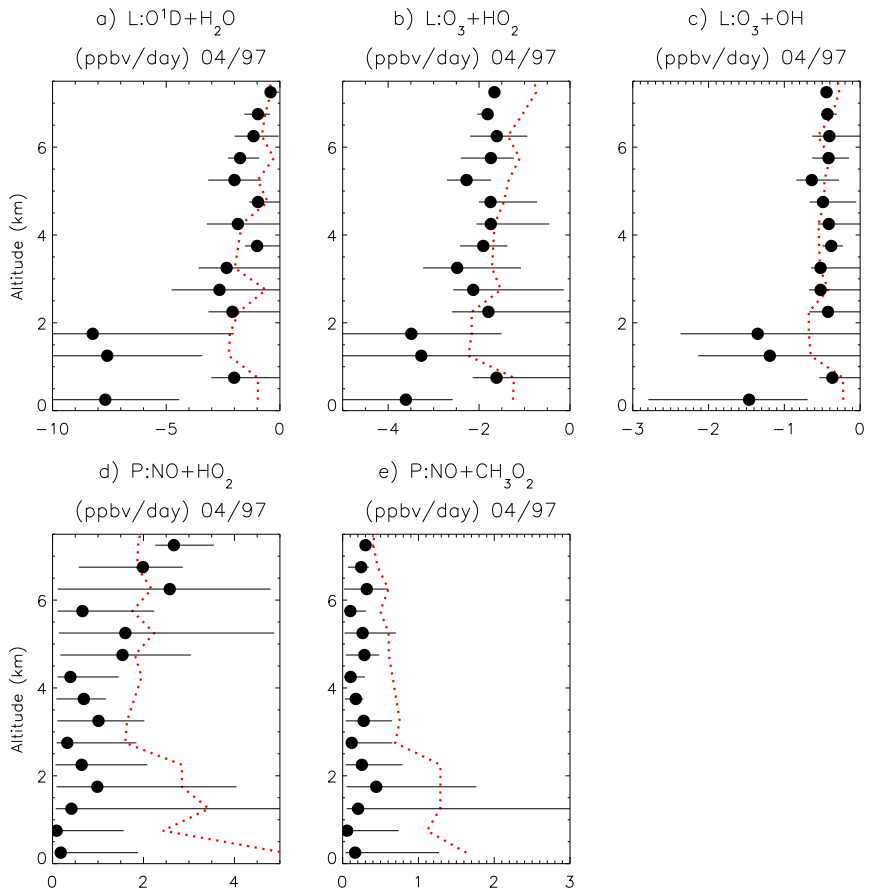

Figure 3.9: Vertical profiles of the median of the individual O_3 loss (a-c) and production (d-e) pathways, binned over 500 metres altitude for the ACSOE flights in April 1997 [*Reeves et al.*, 2002] (in black). GEOS-Chem results (red dotted line) are sampled along the flight tracks at the time and location of the flights. Horizontal bars represent observed 10^{th} and 90^{th} percentile. Units are in ppbv/day. Note that different scales are used for the five panels.

3.7.2 Evolution of the PE and BE characteristics from 60°W to 20°W in spring (Figure 3.10) and summer (Figure 3.11) over the North Atlantic (Complement to sections 3.4.1 and 3.4.2)

As the plumes are expected to chemically evolved as they are travelling, we examined how the chemical tendencies differ between PE and BE in different longitudinal slices (60°W, 40°W, and 20°W) along the north eastward path followed by most of the pollution plumes exported from the North American continent [e.g. *Trickl et al.*, 2003] (Figure 3.5 of the main manuscript). Figures 3.10 and 3.11 show the different quantities averaged at these three slices and can be compared to Figure 3.6 of the main manuscript. In spring, BE CO concentrations remain constant along the transport path. On the contrary, in summer, BE CO concentrations slightly increase from 60°W to 40°W, reflecting a longitudinal gradient (associated with mixing of the U.S. pollution within the background) and a latitudinal gradient (associated with increasing CO lifetime along the transport path) in background CO. Because NO_x has a short lifetime (a few days), PE NO_x (and thus ΔNO_x) decrease rapidly from 60°W eastward to reach BE levels at 20°W for both seasons. The slight increases from 40°W to 20°W seen in both PE CO and NO_x (especially in spring) most probably reflect influences from the European sources. Longitudinal variation in BE NO_x reflects geographical distribution of NO_x ship emissions. The BE netP O_3 also becomes less negative between 2 and 6 km of altitudes from 60° to 20°W, because of a decrease in O_3 loss (rather than an increase in O_3 production) associated with a decrease in water vapour concentrations and temperature along the north-eastward transport path. NetP O_3 is enhanced in plumes in spring at all longitudes for the two models. As expected, ΔNetP O_3 decreases from 60°W to 20°W. In summer, however ΔNetP O_3 in plumes is negative in MOZECH (as discussed in the manuscript) especially at 60°W.

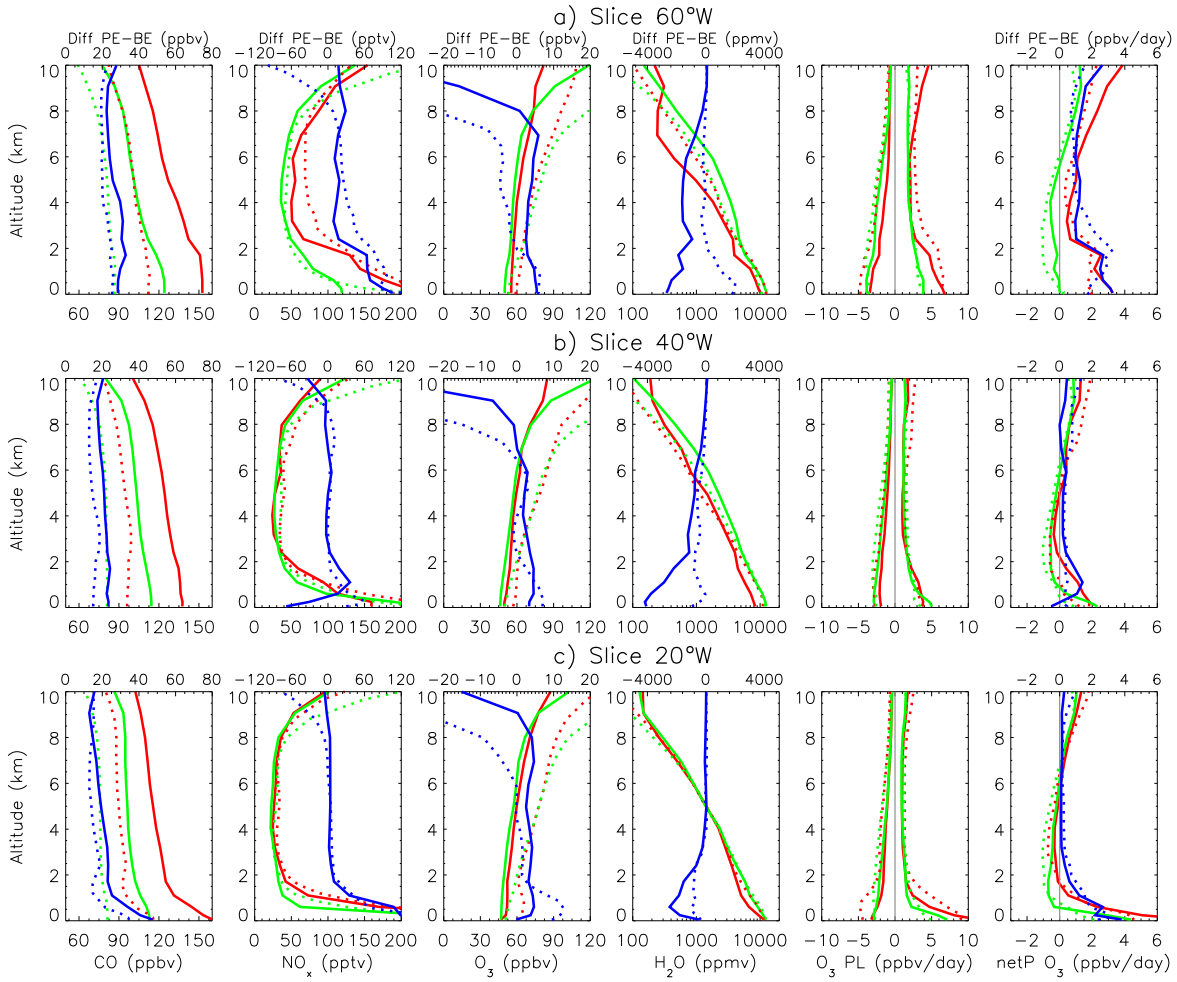

Figure 3.10: Simulated vertical profiles of CO (ppbv), NO_x (pptv), O_3 (ppbv), H_2O (ppmv) and O_3 chemical tendencies (ppbv/day) in April 1997 for three latitudinal slices across the North Atlantic ocean (60°W, 40°W, 20°W, see Figure 3.5). Green line: background environment (BE). Red line: plume environment (PE) (definitions in the text). Blue line: difference between the plume and the background environment (x-axis for the difference between the two environments is given at the top of each panel). Full line: GEOS-Chem. Dotted line: MOZECH.

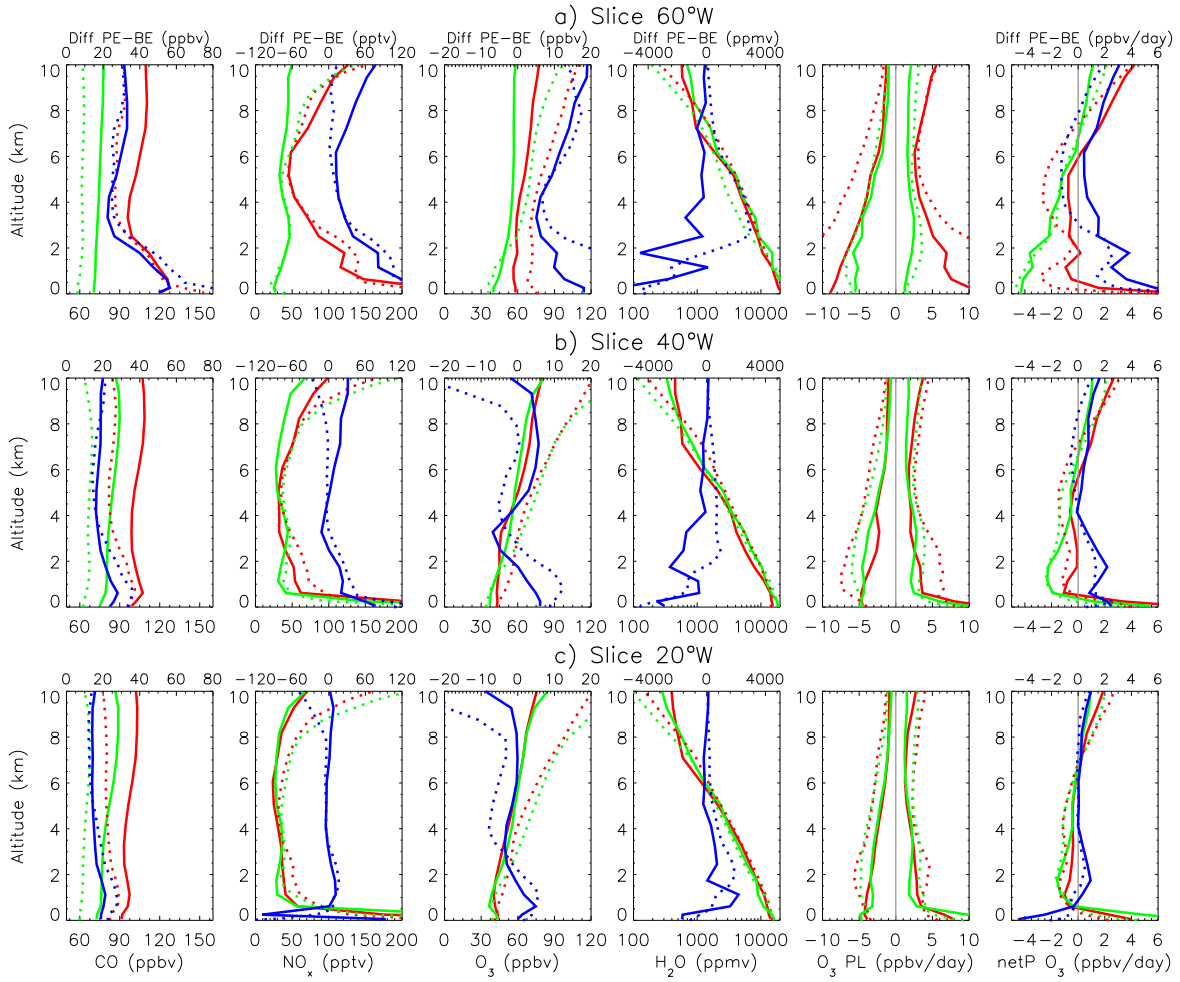

Figure 3.11: Simulated vertical profiles of CO (ppbv), NO_x (pptv), O_3 (ppbv), H_2O (ppmv) and O_3 chemical tendencies (ppbv/day) in July 1997 for three latitudinal slices across the North Atlantic ocean (60°W, 40°W, 20°W, see Figure 3.5). Green line: background environment (BE). Red line: plume environment (PE) (definitions in the text). Blue line: difference between the plume and the background environment (x-axis for the difference between the two environments is given at the top of each panel). Full line: GEOS-Chem. Dotted line: MOZECH.

3.7.3 Example of an outflow episode in summer 1997 as seen by GEOS-Chem and MOZECH. (Complement to section 3.4.2)

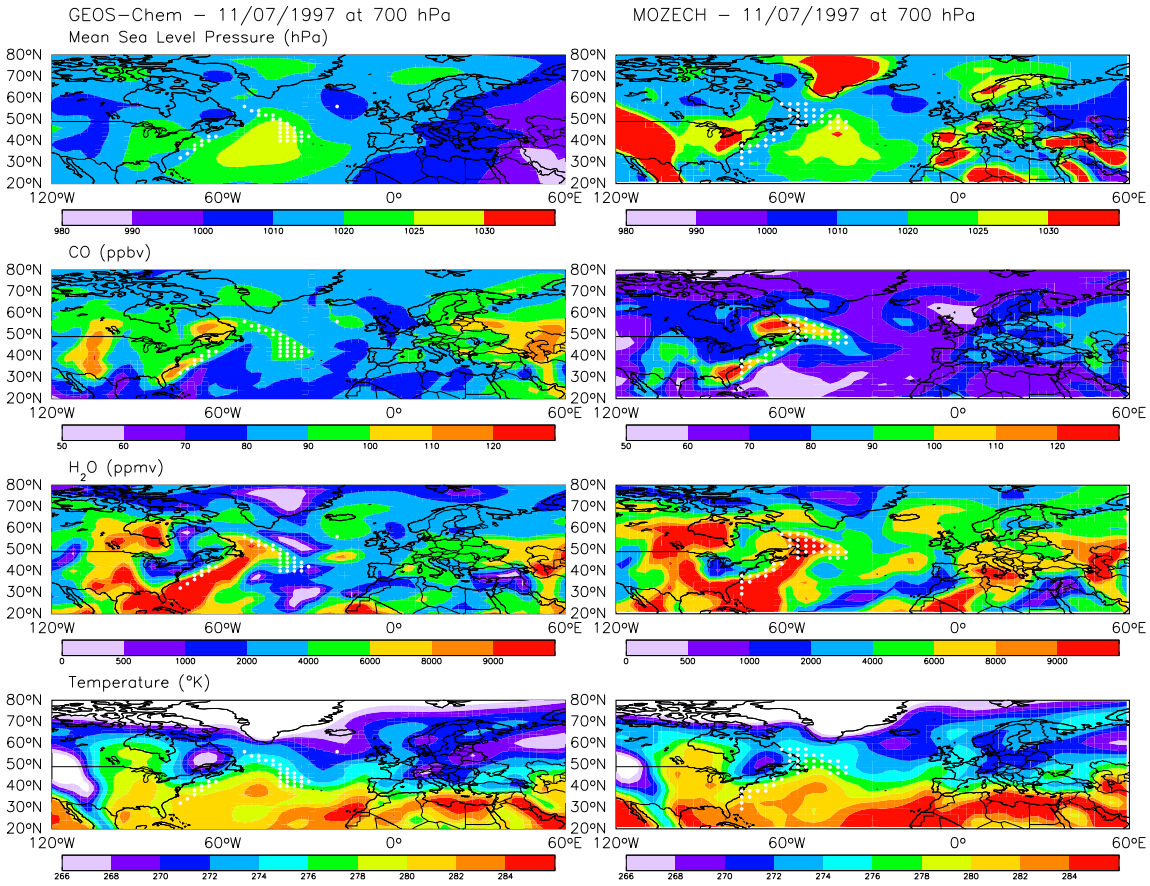

Figure 3.12: Mean sea level surface pressure (hPa), CO concentrations (ppbv), H_2O concentrations (ppmv) and temperature (°K) at 700 hPa for the 11^{th} of July 1997 simulated with GEOS-Chem (first row) and MOZECH (second row). White dots indicate the grid boxes identified as plumes (as defined in section 3.4) at 700 hPa.

3.7.4 PE and BE characteristics in spring and summer 1997 over the Northwest Pacific Ocean (Complement to section 3.5)

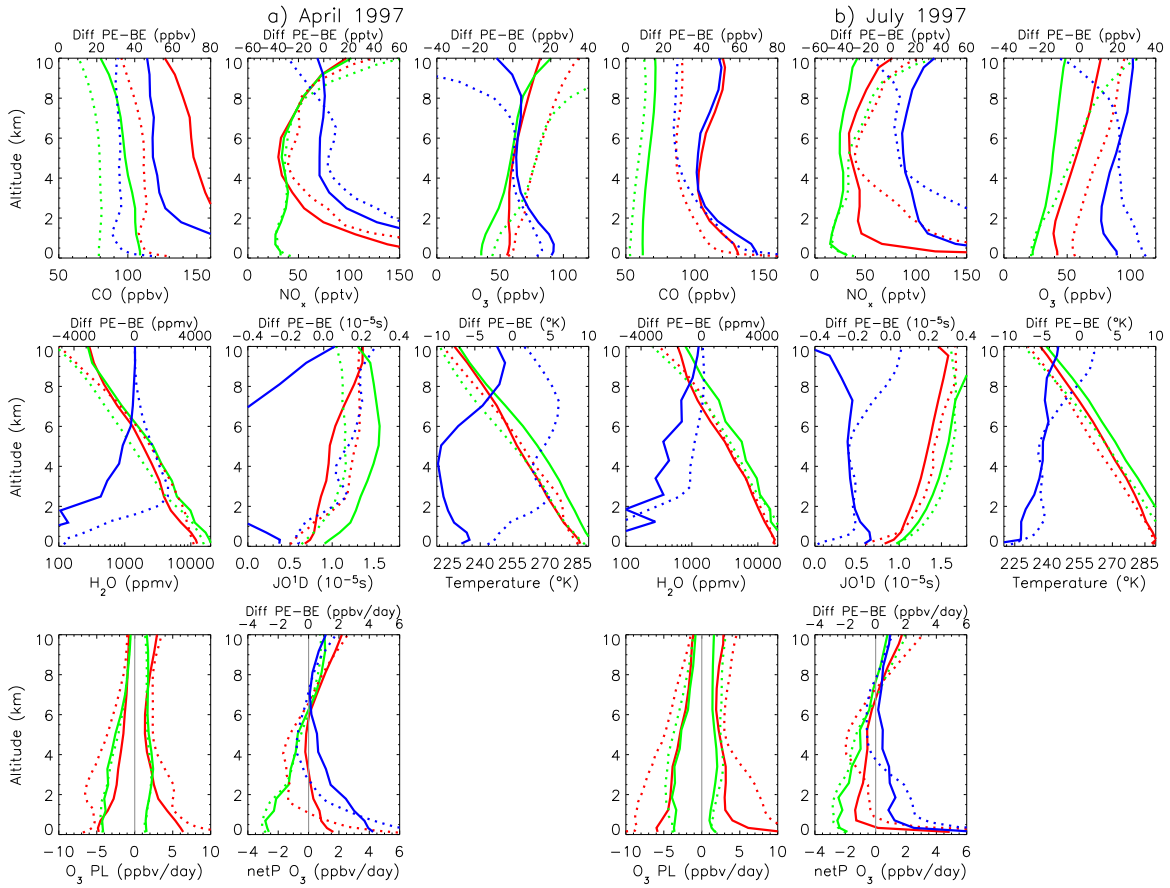

Figure 3.13: Simulated vertical profiles of NO_x (pptv), H_2O (ppmv), O_3 photolysis rate (10^{-5}s), temperature (°K), and O_3 chemical terms (ppbv/day), for April (left 6 panels) and July (right 6 panels) 1997 over the Northwest Pacific ocean (see Figure 3.5 for the definition of the region). Green line: background environment. Red line: plume environment. Blue line: difference between the plume and the background environment (x-axis for the difference between the two environments is given at the top of each panel). Full line: GEOS-Chem. Dotted line: MOZECH.

3.7.5 PE and BE characteristics in spring and summer 2000 over the North Atlantic Ocean (Complement to section 3.6)

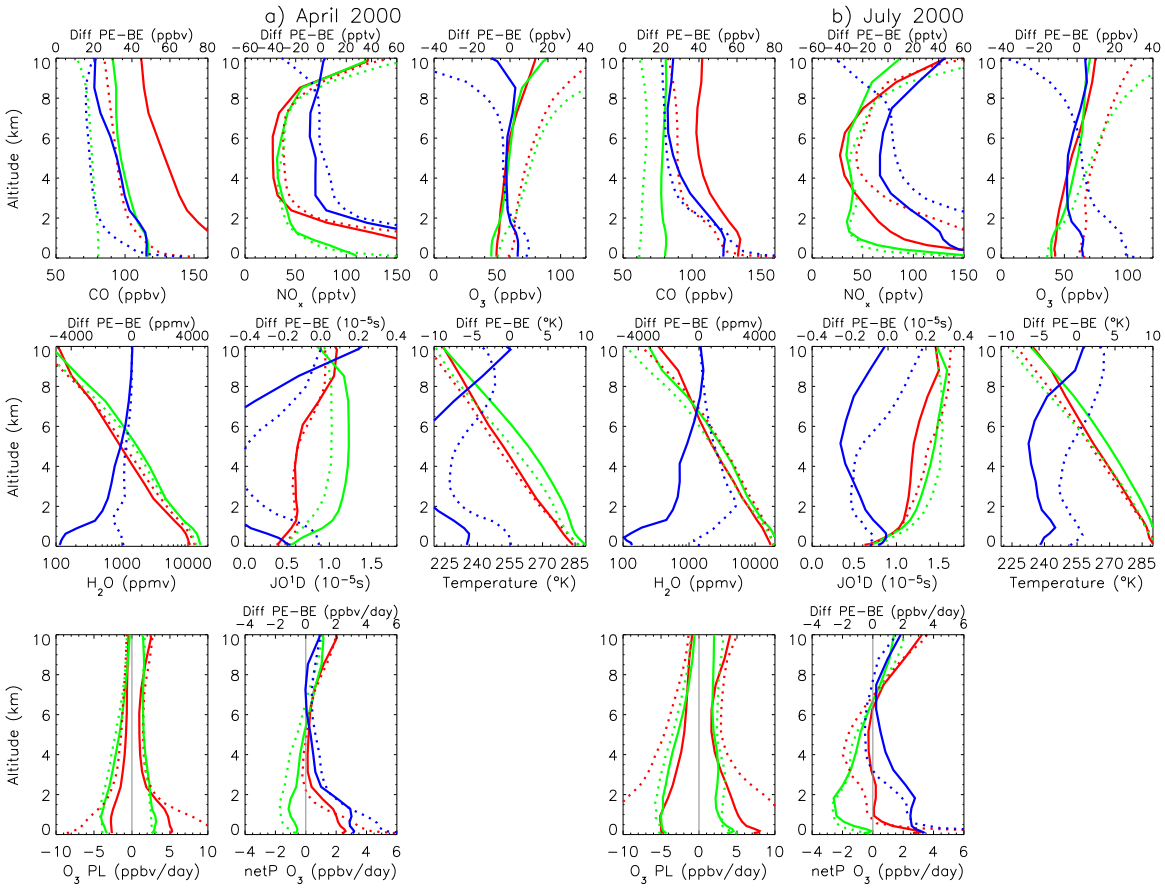

Figure 3.14: Simulated vertical profiles of NO_x (pptv), H_2O (ppmv), O_3 photolysis rate (10^{-5}s), temperature (°K), and O_3 chemical terms (ppbv/day), for April (left 6 panels) and July (right 6 panels) 2000 over the North Atlantic ocean (see Figure 3.5 for the definition of the region). Green line: background environment. Red line: plume environment. Blue line: difference between the plume and the background environment (x-axis for the difference between the two environments is given at the top of each panel). Full line: GEOS-Chem. Dotted line: MOZECH.

3.7.6 PE and BE characteristics in spring and summer 2000 over the Northwest Pacific Ocean (Complement to section 3.6)

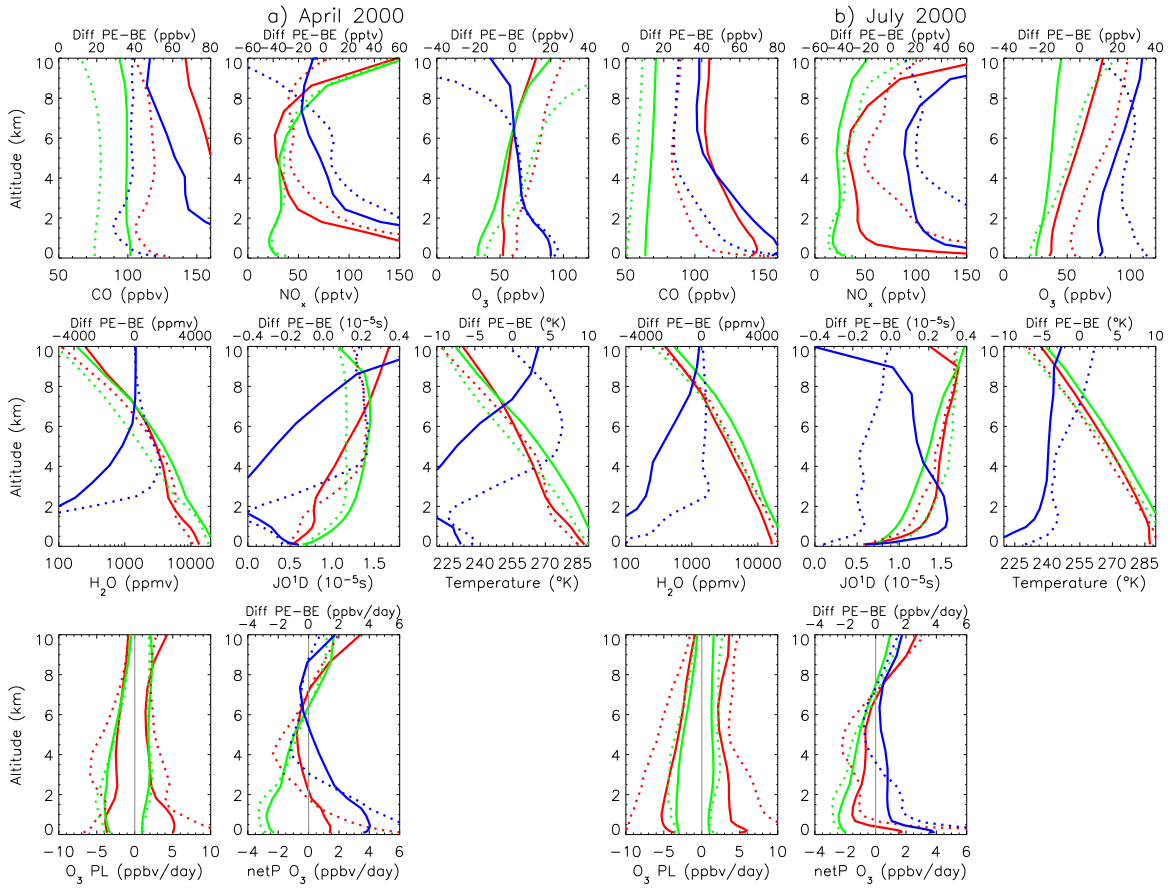

Figure 3.15: Simulated vertical profiles of NO_x (pptv), H_2O (ppmv), O_3 photolysis rate (10^{-5}s), temperature (°K), and O_3 chemical terms (ppbv/day), for April (left 6 panels) and July (right 6 panels) 2000 over the Northwest Pacific ocean (see Figure 3.5 for the definition of the region). Green line: background environment. Red line: plume environment. Blue line: difference between the plume and the background environment (x-axis for the difference between the two environments is given at the top of each panel). Full line: GEOS-Chem. Dotted line: MOZECH.

3.7.7 Seasonal variation in net O_3 production in PE and BE over the North Atlantic Ocean and Northwest Pacific Ocean in 2000 (Complement to section 3.6)

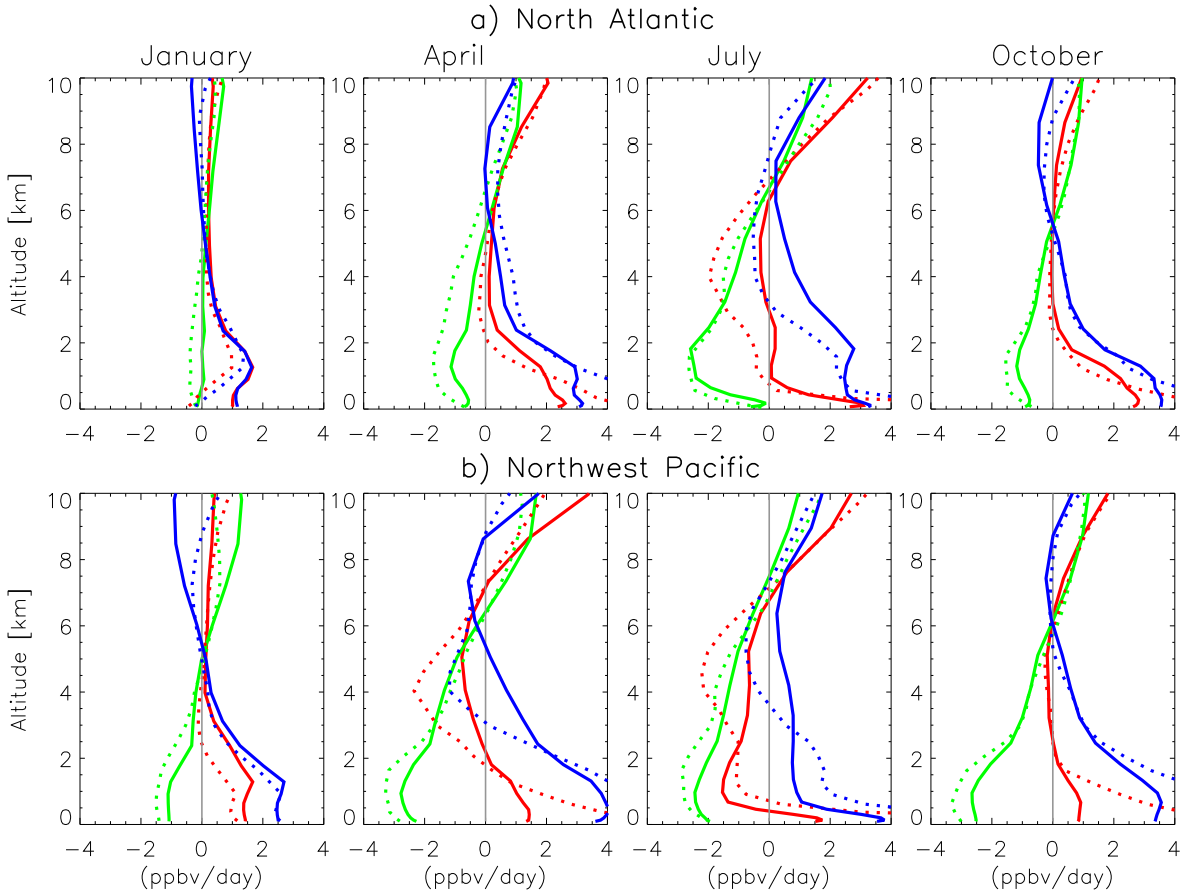

Figure 3.16: Simulated vertical profiles of net O_3 production (ppbv/day), for January, April, July, and October 2000 over the North Atlantic ocean and the Northwest Pacific ocean. Green line: background environment. Red line: plume environment. Blue line: difference between the plume and the background environment (x-axis for the difference between the two environments is given at the top of each panel). Full line: GEOS-Chem. Dotted line: MOZECH.

References

Allen, D. J., R. B. Rood, A. M. Thompson, R. D. Hudson (1996a), Three-dimensional ^{222}Rn calculations using assimilated meteorological data and a convective mixing algorithm, *J. Geophys. Res.*, *101*(D3), 6871–6882, 10.1029/95JD03408.

Allen, D. J., P. Kasibhatla, A. M. Thompson, R. B. Rood, B. G. Doddridge, K. E. Pickering, R. D. Hudson, S.-J. Lin (1996b), Transport-induced interannual variability of carbon monoxide determined using a chemistry and transport model, *J. Geophys. Res.*, *101*(D22), 28655-28670, 10.1029/96JD02984.

Auvray, M., and I. Bey (2005), Long-range transport to Europe: Seasonal variations and implications for the European ozone budget, *J. Geophys. Res.*, *110*, D11303, doi:10.1029/2004JD005503.

Bauguitte, S. (2000), A study of tropospheric reactive nitrogen oxides in the North Atlantic Region, PhD thesis, Univ. of East Anglia, Norwich, UK.

Berntsen, T. K., S. Karlsdottir, and D. A. Jaffe (1999), Influence of Asian emissions on the composition of air reaching the North Western United States, *Geophys. Res. Lett.*, *26*, 2171–2174.

Bey, I., D. J. Jacob, R. M. Yantosca, J. A. Logan, B. D. Field, A. M. Fiore, Q. Li, H. Liu, L. J. Mickley, and M. Schultz (2001a), Global modeling of tropospheric chemistry with assimilated meteorology: Model description and evaluation, *J. Geophys. Res.*, *106*, 23073–23095.

Bey, I., D. J. Jacob, J. A. Logan, and R. M. Yantosca (2001b), Asian chemical outflow to the Pacific in spring: Origins, pathways, and budgets, *J. Geophys. Res.*, *106*, 23097–23114.

Brönnimann, S., E. Schuepbach, P. Zanis, B. Buchmann, and H. Wanner (2000), A climatology of regional background ozone at different elevations in Switzerland (1992-1998), *Atmos. Environ.*, *34*, 5191–5198.

Brönnimann, S., B. Buchmann, and H. Wanner (2002), Trends in near-surface ozone concentrations in Switzerland: the 1990s, *Atmos. Environ.*, *36*, 2841–2852.

Brough, N., et al. (2003), Intercomparison of aircraft instruments on board the C-130 and Falcon 20 over southern Germany during EXPORT 2000, *Atmos. Chem. Phys.*, *3*, 2127–2138.

Carmichael, G. R., I. Uno, M. J. Phadnis, Y. Zhang, and Y. Sunwoo (1998), Tropospheric ozone production and transport in the springtime in east Asia, *J. Geophys. Res.*, *103*, 10649–10672, 10.1029/97JD03740.

Chin, M., P. Ginoux, S. Kinne, O. Torres, B. Holben, B. N. Duncan, R. V. Martin, J. A. Logan, A. Higurashi, and T. Nakajima (2002), Tropospheric aerosol optical thickness from the GOCART model and comparisons with satellite and sunphotometer measurements, *J. Atmos. Sci.*, *59*, 461–483.

Choi, Y., Y. Wang, T. Zeng, R. V. Martin, T. P. Kurosu, K. Chance (2005), Evidence of lightning NO_x and convective transport of pollutants in satellite observations over North America, *Geophys. Res. Lett.*, *32*, L02805, doi:10.1029/2004GL021436.

Collins, W. J., D. S. Stevenson, C. E. Johnson, and R. G. Derwent (2000), The European regional ozone distribution and its links with the global scale for the years 1992 and 2015, *Atmos. Environ.*, *34*, 255–267.

Cooper, O. R., J. L. Moody, D. D. Parrish, M. Trainer, T. B. Ryerson, J. S. Holloway, G. Hübler, F. C. Fehsenfeld, S. J. Oltmans, and M. J. Evans (2001), Trace gas signatures of the airstreams within North Atlantic cyclones: Case studies from the North Atlantic Regional Experiment (NARE'97) aircraft intensive, *J. Geophys. Res.*, *106*, 5437–5456.

Cooper, O. R., J. L. Moody, D. D. Parrish, M. Trainer, T. B. Ryerson, J. S. Holloway, G. Hübler, F. C. Fehsenfeld, and M. J. Evans (2002a), Trace gas composition of midlatitude cyclones over the western North Atlantic Ocean: A conceptual model, *J. Geophys. Res.*, *107*(D7), doi:10.1029/2001JD000901.

Cooper, O. R., J. L. Moody, D. D. Parrish, M. Trainer, J. S. Holloway, G. Hübler, F. C. Fehsenfeld, and A. Stohl (2002b), Trace gas composition of midlatitude cyclones over the western North Atlantic Ocean: A seasonal comparison of O 3 and CO, *J. Geophys. Res.*, *107*(D7), doi:10.1029/2001JD000902.

Crawford, J., et al. (1997), An assessment of ozone photochemistry in the extratropical western North Pacific: impact of continental outflow during the late winter/early spring, *J. Geophys. Res.*, *102*(D23), 28469–28488, 10.1029/97JD02600.

Davis, D. D., et al. (1996), Assessment of ozone photochemistry in the western North Pacific as inferred from PEM-West A observations during the fall 1991, *J. Geophys. Res.*, *101*(D1), 2111–2134, 10.1029/95JD02755.

Davis, D. D., et al. (2003), An assessment of western North Pacific ozone photochemistry based on springtime observations from NASA's PEM-West B (1994) and TRACE-P (2001) field studies, *J. Geophys. Res.*, *108*(D21), 8829, doi:10.1029/2002JD003232.

DeMore, W. B., S. P. Sander, C. J. Howard, A. R. Ravishankara, D. M. Golden, C. E. Kolb, R. F. Hampson, M. J. Kurylo, and M. J. Molina (1997), Chemical kinetics and photochemical data for use in stratospheric modelling: Evaluation number 12, *JPL Publ.*, *97-4*, 14–143.

Dentener, F., D. Stevenson, J. Cofala, R. Mechler, M. Amann, P. Bergamaschi, F. Raes, R. Derwent (2005), The impact of air pollutant and methane emission controls on tropospheric ozone and radiative forcing: CTM calculations for the period 1990–2030, *Atmos. Chem. Phys.*, *5*, 1731–1755.

Derwent, R. G., P. G. Simmonds, S. Seuring, and C. Dimmer (1998), Observation and interpretation of the seasonal cycles in the surface concentrations of ozone and carbon monoxide at Mace Head, Ireland from 1990 to 1994, *J. Atmos. Chem.*, *32*, 145–157.

DiNunno, B., D. Davis, G. Chen, J. Crawford, J. Olson, and S. Liu (2003), An assessment of ozone photochemistry in the central/eastern North Pacific as determined from multiyear airborne field studies, *J. Geophys. Res.*, *108*(D2), 8237, doi:10.1029/2001JD001468.

Duncan, B. N., R. V. Martin, A. C. Staudt, R. Yevich, and J. A. Logan (2003), Interannual and seasonal variability of biomass burning emissions constrained by satellite observations, *J. Geophys. Res.*, *108*(D2), 4100, doi:10.1029/2002JD002378.

Dunlea, E. J., and A. R. Ravishankara (2004), Measurements of the rate coefficient for the reaction of $O(^1D)$ with H_2O and re-evaluation of the atmospheric OH production rate, *Phys. Chem. Chem. Phys.*, *6*, 3333–3340.

EMEP Assessment (2004), Part 1 European perspective, edited by Gun Lövblad, Leonor Tarrasón, Kjetil Tørseth and Sergey Dutchak, Oslo, Norway.

Fehsenfeld, F. C., P. Daum, W. R. Leaitch, M. Trainer, D. D. Parrish, and G. Hübler (1996), Transport and processing of O_3 and O_3 precursors over the North Atlantic: An overview of the 1993 North Atlantic Regional Experiment (NARE) summer intensive, *J. Geophys. Res.*, *101*, 28877–28892.

Fiore, A. M., D. J. Jacob, I. Bey, R. M. Yantosca, B. D. Field, A. C. Fusco, and J. G. Wilkinson (2002), Background ozone over the United States in summer: Origin, trend, and contribution to pollution episodes, *J. Geophys. Res.*, *107*(D15), doi:10.1029/2001JD000982.

Folkins, I., R. Chatfield, D. Baumgardner, and M. Proffitt (1997), Biomass burning and deep convection in southeastern Asia: Results from ASHOE/MAESA, *J. Geophys. Res.*, *102*, 13291–13300.

Gerbig, C., S. Schmitgen, D. Kley, A. Volz-Thomas, K. Dewey, D. Haaks (1999), An improved fast-response vacuum-UV resonance fluorescence CO instrument, *J. Geophys. Res.*, *104*(D1), 1699–1704, 10.1029/1998JD100031.

Grewe, V., D. Brunner, M. Dameris, J. L. Grenfell, R. Hein, D. Shindell and J. Staehelin (2001), Origin and variability of upper tropospheric nitrogen oxides and ozone at northern mid-latitudes, *Atmos. Environ.*, *35*, 3421–3433.

Guerova, G., I. Bey, J.-L. Attié, R. V. Martin, J. Cui, and M. Sprenger (2006), Impact of transatlantic transport episodes on summertime ozone in Europe, *Atmos. Chem. Phys.*, *6*, 2057–2072.

Hannan, J. R., H. E. Fuelberg, J. H. Crawford, G. W. Sachse, and D. R. Blake (2003), Role of wave cyclones in transporting boundary layer air to the free troposphere during the spring 2001 NASA/TRACE-P experiment, *J. Geophys. Res.*, *108*(D20), 8785, doi:10.1029/2002JD003105.

Heald, C. L., et al. (2003), Asian outflow and trans-Pacific transport of carbon monoxide and ozone pollution: An integrated satellite, aircraft, and model perspective, *J. Geophys. Res.*, *108*(D24), 4804, doi:10.1029/2003JD003507.

Heald, C. L., D. J. Jacob, D. B. A. Jones, P. I. Palmer, J. A. Logan, D. G. Streets, G. W. Sachse, J. C. Gille, R. N. Hoffman, and T. Nehrkorn (2004), Comparative inverse analysis of satellite (MOPITT) and aircraft (TRACE-P) observations to estimate Asian sources of carbon monoxide, *J. Geophys. Res.*, *109*, (D23), D23306, doi:10.1029/2004JD005185.

Honrath, R. E., R. C. Owen, M. Val Martin, J. S. Reid, K. Lapina, P. Fialho, M. P. Dziobak, J. Kleissl, D. L. Westphal (2004), Regional and hemispheric impacts of anthropogenic and biomass burning emissions on summertime CO and O_3 in the North Atlantic lower free troposphere, *J. Geophys. Res.*, *109*, D24310, doi:10.1029/2004JD005147.

Horowitz, L. W., J. Liang, G. M. Gardner, and D. J. Jacob (1998), Export of reactive nitrogen from North America during summertime: Sensitivity to hydrocarbon chemistry, *J. Geophys. Res.*, *103*, 13451–13476.

Horowitz, L. W., et al. (2003), A global simulation of tropospheric ozone and related tracers: Description and evaluation of MOZART, version 2, *J. Geophys. Res.*, *108*(D24), 4784, doi:10.1029/2002JD002853.

Hudman, R. C., et al. (2004), Ozone production in transpacific Asian pollution plumes and implications for ozone air quality in California, *J. Geophys. Res.*, *109*, D23S10, doi:10.1029/2004JD004974.

Huntrieser, H., et al. (2005), Intercontinental air pollution transport from North America to Europe: Experimental evidence from airborne measurements and surface observations, *J. Geophys. Res.*, *110*, D01305, doi:10.1029/2004JD005045.

Jacob, D.J. (2000), Heterogeneous chemistry and tropospheric ozone, *Atmos. Environ.*, *34*, 2131–2159.

Jacob, D.J., et al. (1996), Origin of ozone and NO_x in the tropical troposphere: a photochemical analysis of aircraft observations over the South Atlantic Basin, *J. Geophys. Res.*, *101*, 24,235–24,350.

Jacob, D. J., J. H. Crawford, M. M. Kleb, V. S. Connors, R. J. Bendura, J. L. Raper, G. W. Sachse, J. C. Gille, L. Emmons, and C. L. Heald (2003), Transport and Chemical Evolution over the Pacific (TRACE-P) aircraft mission: Design, execution, and first results, *J. Geophys. Res.*, *108*(D20), 9000, doi:10.1029/2002JD003276.

Jaeglé, L., D. J. Jacob, W. H. Brune, D. Tan, I. Faloona, A. J. Weinheimer, B. A. Ridley, T. L. Campos, and G. W. Sachse (1998), Sources of HO_x and production of ozone in the upper troposphere over the United States, *Geophys. Res. Lett.*, *25*, 1705–1708.

Jaffe, D., et al. (1999), Transport of Asian air pollution to North America, *Geophys. Res. Lett.*, *26*, 711–714.

Jaffe, D., I. McKendry, T. Anderson, and H. Price (2003), Six new episodes of trans-Pacific transport of air pollutants, *Atmos. Environ.*, *37*, 391–404.

Kondo, Y., et al. (2004), Impacts of biomass burning in Southeast Asia on ozone and reactive nitrogen over the western Pacific in spring, *J. Geophys. Res.*, *109*(D15), 8522, doi:10.1029/2003JD004203.

Li, Q. B., et al. (2002a), Transatlantic transport of pollution and its effects on surface ozone in Europe and North America, *J. Geophys. Res.*, *107*(D123), 4166, doi: 10.1029/2001JD001422.

Li, Q. B., D. J. Jacob, T. D. Fairlie, H. Y. Liu, R. M. Yantosca, and R. V. Martin (2002b), Stratospheric versus pollution influences on ozone at Bermuda: Reconciling past analyses, *J. Geophys. Res.*, *107*(D22), 4611, doi:10.1029/2002JD002138.

Li, Q. B., D. J. Jacob, R. Park, Y. Wang, C. L. Heald, R. Hudman, R. M. Yantosca, R. V. Martin, M. Evans (2005), North American pollution outflow and the trapping of convectively lifted pollution by upper-level anticyclone, *J. Geophys. Res.*, *110*, D10301, doi:10.1029/2004JD005039.

Liang, Q., L. Jaeglé, D. A. Jaffe, P. Weiss, A. Heckman, and J. Snow (2004), Long-range Transport to the Northeast Pacific: Seasonal variations and transport pathways, *J. Geophys. Res.*, *109*, D23S07, doi:10.1029/2003JD004402.

Lin, S.-J., and R. B. Rood (1996), Multidimensional flux form semi Lagrangian transport schemes, *Mon. Weather Rev.*, *124*, 2046–2070.

Liu, H., D. J. Jacob, L. Y. Chan, S. J. Oltmans, I. Bey, R. M. Yantosca, J. M. Harris, B. N. Duncan, and R. V. Martin (2002), Sources of tropospheric ozone along the Asian Pacific Rim: An analysis of ozonesonde observations, *J. Geophys. Res.*, *107*(D21), 4573, doi:10.1029/2001JD002005.

Liu, H., D. J. Jacob, I. Bey, R. M. Yantosca, B. N. Duncan, and G. W. Sachse (2003), Transport pathways for Asian pollution outflow over the Pacific: Interannual and seasonal variations, *J. Geophys. Res.*, *108*(D20), 8786, doi:10.1029/2002JD003102.

Logan, J. A. (1999), An analysis of ozonesonde data for the troposphere: Recommendations for testing 3-D models and development of a gridded climatology for tropospheric ozone, *J. Geophys. Res.*, *104*(D13), 16115–16150, 10.1029/1998JD100096.

Martin, R. V., D. J. Jacob, R. M. Yantosca, M. Chin, and P. Ginoux (2003), Global and regional decreases in tropospheric oxidants from photochemical effects of aerosols, *J. Geophys. Res.*, *108*(D3), 4097, doi:10.1029/2002JD002622.

McLinden, C. A., S. C. Olsen, B. Hannegan, O. Wild, M. J. Prather, and J. Sundet (2000), Stratospheric ozone in 3-D models: A simple chemistry and the cross-tropopause flux, *J. Geophys. Res.*, *105*, 14653–14665.

Naja, M., H. Akimoto, and J. Staehelin (2003), Ozone in background and photochemically aged air over central Europe: Analysis of long-term ozonesonde data from Hohenpeissenberg and Payerne, *J. Geophys. Res.*, *108*(D2), 4063, doi:10.1029/2002JD002477.

Newell, R. E., E. V. Browell, D. D. Davis, and S. C. Liu (1997), Western Pacific tropospheric ozone and potential vorticity: Implications for Asian pollution, *Geophys. Res. Lett.*, *24*, 2733–2736.

Nordeng, T. E. (1994), Extended versions of the convective parameterization scheme at ECMWF and their impact on the mean and transient activity of the model in the tropics, *Technical Memorandum 206*, ECMWF, Reading, UK.

Olson, J. R., et al. (2001), Seasonal differences in the photochemistry of the South Pacific: A comparison of observations and model results from PEM-Tropics A and B, J. Geophys. Res., 106 (D23), 4437, 32749–32766.

Ordóñez, C., H. Mathis, M. Furger, S. Henne, C. Hüglin, J. Staehelin, A. S. and H. Prévôt (2005), Changes of daily surface ozone maxima in Switzerland in all seasons from 1992 to 2002 and discussion of summer 2003, *Atmos. Chem. Phys.*, *5*, 1187–1203.

Parrish, D. D., J. S. Holloway, M. Trainer, P. C. Murphy, G. L. Forbes, and F. C. Fehenseld (1993), Export of North American ozone pollution to the North Atlantic Ocean, *Science*, *259*, 1436–1439.

Parrish, D. D., M. Trainer, J. S. Holloway, J. E. Yee, M. S. Warshawsky, F. C. Fehsenfeld, G. L. Forbes, J. L. Moody (1998), Relationships between ozone and carbon monoxide at surface sites in the North Atlantic region, *J. Geophys. Res.*, *103*(D11), 13357–13376, 10.1029/98JD00376.

Parrish, D. D., et al. (2004), Changes in the photochemical environment of the temperate North Pacific troposphere in response to increased Asian emissions, *J. Geophys. Res.*, *109*, D23S18, doi:10.1029/2004JD004978.

Penkett, S., et al. (2004), Long-range transport of ozone and related pollutants over the North Atlantic in spring and summer, *Atmos. Chem. Phys. Dis.*, *4*, 4407–4454.

Pickering, K. E., Y. S. Wang, W. K. Tao, C. Price, and J. F. Muller (1998), Vertical distributions of lightning NO_x for use in regional and global chemical transport models, *J. Geophys. Res.*, *103*, 31203–31216, 10.1029/98JD02651.

Price, C., and D. Rind (1992), A simple lightning parameterization for calculating global lightning distributions, *J. Geophys. Res.*, *97*, 9919–9933.

Price, H. U., D. A. Jaffe, O. R. Cooper, P. V. Doskey (2004), Photochemistry, ozone production, and dilution during long-range transport episodes from Eurasia to the northwest United States, *J. Geophys. Res.*, *109*, D23S13, doi:10.1029/2003JD004400.

Purvis, R. M., et al. (2003), Rapid uplift of nonmethane hydrocarbons in a cold front over central Europe, *J. Geophys. Res.*, *108* (D7), 4224, doi:10.1029/2002JD002521.

Randel, W. J., F. Wu, J. M. Russell, A. Roche and J. W. Waters (1998), Seasonal cycles and QBO variations in stratospheric CH_4 and H_2O observed in UARS HALOE data, *J. Atmos. Sci.*, *55*, 163–185.

Ravishankara, A. R., E. J. Dunlea, M. A. Blitz, T. J. Dillon, D. E. Heard, M. J. Pilling, R. S. Strekowski, J. M. Nicovich, and P. H. Wine (2002), Redetermination of the rate coefficient for the reaction of $O(^1D)$ with N_2, *Geophys. Res. Lett.*, *29* (15), doi:10.1029/2002GL014850.

Reeves, C. E., and the EXPORT Team (2003), Results from EXPORT (European EXport of Precursors and Ozone by Long-Range Transport) and lessons learned, in *European export of particulates and ozone by long-range transport (EXPORT-E2 -Final report)*, edited by Penkett S. A., Law K. S., Platt U. and Volz-Thomas A., pp. 147–150, International Scientific Secretariat (ISS), Munich.

Reeves, C. E., et al. (2002), Potential for photochemical ozone formation in the troposphere over the North Atlantic as derived from aircraft observations during ACSOE, *J. Geophys. Res.*, *107*(D23), 4707.

Roeckner, E., et al. (2003), The atmospheric general circulation model ECHAM 5. PART I: Model description, MPI report 349, Max Planck Institute for Meteorology, Hamburg, Germany. (Available at http://www.mpimet.mpg.de/fileadmin/publikationen/Reports/max_scirep_349.pdf).

Sander, S. P., et al., (2000) Chemical kinetics and photochemical data for use in stratospheric modelling: Supplement to evaluation number 12: evaluation number 13, *JPL Publ.*, *00–3*, 10–28.

Schneider, H. R., D. B. A. Jones, M. B. McElroy, G.-Y. Shi (2000), Analysis of residual mean transport in the stratosphere 1. Model description and comparison with satellite data, *J. Geophys. Res.*, *105*(D15), 19991–20012, 10.1029/2000JD900213.

Schultz, M., R. Schmitt, K. Thomas, and A. Volz-Thomas (1998), Photochemical box modeling of long-range transport from North America to Tenerife during the North Atlantic Regional Experiment (NARE) 1993, *J. Geophys. Res.*, *103*(D11), 13477-13488, 10.1029/97JD01481.

Schultz, M., et al. (1999), On the origin of tropospheric ozone and NO_x over the tropical Pacific, *J. Geophys. Res*, *104*, 5829–5844.

Stevenson, D. S., et al. (2006), Multimodel ensemble simulations of present-day and near-future tropospheric ozone, *J. Geophys. Res.*, *111*, D08301, doi:10.1029/2005JD006338.

Simmonds, P. G., R. G. Derwent R. G., A. L. Manning, and G. Spain (2004), Significant growth in surface ozone at Mace Head, Ireland, 1987–2003, *Atmos. Environ.*, *38*, 4769–4778.

Stohl, A. (2001), A 1-year Lagrangian climatology of airstreams in the Northern Hemisphere troposphere and lowermost stratosphere, *J. Geophys. Res.*, *106*, 7263–7280.

Stohl, A., and T. Trickl (1999), A textbook example of long-range transport: Simultaneous observation of ozone maxima of stratospheric and North American origin in the free troposphere over Europe, *J. Geophys. Res.*, *104*, 30445–30462.

Thompson, A. M., K. E. Pickering, R. R. Dickerson, W. G. Ellis, D. J. Jacob, J. R. Scala, W.-K. Tao, D. P. McNamara, and J. Simpson (1994), Convective transport over the central United States and its role in regional CO and ozone budgets, *J. Geophys. Res.*, *99*, 18703–18712.

Tie, X., S. Madronich, S. Walters, D. P. Edwards, P. Ginoux, N. Mahowald, R. Zhang, C. Lou, G. Brasseur (2005), Assessment of the global impact of aerosols on tropospheric oxidants, *J. Geophys. Res.*, 110, D03204, doi:10.1029/2004JD005359.

Tiedtke, M. (1989), A comprehensive mass flux scheme for cumulus parameterization in large-scale models, *Mon. Weather Rev.*, *117*, 1779–1800.

Trickl, T., O. R. Cooper, H. Eisele, P. James, R. Mücke, and A. Stohl (2003), Intercontinental transport and its influence on the ozone concentrations over central Europe: Three case studies, *J. Geophys. Res.*, *108*(D12), 8530, doi:10.1029/2002JD002735.

van der Werf, G. R., J. T. Randerson, G. J. Collatz, and L. Giglio (2003), Carbon emissions from fires in tropical and subtropical ecosystems, *Global Change Biol.*, *9*, 547–562.

Wang, Y., D. J. Jacob, and J. A. Logan (1998), Global simulation of tropospheric O_3-NO_x-hydrocarbon chemistry: 1. Model formulation, *J. Geophys. Res.*, *103*, 10713–10726.

Wild, O., K. S. Law, D. S. McKenna, B. J. Bandy, S. A. Penkett, J. A. Pyle, (1996), Photochemical trajectory modeling studies of the North Atlantic region during August 1993, *J. Geophys. Res.*, *101*(D22), 29269-29288, 10.1029/96JD00837.

Wild, O., X. Zhu, and M. J. Prather (2000), Fast-J: Accurate simulation of in- and below-cloud photolysis in tropospheric chemistry models, *J. Atmos. Chem.*, *37*, 245–282.

Wild, O., and H. Akimoto (2001), Intercontinental transport of ozone and its precursors in a three-dimensional global CTM, *J. Geophys. Res.*, *106*, 27729–27744.

Wild, O., et al. (2004), Chemical transport model ozone simulations for spring 2001 over the western Pacific: Regional ozone production and its global impacts, *J. Geophys. Res.*, *109*, D15S02, doi:10.1029/2003JD004041.

Yienger, J., M. Galanter, T. A. Holloway, M. J. Phadnis, S. K. Guttikunda, G. R. Carmichael, W. J. Moxim, and H. Levy II (2000), The episodic nature of air pollution transport from Asia to North America, *J. Geophys. Res.*, *105*, 26931–26946.

Chapter 4

Long-Range Transport of Ozone to Europe

Originally published as: Auvray, M. and I. Bey (2005), Long-Range Transport to Europe: Seasonal Variations and Implications for the European Ozone Budget, J. Geophys. Res., 110, D11303, doi:10.1029/2004JD005503.

Abstract

We use a chemical transport model (GEOS-Chem) to quantify the contribution of long-range transported pollution to the European ozone (O_3) budget for the year 1997. The model reproduces the main features observed over Europe for O_3, carbon monoxide and nitrogen dioxides, as well as two events of enhanced O_3 of North American origin over the eastern North Atlantic and over Europe. North American O_3 fluxes into Europe experience a maximum in spring and summer, reflecting the seasonal variation in photochemical activity and in export pathways. In summer, North American O_3 enters Europe at higher altitudes and lower latitudes because of deep convection, and because the flow over the North Atlantic is mostly zonal in that season. The low-level inflow is only important in spring, when loss rates in the boundary layer over North Atlantic are weaker. Asian O_3 arrives mainly via the westerlies, and usually at higher altitudes than North American O_3 because of stronger deep convection over Asia. In addition, Asian O_3 fluxes are at a maximum in summer during the monsoon period because of enhanced convection over Asia, increased nitrogen oxides sources from lightning and direct transport towards Europe via the monsoon easterlies. Over Europe, total background accounts for 30 ppbv at the surface. North American and Asian O_3 contribute substantially to the annual O_3 budget over Europe, accounting for 10.9% and 7.7% respectively, while the European contribution only accounts for 9.4%. We find that in summer, at the surface, O_3 decreases over Europe from 1980 to 1997, reflecting the reduction

of European O_3 precursor emissions. In the free troposphere, this decrease is compensated by the increase in O_3 due to increasing Asian emissions. This may explain the lack of trends observed over most of the European region, especially at the mountain sites.

4.1 Introduction

Tropospheric ozone (O_3) results from a complex interaction between transport from the stratosphere [e.g., *Junge*, 1962; *Danielsen*, 1968] and in-situ photochemical production taking place through the oxidation of volatile organic carbons (VOCs) and carbon monoxide (CO) in the presence of nitrogen oxides ($NO_x = NO + NO_2$) [e.g., *Levy*, 1971; *Chameides and Walker*, 1973; *Crutzen*, 1974]. The lifetime of O_3 in the free troposphere ranges from a few days to several months [e.g., *Liu et al.*, 1987], which allows its transport over distances of intercontinental and hemispheric scales. Transport of O_3 and related species may thus have impacts on O_3 concentrations found downwind of industrialised regions of the Northern Hemisphere, where most of the O_3 precursors (VOCs and NO_x) are emitted [*Jacob et al.*, 1999; *Berntsen et al.*, 1999; *Jonson et al.*, 2001; *Wild and Akimoto*, 2001; *Stohl et al.*, 2002; *Wild et al.*, 2004]. *Li et al.* [2002] reported for example that anthropogenic emissions from North America led to an additional 20% of violations of the European Council O_3 standard in the summer 1997 over Europe. There is a crucial need to quantify the relative contributions of the O_3 produced by the precursors emitted within a region and that of the O_3 transported from regions upwind (the so-called background O_3) to provide better information to policy makers [*Holloway et al.*, 2003]. In this paper we examine how the tropospheric composition and, O_3 distributions in particular over Europe, are affected by long-range transport of pollution.

National reports indicate that European emissions of O_3 precursors have decreased from 1990 to 2000 due to control strategies in most of the western and northern European countries. In eastern Europe the decrease is due to modernization or the shut down of air-polluting industrial branches [*Vestreng and Klein*, 2002]. In the mean time, O_3 precursor emissions have more than doubled since the 1990s in Asia because of rapid industrialization [*Van Aardenne et al.*, 1999], while North American emissions have remained fairly constant or have slightly decreased [*EPA*, 1997; 2003]. The decrease in European emissions has likely induced a decrease in O_3 peaks in summer [*Derwent et al.*, 2003; *Brönnimann et al.*, 2002] and an increase in mean O_3 in winter over Europe due to less O_3 titration by NO_x [*Lindskog et al.*, 2001]. For example, *Derwent et al.* [2003] showed a large decline in the annual maximum eight-hour mean O_3 concentrations and in O_3 peaks observed between 1990 and 2000 over the United Kingdom. A decrease in O_3 peaks was also found at several stations in Switzerland from 1991 to 1999 [*Brönnimann et al.*, 2002].

However, recent studies indicate either trends in monthly mean O_3 close to zero or slightly increasing over the last decade for a number of sites over Europe. *Kuebler et al.* [2001] reported, for example, trends close to zero for the 90^{th} percentile summer O_3 concentrations from 1988 to 1998 at some urban and rural sites in Switzerland, as well

at the mountain site of the Jungfraujoch (Switzerland, 3580 m asl) despite a negative trend of NO_x, VOCs, and CO concentrations. *Brönnimann et al.* [2000; 2002] reported that the deseasonalised daily and monthly mean values over the periods 1992-1998 and 1991-1999 increase in a number of rural or urban stations in Switzerland. *Logan et al.* [1999] found trends close to zero in the whole troposphere for two O_3 sounding over Europe (Uccle and Hohenpeissenberg) for the period 1980-1996 and *Pochanart et al.* [2001] reported no change in the average monthly mean O_3 between 1996-1997 and 1989-1991 at Arosa (Switzerland, 1840 m asl). The small or close-to-zero trends in O_3 observed at various sites in Europe, despite the reduction of local anthropogenic emissions, could indicate an increase in the background O_3 over Europe [*Collins et al.*, 2000; *Brönnimann et al.*, 2002].

In this paper, we use the three-dimensional (3-D) chemical transport model (CTM) GEOS-Chem to investigate the processes that contribute to long-range transport of O_3 into Europe. We focus our analysis on the contributions from North America (because of its direct influence on Europe [e.g., *Wild and Akimoto*, 2001; *Stohl et al.*, 2002]), and from Asia, which is expected to contribute the most significantly to global atmospheric changes in the coming decades [*IPCC*, 2001]. We use the model to establish a European O_3 budget and to examine its perturbations by long-range transport. We quantify how changes in O_3 precursor emissions contribute to changes in background and total O_3 over Europe. We focus on the period 1980–1997 over which Asian anthropogenic emissions significantly increased, and we examine to what extent the divergent trends observed over Europe for the last decades could reflect the superposition of various processes, including the decrease in local O_3 precursor emissions and the increase in O_3 transported from other continents.

4.2 Model Description and Simulations

4.2.1 The GEOS-Chem Model

The GEOS-Chem model (http://www-as.harvard.edu/chemistry/trop/geos/) [*Bey et al.*, 2001a] is a global 3-D CTM driven by assimilated meteorological observations provided by the Goddard Earth Observing System (GEOS) of the NASA Global Modeling and Assimilation Office (GMAO). The assimilated meteorological fields include winds, surface pressure, temperature, water content, cloud information, convective mass flux, and other surface properties, with a 3- or 6- hour temporal resolution, depending on the variable. The fields are provided with a horizontal resolution of 2° of latitude by 2.5° of longitude, and 48 sigma levels (up to 0.01 hPa) for the GEOS-STRAT version (December 1995 to 1997). They are degraded in this study to a 4° of latitude by 5° of longitude and to 26 levels for computational expediency. Here we used the 5-02 version of the GEOS-Chem model with some improvements as described below.

The chemical mechanism is based upon that of *Horowitz et al.* [1998] and includes 80 species and over 300 reactions with detailed photooxidation schemes for major anthropogenic hydrocarbons and isoprene. Heterogeneous reactions on aerosols

(sulfate, black carbon, organic carbon, sea salt and dust) are included, following recommendations from *Jacob* [2000]. The aerosol fields are provided by the Global Ozone Chemistry Aerosol Radiation and Transport (GOCART) model [*Chin et al.*, 2002] and are coupled to the GEOS-Chem model as described by *Martin et al.* [2003]. Photolysis frequencies in the troposphere are calculated with the Fast-J algorithm of *Wild et al.* [2000] which accounts for aerosols and clouds. The dry deposition is computed using a resistance-in-series model [*Wesely*, 1989]. The wet deposition, applied to HNO_3 and H_2O_2 follows *Liu et al.* [2001]. Transport of O_3 from the stratosphere is simulated using the Synoz method (synthetic ozone) proposed by *McLinden et al.* [2000], in which stratospheric O_3 is represented as a passive tracer that is released uniformly in the tropical lower stratosphere at a rate constrained to match a prescribed global mean tropopause O_3 flux. On average, we obtain a net stratosphere troposphere exchange of 450 $Tg.yr^{-1}$. The spatial and temporal (year-to-year) variability of the stratospheric O_3 column is accounting for by using the Total Ozone Mapping Spectrometer/Solar Backscatter Ultraviolet (TOMS/SBUV) merged total O_3 data sets. The year-to-year varying methane (CH_4) distributions are specified for each latitudinal band using the Climate Monitoring and Diagnostics Laboratory (CMDL) observations.

Anthropogenic emission inventories in the GEOS-Chem model are based on the NO_x emissions from the Global Emission Inventory Activity (GEIA) inventory [*Benkovitz et al.*, 1996], the nonmethane hydrocarbon emission inventory from *Piccot et al.* [1992], and CO emissions from *Wang et al.* [1998a]. We adjusted this base emission inventory of 1985 to specific years using scaling factors as described in *Bey et al.* [2001a]. In the present work, we used the year-specific European Monitoring and Evaluation Program (EMEP) database inventory for NO_x, CO and VOC over Europe, which significantly improves our simulation of O_3 precursors over Europe (not shown). Biomass burning emissions are from a climatological inventory described by *Wang et al.* [1998a] and its interannual variability is estimated using Along Track Scanning Radiometer (ATSR) fire-counts [*Duncan et al.*, 2003].

4.2.2 Simulations

To investigate the ability of the model to reproduce observations of key atmospheric compounds over Europe, we first conducted a simulation using assimilated meteorology for 1997 (hereafter called the standard simulation). We then conducted a number of sensitivity simulations to distinguish between different components of total O_3, including the hemispheric background and the anthropogenic contributions from Europe, Asia, North America and the rest of the world. In our study, the hemispheric background includes the stratospheric input and the contemporary (1997) O_3 produced by precursors from natural sources (e.g., soils, lightning, biosphere), from biomass burning, and from CH_4 oxidation. The hemispheric background is obtained from a simulation with all anthropogenic sources shut off, including NO_x, CO, and NMHC emissions from fossil fuel and biofuel combustion as well as NO_x from fertilizer and aircraft. The contributions of the main industrialised regions, i.e., North America (northward of 12°N, 132.5°W-62.5°W), Asia (northward of 12°S, 57.5°E-147.5°E), extended Europe (north-

ward of 36°N, 12.5°W-57.5°E) and the rest of the world are calculated by subtracting the results of the sensitivity simulations (with anthropogenic emissions of a given region turned off) from that of the standard simulation. The total background for Europe is thus the sum of the hemispheric background plus the different anthropogenic contributions except Europe. Each sensitivity run is initialised by a one-year simulation. We also conducted sensitivity simulations with anthropogenic emissions scaled for the years 1980 (but with contemporary hemispheric background), to quantify changes in total O_3 that could be attributed to changes in emissions.

The contribution of stratospheric O_3 is obtained by a tagged O_3 simulation following the methods proposed in *Wang et al.* [1998b] and *Fiore et al.* [2002]. Production and loss frequencies are archived from the standard simulation and are further used to drive an offline simulation in which total O_3 is divided into individual tracers produced in different regions of the atmosphere, including the stratosphere.

Table 4.1: Statistical quantities for CO and NO_2 model evaluation

	Observations CO	**Model CO**	**Observations NO_2**	**Model NO_2**
Mean	148.80	147.96	4.34	3.53
Standard deviation	55.00	54.24	2.60	3.05
Minimum	64.04	81.73	0.26	0.30
Maximum	383.72	442.50	14.02	12.68
Model Mean Bias	-0.85 (2.35%)		-0.81 (-17.62%)	
Model Absolute Mean Bias	22.51 (15.61%)		1.66 (42.90%)	
Correlation Coefficient (r^2)	0.63		0.52	

Statistical quantities for monthly mean NOAA/CMDL unfiltered CO data and monthly mean NO_2 sampled at EMEP stations with model monthly mean CO and NO_2 results for 1997 at the surface.

4.3 Model Evaluation of Ozone and Related Species over Europe

The model has been previously the subject of global [*Bey et al.*, 2001a] and more regionally-focussed evaluations, e.g., over the Pacific Rim [*Liu et al.*, 2002], the United States [*Fiore et al.*, 2002; *Li et al.*, 2002], the North Atlantic Ocean [*Li et al.*, 2002; 2004], and Europe [*Duncan and Bey*, 2004]. No obvious global bias was found for a number of species including O_3, CO, and nitrogen dioxide (NO_2), except that monthly mean O_3 shows a too low seasonal amplitude especially in the middle troposphere. In most of the cases, monthly mean CO were too low by 10 to 20 ppbv. Global NO_2 distributions in the model were also found to be in good agreement with the

NO_2 columns retrieved from Global Ozone Monitoring Experiment (GOME) except that the model underestimates the observations in some regions of the world (South Africa and industrial region of U.S. and Europe) [*Martin et al.*, 2002]. *Li et al.* [2004] evaluated the model over the western North Atlantic using observations from the North Atlantic Regional Experiment (NARE) campaign, and found that observed CO were usually overestimated by 10–20 ppbv in the boundary layer, while O_3 concentrations are well reproduced (within 5 ppbv at Sable Island). It was also reported that the nighttime depletion of surface O_3 (due to deposition and chemical loss in shallow boundary layer) is poorly reproduced in the model [*Fiore et al.*, 2002; *Li et al.*, 2002]. In this paper, we focus the model evaluation over Europe using observations for CO, NO_2 and O_3. Tables 4.1 to 4.3 present a number of statistical quantities computed between the model results and atmospheric observations, which allow us to better quantify our evaluation. Correlation coefficient (r^2) indicates the ability of the model to reproduce the seasonal cycle, while mean bias and absolute mean bias indicate whether the model tends to overestimate or underestimate the observed concentrations. We further evaluate the model in section 4.4.1 using observations available for two specific events of O_3 transport over the North Atlantic ocean and Europe.

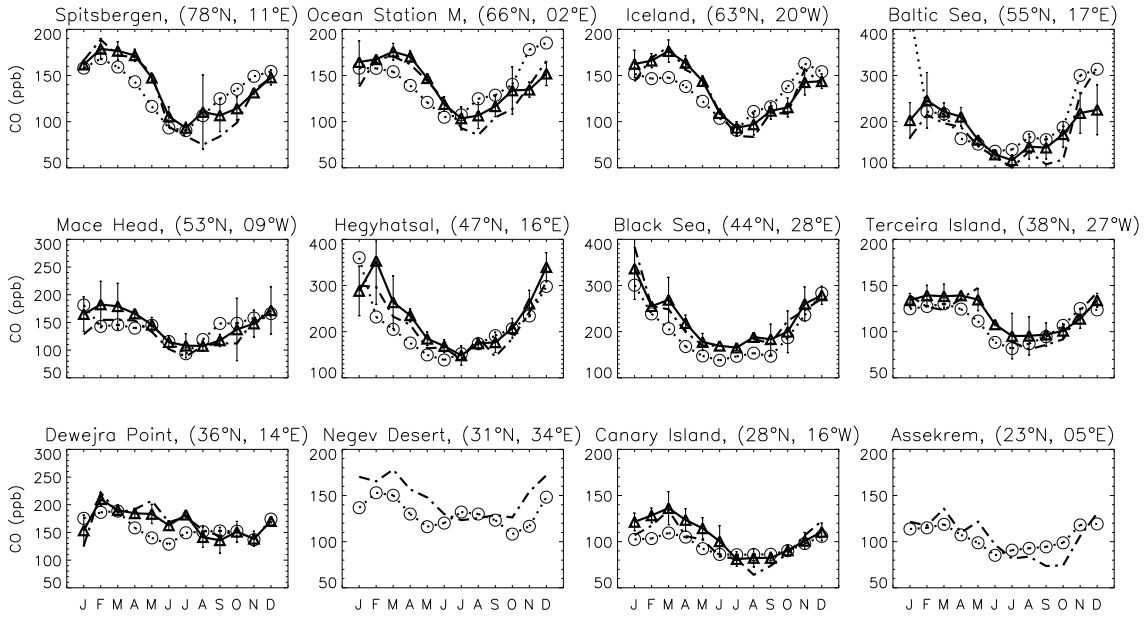

Figure 4.1: Comparison of monthly mean CO between the model results (open circles and dotted lines) and 1997 observed values (NOAA/CMDL unfiltered data: J. Logan, Harvard U., personal communication, 2003) (dot dashed lines) over Europe. Climatological observations (open triangles and solid lines) are from J. Logan (Harvard U., personal communication, 2003). Vertical bars are standard deviations of the climatological observations, corresponding to interannual variability. Note that the climatological observations are not available at the stations of Negev Desert and Assekrem.

4.3.1 Carbon Monoxide

Figure 4.1 compares monthly mean CO simulated by the model and observed from the cooperative National Oceanic and Atmospheric Administration (NOAA)/Climate Monitoring and Diagnostics Laboratory (CMDL) flask sampling program [*Novelli et al.*, 1992; *Jennifer Logan*, Harvard University, personal communication]. For the Negev Desert and Assekrem stations, only one observation is available per month. The model reproduces much of the observed seasonal variation at different sites (r^2=0.63) but the model CO concentrations tend to be too low in winter and spring by about 20 ppbv and too high in summer and fall by about 20 ppbv, resulting in a global absolute mean bias of 15% (Table 4.1). The simulated CO at the Baltic sea station is too high by 200 ppbv in January in comparison with the observed value. *Duncan and Bey* [2004] found however a much better agreement between the model and the observations at that site when the model is sampled in an adjacent box which appears to be more representative of the measurements taken at sea.

4.3.2 Nitrogen Dioxide

Monthly mean NO_2 simulated by the model and provided by EMEP are compared in Figure 4.2. At most of the sites, the model reproduces reasonably well the strong seasonal variation (r^2=0.52) but the low summer concentrations are usually severely underestimated by the model, resulting in a high mean bias of 43% (Table 4.1). Evaluation of NO_2 concentrations is made difficult by their great spatial and temporal variability. In addition, data quality issues should not be discarded, as NO_2 measurements appear to be too high for the low concentrations [*Barrett et al.*, 2000], especially for the German sites. This could partly explain the disagreements seen at the Brotjacklriegel and Schauinsland sites during the summer months.

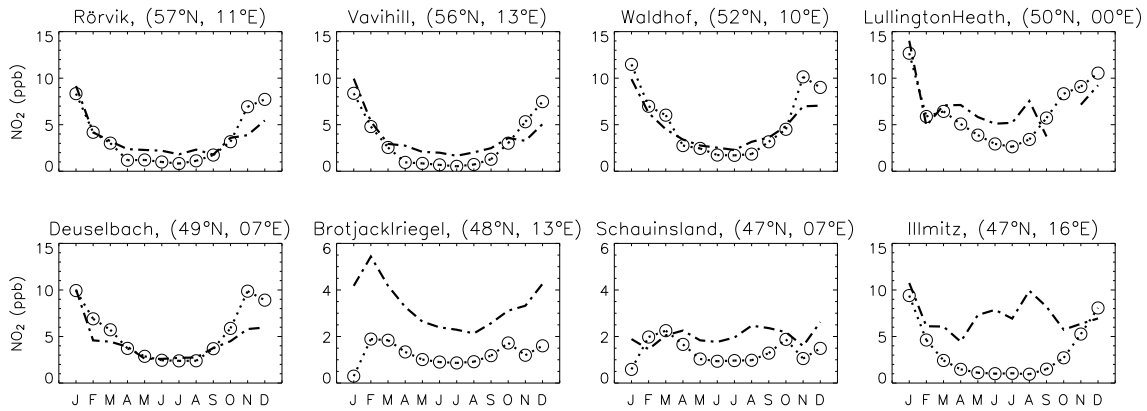

Figure 4.2: Observed (dot dashed lines) and simulated (open circles and dotted lines) monthly mean NO_2 concentrations for 1997 at 8 EMEP sites over Europe. Observations are from EMEP (http://www.nilu.no/projects/ccc/emepdata.html).

4.3.3 Ozone

O_3 distributions over Europe are evaluated using ozonesonde data [*Logan*, 1999], observations from the Measurement of Ozone by Airbus In-service Aircraft (MOZAIC) program [*Marenco et al.*, 1998; *Thouret et al.*, 1998] as well as surface measurements provided by EMEP. Figure 4.3 compares simulated and observed monthly mean O_3 concentrations at 8 sites over Europe at three different altitudes. The model reproduces poorly O_3 concentrations at the 300 hPa level (close to the tropopause) for the more northern stations (e.g., Ny Alesund and Sodankyla). The agreement between observed and model values improves in the upper troposphere for the sites further south, but the amplitude of the seasonal cycle is too weak. These discrepancies are likely due to a vertical resolution that is too coarse around the tropopause and a seasonal cycle that is too weak in the cross-tropopause flux in our model, as already noted by *Bey et al.* [2001a] and *Fusco and Logan* [2003]. The annual cross-tropopause flux (451 Tg $O_3.yr^{-1}$) is however in the range of other studies [*IPCC*, 2001]. Statistical quantities for the middle troposphere are relatively good (r^2=0.59 and absolute mean bias less than 5 ppbv, Table 4.2) but the model shows however a lack of seasonal cycle, and in some cases, underestimates the summer concentrations by 5 to 10 ppbv. The model reproduces well the seasonal cycle in the lower troposphere, including the low values observed in the summer in the northern sites and the large summer increase (especially in August) at the mid-latitude sites (r^2=0.49 and absolute mean bias less than 3.5 ppbv, Table 4.2).

Table 4.2: Statistical quantities for O_3 model evaluation at three different levels

O_3	850-800		550-500		350-300	
	Obs	**Model**	**Obs**	**Model**	**Obs**	**Model**
Mean	44.90	45.64	54.94	51.97	67.83	70.70
Standard deviation	6.64	5.82	7.53	3.56	15.57	6.81
Minimum	30.65	36.20	42.67	45.79	45.22	59.21
Maximum	58.92	58.42	70.19	58.52	127.13	89.35
Model Mean Bias	0.74 (2.63%)		-2.96 (-4.32%)		2.87 (7.74%)	
Model Absolute Mean Bias	3.41 (8.07%)		4.77 (8.16%)		10.44 (15.82%)	
Correlation Coefficient (r^2)	0.49		0.59		0.33	

Statistical quantities are between observed (ozonesonde data and MOZAIC data) and simulated monthly mean O_3 concentrations, for the 7 stations in Europe which have observations for 1997. Model results and observations are used at 800, 500 and 300 hPa for ozonesonde and at 850, 550 and 350 hPa for MOZAIC.

Simulated O_3 is also evaluated at a mountain site (Jungfraujoch, 3580 m asl) with a higher temporal resolution. Figure 4.4 compares the hourly timeseries obtained at the Jungfraujoch from the National Air Pollution Monitoring Network (NABEL) with model results. The mean value is simulated correctly (49 ppbv for the model and 51 ppbv for the observations), but the maximum and minimum concentrations are usually

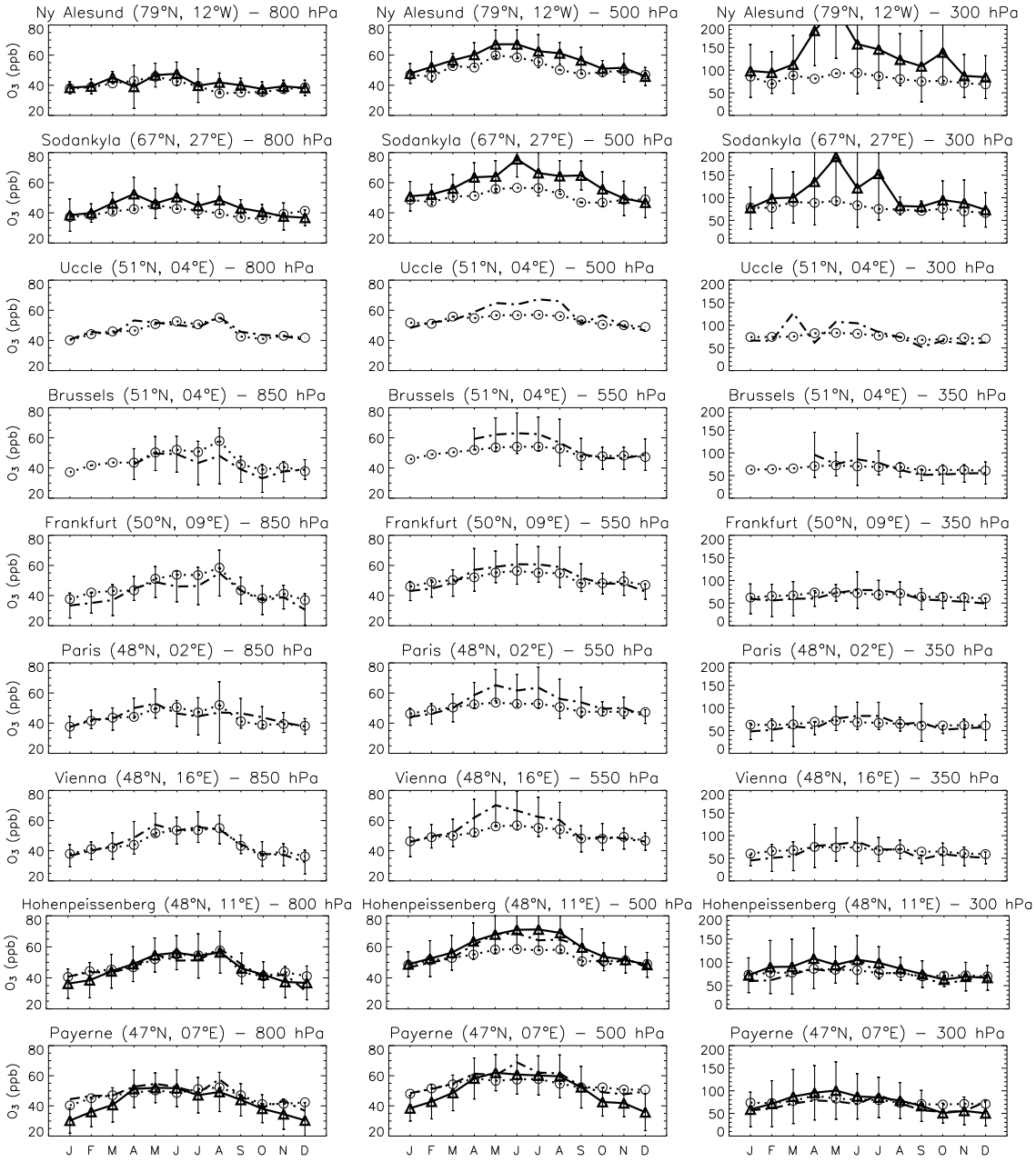

Figure 4.3: Comparison of observed and simulated monthly mean O_3 concentration over Europe. Observed values at Ny Alesund, Sodankyla, Uccle, Hohenpeissenberg and Payerne, sampled at 800, 500 and 300 hPa are from *Logan et al.*, [1999], and observed values at Brussels, Frankfurt, Paris and Vienna, sampled at 850, 550 and 350 hPa are from MOZAIC. Open circles and dotted lines: model values for 1997. Dot dashed lines: observed value for 1997. Open triangles and solid lines: climatological observations [*Logan et al.*, 1999, *Thouret et al.*, 1998]. For ozonesondes, vertical bars are standard deviations of the climatological observations, corresponding to interannual variability (not available for Uccle station). For MOZAIC, the vertical bars are standard deviations and represent daily variability.

not too well represented. This may be related to the too coarse resolution of the model (4°x5°) which makes it difficult to capture the specific meteorology at a mountain site: the Jungfraujoch is often located within the boundary layer in summer, while model results are sampled in the free troposphere. That results in a relatively poor correlation (r^2 of 0.34), and a mean absolute bias of 6.2 ppbv (12.7%).

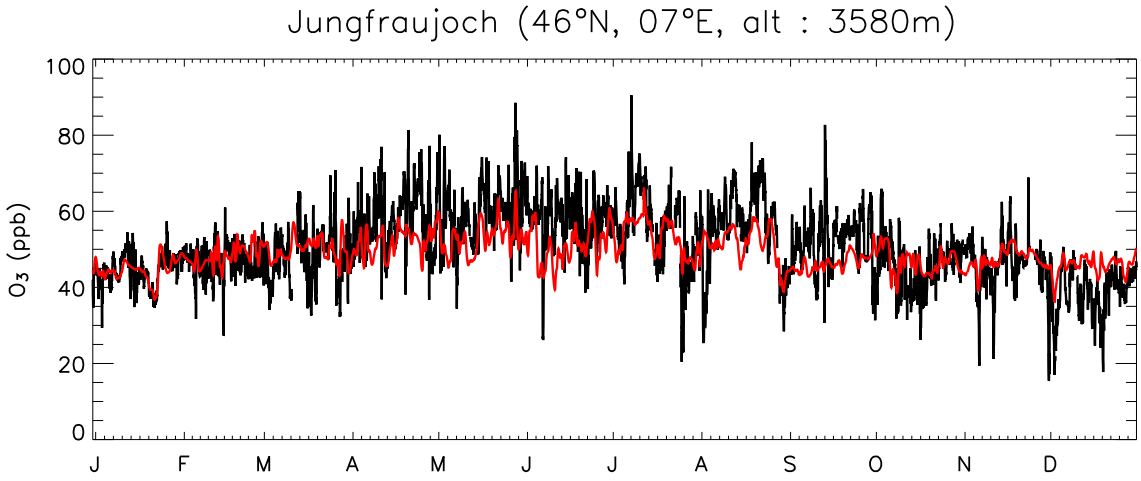

Figure 4.4: Seasonal variation of hourly O_3 at the Jungfraujoch station in 1997. Model results (red lines) are compared to observations (black lines). Observations are from the National Air Pollution Monitoring Network (NABEL).

Table 4.3: Statistical quantities for O_3 model evaluation at the surface

	Monthly Afternoon average O_3		Daily Afternoon average O_3	
	Obs	**Model**	**Obs**	**Model**
Mean	36.05	35.67	44.73	49.98
Standard deviation	11.77	13.49	15.31	11.06
Minimum	7.15	3.78	9.0	21.09
Maximum	62.16	63.72	94.0	81.97
Model Mean Bias	-0.38 (-2.43%)		5.25 (20.04%)	
Model Absolute Mean Bias	4.19 (13.12%)		8.96 (26.19%)	
Correlation Coefficient (r^2)	0.84		0.56	

Statistical quantities between EMEP data and model results for 1997 for monthly afternoon average O_3 concentrations and for daily afternoon average O_3, over June, July and August.

Simulated O_3 concentrations are further evaluated at the surface using observations from EMEP (Figure 4.5). We used monthly afternoon averages for both model and observed data because the model does not resolve correctly the nighttime depletion as mentioned previously. The seasonal variations are well reproduced by the model at most of the sites (r^2=0.84, Table 4.3). The model however overestimates the observed concentrations at some sites in summer (by up to 10 ppbv). This is seen particularly

at some coastal sites (e.g., Yarner-Wood) where NO_x dilution within the model grid box would be critical. The absolute mean bias remains however only of about 4 ppbv (13%).

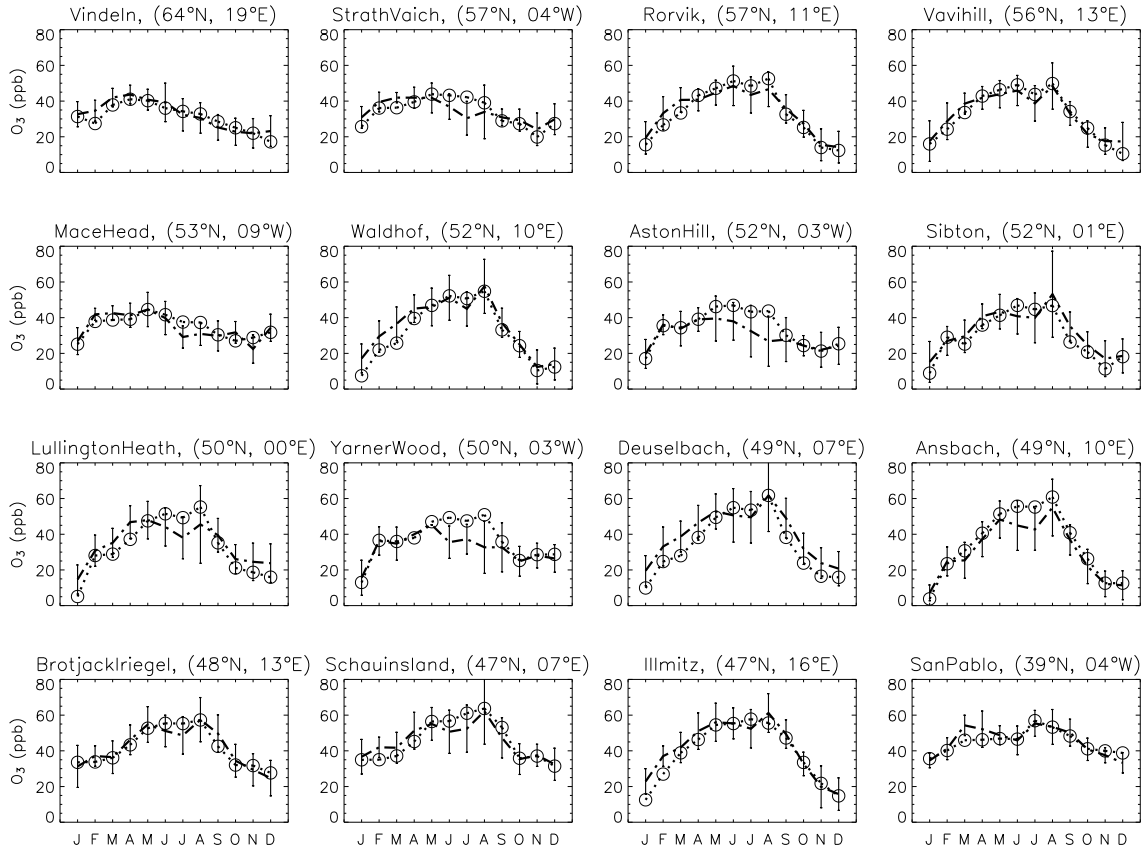

Figure 4.5: Seasonal variation of monthly afternoon average O_3 for a number of EMEP stations in 1997. Model results (open circles and dotted lines) are compared to observations (dot dashed lines) (EMEP: http://www.nilu.no/projects/ccc/emepdata.html). Vertical bars correspond to the standard deviation, and represent the daily variability.

We then proceed to a comparison of the daily afternoon average during the summer period (June-July-August) to determine the abilities of the model to reproduce O_3 during photochemical episodes. Figure 4.6 presents comparison of daily afternoon averages of surface O_3 at different EMEP stations over Europe for the year 1997 from June to August, obtained by the model simulation and provided by the EMEP network. Most of the photochemical events are captured by the model (r^2=0.56), but the model does not capture the lowest O_3 concentrations. This leads to a mean bias of about 5 ppbv (20%) (Table 4.3).

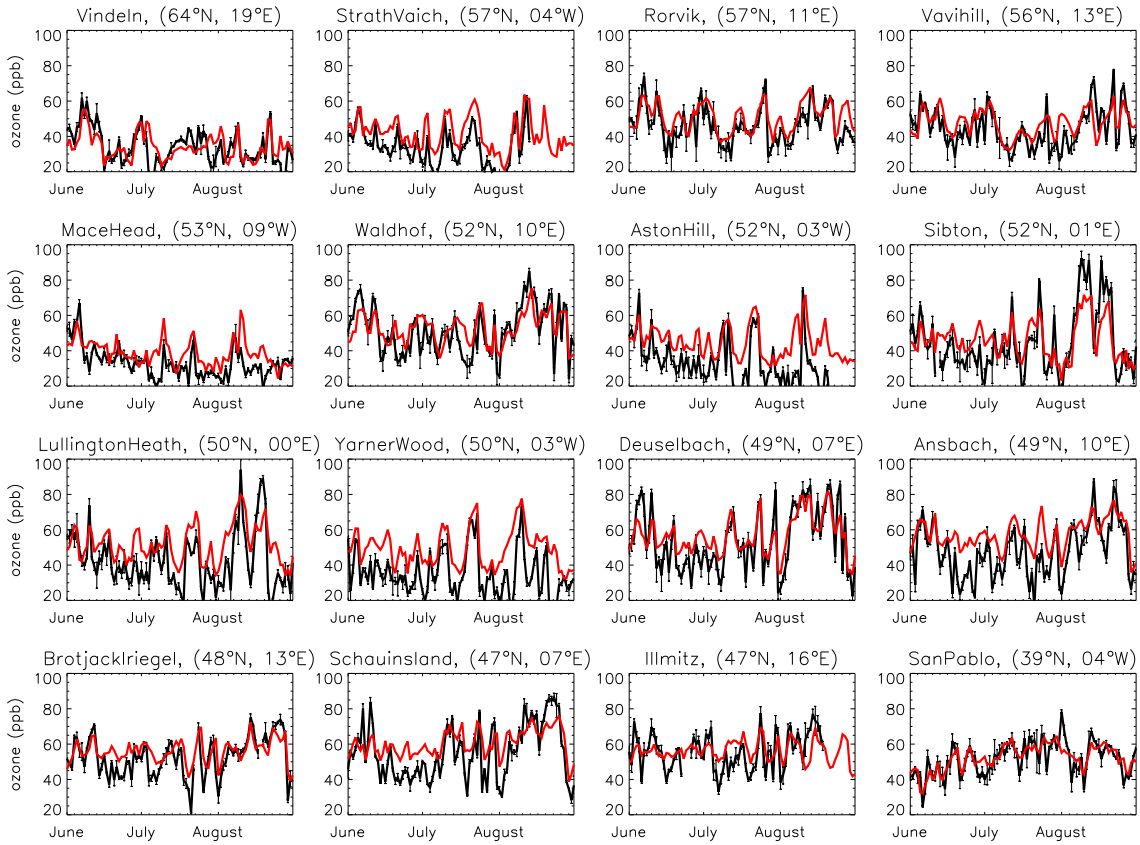

Figure 4.6: Photochemical episodes (afternoon-daily average O_3) during the summer months (June-July-August) for a number of EMEP stations in 1997. Model results (red lines) are compared to observations (black lines) (EMEP: http://www.nilu.no/projects/ccc/emepdata.html). Vertical bars are the standard deviation and represent the afternoon-hourly variability.

4.4 Long-Range Transport from North America to Europe

4.4.1 Export from the North American boundary layer and transport across the Atlantic

The transport associated with mid-latitude cyclones is now recognized as a major pathway for pollution export from the North American boundary layer [*Stohl and Trickl*, 1999; *Cooper et al.*, 2001; 2002; *Stohl*, 2001; *Trickl et al.*, 2003]. In particular, two specific airstreams that compose the mid-latitude cyclones, the warm conveyor belt (WCB) (a rising air mass ahead of the cold front) and the post cold front (PCF) airstream (a low level airstream running behind the cold front) have been shown to contribute to pollution transport [*Cooper et al.*, 2002]. The other important process that ventilates the boundary layer is deep convection [*Thompson et al.*, 1994; *Horowitz et al.*, 1998; *Li et al.*, 2005] which injects air directly and quickly from the surface to

the free troposphere.

Once out of the North American boundary layer, the pollution follows the general circulation over the North Atlantic area which is mainly determined by the strength and position of the Azores High and the Icelandic Low (Figure 4.7). In general, in winter and spring, the westerly flow is mostly zonal out of North America, but it turns anticyclonically before reaching the continent (Figures 4.7a and 4.7c). The pollution path presents thus a curved shape over the North Atlantic ocean, as already mentioned in previous studies (e.g., *Trickl et al.*, [2003]). By late spring-early summer (Figure 4.7e), the Icelandic low weakens while the Azores High expands and move northwards. The westerlies decrease in strength throughout the column in summer (Figures 4.7e and 4.7f). Part of the flow actually turns anticyclonically around the Azores High and goes back towards North America before reaching Europe, especially at lower levels (Figure 4.7e). In the upper levels (350 hPa), the westerlies still run quickly across the Atlantic, but they can reach Europe at lower latitudes than in winter and spring (Figures 4.7b and 4.7d).

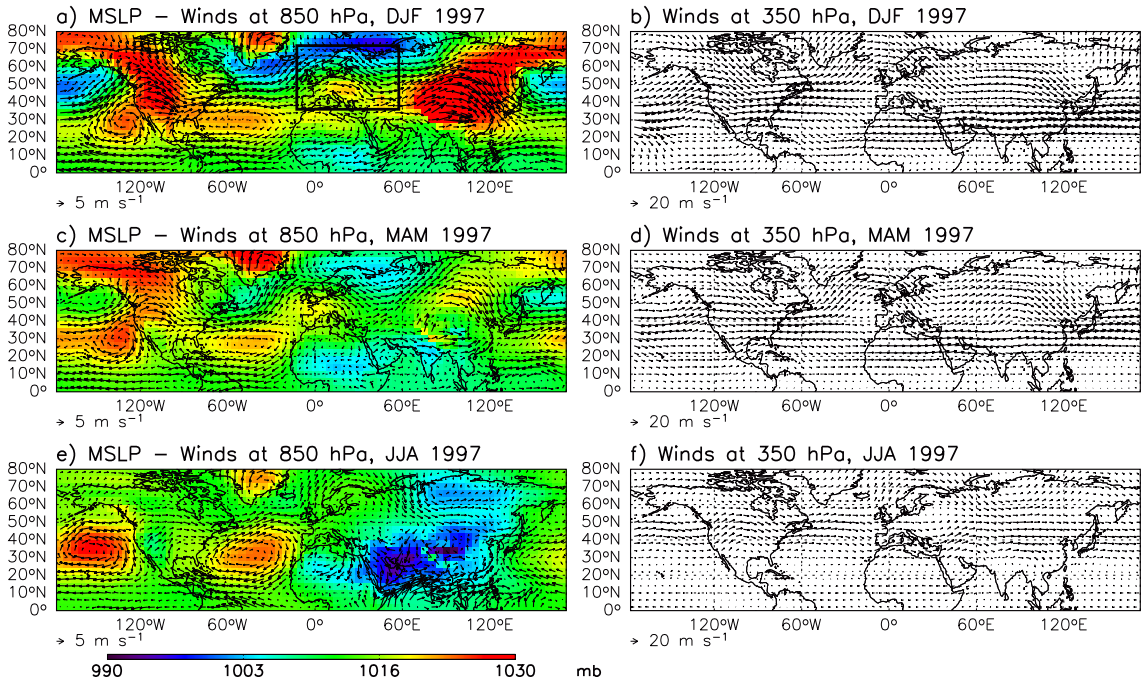

Figure 4.7: Mean sea level pressure (MSLP) and winds at 850 hPa and 350 hPa averaged for winter (DJF), spring (MAM) and summer (JJA) 1997 over the North Hemisphere. The black box represents the European domain in which we examine the O_3 budget (see Section 4.6).

4.4.2 Simulation of Episodic Pollution Transport Events

Ozone transport over the eastern North Atlantic

A first examination of the ability of the model to reproduce episodic transport events over the North Atlantic is conducted using observations from the Atmospheric Chemistry Studies in the Oceanic Environment (ACSOE) campaign. The ACSOE campaign took place in April and in September 1997 over the eastern North Atlantic. The C-130 UK Meteorological Office aircraft (based at the Azores) captured several transatlantic transport events [*Reeves et al.*, 2002; *Penkett et al.*, 2004]. On one of these flights (14^{th} of September), the aircraft flew south of the Azores, then turned west to intercept the outflow of hurricane Erica from 16 UTC onward, before flying back to the Azores (Figure 4.8b). Enhanced O_3 concentrations (up to 90 ppbv) were observed between 5 and 6 km (Figure 4.8b) and backtrajectory analysis indicated that these polluted air masses were uplifted by a frontal system over North America 3 to 6 days earlier [*Penkett et al.*, 2004].

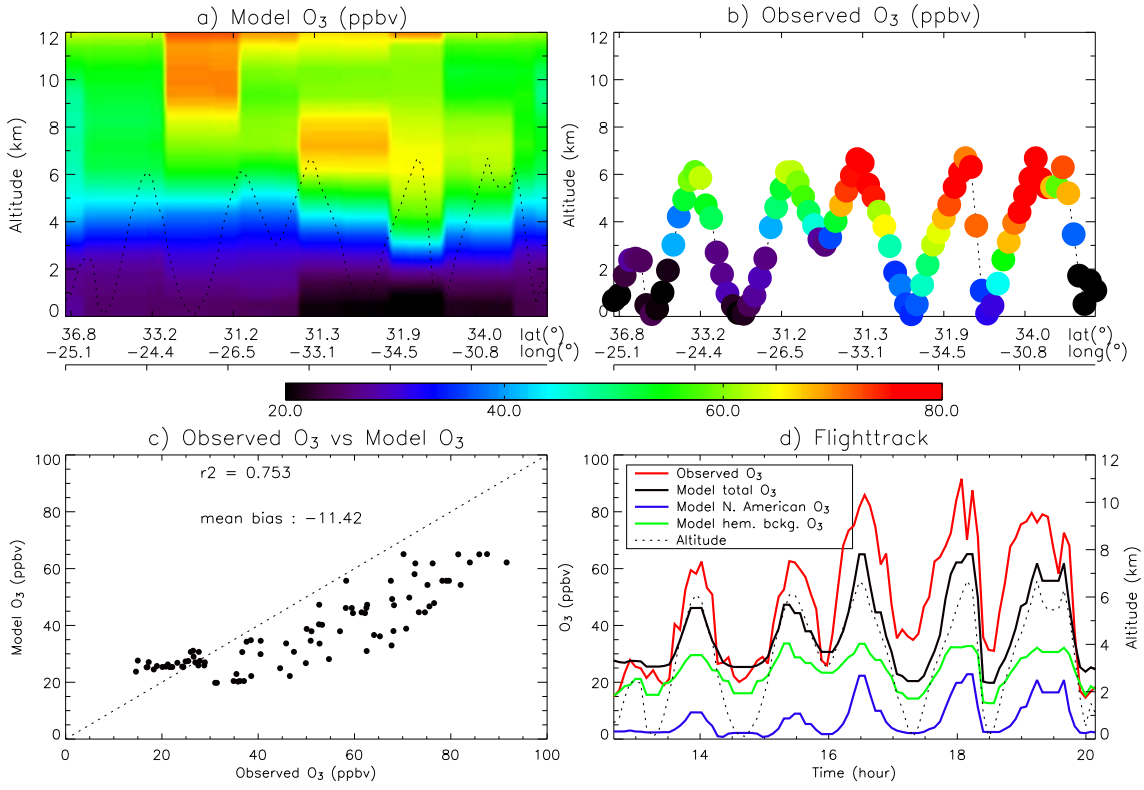

Figure 4.8: Model (a) and observed (b) O_3 (ppbv) along the flight track of the C-130 UK Meteorological Office aircraft on September 14^{th} during the ACSOE campaign over the North Atlantic ocean. The aircraft measurements are 5-minutes averages. (c) Correlation between observed and model O_3. (d) Timeseries along the flight track of observed O_3 (red), model total O_3 (black), hemispheric background O_3 (green), and North American O_3 (blue).

The model underestimates O_3 by about 10 ppbv (Figure 4.8c and 4.8d), but reproduces quite well the variations along the flight track (r^2=0.75). The model total O_3 is enhanced by 20 ppbv between 6 and 8 km from 16 UTC onward, reaching up to 65 ppbv. We find that the simulated hemispheric contribution remains constant at this altitude and at this time, while the North American contribution increases up to 20 ppbv. The model O_3 enhancement is thus mostly due to an increase in North American O_3, consistently with the backtrajectory analysis.

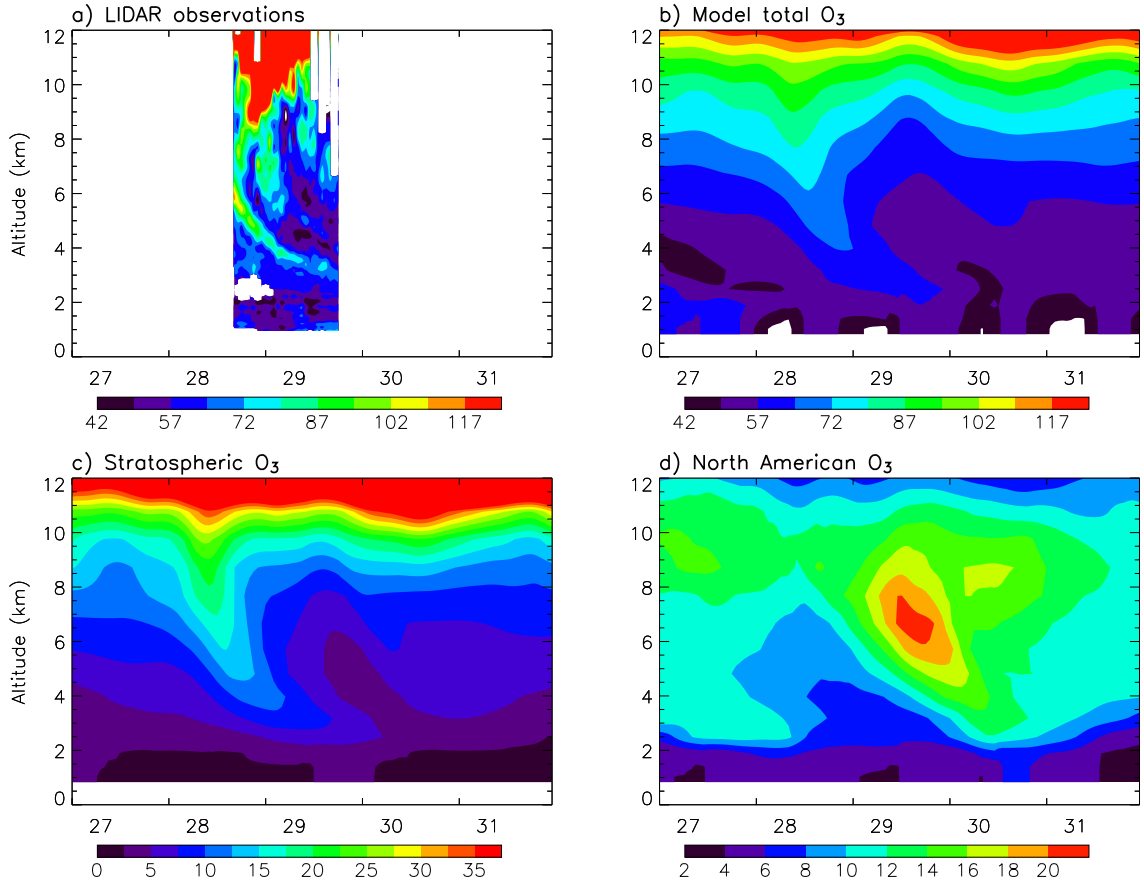

Figure 4.9: Hourly O_3 timeseries as function of altitude at Garmisch Partenkirchen (47°N, 11°E), Germany, for 27-31 May 1997. Lidar measurements of O_3 (ppbv) are from the 28 of May at 16 UTC to the 29 of May at 18 UTC [T. Trickl, personal communication]. White area corresponds to cloud layers, for which no data have been obtained. Model results for total O_3, stratospheric O_3 and North American O_3 are also shown. Units are in ppbv.

Ozone import into the European upper troposphere

We examine here an episode of elevated O_3 levels observed in the free troposphere over Europe [*Stohl and Trickl*, 1999]. The 1997 May 28-29 episode is illustrated in Figure 4.9a that shows a 26-hour record of O_3 concentrations taken by a high-resolution lidar

at Garmisch-Partenkirchen in Germany. The lidar observations show the presence of a thin O_3 tongue of about 65 to 110 ppbv of stratospheric origin that penetrated deeply into the troposphere as far down as 3 km over the course of 28 and 29 May [*Stohl and Trickl*, 1999]. This stratospheric intrusion leads to the O_3 peak of about 80 ppbv observed at the Jungfraujoch on May 28 and 29 (Figure 4.4). Figure 4.9a also shows the presence of pockets of high O_3 concentrations (up to 80 ppbv) at 00 UTC between 6 and 8 km and between 07 and 12 UTC at 8 km on May 29. Air trajectory calculations performed by *Stohl and Trickl* [1999] revealed that these elevated O_3 concentrations were produced in the North American boundary layer and were subsequently lifted to the free troposphere through a WCB ahead of a cold front and transported to the European free troposphere.

Figure 4.9b shows that the model reproduces the enhanced O_3 concentrations on May 28–29 in the upper and middle troposphere. Even though the presence of high O_3 pockets is not evident in the simulated total O_3 concentrations at high altitudes, tagged O_3 and sensitivity simulations clearly reveal that both stratospheric and North American contributions are also found in our model. Figure 4.9c shows the concentration of stratospheric O_3 as simulated by the model over the period May 27-31, and an O_3 tongue is clearly seen from May 28 to May 29 that descends down to 3 km, although it is thicker and presents lower concentrations than in the observed data. On May 29, the model shows a pocket of O_3 concentrations originated from North America (Figure 4.9d), with concentrations as high as 20 ppbv and located above the stratospheric tongue between 6 and 8 km, similar to that described in *Stohl and Trickl* [1999]. One should note that the arrival of the high North American concentration is delayed by 16 hours in the model, in comparison with the observed data.

4.4.3 Seasonal Variation of North American Ozone Entering Europe

We further extend our analysis of long-range transport to a one-year period by examining the O_3 mass fluxes from North America entering Europe through the western, northern and southern European boundaries, as diagnosed by the model sensitivity simulations (Figure 4.10a; see Figure 4.7a for the definition of the European domain). North American O_3 enters Europe mainly through its western side, but also, to some extent, through the northern boundary because of the anticyclonic curvature of the flow reaching Europe (see Section 4.4.1). The May episode (Section 4.4.2, second part) is shown with a black arrow. The September episode (Section 4.4.2, first part) is not visible in these fluxes as the pollution was entrained around the Azores high towards North Africa, avoiding continental Europe.

North American O_3 enters Europe all-year round but with a strong seasonality, reflecting the seasonality of both the photochemical activity and the transport pathways. *Stohl* [2001] reported that the WCB originate from the eastern seaboard of North America all-year round, but their frequency is higher in winter, spring and fall than in summer. The smaller O_3 fluxes in winter and early spring are due to the lower O_3

production and thus reflect predominantly the strength of the winds.

North American O_3 enters Europe throughout the column in spring while it is restricted to higher altitudes in summer because of a greater chemical loss in the marine boundary layer in summer. In general, low-level transport only contributes to a small extent to the import of O_3 into Europe, as winds are weaker and that O_3 is efficiently destroyed in the marine boundary layer due to higher water vapour and dry deposition [*Fehsenfeld et al.*, 1996].

The highest O_3 fluxes are seen in the middle and upper troposphere between 8 and 12 km in late spring and summer (Figure 4.10a). These high altitude fluxes are due to deep convection which lifts pollutants higher than the WCB, as diagnosed by a sensitivity run. Deep convection is especially important in summer over the central and south-eastern United States (*Li et al.*, [2005]). In addition to this shift in altitude between spring and summer, a seasonal shift in the latitudinal distribution of the O_3 fluxes entering the western side of Europe is also observed in our model (Figure 4.11). In spring, O_3 fluxes are at a maximum around 50 to 60°N (because of the anticyclonic curvature of the flow reaching Europe), while the summer O_3 fluxes are at a maximum around 40°N, thus having a stronger effect on the Mediterranean basin.

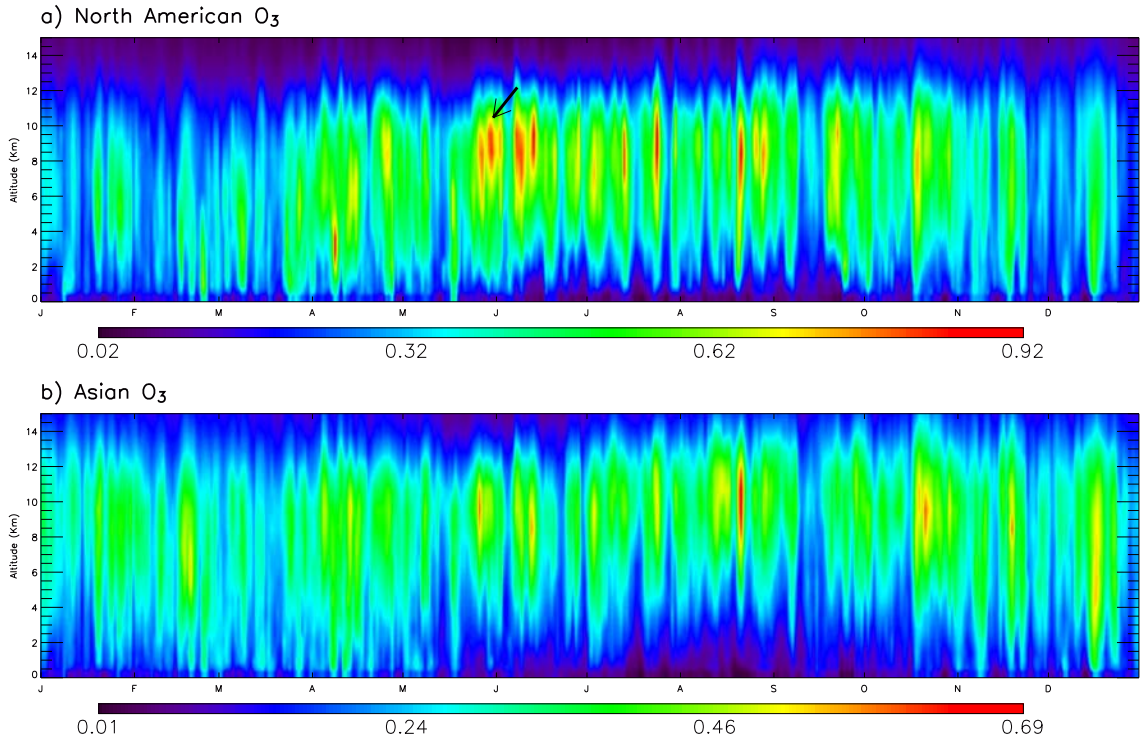

Figure 4.10: Daily timeseries of North American and Asian O_3 fluxes entering the west, north and south side of Europe for the year 1997 (coordinate of the European box: 36°N-72°N, 12.5°W-57.5°E, c.f. Figure 4.7). Note that the scale is different for North American and Asian O_3 fluxes. Units are in 10^4 mol.cm^{-2}.day^{-1}. The black arrow represents the episode of the 29^{th} of May 1997.

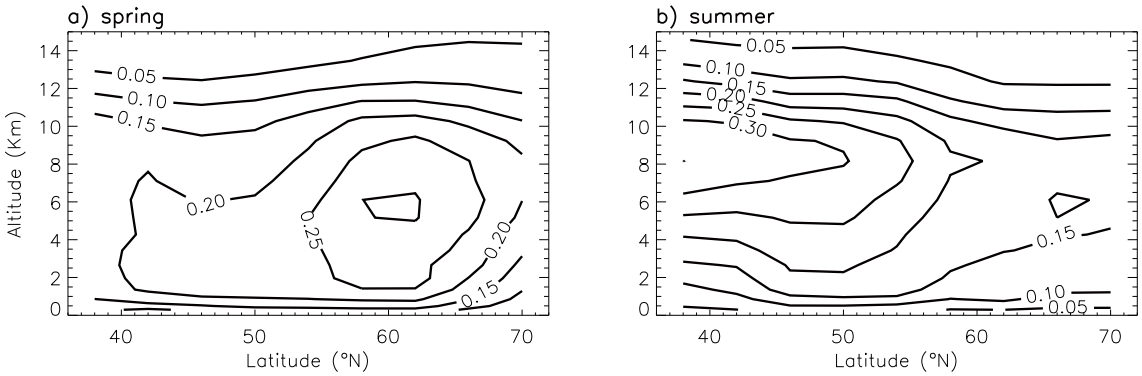

Figure 4.11: Seasonal North American O_3 fluxes entering the west side of Europe (12.5°W) in spring and summer 1997. Units are in 10^4 mol.cm^{-2}.day^{-1}.

4.5 Long-Range Transport from Asia to Europe

Pollution export from Asia has been well documented by several aircraft experiments and modeling studies, such as the recent Transport and Chemical Evolution over the Pacific (TRACE-P) campaign [*Jacob et al.*, 2003]. Similar to that found for North America, both convection [*Folkins et al.*, 1997; *Newell et al.*, 1997; *Bey et al.*, 2001b; *Liang et al.*, 2004; *Cooper et al.*, 2004] and mid-latitude cyclones [*Carmichael et al.*, 1998; *Yienger et al.*, 2000; *Hannan et al.*, 2003; *Liu et al.*, 2003; *Liang et al.*, 2004] contribute to pollution export from the Asian boundary layer. Orographic lifting have also been reported as a significant pathway [*Hannan et al.*, 2003; *Liu et al.*, 2003]. The Asian pollution is then entrained in the general westerly flow around the globe and may have been observed as far as over the North Atlantic region [*Reeves et al.*, 2002; *Penkett et al.*, 2004].

In addition, the Mediterranean Intensive Oxidant Study (MINOS) aircraft experiment recently pointed out another export process that directly affects Europe [*Lelieveld et al.*, 2002]. From the end of May to the end of August, a warm upper tropospheric anticyclone forms at around 450 hPa over the Tibetan plateau due to its heating after the winter period [*Barry and Chorley*, 2003]. This leads to an upper easterly current (Figure 4.12a), delimited by the Intertropical Convergence Zone (ITCZ) at the south end of the Tibetan plateau. These strong easterlies extented westward across South Arabia and Africa and overlay the southwest monsoon winds of the lower troposphere. During MINOS, pollution with an Asian origin was frequently found as far as the Mediterranean Basin in the upper troposphere and even in the lower stratosphere [*Lawrence et al.*, 2003; *Scheeren et al.*, 2003; *Roelofs et al.*, 2003; *Traub et al.*, 2003].

Figure 4.10b shows the timeseries of daily Asian O_3 mass fluxes entering Europe through its west, south and north sides. Asian O_3 fluxes are imported into Europe all year-round. The Asian O_3 fluxes present a strong seasonal variation with a maximum in summer, especially at high altitude (8 to 12 km). Those high-altitude fluxes reach Europe through its southern boundary in the Mediterranean basin and are associated

with the monsoon easterly winds as described previously (Figure 4.12b). The enhanced convection over Asia injects the pollution in the free troposphere [*Scheeren et al.*, 2003], which explains the high altitude (between 8 km and 12 km) of O_3 Asian fluxes simulated in the summer period (Figure 4.10b).

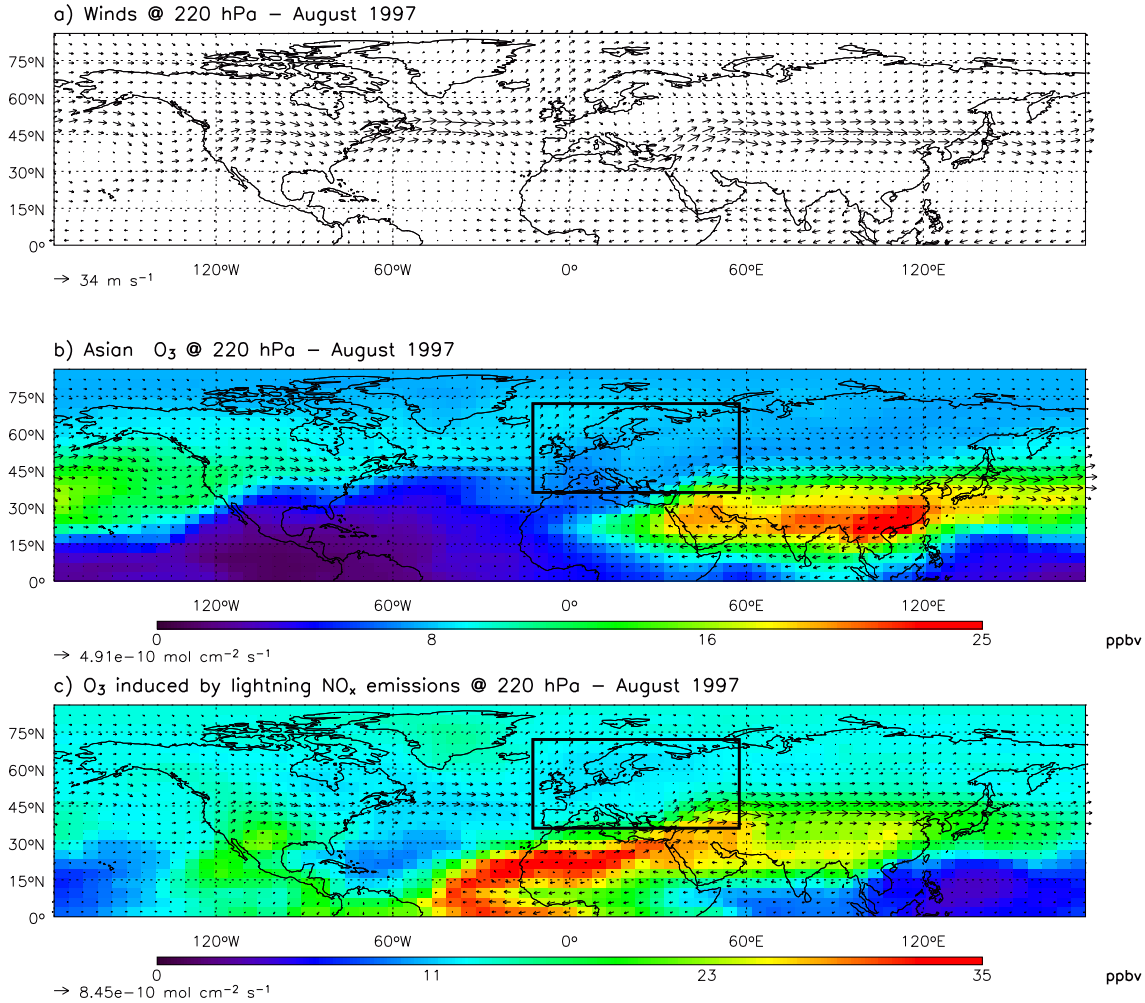

Figure 4.12: a) Model winds at 220 hPa for August 1997; b) Asian O_3 concentration (ppbv) and fluxes (mol.cm^{-2}.s^{-1}); c) O_3 concentration (ppbv) and fluxes (mol.cm^{-2}.day^{-1}) induced by lightning NO_x emissions.

Convection during the monsoon season is accompanied by thunderstorms and leads to a high source of NO_x from lightning, particularly along the ITCZ [*Christian and Latham*, 1998; *Nesbitt et al.*, 2000; *Li et al.*, 2001]. By conducting a sensitivity run in which we isolate the role of lightning emissions, we find several events during the summer period in which O_3 due to lightning is clearly linked to the enhanced convection and winds system associated with the monsoon. Figure 4.12c presents those concentrations and fluxes averaged for August. O_3 produced by lightning emissions is at a maximum along the ITCZ and at the east of the Tibetan plateau, and is then transported towards Europe by the easterly upper tropospheric winds.

4.6 Tropospheric O_3 Budget over Europe

In this section, we define O_3 as the extended odd oxygen family ($O_x = O_3 + NO_2 + 2NO_3 + PANs + HNO_4 + HNO_3 + 3N_2O_5$). We will refer to O_x as O_3, since O_3 usually accounts for 99% of O_x. The European O_3 budget calculated with the model is given in Table 4.4. Figure 4.13 shows the seasonal variations of the different processes contributing to the European budget for the boundary layer and for the whole troposphere. Positive values correspond to a source for the given region. We also examine the O_3 budget over Europe by dividing total O_3 into different components (Figure 4.14), as diagnosed with model sensitivity simulations. Interpretation of the different contributions to total O_3 requires caution because of the non-linear chemistry involved in O_3 production. We find that, averaged over the whole European troposphere, the sum of the O_3 components does not differ from the total O_3 burden (obtained from the standard simulation) by more than 7% in summer and by 4% in winter. The difference is maximal in the boundary layer in summer and can reach up to 10% in June. The non-linearity in O_3 burden is smaller when averaged globally, as the sum of the components does not differ annually by more than 2%. The one-year averaged sums of production and loss rates of individual contributions do not differ from the total O_3 production and loss rates by more than 9% and 4%, respectively for the European troposphere, and by more than 2% and 1.6%, respectively on a global scale.

4.6.1 Chemical production and deposition

Net O_3 production occurs over Europe all year round (Figure 4.13) accounting for a total of about 105 Tg O_3.yr^{-1} (Table 4.4), and is mainly due to European precursors. Net O_3 production is more efficient in the boundary layer (due to the proximity of European precursors) and reaches a maximum in summer. This is consistent with the expected increase in summertime photochemical production and vertical extend of the boundary layer. Deposition accounts for a total of 100 Tg.yr^{-1} and is also at a maximum in summer, following the seasonal variation of chemical production. About half of this process is due to deposition of European O_3 and the other half is due to the deposition of the total background O_3.

4.6.2 Transport

Horizontal fluxes of total O_3 over the European domain, in the whole troposphere, tend to act as a source (sink) of O_3 for Europe in winter (summer) (Figure 4.13). They present a high variability, also reported by *Laurila* [1999] in Northern Europe, due to the high variability of the horizontal transport of hemispheric background O_3. As expected, the fluxes through the western and northern boundaries act as a source for total O_3, while those through the eastern and southern boundaries act as sink (Table 4.4). Horizontal advection has a larger impact in the free troposphere as winds are stronger. Throughout the tropospheric column, European O_3 is exported all year

Table 4.4: European budget for tropospheric O_x in the GEOS-Chem model

	Europe [1]	
	Boundary layer [2]	Troposphere [3]
Sources (Tg O_x.yr^{-1})		
Chemical production	167.4	206.0
Horizontal advection	195.7	972.9
West	175.2	857.1
North	20.5	115.8
Vertical non convective transport [4]	22.8	56.2
Vertical convective transport [5]	12.8	-
Total	398.7	1235.1
Sinks (Tg O_x.yr^{-1})		
Chemical loss	81.0	100.8
Deposition [6]	100.0	100.4
Horizontal advection	228.1	989.8
East	185.8	934.9
South	42.3	54.9
Total	409.1	1191.0
Burden (Tg O_x)	5.8	13.8

[1]The budget is for the extended odd oxygen family defined as O_3 + NO_2 + $2NO_3$ + PANs + HNO_4 + HNO_3 + $3N_2O_5$ and is calculated over the European region (36°N-72°N, 12.5°W- 57.5°E). Values are annual mean for 1997. [2]The boundary layer is taken from the surface up to 600 hPa (4.1 km). [3]The troposphere is taken from the surface to the tropopause. [4]Vertical transport corresponds here to non-convective transport associated with subsiding air for the boundary layer and with transport from the stratosphere for the whole troposphere. [5]Vertical transport corresponds here to convective downdraft from the free troposphere to the boundary layer. [6]The deposition term includes both dry deposition on the ground and wet deposition of O_3-related species (e.g., HNO_3), therefore it is slightly higher in the whole troposphere than in the boundary layer.

round, while North American and Asian O_3 are imported all year round. North American horizontal O_3 fluxes are greater than the Asian ones because North American sources are closer to Europe. We can note that, as discussed in the previous section, transport of North American and Asian O_3 through the southern boundary acts as a source, especially in summer. Total O_3 mass horizontal fluxes act as a net sink in the boundary layer; although North American and Asian O_3 are imported all year-round, they do not compensate the export of European O_3. European horizontal (advective) fluxes are higher in the boundary layer than in the free troposphere, as already noticed by *Wild et al.* [2004] and present a maximum in summer. *Duncan and Bey* [2004] showed that the major pathways for pollution export in summer is towards Russia and the Mediteranean Basin/North Africa.

Vertical transport includes convective processes (when O_3-rich air is transported

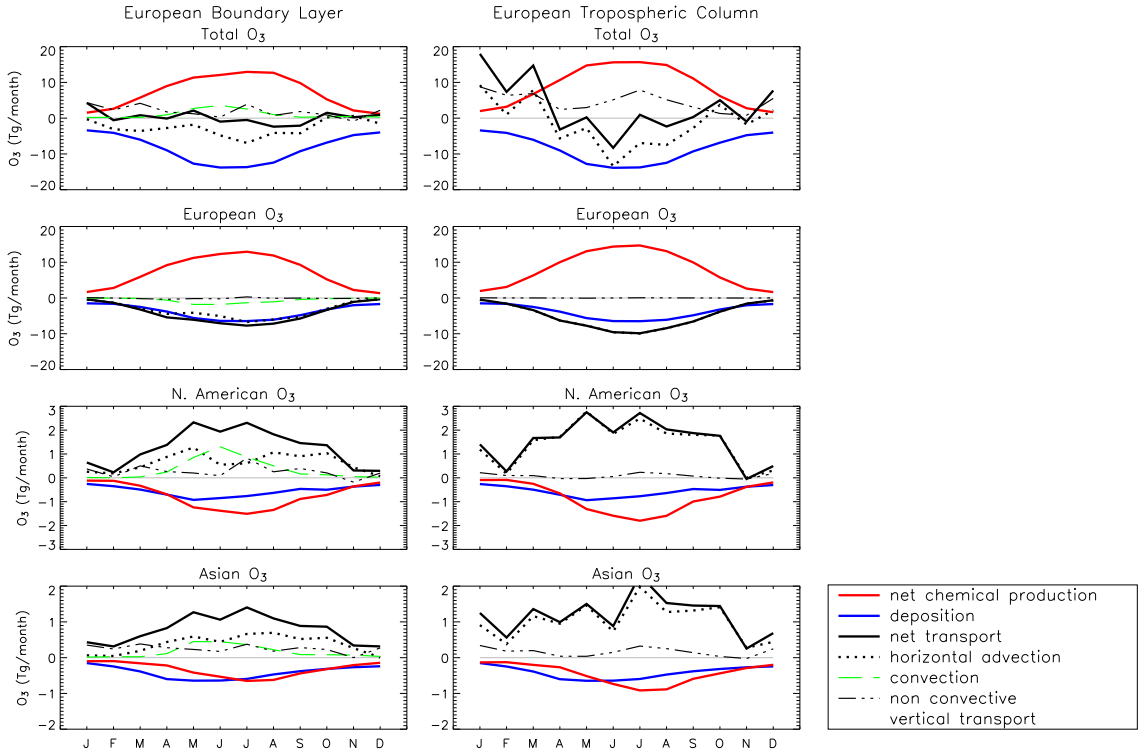

Figure 4.13: Seasonal variation of the processes contributing to the European tropospheric O_3 budget for 1997 in the boundary layer (from the surface to 600 hPa), and throughout the tropospheric column (from the surface to the tropopause) for total O_3, European, North American and Asian O_3. Net transport corresponds to the sum of all O_3 fluxes integrated over the 4 vertical boundaries and the top of the region. Advective horizontal fluxes are net fluxes through the 4 vertical boundaries of Europe. Non-convective vertical flux corresponds to the flux exchanged between the boundary layer and the free troposphere for the "boundary layer" domain and to the net stratospheric input through the tropopause, for the "tropospheric column" domain.

in the convective downdrafts from the free troposphere to the boundary layer) and non-convective processes (when air subsides from the free troposphere to the boundary layer).

Convective downdraft of total O_3 is a small net source for the boundary layer, as already reported by *Langmann et al.* [2003], especially in summer (Table 4.4 and Figure 4.13). However, convective lifting of European O_3 leads to a net export of O_3 from the boundary layer, especially during the summer months. This is consistent with previous findings of *Duncan and Bey* [2004], who reported that areas over Germany and the Ural Mountains in Russia frequently experience deep convection, and participate to pollution export from Europe. Conversely, convective downdraft of North American, Asian and hemispheric background (not shown) fluxes act as a net source for the boundary layer, and are at a maximum in summer. During that season, convective downdraft and horizontal transport of North American and Asian O_3 to the boundary layer contribute to the same extent.

Non-convective subsidence, which is a source for both the boundary layer and the whole troposphere should be either associated with large-scale synoptic systems [*Cooper et al.*, 2004; *Heald et al.*, 2003] or with dry air intrusions [*Stohl and Trickl*, 1999; *Trickl et al.*, 2003; *Jaeglé et al.*, 2003]. North American, Asian and hemispheric background O_3 subside into the European boundary layer, acting as a net source. Subsidence of Asian O_3 in the boundary layer is constant all year round, while subsidence of North American O_3 peaks in July. The non-convective mass flux entering at the top of the tropospheric column corresponds to input from the stratosphere (56 Tg.yr^{-1}, Table 4.4) and shows two maxima, in late winter-early spring and mid-summer. *James et al.* [2003] reported that the contribution of stratospheric O_3 to tropospheric O_3 throughout the whole troposphere in the Northern Hemisphere is likely to be higher from February to May and lower during the fall months, in agreement with our findings. Moreover, this seasonal cycle is somewhat consistent with the findings of *Sprenger and Wernli* [2003], who reported that the net stratosphere-troposphere exchange in the extratropical Northern Hemisphere is at a maximum in winter, but also noted a significant downward flux in summer over the continents.

4.6.3 Burden over Europe

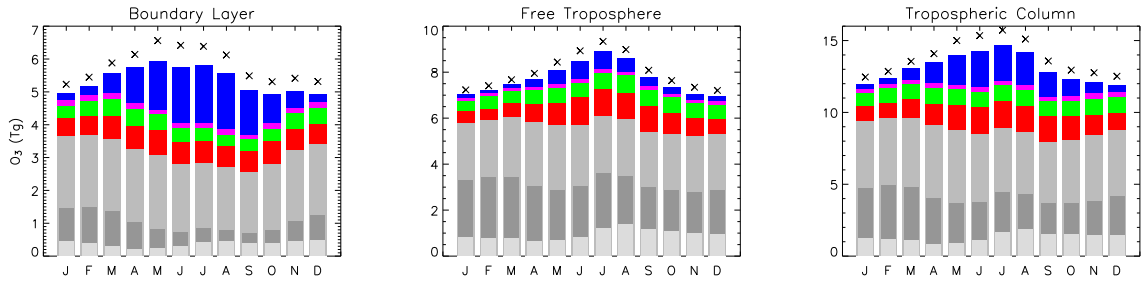

Figure 4.14: Seasonal O_3 burden over continental Europe for 1997. Red: North American contribution; Green: Asian contribution; Blue: European contribution; Pink: Anthropogenic emission contribution from other regions (e.g., middle-east, southern hemisphere). Grey: Total hemispheric background which includes O_3 produced by precursors from natural sources (e.g., soils, biosphere), from biomass burning, from CH_4 oxidation, O_3 induced by lightning NO_x emissions (light grey) and stratospheric O_3 input (dark grey). Crossmarks show the burden for total O_3, and the difference between the crossmarks and the top of the bar graph indicates the effect of non-linearity in O_3 chemistry. Left panel: boundary layer (from the surface to the top of the boundary layer, i.e., 600 hPa). Middle panel: free troposphere (from 600 hPa to the tropopause); Right panel: throughout the tropospheric column (from the surface to the tropopause).

The total O_3 burden integrated over the European tropospheric column ranges from 12.5 Tg (January) to 15.7 Tg (July) (Figure 4.14). Integrated over the whole troposphere, the hemispheric background O_3 (9.0 Tg) accounts for 64% of total tropospheric O_3 burden (including 10% due to lightning and 20% due to stratospheric O_3) and shows only little seasonal variation. The hemispheric background O_3 reaches

a maximum over the Mediterranean basin, as well as the lightning and stratospheric contributions (not shown). A lot of the seasonal variation of the total O_3 burden in the whole troposphere is driven by the summer increase in the European contribution, which accounts for 16% of the total O_3 in summer and less that 3% in winter. At the surface, we find that European contribution is negative for some winter months due to the O_3 titration by NO_x (see Figure 4.15). As also reported by *Wild et al.* [2004], the contribution of European O_3 is greater in the boundary layer (e.g., 27% in July) than in the free troposphere (e.g., 8% in July), due to the proximity of local sources and to a relatively low venting of the boundary layer. The European O_3 is at a maximum over the Mediterranean basin at the surface (35 ppbv in summer), over southern central Europe in the boundary layer and over eastern central Europe in the free troposphere (not shown).

North American and Asian O_3 contribute to about 11.0% and 7.7%, respectively, to the total tropospheric column over Europe on annual average. Those contributions present two maxima in spring and fall in the boundary layer (as well as at the surface, see Figure 4.15), due to stronger low-altitude fluxes during these seasons (see Section 4.4), and a maximum in summer in the free troposphere due to enhanced O_3 production over the source regions. In fact, we find that the sum of the North American and Asian contributions is higher than the European contribution all year round both in the free troposphere and in the whole troposphere, indicating the significance of intercontinental transport of pollution to the total O_3 budget over Europe. Even taken individually, both contributions of North America and Asia are higher than that of Europe in the free troposphere. North American and Asian contributions experience a maximum at the surface in spring over Western, Northern Europe and at the north of the Mediterranean basin (7.5 ppbv). These contributions in the free troposphere go through a maximum in summer over the Mediterranean basin, the European region with the highest O_3 concentration [*Lelieveld and Dentener*, 2000; *Kourtidis et al.*, 2002].

We find that total background O_3 averaged over continental Europe reaches a maximum at the surface (30 ppbv) in early spring and in the free troposphere (52 ppbv at 550 hPa) in summer (not shown). The highest concentrations are found in the Mediterranean basin. At the surface, this appears to be slighty lower than observations (28-42 ppbv [*Simmonds et al.*, 1997; *Derwent et al.*, 1998; *Brönnimann et al.*, 2000; *Pochanart et al.*, 2001; *Naja et al.*, 2003]). However, the spring maximum is well reproduced by the model and appears to be due to several factors, including a maximum in North American and Asian contribution, as well as stratospheric inputs. The background O_3 concentrations increase with altitude and are observed to range from 46 to 55 ppbv in locations representative of free tropospheric conditions [*Brönnimann et al.*, 2000; *Bonasoni et al.*, 2000; *Naja et al.*, 2003], in agreement with our findings.

4.7 Impact of Anthropogenic Emission Changes for the Period 1980-1997

As already pointed out, it is difficult to draw a clear picture of the trends in O_3 over Europe for the last two decades, partly because different trends are found in the lower troposphere in comparison with those observed at higher altitudes (e.g., at the mountain sites) and also because they depend on the quantities examined (e.g., average v.s. maximum). The major parameters contributing to long-term changes in tropospheric O_3 concentrations include O_3 precursor emissions, stratospheric O_3 input, CH_4 levels, ultraviolet (UV) radiation, meteorology, and temperature and humidity [e.g., *Vukovich et al.*, 1977; *Guicherit and Van Dop*, 1977; *Beekmann et al.*, 1994; *Fuglestvedt et al.*, 1994; *Sillman and Samson*, 1995; *Lelieveld and Dentener*, 2000; *Fusco and Logan*, 2003]. *Fusco and Logan* [2003] have investigated the changes in those different processes from 1970 to 1995. They find that the major factors influencing summer tropospheric O_3 are the decline of the stratospheric O_3 flux in the free troposphere, the global increase in NO_x surface emissions and the increase in the lower troposphere temperature.

Previous sections of this paper have also clearly highlighted that long-range transport of O_3 significantly affects the levels of O_3 over Europe, especially in the middle and upper troposphere, while the effect of regional (European) emissions is preferentially seen in the lower troposphere. We suggest that the variation with altitude of the O_3 trends observed over Europe may also reflect, to some extent, the impact of the long-range transport of O_3 pollution. We further investigate this point by examining the variations in O_3 concentrations over Europe at various altitudes due only to the changes in anthropogenic emissions in Europe, North America and Asia over the last two decades. For that purpose, we conducted a number of sensitivity studies where anthropogenic emissions from North America, Asia and Europe were successively fixed to 1980 levels, while keeping the 1997 meteorology, and the CH_4 level, UV radiation, stratospheric input at their 1997 levels.

Table 4.5: NO_x, CO and VOC emissions in the different geopolitical regions in the GEOS-Chem model

	NO_x (Tg N.yr^{-1})		CO (Tg CO.yr^{-1})		VOC (Tg C.yr^{-1})	
	1980	**1997**	**1980**	**1997**	**1980**	**1997**
Europe	7.55	6.37	114.84	72.04	3.28	2.34
North America	6.71	7.12	118.27	103.22	15.59	13.50
Asia	3.67	8.16	63.81	166.02	8.51	19.20
All world	20.02	25.05	331.31	390.47	33.34	44.50

The O_3 precursor emissions used in our model for these two years are presented in Table 4.5. NO_x decreased by 15%, CO by 37% and VOC by 29% over the period 1980-1997 over Europe, following the EMEP recommendations. This decrease is maximal over Central Europe, but there is a local increase in NO_x emissions in Iceland, Ireland

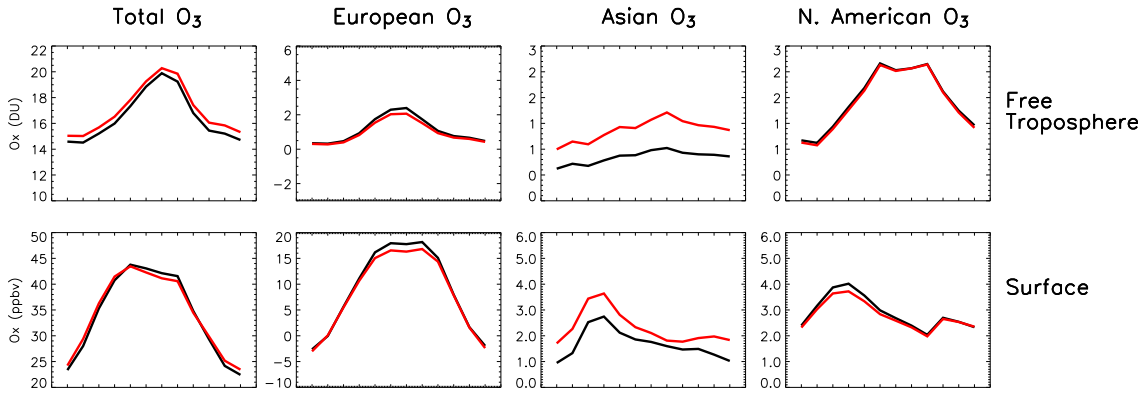

Figure 4.15: Seasonal variations of total O_3, European, Asian and North American O_3 contributions as calculated in the model over continental Europe at the surface (in ppbv, top panels) and in the free troposphere (in DU, bottom panels). Black: 1980 emissions. Red: 1997 emissions. Note that the plots use different scales.

and in the southwest Europe (Spain and Portugal) and the southeast Europe (Croatia, Cyprus, Greece and Turkey) [*Vestreng and Klein*, 2002]. We used data from *EPA* [2000] to estimate the 1980 emissions over North America, as described by *Fusco and Logan* [2003]. In our model, NO_x emissions increase by 6%, while CO and VOC emissions decrease respectively by 12.5% and 13%. However, it should be noted that a new emission database recently provided by EPA [2003] indicates that both NO_x and CO emissions have declined by 8.5% and 36%, respectively over the period 1980-1997. These newer numbers appear to be closer to the reality, at least for CO, as discussed by *Parrish et al.* [2002], who found a larger decrease in CO emissions due to on-road vehicles than previously reported in the *EPA* [2000]. However, the authors also suggest an increase in vehicle NO_x emissions over North America of 2-3% per year due to the use of heavy-duty diesel-powered trucks, which is more in agreement with *EPA* [2000]. For Japan, we use data from the Organization for Economic Cooperation and Development [*OECD*, 1997], while for the rest of Asia, we used emissions scaled to annual fossil fuel CO_2 emission statistics provided by the Carbon Dioxide Information Analysis Center (CDIAC) [*Marland et al.*, 2001]. For the period 1980-1997, we found a large increase in NO_x (x2.2), CO (x2.6) and VOC (x1.3) anthropogenic emissions over Asia. Asian emissions are still largely uncertain, however, previous modelling studies have shown that O_3 simulated over that region with GEOS-Chem are in good agreement with observations [e.g., *Bey et al.*, 2001b; *Liu et al.*, 2003]. *Van Aardenne et al.* [1999] reported an increase by a factor of 1.7 for NO_x over Asia from 1990 to 2000, in good agreement with our number.

Figure 4.15 shows the seasonal variation in 1980 and 1997 of total O_3 and of the European, Asian and North American O_3 contributions (all quantities are averaged over continental Europe). Figure 4.16 shows the spatial distribution at the surface in winter and summer of the change between 1980 and 1997 in total O_3, European O_3 and total background O_3. As hemispheric background does not vary in our simulations, total background O_3 represents only changes in Asian O_3 and in North American O_3. Because of the non-linearity in the O_3 chemistry, more emphasis should be given to the

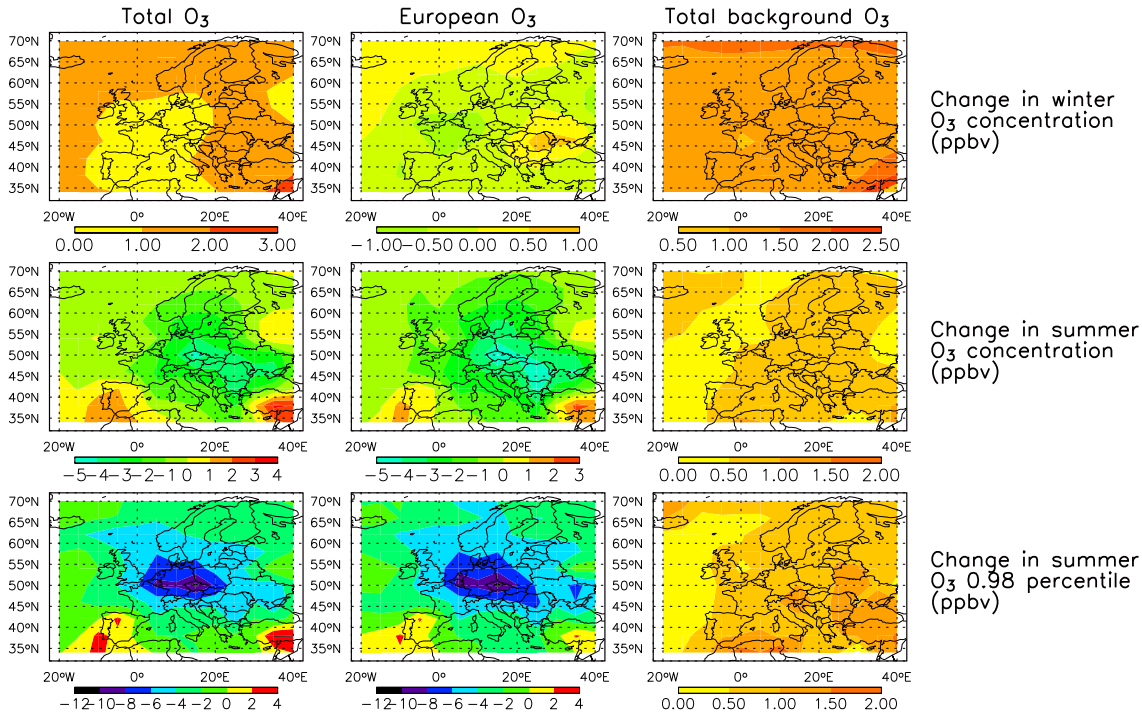

Figure 4.16: Geographical distribution at the surface over Europe of the change between 1980 and 1997 of the mean O_3 concentration (ppbv) (winter and summer) and of the change between 1980 and 1997 in the O_3 0.98 percentile (in summer 1997). Left panel: total O_3. Middle panel: European O_3. Right panel: Total background O_3. Positive values indicate an increase in O_3 concentration or O_3 peaks from 1980 to 1997.

tendencies rather than the actual concentrations or changes in concentrations.

Between 1980 and 1997, we find that the North American O_3 contribution remains fairly constant, while the Asian O_3 contribution increases by about 1 ppbv at the surface (Figure 4.15). This results in a net increase in the total background seen in all seasons at the surface over the whole continental Europe (Figure 4.16). The annual mean continental-averaged European O_3 decreases by 0.6 ppbv, between 1980 and 1997 and up to 1.5 ppbv in July (Figure 4.15) due to the reduction of local O_3 precursor emissions. As the O_3 distributions at the surface over Europe are mostly driven by the European emissions (see Section 4.6 and *Wild et al.* [2004]), the change in emissions between 1980 and 1997 leads to a decrease in total O_3 at the surface in summer. One should note however that, in summer, at the surface, total O_3 and European O_3 decrease by up to 5 ppbv over Central Europe, while they increase by up to 2–3 ppbv over southwest and southeast Europe (Figure 4.16). In winter, European O_3 increases in central Europe due to the reduced NO_x titration, and decreases over the other parts of Europe (Figure 4.16). However, as total background increases, total surface O_3 also increases over all Europe in winter.

At higher altitudes, we find that the decrease in European O_3 due to the reduction of local emissions is compensated by the increase in Asian O_3, resulting in a small

increase in total O_3 concentrations (Figure 4.15). Even though it should be recognized that only changes in emissions are accounting for in our simulations, this compensating effect may explain the small (or lack of) trends observed in O_3 over Europe for the last two decades, especially at the mountain sites.

We also examine the sensitivity of O_3 to the change in CH_4 levels from 1980 to 1997. CH_4 levels are specified in the model using the set of CMDL observations. These observations are available for 1983-2001, and were scaled for the year 1980 using a polynomial regression for each latitude band. CH_4 increases globally from 1560 to 1730 ppbv between 1980 and 1997. We find that, over Europe, the changes in O_3 concentrations due to the changes in CH_4 levels are smaller that those induced by the changes of other anthropogenic emissions: hemispheric O_3 background increases up to 1.2% (0.3 ppbv), while Asian O_3 contribution increases up to 1.6% (1.4 ppbv) in the whole troposphere (at the surface).

Figure 4.16 presents the change in peak O_3 (computed as a 0.98^{th} percentile) for the summer period, between 1980 and 1997, for total O_3, European O_3 and total background O_3. In summer, total O_3 peaks decrease in central Europe by up to 12 ppbv. This is in accordance with previous studies over England [*Derwent et al.*, 2003] and Switzerland [*Brönnimann et al.*, 2002]. However, in southwest Europe and southeast Europe O_3 peaks increased by up to 4 ppbv.

Figure 4.17 shows the change between 1980 and 1997 in hourly mean for total O_3, European, Asian and North American O_3 for different locations representative of western Europe (Mace Head), central Europe (Waldhof), and the alpine site of the Jungfraujoch. For each station, the change in total O_3 has to be interpreted differently, although change in North American O_3 is systematically close to zero while Asian O_3 increases at all sites. Mace Head is a coastal station where European emissions have only a small impact (Figure 4.16, 2^{nd} row, 2^{nd} column), and thus presents only a small decrease in European O_3 in summer (< 2 ppbv) but an episodic increase in the European O_3, particularly in fall and winter (up to 6 ppbv) due to a weaker O_3 titration by NO_x. Asian O_3 increases all year-round by less than 2 ppbv with a minimum impact in summer, leading to an increase in total O_3 in fall, winter and spring. In summer, total O_3 is consequently driven by European O_3. The Waldhof station is at the heart of the area impacted by the changes due to European emissions (Figure 4.16), and presents an increase in O_3 in winter and a decrease in summer. Asian O_3 increases (of 0.8 ppbv averaged on the year), while North American O_3 presents a small increase in winter. At that station, the change in total O_3 is thus driven by the change due to European emissions all year-round. The Jungfraujoch station (altitude: 3580 m) is less sensitive to the local emissions as it is usually typical of free tropospheric conditions (see Section 4.6). European O_3 decreases during photochemical episodes in summer and Asian O_3 increases all year-round by 1.5 ppbv, while North American O_3 remains more or less constant. Thus, total O_3 increases all-year round ($+1.4$ ppbv) due to the change in Asian O_3 except during strong photochemical episodes in summer. This last section illustrates the difficulty of assessing O_3 trends over Europe, as each station appears to be differently impacted by various contributions.

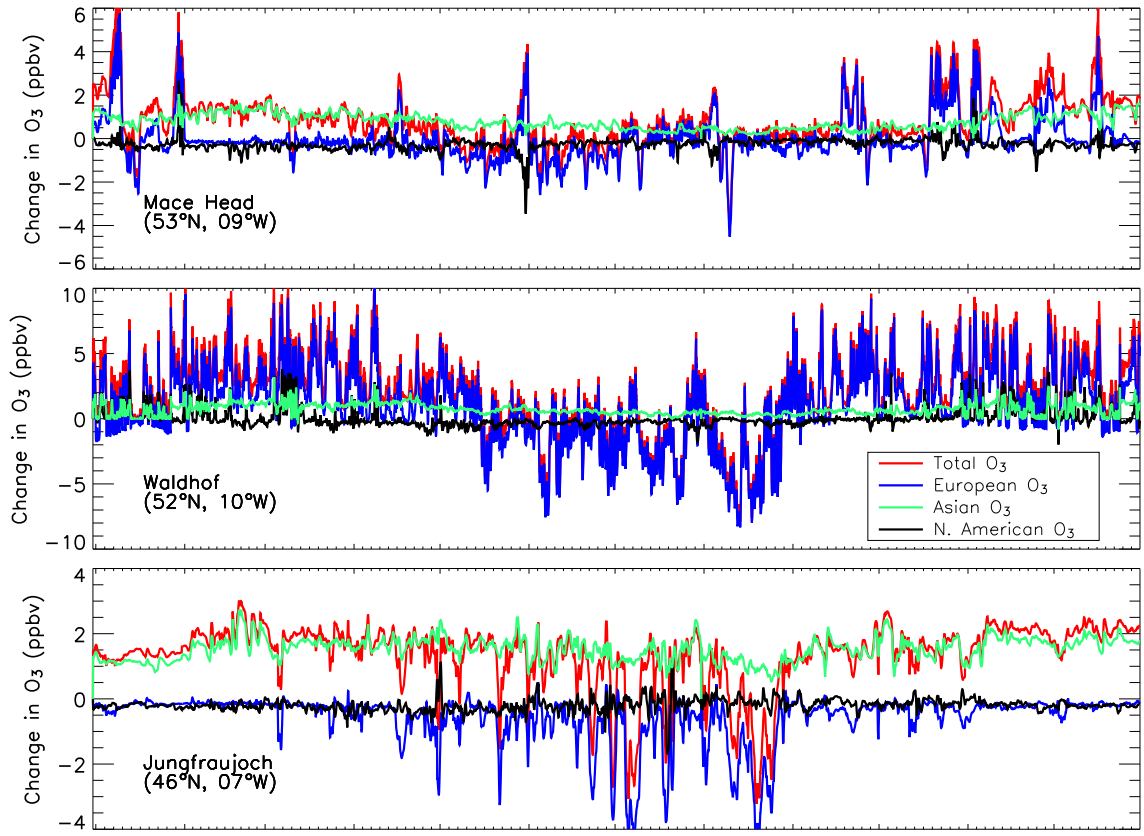

Figure 4.17: Change in hourly O_3 concentrations between 1980 and 1997 for total O_3 and for the European, Asian and North American O_3 contribution for three sites over Europe.

4.8 Summary and Conclusion

We use a global chemical transport model to investigate the processes associated with pollution import into Europe and to assess its impact on the European O_3 budget. Sensitivity simulations enable us to separate O_3 fluxes and concentrations into different components, including hemispheric background (which includes stratospheric input and O_3 produced by precursors from natural sources, biomass burning, and by CH_4 oxidation) and the contribution due to anthropogenic sources over Europe, North America and Asia. We also examine the change in different O_3 contributions over Europe due to the change in local and continental emissions over the period 1980–1997.

The model reproduces generally well O_3 concentrations over Europe throughout the column with the exception that O_3 concentrations are overestimated in summer at the surface at some sites, underestimated in the middle troposphere in summer, and that the seasonal cycle of O_3 is too flat in the upper troposphere. We also examined two events of O_3 enhancements of North American origin over the eastern North Atlantic and over Europe, and showed that the model reproduces well the features associated with long-range transport of pollution.

The altitudinal and latitudinal distributions of North American O_3 fluxes entering Europe show a clear seasonal signal, reflecting the seasonal variation in export pathways and photochemical activity. North American O_3 fluxes into Europe are at a maximum in spring and summer because of the stronger photochemical activity. The pollution usually follows a curved shape over the North Atlantic, and therefore enters Europe on both its western and northern sides. In summer, North American O_3 enters Europe at higher altitudes and lower latitudes because deep convection lifts pollution to higher altitudes than warm conveyor belts in general, and the flow over the North Atlantic is mostly zonal in that season. The low-level inflow is only important in spring, when loss rates in the boundary layer over the North Atlantic is at a minimum.

Asian O_3 reaches Europe all-year round, but usually at higher altitudes than North American O_3. Over Asia, the pollution is rapidly lifted to the free troposphere through convection or mid-latitude cyclones and is then transported around the world in the westerly flow. In addition, during the monsoon season (summer), the anticyclone centred over the Tibetan plateau extends far to the west and induces an easterly flow by which Asian pollution is directly transported towards Europe, especially in the Mediterranean area. We note both a strong contribution of lightning and Asian pollution in this O_3 import.

Total O_3 burden integrated throughout the tropospheric column over Europe ranges between 12.4 Tg in winter and 15.8 Tg in summer. Hemispheric background accounts annually for 64.4% of total O_3 burden, while North American, Asian and European contributions account for 10.9%, 7.7% and 9.4% respectively. Most of the seasonal variation of the European O_3 burden is driven by the European emissions. In the free troposphere, Asian and North American contributions are highest in summer due to the greatest chemical O_3 production over the source region. This is also the case in the low troposphere in spring and fall, when net chemical O_3 loss are weaker over the

North Atlantic. Total background (the sum of the hemispheric background plus the Asian and North American contributions) at the surface presents a maximum in spring of 30 ppbv.

From 1980 to 1997, we find that O_3 concentrations at the surface decreased in summer because of the decrease in European O_3 precursor emissions and increased in winter because of i) the weaker O_3 titration by NO_x and ii) the increase in Asian contribution. In the free troposphere, the change in O_3 is driven by the increase in Asian contribution, which compensates for the decrease due to the local emission reductions in all seasons. We find that these changes are larger than those due to the global CH_4 increase. This result has political implications as the effect of the European emissions reductions may be offset, to some extent, by the increase in foreign emissions. The need for international treaties regulating the emissions is thus reinforced [e.g., *Holloway et al.*, 2003].

It should be noted that the results presented here are for 1997. It has been suggested that the distributions of different chemical tracers over the North Atlantic is related to the North Atlantic Oscillation (NAO) [*Li et al*, 2002; *Creilson et al.*, 2003; *Duncan and Bey*, 2004], which has a strong year-to-year variability. Further work is required to investigate the sensitivity of our results to interannual variability of NAO.

Finally, uncertainties still remain about the model's quantitative ability to reproduce events of long-range transport. In particular, only limited data are available to constrain the evaluation of the model's chemical loss and production rates. In future work, we will examine the O_3 production terms during long-rang transport events with a special focus on the individual chemical reactions driving those chemical terms. The Intercontinental Transport of Ozone and Precursors (ITOP) campaign, which took place over the North Atlantic in summer 2004, will provide a valuable database to better characterize the chemical environment in the polluted air masses travelling over the North Atlantic and their impact on Europe.

Acknowledgements

The GEOS-Chem model is managed by the Atmospheric Chemistry Modeling Group at Harvard University with support from the NASA Atmospheric Chemistry Modeling and Analysis Program. We are very grateful to Anne-Gunn Hjellbrekke for providing the EMEP ozone observations, the Swiss Agency for Environment Forests and Landscape (SAEFL) for providing NABEL data at the Jungfraujoch, and Thomas Trickl for the lidar observations at Garmisch-Partenkirchen. We would like to express our appreciation to Philippe Thunis for his assistance with the EMEP emission inventories. Discussions with Bryan Duncan, Arlene Fiore, Mathew Evans, David Parrish, and Johannes Staehelin were very helpful.

References

Barrett, K., J. Schaug, A. Bartonova, A. Semb, A. G. Hjellbrekke, and J.E. Hanssenn (2000), A contribution from CCC to the reevaluation of the observed trends in sulphur and nitrogen in Europe 1978–1998, *EMEP/CCC-Report 7/2000*, 195 pp., Norwegian Institute for Air Research, Kjeller, Norway.

Barry, R. G., and R. J. Chorley (2003), *Atmosphere, weather and climate*, 8th ed., 421pp., Routledge, London, England.

Beekmann, M., G. Ancellet, and G. Mégie (1994), Climatology of tropospheric ozone in southern Europe and its relation to potential vorticity, *J. Geophys. Res.*, *99*, 12841–12854.

Benkovitz, C. M., M. T. Scholtz, J. Pacyna, L. Tarrasón, J. Dignon, E. C. Voldner, P. A. Spiro, J. A. Logan, and T. E. Graedel (1996), Global gridded inventories of anthropogenic emissions of sulfur and nitrogen, *J. Geophys. Res.*, *101*, 29239–29254.

Berntsen, T. K., S. Karlsdottir, and D. A. Jaffe (1999), Influence of Asian emissions on the composition of air reaching the North Western United States, *Geophys. Res. Lett.*, *26*, 2171–2174.

Bey, I., D. J. Jacob, R. M. Yantosca, J. A. Logan, B. D. Field, A. M. Fiore, Q. Li, H. Liu, L. J. Mickley, and M. Schultz (2001a), Global modeling of tropospheric chemistry with assimilated meteorology: Model description and evaluation, *J. Geophys. Res.*, *106*, 23073–23095.

Bey, I., D. J. Jacob, J. A. Logan, and R. M. Yantosca (2001b), Asian chemical outflow to the Pacific in spring: Origins, pathways, and budgets, *J. Geophys. Res.*, *106*, 23097–23114.

Bonasoni, P., A. Stohl, P. Cristofanelli, F. Calzolari, T. Colombo, and F. Evangelisti (2000), Background ozone variations at Mt. Cimone Station, *Atmos. Environ.*, *34*, 5183–5189.

Brönnimann, S., E. Schuepbach, P. Zanis, B. Buchmann, and H. Wanner (2000), A climatology of regional background ozone at different elevations in Switzerland (1992–1998), *Atmos. Environ.*, *34*, 5191–5198.

Brönnimann, S., B. Buchmann, and H.Wanner (2002), Trends in near-surface ozone concentrations in Switzerland: the 1990s, *Atmos. Environ.*, *36*, 2841–2852.

Carmichael, G. R., I. Uno, M. J. Phadnis, Y. Zhang, and Y. Sunwoo (1998), Tropospheric ozone production and transport in the springtime in east Asia, *J. Geophys. Res.*, *103*, 10649–10672, 10.1029/97JD03740.

Chameides, W. L. and J. C. G. Walker (1973), Photochemical theory of tropospheric ozone, *J. Geophys. Res.*, *78*, 8751–8760.

Chin, M., P. Ginoux, S. Kinne, O. Torres, B. Holben, B. N. Duncan, R. V. Martin, J. A. Logan, A. Higurashi, and T. Nakajima (2002), Tropospheric aerosol optical thickness from the GOCART model and comparisons with satellite and sunphotometer measurements, *J. Atmos. Sci.*, *59*, 461–483.

Christian, H. J., and J. Latham (1998), Satellite measurements of global lightning, *Q. J. R. Meteorol. Soc.*, *124*, 1771–1773.

Collins, W. J., D. S. Stevenson, C. E. Johnson and R. G. Derwent (2000), The European regional ozone distribution and its links with the global scale for the years 1992 and 2015, *Atmos. Environ.*, *34*, 255–267.

Cooper, O. R., J. L. Moody, D. D. Parrish, M. Trainer, T. B. Ryerson, J. S. Holloway, G. Hübler, F. C. Fehsenfeld, S. J. Oltmans, and M. J. Evans (2001), Trace gas signatures of the airstreams within North Atlantic cyclones: Case studies from the North Atlantic Regional Experiment (NARE'97) aircraft intensive, *J. Geophys. Res.*, *106*, 5437–5456.

Cooper, O. R., J. L. Moody, D. D. Parrish, M. Trainer, J. S. Holloway, G. Hübler, F. C. Fehsenfeld, and A. Stohl (2002), Trace gas composition of midlatitude cyclones over the western North Atlantic Ocean: A seasonal comparison of O^3 and CO, *J. Geophys. Res.*, *107*(D7), doi:10.1029/2001JD000902.

Cooper, O.R., et al. (2004), A case study of transpacific warm conveyor belt transport: Influence of merging airstreams on trace gas import to North America, *J. Geophys. Res.*, *109*, D23S08, doi:10.1029/2003JD003624.

Creilson, J., Fishman, J. and A. Wozniak (2003), Intercontinental transport of tropospheric ozone: A study of its seasonal variability across the North Atlantic utilizing tropospheric ozone residuals and its relationship to the North Atlantic Oscillation, *Atmos. Chem. Phys.*, *3*, 2053–2066.

Crutzen, P. J. (1974), Photochemical reactions initiated by and influencing ozone in the unpolluted tropospheric air, *Tellus*, *26*, 47–57.

Danielsen, E. F. (1968), Stratospheric-tropospheric exchange based on radioactivity ozone and potential vorticity, *J. Atmos. Sci.*, *25*, 502–518.

Derwent, R. G., P. G. Simmonds, S. Seuring, and C. Dimmer (1998), Observation and interpretation of the seasonal cycles in the surface concentrations of ozone and carbon monoxide at Mace Head, Ireland from 1990 to 1994, *J. Atmos. Chem.*, *32*, 145–157.

Derwent, R. G., M. E. Jenkin, S. M. Saunders, M. J. Pilling, P. G. Simmonds, N. R. Passant, G. J. Dollard, P. Dumitrean, and A. Kent (2003), Photochemical ozone formation in north west Europe and its control, *Atmos. Environ.*, *37*, 1983–1991.

Duncan, B. N., and I. Bey (2004), A modeling study of the export pathways of pollution from Europe: Seasonal and interannual variations (1987–1997), *J. Geophys. Res.*, *109*, D08301, doi:10.1029/2003JD004079.

Duncan, B. N., R. V. Martin, A. C. Staudt, R. Yevich, and J. A. Logan (2003), Interannual and seasonal variability of biomass burning emissions constrained by satellite observations, *J. Geophys. Res.*, *108*(D2), 4100, doi:10.1029/2002JD002378.

Environmental Protection Agency (EPA) (1997), National air pollutant emission trends: 1900-1996, *Rep. EPA-454/R-97-011*, Research Triangle Park, N.C.

Environmental Protection Agency (EPA) (2000), National air pollutant emission trends: 1900-1998, *Rep. EPA-454/R-00-002*, Research Triangle Park, N.C.

Environmental Protection Agency (EPA) (2003), Average Annual Emissions, all criteria pollutants years including 1970–2001/updated August 2003, Research Triangle Park, N.C. (Available at http://www.epa.gov/ttn/chief/trends/index.html)

Fehsenfeld, F. C., P. Daum, W. R. Leaitch, M. Trainer, D. D. Parrish, and G. Hübler (1996), Transport and processing of O_3 and O_3 precursors over the North Atlantic: An overview of the 1993 North Atlantic Regional Experiment (NARE) summer intensive, *J. Geophys. Res.*, *101*, 28877–28892.

Fiore, A. M., D. J. Jacob, I. Bey, R. M. Yantosca, B. D. Field, A. C. Fusco, and J. G. Wilkinson (2002), Background ozone over the United States in summer: Origin, trend, and contribution to pollution episodes, *J. Geophys. Res.*, *107*(D15), doi:10.1029/2001JD000982.

Folkins, I., R. Chatfield, D. Baumgardner, and M. Proffitt (1997), Biomass burning and deep convection in southeastern Asia: Results from ASHOE/MAESA, *J. Geophys. Res.*, *102*, 13291–13300.

Fuglestvedt, J. S., J. E. Jonson, and I. Isaksen (1994), Effects of reductions in stratospheric ozone on tropospheric chemistry through changes in photolysis rates, *Tellus*, *46B*, 172–192.

Fusco, A. C., and J. A. Logan (2003), Analysis of 1970–1995 trends in tropospheric ozone at Northern Hemisphere midlatitudes with the GEOS-CHEM model, *J. Geophys. Res.*, *108*(D15), 4449, doi:10.1029/2002JD002742.

Guicherit, R., and H. Van Dop (1977), Photochemical production of ozone in western-Europe (1971–1975) and its relation to meteorology, *Atmos. Environ.*, *11*, 145–155.

Hannan, J. R., H. E. Fuelberg, J. H. Crawford, G. W. Sachse, and D. R. Blake (2003), Role of wave cyclones in transporting boundary layer air to the free troposphere during the spring 2001 NASA/TRACE-P experiment, *J. Geophys. Res.*, *108*(D20), 8785, doi:10.1029/2002JD003105.

Heald, C. L., et al. (2003), Asian outflow and trans-Pacific transport of carbon monoxide and ozone pollution: An integrated satellite, aircraft, and model perspective, *J. Geophys. Res.*, *108*(D24), 4804, doi:10.1029/2003JD003507.

Holloway, T., A. Fiore, and M. G. Hastings (2003), Intercontinental Transport of air pollution: Will emerging science lead to a new hemispheric treaty?, *Environ. Sci. & Technol.*, *37*, 4535–4542.

Horowitz, L. W., J. Liang, G. M. Gardner, and D. J. Jacob (1998), Export of reactive nitrogen from North America during summertime: Sensitivity to hydrocarbon chemistry, *J. Geophys. Res.*, *103*, 13451–13476.

Intergovernmental Panel on Climate Change (IPCC) (2001), *Climate Change 2001: The Scientific Basis*, Edited by J.T. Houghton et al., Cambridge Univ. Press, New York.

Jacob, D. J. (2000), Heterogeneous chemistry and tropospheric ozone, *Atmos. Environ.*, *34*, 2131–2159.

Jacob, D. J., J. A. Logan, and P. P. Murti (1999), Effect of rising Asian emissions on surface ozone in the United States, *Geophys. Res. Lett.*, *26*, 2175–2178.

Jacob, D. J., J. H. Crawford, M. M. Kleb, V. S. Connors, R. J. Bendura, J. L. Raper, G. W. Sachse, J. C. Gille, L. Emmons, and C. L. Heald (2003), Transport and Chemical Evolution over the Pacific (TRACE-P) aircraft mission: Design, execution, and first results, *J. Geophys. Res.*, *108*(D20), 9000, doi:10.1029/2002JD003276.

Jaeglé, L., D. A. Jaffe, H. U. Price, P. Weiss-Penzias, P. I. Palmer, M. J. Evans, D. J. Jacob, and I. Bey (2003), Sources and budgets for CO and O_3 in the northeastern Pacific during the spring of 2001: Results from the PHOBEA-II Experiment, *J. Geophys. Res.*, *108*(D20), 8802, doi:10.1029/2002JD003121.

James, P., A. Stohl, C. Forster, S. Eckhardt, P. Seibert, and A. Frank (2003), A 15-year climatology of stratosphere-troposphere exchange with a Lagrangian particle dispersion model 2. Mean climate and seasonal variability, *J. Geophys. Res.*, *108*(D12), 8522, doi:10.1029/2002JD002639.

Jonson, J. E., J. K. Sundet, and L. Tarrason (2001), Model calculations of present and future levels of ozone and ozone precursors with a global and a regional model, *Atmos. Env.*, *35*, 525–537.

Junge, C. E. (1962), Global ozone budget and exchange between stratosphere and troposphere, *Tellus*, *14*, 363–377.

Kourtidis, K., et al. (2002), Regional levels of ozone in the troposphere over eastern Mediterranean, *J. Geophys. Res.*, *107*(D18), 8140, doi:10.1029/2000JD000140.

Kuebler, J., H. Van Den Bergh, A. G. Russell (2001), Long-term trends of primary and secondary pollutant concentrations in Switzerland and their response to emission controls and economic changes, *Atmos. Environ.*, *35*, 1351–1363.

Langmann, B., S. E. Bauer, and I. Bey (2003), The influence of the global photochemical composition of the troposphere on European summer smog, Part I: Application of a global to mesoscale model chain, *J. Geophys. Res.*, *108*(D4), 4146, doi:10.1029/2002JD002072.

Laurila, T. (1999), Observational study of transport and photochemical formation of ozone over northern Europe, *J. Geophys. Res.*, *104*, 26235–26244.

Lawrence, M. G., et al. (2003), Global chemical weather forecasts for field campaign planning: Predictions and observations of large-scale features during MINOS, CONTRACE and INDOEX, *Atmos. Chem. Phys.*, *3*, 267–289.

Lelieveld, J., and F. J. Dentener (2000), What controls tropospheric ozone?, *J. Geophys. Res.*, *105*, 3531–3552.

Lelieveld, J., et al. (2002), Global air pollution crossroads over the Mediterranean, *Science*, *298*, 794–799.

Levy, H. (1971), Normal atmosphere: large radical and formaldehyde concentrations predicted, *Science*, *173*, 141–143.

Li, Q. B., et al. (2001), A tropospheric ozone maximum over the Middle East, *Geophys. Res. Lett.*, *28*, 3235-3238

Li, Q. B., et al. (2002), Transatlantic transport of pollution and its effects on surface ozone in Europe and North America, *J. Geophys. Res.*, *107*(D123), 4166, doi: 10.1029/2001JD001422

Li, Q. B., D. J. Jacob, R. M. Yantosca, J. W. Munger, and D. D. Parrish (2004), Export of NO_y from the North American Boundary Layer: Reconciling Aircraft Observations and Global Model Budgets, *J. Geophys. Res.*, *109*, D02313, doi:10.1029/2003JD004086.

Li, Q. B., D. J. Jacob, R. Park, Y. Wang, C. L. Heald, R. Hudman, R. M. Yantosca, R. V. Martin, M. Evans (2005), North American pollution outflow and the trapping of convectively lifted pollution by upper-level anticyclone, *J. Geophys. Res.*, *110*, D10301, doi:10.1029/2004JD005039.

Liang, Q., L. Jaeglé, D. A. Jaffe, P. Weiss, A. Heckman, and J. Snow (2004), Long-range Transport to the Northeast Pacific: Seasonal variations and transport pathways, *J. Geophys. Res.*, *109*, D23S07, doi:10.1029/2003JD004402.

Lindskog, A., M. Beekmann, P. Builtjes, P. Monks, M. Roemer, E. Schuepbach, and S. Solberg (2001), Tropospheric Ozone Research, *Annual Report 2000*, National Research Center for Environment and Health, Munich, Germany.

Liu, H., D.J. Jacob, I. Bey, and R.M. Yantosca (2001), Constraints from 210Pb and 7Be on wet deposition and transport in a global three-dimensional chemical tracer model driven by assimilated meteorological fields, *J. Geophys. Res.*, *106*, 12109–12128.

Liu, H., D. J. Jacob, L. Y. Chan, S. J. Oltmans, I. Bey, R. M. Yantosca, J. M. Harris, B. N. Duncan, and R. V. Martin (2002), Sources of tropospheric ozone along the Asian Pacific Rim: An analysis of ozonesonde observations, *J. Geophys. Res.*, *107*(D21), 4573, doi:10.1029/2001JD002005.

Liu, H., D. J. Jacob, I. Bey, R. M. Yantosca, B. N. Duncan, and G. W. Sachse (2003), Transport pathways for Asian pollution outflow over the Pacific: Interannual and seasonal variations, *J. Geophys. Res.*, *108*(D20), 8786, doi:10.1029/2002JD003102.

Liu, S. C., M. Trainer, F. C. Fehsenfeld, D. D. Parrish, E. J. Williams, D. W. Fahey, G. Hübler and P. C. Murphy (1987), Ozone production in the rural troposphere and the implications for regional and global ozone distributions, *J. Geophys. Res.*, *92*, 4191–4207.

Logan, J. A., et al. (1999), Trends in the vertical distribution of ozone: a comparison of two analyses of ozonesonde data, *J. Geophys. Res.*, *104*, 26373–26399.

Marenco, A., et al. (1998), Measurement of ozone and water vapor by Airbus in-service aircraft: The MOZAIC airborne program, an overview, *J. Geophys. Res.*, *103*, 12855–12861.

Marland, G., T. A. Boden, and R. J. Andres (2001), Global, regional, and national annual CO2 emissions from fossil-fuel burning, cement production, and gas flaring: 1751-1998, *Carbon dioxide Inf. Anal. Cent.*, Oak Ridge, Tenn.

Martin, R. V., et al. (2002), An improved retrieval of tropospheric nitrogen dioxide from GOME, *J. Geophys. Res.*, *107*(D20), 4437, doi:10.1029/2001JD001027.

Martin, R. V., D. J. Jacob, R. M. Yantosca, M. Chin, and P. Ginoux (2003), Global and regional decreases in tropospheric oxidants from photochemical effects of aerosols, *J. Geophys. Res.*, *108*(D3), 4097, doi:10.1029/2002JD002622.

McLinden, C. A., S. C. Olsen, B. Hannegan, O. Wild, M. J. Prather, and J. Sundet (2000), Stratospheric ozone in 3-D models: A simple chemistry and the cross-tropopause flux, *J. Geophys. Res.*, *105*, 14653–14665.

Naja, M., H. Akimoto, and J. Staehelin (2003), Ozone in background and photochemically aged air over central Europe: Analysis of long-term ozonesonde data from Hohenpeissenberg and Payerne, *J. Geophys. Res.*, *108*(D2), 4063, doi:10.1029/2002JD002477.

Nesbitt, S. W., R. Y. Zhang, and R. E. Orville (2000), Seasonal and global NO_x production by lightning estimated from the Optical Transient Detector (OTD), *Tellus*, *52B*, 1206–1215.

Newell, R. E., E. V. Browell, D. D. Davis, and S. C. Liu (1997), Western Pacific tropospheric ozone and potential vorticity: Implications for Asian pollution, *Geophys. Res. Lett.*, *24*, 2733–2736.

Novelli, P. C., L. P. Steele, and P. P. Tans (1992), Mixing ratios of carbon monoxide in the troposphere, *J. Geophys. Res.*, *97*, 20731–20750.

Organization for Economic Cooperation and Development (OECD) (1997), *Environmental Data Compendium* - 1997, Paris, France.

Parrish, D. D., M. Trainer, D. Hereid, E. J. Williams, K. J. Olszyna, R. A. Harley, J. F. Meagher, and F. C. Fehsenfeld (2002), Decadal change in carbon monoxide to nitrogen oxide ratio in U.S. vehicular emissions, *J. Geophys. Res.*, *107*(D12), doi:10.1029/2001JD000720.

Penkett, S., et al. (2004), Long-range transport of ozone and related pollutants over the North Atlantic in spring and summer, *Atmos. Chem. Phys. Dis.*, *4*, 4407–4454.

Piccot, S. D., J. J. Watson, and J. W. Jones (1992), A global inventory of volatile organic-compound emissions from anthropogenic sources, *J. Geophys. Res.*, *97*, 9897–9912.

Pochanart, P., H. Akimoto, S. Maksyutov, and J. Staehelin (2001), Surface ozone at the Swiss Alpine site Arosa: the hemispheric background and the influence of large-scale anthropogenic emissions, *Atmos. Environ.*, *35*, 5553–5566.

Reeves, C. E., et al. (2002), Potential for photochemical ozone formation in the troposphere over the North Atlantic as derived from aircraft observations during ACSOE, *J. Geophys. Res.*, *107*(D23), 4707.

Roelofs, G.-J., B. Scheeren, J. Heland, H. Ziereis and J. Lelieveld (2003), A model study of ozone in the eastern Mediterranean free troposphere during MINOS (August 2001), *Atmos. Chem. Phys.*, *3*, 1199–1210.

Scheeren, H. A., et al. (2003), The impact of monsoon outflow from India and Southeast Asia in the upper troposphere over the eastern Mediterranean, *Atmos. Chem. Phys.*, *3*, 1589–1608.

Sillman, S., and P. J. Samson (1995), Impact of temperature on oxidant photochemistry in urban, polluted rural and remote environments, *J. Geophys. Res.*, *100*, 11497–11508.

Simmonds, P. G., S. Seuring, G. Nickless, and R. G. Derwent (1997), Segregation and interpretation of ozone and carbon monoxide measurements by air mass origin at the TOR Station Mace Head, Ireland from 1987 to 1995, *J. Atmos. Chem.*, *28*, 45–59.

Sprenger, M., and H. Wernli (2003), A northern hemispheric climatology of cross-tropopause exchange for the ERA15 time period (1979–1993), *J. Geophys. Res.*, *108*(D12), 8521, doi:10.1029/2002JD002636.

Stohl, A. (2001), A 1-year Lagrangian "climatology" of airstreams in the Northern Hemisphere troposphere and lowermost stratosphere, *J. Geophys. Res.*, *106*, 7263–7280.

Stohl, A., and T. Trickl (1999), A textbook example of long-range transport: Simultaneous observation of ozone maxima of stratospheric and North American origin in the free troposphere over Europe, *J. Geophys. Res.*, *104*, 30445–30462.

Stohl, A., S. Eckhardt, C. Forster, P. James, and N. Spichtinger (2002), On the pathways and timescales of intercontinental air pollution transport, *J. Geophys. Res.*, *107*(D23), 4684, doi:10.1029/2001JD001396.

Thompson, A. M., K. E. Pickering, R. R. Dickerson, W. G. Ellis, D. J. Jacob, J. R. Scala, W.-K. Tao, D. P. McNamara, and J. Simpson (1994), Convective transport over the central United States and its role in regional CO and ozone budgets, *J. Geophys. Res.*, *99*, 18703–18712.

Thouret, V., A. Marenco, P. Nédélec, and C. Grouhel (1998), Ozone climatologies at 9–12 km altitude as seen by the MOZAIC airborne program between September 1994 and August 1996, *J. Geophys. Res.*, *103*, 25653–25680.

Traub, M., et al. (2003), Chemical characteristics assigned to trajectory clusters during the MINOS campaign, *Atmos. Chem. Phys.*, *3*, 459–468.

Trickl, T., O. R. Cooper, H. Eisele, P. James, R. Mücke, and A. Stohl (2003), Intercontinental transport and its influence on the ozone concentrations over central Europe: Three case studies, *J. Geophys. Res.*, *108*(D12), 8530, doi:10.1029/2002JD002735.

Van Aardenne, J. A., G. R. Carmichael, H. Levy, D. Streets, and L. Hordijk (1999), Anthropogenic NO_x emissions in Asia in the period 1990–2020, *Atmos. Environ.*, *33*, 633–646.

Vestreng, V. and H. Klein (2002), Emission data reported to UNECE/EMEP: Quality insurance and trend analysis & Presentation of WebDab, *MSC-W Status Report 2002*, 101pp., Norwegian Meteorological Institute, Oslo, Norway. (Available at http://www.emep.int/publ/reports/2002/mscw_note_1_2002.pdf)

Vukovich, F. M., W. D. Bach, B. W. Crissman, and W. J. King (1977), Relationship between high ozone in rural surface-layer and high-pressure systems, *Atmos. Environ.*, *11*, 967–983.

Wang, Y., D. J. Jacob, and J. A. Logan (1998a), Global simulation of tropospheric O_3-NO_x-hydrocarbon chemistry: 1. Model formulation, *J. Geophys. Res.*, *103*, 10713–10726.

Wang, Y., D. J. Jacob, and J. A. Logan (1998b), Global simulation of tropospheric O_3-NO_x-hydrocarbon chemistry: 3. Origin of tropospheric ozone and effects of non-methane hydrocarbons, *J. Geophys. Res.*, *103*, 10757–10768.

Wesely, M. L. (1989), Parameterization of surface resistances to gaseous dry deposition in regional-scale numerical-models, *Atmos. Environ.*, *23*, 1293–13042.

Wild, O., and H. Akimoto (2001), Intercontinental transport of ozone and its precursors in a three-dimensional global CTM, *J. Geophys. Res.*, *106*, 27729–27744.

Wild, O., X. Zhu, and M. J. Prather (2000), Fast-J: Accurate simulation of in- and below-cloud photolysis in tropospheric chemistry models, *J. Atmos. Chem.*, *37*, 245–282.

Wild, O., P. Pochanart, and H. Akimoto (2004), Trans-Eurasian transport of ozone and its precursors, *J. Geophys. Res.*, *109*, D11302, doi:10.1029/2003JD004501.

Yienger, J., M. Galanter, T. A. Holloway, M. J. Phadnis, S. K. Guttikunda, G. R. Carmichael, W. J. Moxim, and H. Levy II (2000), The episodic nature of air pollution transport from Asia to North America, *J. Geophys. Res.*, *105*, 26931–26946.

Chapter 5

Long-Range Transport of Aerosols

In preparation for submission: Auvray, M. et al., Impact of long-range transport on the aerosol burden over Europe: A focus on the ICARTT campaign.

Abstract

We used a global 3D-chemical transport model (GEOS-Chem) conjointly with satellite (MODIS) observations of aerosol optical depth (AOD) and ground-based measurements of AOD and particulate matter less than 2.5 μm ($PM_{2.5}$) to establish an aerosol budget over Europe for the year 2004. A special focus is given to the impact of long and medium-range transport. The model overestimates aerosol local sources over Europe but represents correctly $PM_{2.5}$ mass and AOD over Europe. This might reflect some compensation between individual components, including an overestimate of sulfate and ammonium, and an underestimate of organic matter and dust. Outflow from the United States is also well captured, although underestimated during specific episodes. The European aerosol budget is driven by local sources and by dust from North Africa and Middle-East. North American anthropogenic aerosols (and particularly sulfate) reach Europe all year-round at the altitude range of 2 to 4 km and with a maximum in spring, the season of lowest scavenging. High biomass burning events over Alaska and Canada in summer 2004 emitted strong OC concentrations, which influence the aerosol budget over Europe. Some of these events were observed during the ICARTT campaign and could be traced with aircraft measurements, satellite observations, lidar measurements and the model. Effects of these plumes are quantified by the model. In summer, North American anthropogenic plumes can contribute up to 3 $\mu g/m^3$ to sulfate concentrations and North American biomass burning plumes more than 50% to OC concentrations. Dust sources have a strong impact on the European aerosol budget as they can exceed the contribution of local anthropogenic sources, especially in southern Europe.

5.1 Introduction

During the summer 2004, the International Consortium for Atmospheric Research on Transport and Transformation (ICARTT) regrouped several field efforts from North America and Europe to carry out a large atmospheric chemistry field experiment over the eastern coast of North America, the North Atlantic ocean, and the western coast of Europe. Coordinated flights were conducted to sample polluted outflow from the United States and to follow the plumes through their way across the North Atlantic ocean, over the Azores and the European West coast. Extensive measurements of greenhouse gases, oxidants and aerosols provide an opportunity to better understand export of pollution from North America and the chemical transformation and removal processes of aerosols, oxidants and their precursors during intercontinental transport. During the course of the campaign, several events of long-range transport of pollution were observed across the Atlantic and several events actually reached continental Europe [e.g. *Methven et al.*, 2006]. The main goal of the present work is to assess the contribution of long-range transport events to the overall aerosol loading over Europe, in the free troposphere as well as at the surface.

Despite the relatively short lifetime of aerosols (days to weeks [*Seinfeld and Pandis*, 1998]), there are some indications that they can be transported over distances greater than hundred of kilometers. Studies on long-range transport of aerosols first focused on mineral dust. For example, long and medium-range transport of dust from China over the Pacific and over the Mediterranean basin have been documented with satellite observations [e.g. *Moulin et al.*, 1998; *Wilkening et al.*, 2000; *Husar et al.*, 2001; *Prospero et al.*, 2002; *Darmenova et al.*, 2005]. Consecutive enhanced aerosols concentrations have been reported at surface site over the U.S. [*McKendry et al.*, 2001; *Husar et al.*, 2001]. Dust fallout from China has been also observed as far as the French Alps [*Grousset et al.*, 2003]. Backward trajectory analysis have indicated that, in some cases, enhanced lidar signals captured in Greece [*Amiridis et al.*, 2005] and Germany [*Mattis et al.*, 2002; *Mattis et al.*, 2004] can be attributed to Saharan dust. *Barkan et al.* [2005] reported however that these dust events rarely reach Europe north of the Alps.

More recently, transport of aerosols associated with anthropogenic activities and biomass burning fires have been also reported. Two long-range transport events of forest fire aerosols over Europe have been discussed in the literature. In August 1998 the Total Ozone Mapping Spectrometer (TOMS) space-borne instrument observed Canadian smoke plume over Greenland and the North Atlantic [*Hsu et al.*, 1999; *Forster et al.*, 2001]. Several lidars captured this aerosol layer in the free troposphere over Germany [*Forster et al.*, 2001; *Wandinger et al.*, 2002]. During the same month when washout was inefficient, surface measurement of black carbon concentrations at Mace Head (Ireland) in air masses influenced by forest fire were above the normal background concentrations [*Forster et al.*, 2001]. In spring and summer 2003, intense fires in southeast Russia and subsequent long-range transport of aerosol plumes were observed through satellite observations [*Edwards et al.*, 2004, *Damoah et al.*, 2004]. In May, one of the plumes passed through the Bering Sea to Alaska, crossed the eastern Canada and

made its way through the Atlantic before reaching Europe where it was observed over Germany by lidar measurements [*Mattis et al.*, 2003; *Damoah et al.*, 2004]. The same year, strong events of forest fire were reported over Canada after mid-June [*Müller et al.*, 2005]. The enhanced extinction coefficient observed over Germany for spring and summer 2003 may result from those high fire activities [*Mattis et al.*, 2003; *Müller et al.*, 2005].

Long-range transport of anthropogenic aerosols has only been reported between Asia and the western coast of North America. Until recently these events were only observed at surface island sites over the Pacific [*Huebert et al.*, 2001; *Prospero et al.*, 2003] or in aircraft campaigns [*Jaffe et al.*, 2003; *Price et al.*, 2003; *Bertschi et al.*, 2004]. Recent developments in aerosol retrievals from satellite observations allow the detection of fine aerosols [*Deuzé*, 2001; *Remer et al.*, 2005], which can be used to provide quantitative information on the anthropogenic fraction of aerosols [*Kaufman et al.*, 2005]. A concomitant analysis of satellite observations, measurements at surface sites and modelling studies indicated that long-range transport of anthropogenic aerosols from Asia have a direct impact on the aerosol burden over the north-western U.S. surface sites [*Heald et al.*, 2006].

Satellite observations reported outflow of aerosols out of the North American east coast [*Li et al.*, 2005], but no events of long-range transported anthropogenic aerosols have been examined in detail in the literature. *Müller et al.* [2005], however, used lidar observations in Germany to examine an episode of aerosol enhancement on the 25^{th} of August 2003. Based on the aerosol optical properties and on the particles size, they suggested that this plume shows signatures of North American anthropogenic sources. Analyzing the chemical composition at Chebogue Point during the summer 2004, *Millet et al.* [2006] reported enhanced ozone (O_3), CO and aerosol concentrations during U.S. outflow periods. *Quinn and Bates* [2003] analyzed O_3 concentrations and aerosol levels obtained during the New England Air Quality Study (NEAQS) field campaign and found that U.S. pollution plumes can be as intense (in terms of aerosol mass concentration, aerosol optical depth, and O_3 mixing ratio) as those found downwind of India and Asia. Given the observed impact of Asian aerosols on the western United States, the *Quinn and Bates* [2003] results suggest that aerosol transport from North America could be important for the European aerosol burden, especially if one considers the shorter distance between the two continents.

Measurements of aerosol loads remain sparse and concern mainly western Europe. Nevertheless, available observations over Europe clearly indicate that aerosol concentrations at the surface often exceed the U.S EPA annual average $PM_{2.5}$ (i.e. particulate matter of diameter smaller than 2.5 μm) standard of 15 $\mu g/m^3$ [*van Dingenen et al.*, 2004]. Because of the lack of observations for $PM_{2.5}$ over Europe, recommended standards of the European council are only set for PM_{10} (particulate matter of diameter smaller than 10 μm) [*Technical working group on particles*, 1997]. Council directive 1999/30/EC of April 22, 1999 fixed PM_{10} annual standard to 40 $\mu g/m^3$ for 2005 and to 20 $\mu g/m^3$ for 2010; daily mean value of 50 $\mu g/m^3$ should not be exceeded more than 35 times in a year in 2005 and 7 times in 2010. The 2005 annual average PM_{10} standard is currently exceeded at a few sites over Europe each year, and the 2010 an-

nual average PM_{10} standard is exceeded at all suburban and urban sites [*van Dingenen et al.*, 2004].

Van Dingenen et al. [2004] analyzed observed ground-based concentrations taken at 31 sites over Europe and found a PM_{10} and a $PM_{2.5}$ background annual average mass concentrations of 7 $\pm$ 4.1 and 4.8 $\pm$ 2.4 $\mu g/m^3$, respectively. The European aerosol burden has also been investigated by *Gonzales et al.* [2000; 2003] using aerosol optical depth (AOD) retrieved with the Along Track Scanning Radiometer (ATSR2) for August 1997. They found that there is a large spatial variation and strong gradients around industrialized area, indicating the influence of local emissions. *Wandinger et al.* [2004] analyzed European aerosol load reported by the European Aerosol Research LIdar NETwork (EARLINET) and found that the aerosol load is smaller above western Europe than over Poland and south-eastern Europe. Higher AOD are also found in southern Europe compared to the northern part [*Matthias et al.*, 2004]. The authors suggest that these higher values, which are mainly seen at high altitudes, are associated with transport from Sahara and other continental sources.

The aim of this study is thus 1) to better quantify and characterize the aerosol load over Europe both in term of AOD and concentrations, and 2) to determine the contribution of local pollution versus that of the medium and long-range transport of aerosols associated with anthropogenic sources, forest fire emissions, and mineral dust. To that purpose, we employ a three-dimensional global model of oxidant-aerosol chemistry and transport conjointly with satellite observations, surface measurements and data collected during the ICARTT campaign. Section 5.2 provides information on the model as well as on the different experimental data set used in this study. The capabilities of the model to reproduce aerosol concentrations and aerosol optical depths are discussed in Section 5.3. Section 5.3 also provides a chemical characterization of the aerosol load over Europe as seen by our global model. In Section 5.4 we investigate the seasonal variation of the aerosol transport over the North Atlantic and examine individual events of long and medium-range transport, including two events observed during ICARTT. The impact of aerosol import on the aerosol load is quantitatively described in section 5.5. Section 5.6 provides a summary and some conclusions.

5.2 Methods

5.2.1 The GEOS-Chem Model

The GEOS-Chem model (http://www.as.harvard.edu/chemistry/trop/geos), a global three-dimensional chemical transport model (CTM) of coupled oxidant-aerosol chemistry [*Bey et al.*, 2001; *Martin et al.*, 2003; *Park et al.*, 2004] is used to conduct simulations for 2004. The model (version v7-02-04) is driven by assimilated meteorological observations from the NASA Goddard Earth Observing System (GEOS-4). The meteorological fields of the GEOS-4 version used in this study (including winds, temperature, surface pressure, water content, clouds, precipitation, convective mass fluxes, mixed layer depth and surface properties) are available with a 3- or 6-hour temporal

resolution (depending on the variable) at 1.25° of latitude by 1.25° of longitude on 55 hybrid levels, extending from the surface to 0.01 hPa. The first 14 levels from the surface upward are pure sigma levels while the top levels are fixed pressure levels. For computational expediency, meteorological fields are degraded to an horizontal resolution of 2° of latitude by 2.5° of longitude and are reduced to 30 levels.

The GEOS-Chem oxidant-aerosol simulation includes H_2SO_4-HNO_3-NH_3 aerosol thermodynamics coupled to an O_3-NO_x-hydrocarbon chemical mechanism [*Park et al.*, 2004], as well as organic carbon (OC) and black carbon (BC) [*Park et al.*, 2003], secondary organic aerosol (SOA) [*Chung and Seinfeld*; 2002], sea-salt aerosols [*Alexander et al.*, 2005] and soil dust [*Fairlie et al.*, 2006]. The chemical mechanism includes around 90 species and over 350 reactions. The photolysis rates in the troposphere are calculated with the Fast-J algorithm [*Wild et al.*, 2000]. The aerosol and oxidant simulations are coupled through formation of sulfate, nitrate and SOA, $HNO_{3(g)}/NO_3^-$ partitioning of total inorganic nitrate, heterogeneous chemistry [*Jacob*, 2000] and aerosol effects on photolysis rates [*Martin et al.*, 2003]. Dry deposition of dust and sea-salt aerosols follows the resistance in series formulation of *Zhang et al.* [2001], based on particles size and density, which accounts for hygroscopic growth in function of relative humidity. Dry deposition for all other aerosols and gases is computed using a resistance in series model [*Wesely et al.*, 1989]. Wet deposition applies to gases, dust and hydrophilic aerosols, following the scheme of *Liu et al.* [2001]. 80% of BC and 50% of OC emitted from primary sources are assumed to be hydrophobic [*Cooke et al.*, 1999; *Chin et al.*, 2002; *Chung and Seinfeld*, 2002], and become hydrophilic with an exponential decay lifetime of 1.2 days [*Cooke et al.*, 1999; *Chin et al.*, 2002]. All SOA are assumed to be hydrophilic.

In the following, we will refer to particulate organic matter (POM) as the sum of primary OC and secondary organic aerosol (SOA). In the model, OC are expressed in mass of C, while SOA are in mass of particulate matter. A factor of 1.4 is used on-line to account for the non-carbon mass of SOA. We use the same factor to convert primary OC into POM, although *Turpin and Lim* [2001] suggested the use of a value of 1.6 $\pm$ 0.2 for urban aerosols and 2.1 $\pm$ 0.2 for non-urban aerosols. However, we expect this conversion to be of minor impact on our results. In the following, we will refer to carbonaceous aerosols as the sum of POM plus BC.

AOD (τ) is linked to aerosol mass loading per unit area (M) through the relation $\tau = 3QM/(4\rho r_e)$ where ρ is the particle density, r_e the effective radius and Q the extinction coefficient calculating from the Mie-scattering theory. The variables τ and Q are wavelength dependent. Aerosol optical properties are calculated for each aerosol component as a function of local relative humidity for the 400, 550 and 865 nm wavelengths.

Table 5.1 summarizes the anthropogenic sources of major gases and aerosols used in the model for the whole world, and for specific regions including North America (14°N-90°N; 130°W-65°W) and Europe (38°N-90°N; 15°W-55°E). Inventories used for anthropogenic emissions of NO_x, CO, hydrocarbons and sulfur are from the Global Emissions Inventory Activity (GEIA) for 1985 [*Benkovitz et al.*, 1996] with updated

national emissions inventories [*Bey et al.*, 2001] and scaled for specific years [*Bey at al.*, 2001; *Park et al.*, 2004]. Over Europe and North America, anthropogenic NO_x, CO, hydrocarbons and sulfur emissions are from the European Monitoring and Evaluation Program (EMEP) for the year 2000 [*Vestreng and Klein* 2002] and the EPA National Emissions Inventory (NEI99) for the year 1998 respectively, as described in [*Park et al.*, 2004; *Auvray and Bey*, 2005; *Hudman et al.*, Surface and lightning sources of nitrogen oxides in the United States: magnitudes, chemical evolution and outflow, in preparation for submission to *Journal of Geophysical Research*, (hereinafter referred as *Hudman et al.*, in preparation)]. Anthropogenic sulfur is emitted as SO_2 except for 5% in Europe and 3% elsewhere that are emitted as sulfate [*Chin et al.*, 2000; *Park et al.*, 2004]. Anthropogenic sources of ammonia are as described in *Park et al.* [2004]. Carbonaceous aerosol anthropogenic emissions are from *Bond et al.* [2004] except from North America for which Park et al [2003] have imposed seasonality of *Cooke et al.* [1999] emissions. One has to keep in mind that several studies suggested that BC emissions in the *Bond et al.* [2004] inventory are likely to be too low, especially over Asia [*Carmichael et al.*, 2003; *Clarke et al.*, 2004; *Park et al.*, 2005].

Vestreng et al. [2005] recently reported a new set of EMEP emissions, which may be more representative of the 2004 emissions than the ones used in the present study. Both CO and NO_x emissions reported in *Vestreng et al.* [2005] have decreased compared to the ones of *Vestreng and Klein* [2002] used in the present work. NH_3 and SO_2 GEOS-Chem emissions are also higher than those from *Vestreng et al.* [2005] by a factor of 1.25. In *Vestreng et al.* [2005], only particulate matter (PM) emissions are reported (e.g. rather than emissions of individual types of aerosols). According to *Vestreng et al.* [2005], $PM_{2.5}$ European emissions are of 3.2 Tg/yr, which is only slightly higher than the ones used in GEOS-Chem (2.7 Tg/yr). *Schaap et al.* [2004] reported BC emissions for Europe (excluding former Soviet Union and ship emissions) of 0.47 Tg/yr, which is in the same order as GEOS-Chem emissions (0.38 Tg/yr).

NEI Air Pollutant Emissions Trends (table of the 18^{th} of August 2005, http://www.epa.gov/ttn/chief/trends/index.html#tables, referred hereafter as NEI05) provides total North American emissions estimate for 2002. CO emission estimates from our model appear to be consistent with those provided by EPA, but NO_x emissions are lower in the model. Both North American NH_3 and SO_2 are higher by a factor 1.2 and 1.7, respectively, in the model compared to EPA. *Parrish et al.* [2006] examined the different estimates of EPA on-road vehicle emissions (77.3% of total CO emissions for 2002) and found that CO are overestimated by a factor of two in the EPA estimates. Moreover *Hudman et al.* [in preparation] showed that NO_x emissions have sharply decreased in power plant and industry emissions since 1999 (NEI99 used as reference inventory). This indicates that the set of anthropogenic emissions of NO_x and CO currently used in the model for the United States are likely to be too high.

	CO (TgCO/yr)	NO_x ($TgNO_2$/yr)	NH_3 ($TgNH_3$/yr)	SO_2 ($TgSO_2$/yr)	SO_4^{2-} ($TgSO_2$/yr)	BC (TgC/yr)	OC (TgC/yr)	$PM_{2.5}$ (Tg/yr)
World	386.7	80.0	40.6	119.5	5.9	3.5	2.7	12.1
North Am.	100.5	22.7	4.0	24.3	0.72	0.74	0.62	2.08
Europe	64.0	18.7	7.0	22.3	1.76	0.56	0.38	2.7
EMEP	53.5	17.9	5.6	17.3	-	-	-	3.2
EPA	101.7	27.9	3.4	13.9	-	-	-	6.2

Table 5.1: First three rows: Anthropogenic emissions of CO, NO_x, NH_3, SO_2, SO_4^{2-}, BC and OC in GEOS-Chem used in that study. Fourth row: Emissions as reported by EMEP expert emissions [*Vestreng et al.*, 2005] for the year 2003 and averaged over the same European region. Fifth row: Emissions as reported by EPA NEI05 for the year 2002 (see text for further detail).

	CO (TgCO/yr)	NO_x ($TgNO_2$/yr)	NH_3 ($TgNH_3$/yr)	SO_2 ($TgSO_2$/yr)	BC (TgC/yr)	OC (TgC/yr)
World	479.9	22.6	7.3	2.6	2.9	24.5
North Am.	27.6	1.36	0.27	0.17	0.11	1.67
Europe	8.3	0.32	0.10	0.05	0.04	0.47

Table 5.2: GEOS-Chem biomass burning emissions of CO, NO_x, NH_3, SO_2, BC and OC in different geopolitical regions.

Biomass burning trace gas and aerosol emissions are derived from a climatological dry mass burned inventory with spatial and monthly resolution [*Duncan et al.*, 2003] to which vegetation specific emission factors from *Andreae and Merlet* [2001] have been applied, as described in *Park et al.* [2006]. In the summer 2004 strong fires occur over North America, mainly in Alaska, Yukon, and Central Canada. In order to take into account the impact of large fire events, *Turquety et al.* [2006] have developed a daily inventory based on daily reports from fire agencies (U.S. National Interagency Fire Center) and on hot spots detected from space by the Moderate Resolution Imaging Spectroradiometer (MODIS) instrument. Peat emissions, which are expected to have a large contribution in boreal regions [*Zoltai et al.*, 1998], are included in this inventory. Injection heights play a significant role on the distribution of aerosols and trace gases [*Fromm et al.*, 2000; 2005; *Colarco et al.*, 2004]. Following *Turquety et al.* [2006], we assumed that 40% of biomass burning emissions for North America are injected in the model-diagnosed boundary layer and 60% in the free troposphere. According to the ATSR web fire atlas (http://dup.esrin.esa.it/ionia/wfa/index.asp), only few fires occurred over Europe in 2004 in comparison to other years (e.g. 2003). Therefore it may be possible that the climatological inventory used in this study for European biomass burning emissions slightly overestimates the aerosol biomass burning emissions for that year. Table 5.2 summarizes global, North American (42°N-90°N; 170°W-65°W) and European (38°N-90°N; 15°W-55°E) biomass burning emissions for 2004.

The SOA formation is based on the scheme described by *Chung and Seinfeld* [2002]. The oxidation of biogenic hydrocarbons produces semi-volatile compounds which are partitioned between the gas and aerosol phases. Five classes of biogenic hydrocarbons are taken into account in GEOS-Chem, including (1) a-pinene, b-pinene, sabinene, carene, terpenoid ketones, (2) limonene, (3) a-terpinene, r-terpinene, terpinolene, (4) myrcene, terpenoid alcohols, ocimene, and (5) sesquiterpenes. Biogenic emissions in the model are computed on-line using the scheme of *Guenther et al.* [1995]; they depend on vegetation type and are adjusted monthly by leaf area index and temperature.

Finally, for dust emissions, we tested different schemes available from the literature (see detailed discussion in Section 5.3.2) in order to better reconcile model outputs with observations of AOD over Europe and over dust source regions of interest for Europe (e.g. Sahara).

We conducted four simulations for the year 2004 including a standard simulation as described above, and three sensitivity simulations in which North American anthropogenic emissions (14°N-90°N; 130°W-65°W), North America biomass burning emissions (42°N-90°N; 170°W-65°W) and European anthropogenic emissions (38°N-90°N; 15°W-55°E) were turned off. Each simulation was initialized with a one-year run. Anthropogenic emissions refer in this context to fossil fuel, biofuel, aircraft and fertilizer emissions. These simulations allowed us to quantify the contribution of North American sources and European sources to the European burden in aerosols by subtracting the results of the sensitivity simulations to that of the standard run. Additional tests were performed with offline aerosol chemistry (i.e. without computing the full O_3-NO_x-VOC chemistry but using archived monthly mean fields for OH for example) to test different dust emission schemes and the inclusion of isoprene as a precursor of SOA (Section

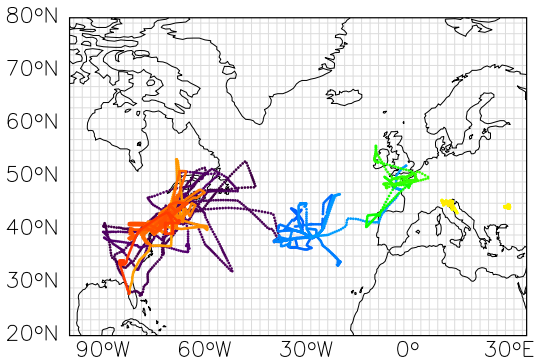

Figure 5.1: Flight tracks for INTEX-NA (red), ITCT 2k4 (purple), ITOP-BAE146 (blue), ITOP-Falcon (green) and ADRIEX-BAE146 (yellow) aircraft campaigns.

5.3.2 and 5.3.3). Section 5.3 provides a thorough evaluation of the aerosols concentrations and optical depths simulated by GEOS-Chem over Europe, the Saharan region and in the North American aerosol outflow as observed in ICARTT.

5.2.2 Aircraft observations

Several mobile platforms were deployed during the summer 2004, time window of the ICARTT campaign, to characterize chemical environment over the North Atlantic, and more specifically outflow from North America to Europe. Three major fields efforts were the NOAA New England Air Quality Study/Intercontinental Transport and Chemical Transformation (NEAQS-ITCT2k4), NASA Intercontinental Transport Experiment - North America, phase A (INTEX-NA) and the ITOP (Intercontinental Transport of Ozone and Precursors) program (Table 5.3). Figure 5.1 shows the flight tracks of these missions and Table 5.4 summarizes the different instruments used onboard of each aircraft.

Another campaign, the Aerosol Direct Radiative Impact Experiment (ADRIEX), was conducted over the end of the summer 2004 over Northern Italy, the Adriatic Sea and between Northern Italy and the West coast of the Black Sea. Its aim was to improve the understanding of the radiative effects of anthropogenic gases and aerosols.

Campaign name	Period (in 2004)	Region	Plane	Flight-days used in this study [a]
NOAA NEAQS-ITCT2k4	July 1 - August 15	North-West Atlantic, eastern United States	NOAA WP-3D [b]	5–9–11–15–20–21–22–25–27–28–31 July 3–6–7–9–11–14–15 August
NASA INTEX-NA	July 1 - August 15	Central and eastern United States	NASA DC-8	18–20–22–25–28–31 July 2–6–7-11 August
ITOP (British part)	July 12 - August 4	Azores	FAAM BAe146–300 [c]	15–17–19–20–22–25–28–29–31 July 1–3 August
ITOP (German part)	July 19 - August 6	Western Europe and eastern North Atlantic	DLR Falcon	22–23–25–26–30–31 July
ADRIEX	August 27 - September 6	Northern Italy, Adriatic Sea, west coast of the Black Sea	FAAM BAe146-300[c]	27–28–29–30 August 2–3–5–6 September

Table 5.3: Summary of the field campaigns and research aircrafts from which observations were used in the frame of our study. Rows 1 to 4: ICARTT components. Row 5: ADRIEX campaign.

[a]For NOAA NEAQS-ITCT2k4 and NASA INTEX-NA, we only used aircraft flights performed over the eastern coast of U.S. and over the North Atlantic ocean, as we are only interested in features of the outflow.

[b]the NOAA WP-3D is further referred to as P3.

[c]the FAAM BAe146–300 is further referred to as BAE146.

	P3	DC-8	BAE146	Falcon
O_3	NO/O_3 chemilumimescence	NO/O_3 chemiluminescence	UV	UV-O_3-photometer
CO	Diode laser spectrometer measurements	VUV resonance fluorescence	VUV fluorescence	CO Analysator AL 5001 fluorescence technique
NO	NO chemiluminescence	NO/O_3 chemiluminescence	-	NO/O_3 chemiluminescence
NO_2	Thermal Dissociation Laser Induced Fluorescence	Photolysis and NO/O_3 chemiluminescence	-	-
PAN	Automated dual GC with cryofocusing	Chemical Ionization Mass Spectrometer	Dual channel IGC-ECD	-
HNO_3	Chemical Ionization Mass Spectrometer	Chemical Ionization Mass Spectrometer	-	-
NO_y	-	Au converter and NO/O_3 chemiluminescence	- -	NO_y-AU-Converter NO-O_3-chemiluminescence
SO_2	Chemical Ionization Mass Spectrometry	Miniturized Differential Absorption Spectroscopy	-	-
NH_4^+, NO_3^-, SO_4^{2-}	PILS coupled to ICs	Dual ICs coupled to a PILS R	Aerodyne Aerosol Mass Spectrometer	-
Water Soluble Organic Carbon [a]	- -	Sievers Total OC instrument coupled with a PILS with syringe liquid pumping system and 0.5 μm pore (Upchurch) PEEK liquid filter	-	-
Organic Aerosol [a]	-	-	Aerodyne Aerosol Mass Spectrometer	-
AOD	-	UV Lidar	-	-

Table 5.4: Method of measurement onboard of each aircraft involved during ICARTT and ADRIEX.
[a]Observed organic carbon concentrations were transformed into POM by using an organic carbon factor of 1.4 to be consistent with the value used in GEOS-Chem. It is further referred as observed POM.

We used ten-second averaged measurements for all flights. We choose to use such a fine period to better capture the variability observed during the aircraft ascend and descend profiles. GEOS-Chem results were sampled along the flight tracks. Vertical profiles shown in Section 5.3 and 5.4 are the 10-seconds median value binned over 500 meters of altitude for all flights indicated in the fifth column of Table 5.3 of a given plane.

5.2.3 Ground-based measurements

Aerosol concentrations are measured at several sites over Europe and results are made available through the Airbase and EMEP networks.

Prior to submission to the EMEP Chemical Coordinating Centre (CCC), the data are subject to national quality assessment. The submitted data are further assessed by the EMEP-CCC in collaboration with the data originators before they are reported on an annual basis. Measurements of individual aerosol compound like sulfate, nitrate and ammonium as well as PM aerosol concentrations are provided up to 2003 [*Hjellbrekke*, 2005]. Due to sampling artefacts, separation between gases and particles could be unreliable [*Hjellbrekke*, 2005], and thus only the sum of nitric acid and nitrate as well as the sum of ammonium and ammonia are unbiased. Measurements of wet deposition fluxes of sulfate, nitrate and ammonium are also available [*Hjellbrekke*, 2005]. Data are provided on a daily basis. We build annual and monthly mean climatologies using observations (averaged over a same model grid-box) for the period 2000–2003 to compare with our 2004 model results.

Airbase data are provided by the European air quality database. The data originate from national reports within the context of EoI (Exchange of Information) and EuroAirnet (European Air Quality monitoring network). These networks were set to support the European Environment Agency (EEA) to provide European Community (EC) member states with objective, reliable and comparable measurements at the European level. Because different methods are used to collect PM_{10} measurements, correcting factors are applied as described in *Buijsman and de Leeuw* [2004] in order to have a data set as homogeneous as possible. These correcting factors are however not always provided by individual countries, which leads *Buijsman and de Leeuw* [2004] to suggest that comparing PM_{10} (and thus $PM_{2.5}$) measurements form different countries may be difficult. Measurements of PM are available for 2004 on a daily basis. Despite the above-mentioned problems, measurements can provide useful information to find possible bias or deficiencies in our aerosol simulations. For a fair comparison of our model to data provided by the air quality networks, only rural and suburban background stations of Airbase are considered and the model is sampled only on the days for which observations are available at a given site.

AOD are measured routinely from ground-based sunphotometers of the AErosol RObotic NETwork (AERONET) [*Holben*, 1998]. The measurements used in this study are level-2 quality-assured data of the Version 2 Direct Sun Algorithm products. We used observations from stations over Europe and North Africa which are provided at

500 and 440 nm, respectively. The total uncertainty of a new calibrated field instrument is typically lower than $\pm$ 0.01 for such wavelengths [*Holben et al.*, 1998]. The World Data Center for Aerosols (WDCA) in Ispra archives also AOD from several Global Atmosphere Watch (GAW) stations, including the high alpine sites of Jungfraujoch and Hohenpeissenberg in 2004. We computed daily, monthly and annual values from individual measurements. GEOS-Chem outputs are sampled on a daily basis and monthly mean values are constructed using model outputs only for those days with observations.

We also used observations from EARLINET which coordinates aerosol lidar measurements over Europe. Specific measurements were performed during ICARTT. We used measurements that were provided for the Leipzig station at the 532 nm wavelength. Hourly values of extinction coefficient were interpolated for each model level and further converted to AOD by multiplying the extinction coefficient with the depth of the model grid-box.

5.2.4 Satellite observations

The AOD observations used in this study are provided by MODIS, onboard of the NASA EOS-Terra satellite. Local time overpass is at 10.30 am. AOD (for total, fine and coarse modes) are derived over land and ocean using two independent algorithms [*Remer et al.*, 2005 and references therein]. We used version 4 products at the 550 nm wavelength with a 1°x1° resolution regridded on the 2°x2.5° model resolution. Comparison of MODIS products over land to AERONET measurements provided quantitative information of the MODIS error [*Remer et al.*, 2005]. A prelaunch uncertainty of $\tau = \pm 0.05 \pm 0.15\tau$ was predicted for MODIS AOD over land, and an extensive validation with AERONET measurements on a 2-year period shows that 68% of the 550 nm retrievals fall within this uncertainty. *Remer et al.* [2005] also noted MODIS shows a positive bias over land (relative error of 41%). Over the ocean, the predicted prelaunch uncertainty was of $\tau = \pm 0.03 \pm 0.05\tau$, and 62% of the 550 nm retrieval fall within. No bias is found and the relative error between MODIS and AERONET is very low (1%). However *Remer et al* [2005] reported a possible lower performance of the ocean algorithm on a dust-loaded atmosphere.

For comparison with MODIS AOD, GEOS-Chem outputs at 550 nm are sampled between 10 and 11 am and only for the days when MODIS observations are available. The model fine mode includes sulfate, nitrate, ammonium, carbonaceous and fine sea-salt aerosols.

5.3 Model evaluation and characterization of the aerosol load over Europe

GEOS-Chem simulations of the trace gas distributions over the North Atlantic/European area have been discussed previously (Chapters 3 and 4); therefore we only present here a short evaluation of the simulated North American outflow in terms of

trace gases (Section 5.3.1), as this could provide some useful insights for understanding our simulations aerosol outflow. We then focus our discussion on the aerosol simulation (Sections 5.3.2, 5.3.3, and 5.3.4), especially in the North Atlantic/Europe/North Africa area, which has not been the subject of any thorough evaluations yet.

5.3.1 Trace gas simulations of the North American outflow

Previous works have indicated that GEOS-Chem reproduces well the general features of the North American outflow as well as the European distribution of O_3 and O_3-related species [*Li et al.*, 2004; *Auvray and Bey*, 2005; *Li et al.*, 2005; *Guerova et al.* 2006; *Auvray et al.*, 2006]. A comparison of model results to observed vertical profiles of CO, NO, NO_y and O_3 over the North Atlantic sampled during the ACSOE campaign indicated that GEOS-Chem reproduces well the general features of that region, although the simulated NO and NO_y concentrations in the marine boundary layer present some discrepancies that could be associated with the representation of NO_x ship emissions [Chapter 3, *Auvray et al.*, 2006]. Further evaluation of the trace gas simulation is provided here in the frame of the ICARTT campaign (Figure 5.2). In general, the model agrees well with the observations (in particular for O_3 and CO), indicating that the main features of the North American outflow and its transport over the North Atlantic are correctly represented in general during that period. For example, both longitudinal and vertical patterns are well reproduced. In particular, the high CO and NO_y concentrations sampled by the Falcon at 6km altitude and which are likely to be associated with biomass burning sources over North America, are well reproduced by the model. Boundary layer CO, NO, NO_2 and NO_y are too high in the North American outflow and over western Europe. This may reflect the too high anthropogenic emissions over both U.S. and Europe as discussed in Section 5.2.1. The large upper tropospheric NO/NO_2 bias is likely due to the lightning NO_x sources over North America which are underestimated [*Hudman et al.*, in preparation].

Pollution export from the boundary layer is driven by frontal passages and deep convection associated with thunderstorms. *Auvray et al.* [2006] examined the chemical environment in plumes transported over the North Atlantic in two global models and found significant differences, in particular in term of water content of the plumes (Chapter 3). *Auvray et al.* [2006] suggested that these differences could be due to differences in convection schemes between the two models. This was found to have some significant impacts on the chemical tendencies of the plumes, but this could also have large impacts on the amount of aerosols exported in plumes as they can be more easily washed out than trace gases in general.

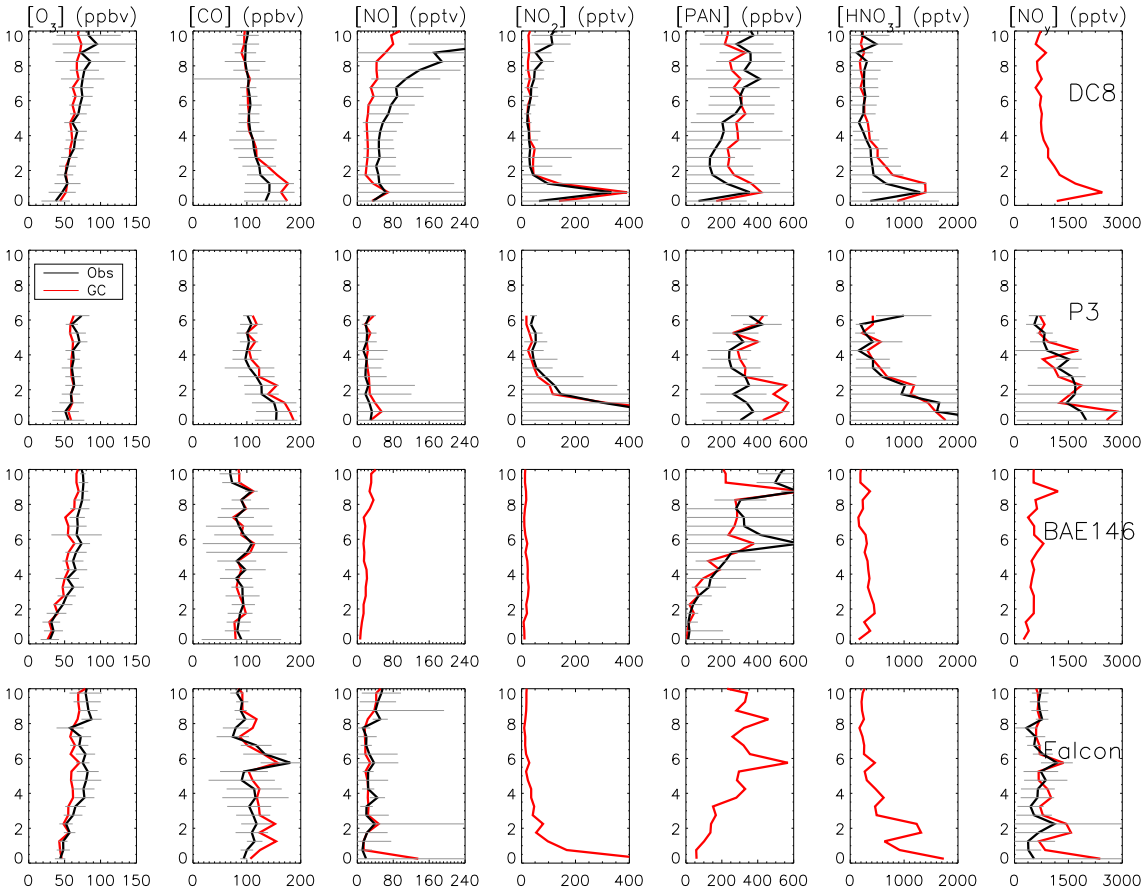

Figure 5.2: Observed (black line) vertical profiles of ten-second median O_3, CO, NO, NO_2, PAN, HNO_3 and NO_y binned over 500 metres of altitude as provided by the flights of the DC-8 (first row), P3 (second row), BAE-146 (third row) and Falcon (fourth row) aircrafts during the ICARTT campaigns. GEOS-Chem results (red line) are sampled along the flight tracks at the time and location of the observations. The horizontal bars show the observed standard deviations, reflecting the variability found over the ensemble of flights for a given plane. NO_y observations are not available for the DC-8; NO, NO_2, NO_y and HNO_3 observations are not available for the BAE-146; NO_2, PAN, HNO_3 observations are not available for the Falcon.

5.3.2 Aerosol chemical composition

Sulfate

Sulfate aerosol concentrations and wet deposition fluxes are measured in several EMEP stations distributed over 76 and 75 different 2°x2.5° model grid-boxes, respectively (Figure 5.3 and 5.4). Dry deposition is also an important process for removing aerosols (GEOS-Chem predicts that it is as important as wet deposition, e.g. *Dentener et al. [2006]*) but no data are available over Europe to evaluate this process.

EMEP sulfate concentrations show rather large gradients across Europe, with higher concentrations over Poland, Slovakia, Turkey and north of Spain and lower concentrations for Ireland and Scandinavian countries. The model has some success in reproducing the annual spatial variability (correlation coefficient r=0.61) but it tends to overestimate concentrations observed at the EMEP sites by a factor 2 (annual bias of 0.5 $\mu gS/m^3$). This is especially true in spring and summer, except in Turkey where the model simulates too low values. Similar results are found when the model is compared to observations taken during the ADRIEX campaign (Figure 5.5). Both observed and simulated vertical profiles decrease rapidly with altitude but the model overestimates observed concentrations below 3 km. Too high SO_2 emissions over Europe used in the model (see discussion in Section 5.2.1 and Table 5.1) could explain this overestimate; comparison of simulated SO_2 to EMEP SO_2 concentrations also indicated a clear overestimate (not shown). This could also indicate a too high rate of SO_2 oxidation in the model as further discussed in the following. Finally, deposition may also be too low. As shown in Figure 5.4, the spatial variation of non sea-salt sulfate wet deposition fluxes is represented correctly (r=0.65) by the model (with maximal fluxes found in central Europe) but the model simulates systematically too low fluxes (despite having too high concentrations). Combining simulated sulfate and SO_2 deposition fluxes for comparison with the non sea-salt sulfate observations enhances the correlation (r=0.71) and reduces the bias (from -12 to -7 $\mu gS/m^3$). Note that our evaluation is based on observations averaged over the period 2000–2003 (as no observations are available for 2004 yet). Interannual variability in precipitations could be an additional cause of discrepancy between simulated values for 2004 and observed values averaged over a 3-year period.

Sulfate concentrations in the outflow from North America are evaluated with profiles observed during ICARTT (Figure 5.5). The transformation of SO_2 into sulfate through oxidation by OH could be an additional source of sulfate while plumes are travelling to Europe. Therefore we are interested in the ability of the model to reproduce both the sulfate and the SO_x (defined as the sum of sulphate + SO_2) concentrations in the outflow. Measurements of sulfate are available from the DC-8, the P3 and the BAE146 aircrafts, and SO_x measurements are available from the DC-8 and P3 aircrafts. Observations show enhanced concentrations in the outflow below 2 km for DC-8 and P3 planes. The model shows also an enhancement at the same altitude but the simulated sulfate concentrations are too high by 50%. Simulated SO_x agree better with observations than sulfate alone, indicating that the rate of SO_2 oxidation may be too

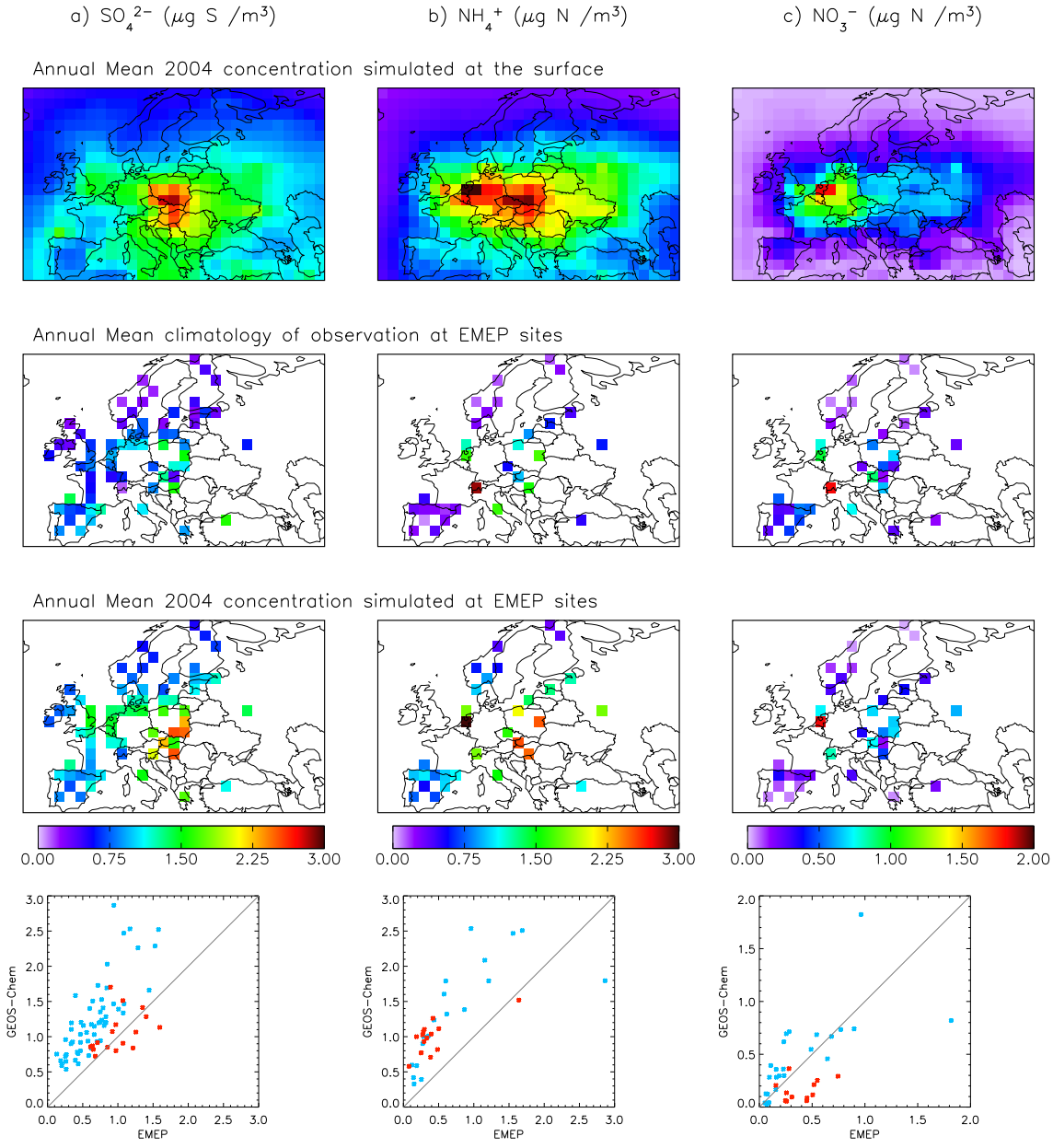

Figure 5.3: Annual averaged concentrations (μg/m^3) of (a) SO_4^{2-}, (b) NO_3^-, (c) NH_4^+. First row: Simulated 2004 concentrations at the surface. Second row: Annual average over the period 2000–2003 at EMEP sites (2004 observations are not available yet). Third row: Simulated 2004 annual concentrations at EMEP sites. Fourth row: Scatterplot of simulated versus observed concentrations at EMEP sites with regression line. Blue dots are stations located North of 46°N and red dots South of 46°N.

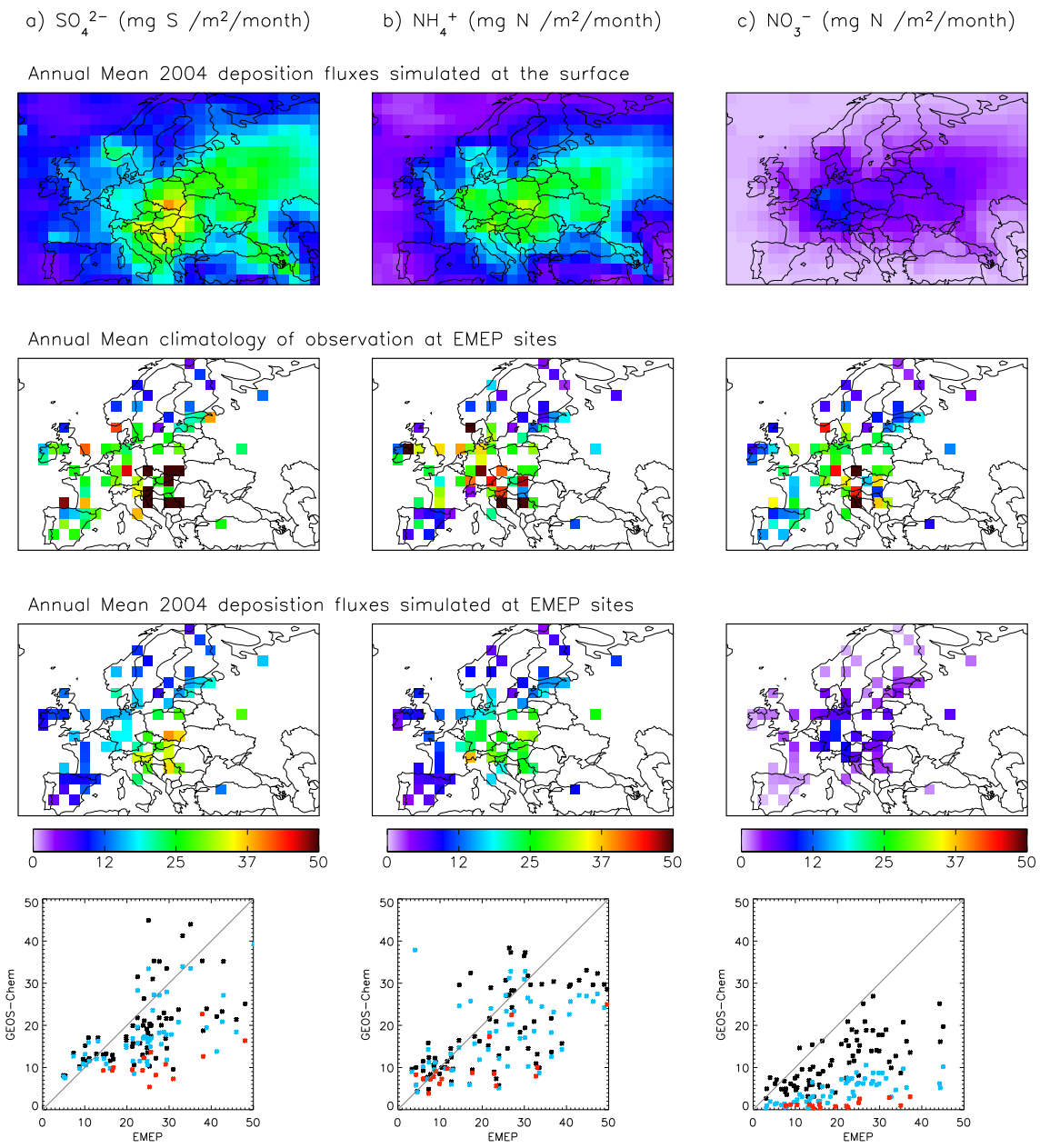

Figure 5.4: Annual averaged deposition fluxes (mg/m^2/month) of (a) SO_4^{2-}, (b) NO_3^-, (c) NH_4^+ . First row: Simulated 2004 deposition fluxes at the surface. Second row: Average of 2000–2003 annual deposition fluxes for EMEP sites. Third row: Simulated 2004 annual deposition fluxes for EMEP sites. Fourth row: Scatterplot of simulated versus observed deposition fluxes at EMEP sites with regression line. Blue dots are stations located North of 46°N and red dots South of 46°N.

high in the model. Similar results are found for the Asian outflow [*Heald et al.*, 2005]. Sulfate concentrations sampled by the BAE146 are lower than the ones found in the North American outflow (Figure 5.5). The simulated values are again higher than the observed ones but no SO_x concentrations are available to further discuss the model's capability.

Ammonium

Ammonium concentrations and wet deposition are measured in several EMEP stations distributed over 36 and 77 different model 2°x2.5° grid-boxes, respectively. Annual mean 2000–2003 ammonium concentrations are higher in Switzerland, Netherlands, Italy, and eastern European countries (Figure 5.3). The model reproduces relatively well the ammonium spatial variability (r=0.76) but overestimates the observed concentrations by a factor 1.75 (0.6 $\mu g/m^3$). Similar results are found for the vertical profiles over Northern Italy during the ADRIEX campaign (Figure 5.5). We attribute part of this overestimate to too low simulated wet deposition fluxes in comparison with available observations for the period 2000–2003 (Figure 5.4).

Over North America, *Park et al.* [2004] found that ammonium spatial variability is well represented both in term of annual and seasonal cycle, although ammonia emissions are excessive in fall over the U.S. The DC-8 and BAE146 aircrafts sampled ammonium concentrations during the ICARTT campaign (Figure 5.5). Large concentrations were found in the boundary layer and at around 6 km by the DC-8 in the vicinity of U.S. while smaller concentrations were found by the BAE146 around the Azores. The model reproduces well the observed concentrations over the Azores but underestimates significantly the elevated concentrations observed in the upper level by the DC-8.

Nitrate

Nitrate is predominantly present in the form of ammonium nitrate (NH_4NO_3). Nitrate concentration is linked to the relative abundance of ammonium and sulfate. Nitrate is produced if ammonia is available in excess of the amount required to neutralize sulphuric acid. Annual mean 2000–2003 nitrate concentrations are higher over Switzerland, Netherlands, Poland and Slovakia (Figure 5.3). The model reproduces some of these features (annual spatial variability, r=0.59) but tends to underestimate nitrate concentrations, especially in Southern Europe. This is also shown by the ADRIEX observations (Figure 5.5). Vertical profiles drop rapidly with altitude due to scavenging processes. Deposition fluxes are underestimated by the model (Figure 5.4). Combining simulated nitrate and HNO_3 deposition fluxes for comparison with the observations enhances the correlation (r=0.45 to 0.58) and reduces the bias by half.

The gas ratio (GR) is defined as $GR = ([NH_x] - 2[SO_4^{2-}])/[HNO_3^T]$ where NH_x is defined as the sum of $NH_{3(g)}$ plus ammonium, HNO_3^T is defined as the sum of aerosol phase nitrate and $HNO_{3(g)}$, and $([NH_x] - 2[SO_4^{2-}])$ is the free ammonia which could

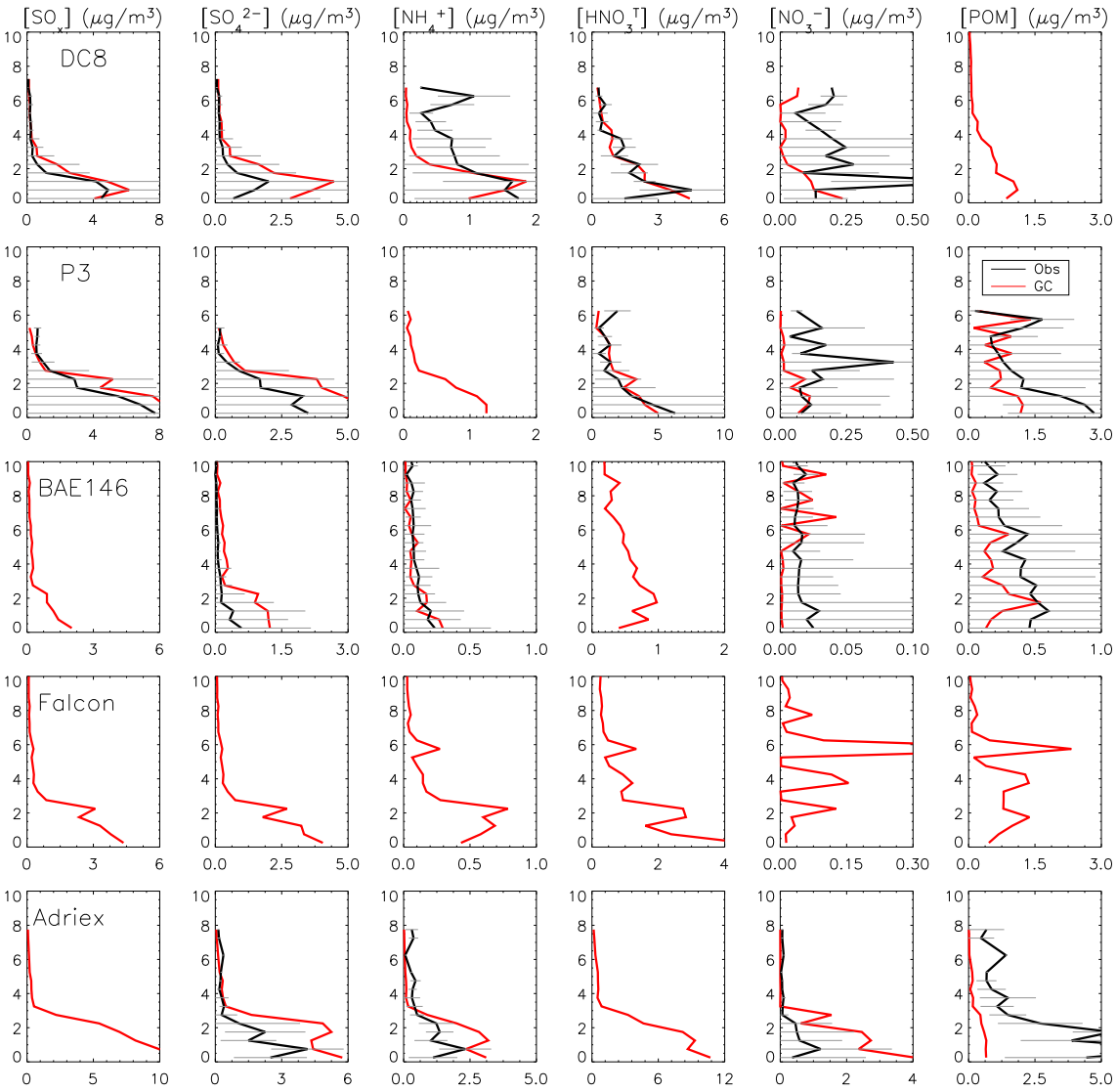

Figure 5.5: Observed (black line) vertical profiles of the ten-second median SO_x (defined as the sum of SO_2 and sulfate aerosol), SO_4^{2-}, NH_4^+, HNO_3^T (defined as the sum of HNO_3 and inorganic nitrate aerosol), NO_3^- and POM binned over 500 metres of altitude for the flights of the DC-8 (first row), P3 (second row), BAE-146 (third row) and Falcon (fourth row) aircrafts during the ICARTT campaigns and by the BAE-146 (fifth row) during the ADRIEX campaign. For the P3, only the water soluble part of POM is measured (and simulated as well). GEOS-Chem results (red line) are sampled along the flight tracks at the time and location of the flights. The horizontal bars show the observed standard deviations, reflecting the variability over the ensemble of flights for a given plane. OC observations are not available for the DC-8. NH_4^+ observations are not available for the P3. SO_x and HNO_3^T observations are not available for the BAE-146. No aerosol observation is available for the Falcon flight and no trace gas observation is available for ADRIEX.

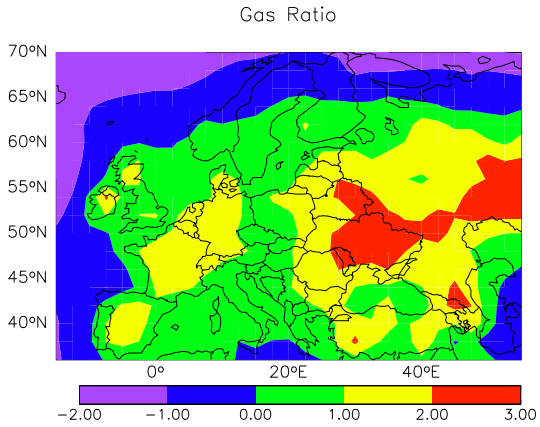

Figure 5.6: Simulated annual 2004 gas ratio (GR) in surface air defined as the available ammonia concentration beyond that required for sulfate neutralization, divided by the total inorganic nitrate concentration (gas plus aerosol) [*Ansari and Pandis*, 1998]. Formation of nitrate aerosol is limited by the availability of nitric acide if GR>1 and by the availability of ammonia if 0<GR<1, and is totally suppressed if GR<0.

react with HNO_3^T. GR diagnoses the limitant reaction for the formation of ammonium nitrate [*Ansari and Pandis*, 1998]. Figure 5.6 shows nitrate simulated with GEOS-Chem in western and eastern Europe is generally limited by the supply of nitric acid (GR>1). In central, southern and northern Europe, the ammonium nitrate formation is limited by the supply of ammonia (GR<1). For this region, a decline in sulfate concentrations may result in a subsequent rise of nitrate level [*Ansari and Pandis*, 1998]. Negative GR value, indicating no presence of nitrate are mainly confined to the ocean and at high latitude (>65°N).

Nitrate outflow from North America is further evaluated with the measurements from the DC-8, the P3 and the BAE146 during the ICARTT campaign. *Park et al.* [2004] indicated that nitrate concentrations are clearly overestimated by GEOS-Chem over North America. However, nitrate outflow from North America is underestimated during July and August 2004 in comparison with observations from the DC-8 and P3 (Figure 5.5). HNO_3^T observations agree better with the model. The model also underestimates the nitrate concentrations observed by the BAE146 measurements below 4 km but the agreement is better at higher altitudes. Analysis of our model sensitivity simulations indicated that the high concentrations simulated above 5 km are due to North American anthropogenic sources.

Dust

Dust emissions depend mainly of wind speed, soil moisture and size distribution, vegetation cover and surface roughness. Dust entrainment into the atmosphere can only occur when wind speed exceed a certain threshold. Given the cubic dependence of emission fluxes to wind speed, small-scale high winds can induce dust emissions that may not be accounted for if one uses regional averaged winds. The spatial resolution

of wind fields is thus an important factor to represent accurately dust emissions, and global models with coarse resolution have encountered difficulties to achieve a good representation of dust emissions [*Cakmur et al.*, 2004]. Moreover, one has to keep in mind that few observations are available over desert regions for being used into meteorological reanalysis.

Preliminary comparisons of our simulated AOD over North Africa with those provided by AERONET pointed out a significant overestimate of the model results (see Figure 5.8 and the following discussion). We noted also a large positive bias in our simulation of AOD over Europe, especially in the southern part. Both were likely to reflect too high simulated dust sources. Therefore, we tested several dust emission schemes in order to achieve a better agreement between simulated and measured AOD over both North Africa and Europe.

We first tested the Dust Emission And Deposition (DEAD) scheme of *Zender et al.* [2003] and the Goddard Global Ozone Chemistry Aerosol Radiation and Transport (GOCART) scheme of *Ginoux et al.* [2001]. The main difference between these two schemes lay in the regions that are considered as potential dust sources. The GOCART scheme restricts dust mobilization to vegetation-free arid regions (e.g. deserts) while the DEAD scheme account for changing vegetation cover (derived from satellite observations of leaf area index). This can result in large regional differences [*Fairlie et al.*, 2006]. The two schemes also differ slightly by their emission formulation. The third scheme that we have tested is a mix of the two previous schemes: mobilization is derived by multiplying the source area from *Ginoux et al.* [2001] by the mobilization calculated using the DEAD emission formulation [*Luo et al.*, 2003; *Fairlie et al.*, 2006]. Table 5.5 provides the dust emissions over the Sahara and globally computed with the different schemes.

Tg/yr	DEAD	GOCART	GOCART Source function + DEAD emission formulation	DEAD emissions scaled on *Laurent* [2005] over the Sahara
World	2364	3679	2363	1214
Sahara	1823	2363	1901	674

Table 5.5: Dust emissions globally and over the Sahara (10°N-36°N; 20°W-40°E) with the 4 different schemes tested in the GEOS-Chem model.

Figure 5.7 shows the simulated seasonal variations of dust emissions over the Sahara and its occidental and oriental parts. We compared our simulated dust emissions with available inventories taken from the literature, including data from *d'Almeida* [1986], *Marticorena and Bergametti* [1996] and *Laurent* [2005]. *D'Almeida* [1986] derived dust emissions over the Sahara from a box-model constrained by measurements from a turbidity network and from associated meteorological observations for the years 1981 and 1982. *Marticorena and Bergametti* [1996] used a dust emission scheme derived from soil properties [*Marticorena and Bergametti*, 1995] and European Centre for Medium-range Weather Forecasts (ECMWF) wind fields with a square degree resolution to compute 1991–1992 source emissions in the western Sahara. *Laurent* [2005] improved the work

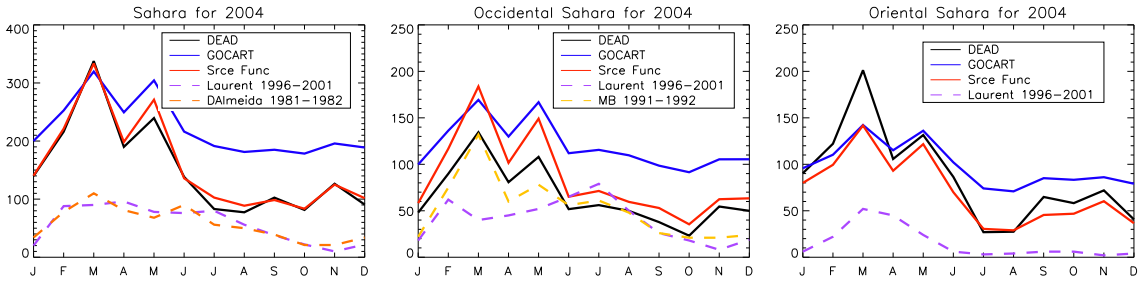

Figure 5.7: Dust emissions for the entire Sahara (left), occidental Sahara (middle) and oriental Sahara (right). Continuous lines: Dust emissions (Tg) simulated with GEOS-Chem with the DEAD module (black line), the GOCART module (blue line) and a mix of the two schemes (red line); Orange dotted line: emissions from *d'Almeida* [1986]. Yellow dotted line: emissions from *Marticorena and Bergametti* [1996]; Purple dotted line: emissions from *Laurent* [2005].

of *Marticorena and Bergametti* [1995; 1996] in two ways: roughness lengths were estimated from observations provided by POLDER-1 space-borne sensor and improved soil size distributions and textures for Saharan soils were determined [*Chatenet et al.*, 1996; *Callot et al.*, 2000]. *Laurent* [2005] used ECMWF 40 year Re-Analysis (ERA-40) wind fields from 1996 to 2001 with a 0.25°x0.25° resolution. Further details of the improvements presented in *Laurent* [2005] are given in *Marticorena et al.* [2004] and *Laurent et al.* [2005].

Similarities are found between the emissions computed by the DEAD scheme and *Marticorena and Bergametti* [1996] results, as expected since both schemes follow *Marticorena and Bergametti* [1995]'s formulation to compute the horizontal saltation fluxes (direct mobilization of particles by the wind). Both fluxes overestimate those found by *Laurent* [2005] and *d'Almeida* [1986]. The improvement proposed by *Luo et al.* [2003] and *Fairlie et al.* [2006] results also in much larger emissions than those from *Laurent* [2005] and *d'Almeida* [1986] and would not allow us to significantly reduce the bias found between observed and simulated AOD over North Africa (see also discussion further below). An additional test was thus performed, in which the GEOS-Chem dust emissions were calculated with the DEAD scheme (providing the different dust classes) and total emissions were then scaled on a monthly basis to those proposed by *Laurent* [2005].

We evaluated the skill of these different schemes using AERONET AOD (440 nm) at several stations in North Africa and southern Europe (see first panel of Figure 5.8. Simulated AOD using the DEAD, GOCART and mix schemes clearly overestimate observed AOD at all the stations. We find that the bias is largely reduced when the model DEAD emissions are scaled to those of *Laurent* [2005]. However, south of 14°N, the simulated AOD are slightly too low. This can reflect an underestimate of dust sources in that region but also of the prescribed biomass burning sources, which are of particularly influence in this region from November to March, and/or the anthropogenic emissions from the nearby cities (e.g. Ouagadougou). Using the DEAD emissions scaled to those of *Laurent* [2005] induced a slight increase (from 0.37 to 0.46) of correlation

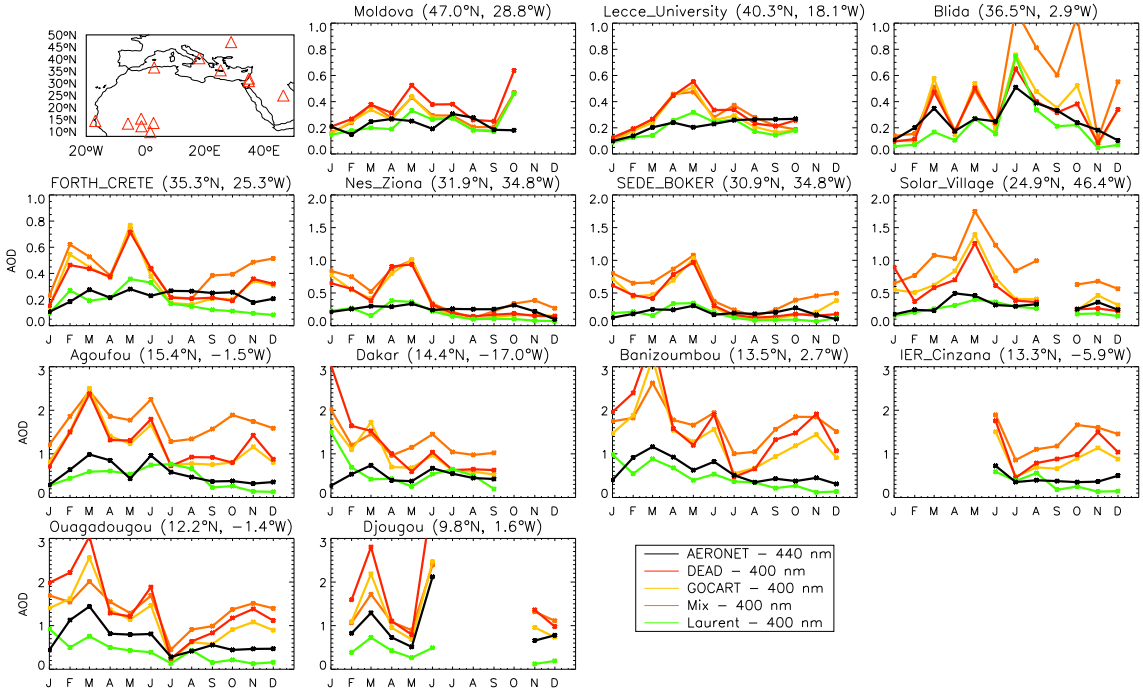

Figure 5.8: Comparison between monthly AERONET AOD at 440 nm (black line) and simulated monthly AOD at 400 nm with different dust modules, including DEAD (red line), GOCART (yellow line), mix scheme (orange line) and using DEAD emissions scaled to those of *Laurent* [2005] (green line). The first graph shows the location of AERONET stations used in this figure. The latitude and longitude coordinates indicated at the top of each graph correspond to the coordinate at the center of the model grid-box, and the following figure is the number of stations present in each grid-box.

coefficient in the stations north of 16°N but a small decrease (from 0.63 to 0.43) in the southernmost stations. Despite this partial lost in seasonal variability, we choose to use the DEAD scheme scaled to *Laurent* [2005]'s dust emissions in order to avoid a systematic overestimate of the dust burden over Europe. In the following, unless stated otherwise, we used the DEAD scheme and scaled the emissions over the Sahara to those of *Laurent* [2005]. Further results of the inter-comparison between the different simulations will be presented in Section 5.3.3.

Carbonaceous aerosol

A lack of BC and POM measurements over Europe do not allow comparison between ground-based measurements and the model. However, during the ADRIEX campaign, POM was measured by the BAE146 in southern Europe (Figure 5.5). Vertical profiles observed during ADRIEX show a decrease in POM concentrations with altitude but less rapid than for sulfate aerosols, which has already been noticed during the Asian Pacific Regional Aerosol Characterization Experiment (ACE-Asia) [*Heald et al.*, 2005] and the Transport and Chemical Evolution over the Pacific (TRACE-P) observations [*Park et*

al., 2005]. The model underestimates POM concentrations over the whole tropospheric column up to 95%. This does not appear to be related with missing biomass burning sources in the model, as ATSR fire-counts indicated no large fires during the period of the measurements.

In fact, the mechanisms for the formation of SOA remain largely uncertain. *Heald et al.* [2005] observed a similar discrepancy over east Asia and suggested that this underestimate could be due to a missing source from sustained formation of SOA in ageing air masses, related to successive generation of oxidation products of VOCs. In the present version, the SOA formation in the model is based on the scheme described by *Chung and Seinfeld* [2002], which assumes that SOA are produced after oxidation of heavy biogenic compounds such as monoterpenes. Several studies have however suggested that isoprene could also provide an additional source of SOA [*Claeys et al.*, 2004a; 2004b; *Edney et al.*, 2005; *Matsunaga et al.*, 2005]. Following *van Donkelaar et al.* [2006a], we investigated the sensitivity of the model to direct SOA production through isoprene. However, this test provided no improvement in the ADRIEX profiles (maximal increase of 0.02 $\mu g/m^3$ in the boundary layer). Further results of this test are presented in Sections 5.3.3.

Vertical profiles of the outflow from the North American east coast and over the middle of the Atlantic sampled respectively with the P3 (soluble fraction) and the BAE146, show decreasing POM concentrations with altitude, but less rapidly than for the sulfate aerosols (Figure 5.5). Simulated POM are too low in general compared to the observations, especially below 3 km in the vicinity of U.S. and for the whole column over the Azores, suggesting, again, that SOA formation may take place as the air masses travel far away from sources. Both the P3 and the BAE146 aircrafts measured enhanced layers of POM at around 6 km which are reproduced by the model, to some extent. Sensitivity tests indicated that these enhancements are associated with biomass burning sources.

5.3.3 Aerosol optical depth

In this section, we first present results of sensitivity tests on the different dust modules and on SOA formation through isoprene. Then we present an evaluation of the model with AERONET and GAW measurements and with MODIS AOD retrieval. We finish with a generalization of our findings over Europe.

Quantitative analysis of the sensitivity tests

We performed a quantitative comparison of the different sensitivity tests with AOD observations. In order to synthesize all the resulting information, we present the results using Taylor diagrams (Figure 5.9). Taylor diagrams allow statistical quantification of the degree of similarity between two fields [*Taylor*, 2001], namely model results (f_m) and observations (f_o). Such a diagram provides information (i) on the variation between observations and simulations average via the correlation coefficient r, (ii) on

the difference between the two fields via the centered root mean square difference (RMS_c), and (iii) on the standard deviation (σ) of each field.

$$\mathrm{RMS_c} = \sqrt{\frac{1}{N}\sum_{n=1}^{N}[(f_n - \bar{f}) - (r_n - \bar{r})]^2}$$

$$\sigma = \sqrt{\frac{1}{N}\sum_{n=1}^{N}(f_n - \bar{f})^2}$$

$$r = \frac{\frac{1}{N}\sum_{n=1}^{N}(f_n - \bar{f}) - (r_n - \bar{r})}{\sigma_m \sigma_o}$$

Here, we used a normalized version of Taylor diagram for which standard deviations and RMS_c are normalized by the standard deviation of the observed field. Each sensitivity test (symbolized by a letter in Figure 5.9) is represented by a given point. The radial distance from the origin to each point is proportional to the ratio of the standard deviation of the model and the observations ($\hat{\sigma}_m = \sigma_m/\sigma_o$). The azimuthal position gives the correlation coefficient. The ratio of the RMS_c with the standard deviation of the observed data set is proportional to the distance between the point and its reference point. To discriminate between two simulated fields when the correlation coefficient decreases but the RMS_c is reduced, we used the skill score S which increases with increasing RMS_c error but is penalized for too low correlations:

$$S = \frac{4(1+r)}{(\hat{\sigma}_f + 1/\hat{\sigma}_f)^2(1+r_0)},$$

where r_0 is the maximum attainable correlation (set to 1, although it should be less because of spatial and time resolution differences) [*Taylor*, 2001]. The contours of constant skill score are plotted in the figures. Statistical quantities are computed annually and seasonally.

Figure 5.9 shows that the simulation that uses *Laurent* [2005]'s dust emissions presents a better skill score in comparison to simulations using the other dust schemes, for the global year and the winter and spring seasons, when dust emissions are at a maximum. This result supports our choice of using dust emissions scaled to the ones of *Laurent* [2005]. The simulation that uses isoprene as a source of SOA provides only a small (if any) improvement of the simulated AOD.

Comparison to AERONET, GAW and MODIS observations

In this section, GEOS-Chem AOD (calculated at 550 nm) are compared to AERONET and GAW observations (provided at 500 nm) as well as MODIS retrievals (provided at 550 nm) sampled at the same location. We first investigated to what extent the AOD at 550 and 500 nm differ in order to interpret the bias between AERONET/GAW and the model/MODIS AOD. AOD (τ_0 and τ_1) at two wavelengths ($\lambda_0 = 550$ nm and $\lambda_1 = 500$ nm) are linked through the following relation: $\tau_0/\tau_1 = (\lambda_1/\lambda_0)^{-\alpha}$ where α is

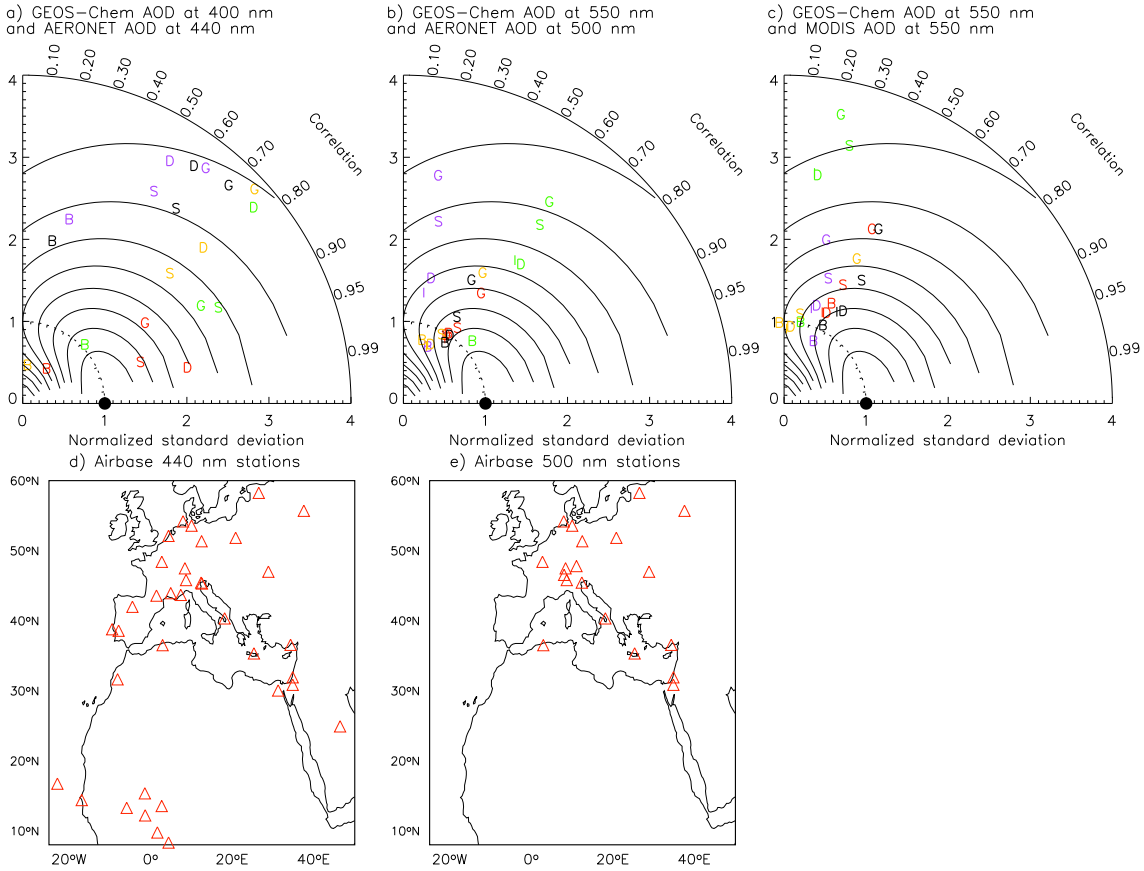

Figure 5.9: Taylor diagrams comparing GEOS-Chem simulations with (a) AOD (440 nm) at AERONET stations (b) AOD (550 nm) at AERONET stations, (c) AOD (550 nm) retrived from MODIS at the location of AERONET stations (500 nm). The black dot is used as the reference to which simulated fields are compared. Each letter corresponds to a given simulation; D: simulation performed with the DEAD dust emission module of *Zender et al.* [2003]; G: simulation performed with the GOCART module [*Ginoux et al.*, 2001]; S: mix scheme combining the source function of GOCART with the DEAD emission formulation [*Luo et al.*, 2003; *Fairlie et al.*, 2006]; B: DEAD emissions scaled to *Laurent* [2005]'s emissions; I: simulation performed with the DEAD dust module and including a direct SOA production by isoprene (see test for further detail). The statistical quantities presented are based on simulated and observed annual mean (black), winter (purple), spring (green), summer (red) and fall (yellow). Continuous black line show iso-contours of skill score, starting at 0.9 (for the one closed to the black point) and decreasing by unity of 0.1. (d) Location of the AERONET stations (440 nm) used in (a). (e) Location of the AERONET stations (500 nm) used in (b) and (c).

the Angström exponent which depends on the aerosol size [*Angström*, 1964]. Typical values of α range from 0 (coarse aerosol) to 3 (fine aerosol) (see for instance satellite observations, http://smsc.cnes.fr/POLDER/ A_produits_scie.htm), thus we expect the difference to be negligible for coarse-only loaded atmosphere and within 25% when fine aerosols are dominant. We verified this relative error using AOD directly measured at 555 and 500 nm at the AERONET Venice site. We found that the difference could reach up 20% on a monthly-basis and annually, the AOD at 555 nm is lower than that at 500 nm by 13.7% on an annual basis.

We first compare spatially the simulated annual mean AOD over Europe to AERONET and GAW measurements and to AOD retrieved from MODIS (Figure 5.10). AERONET and GAW stations are distributed over 19 grid-boxes of the model and MODIS is retrieved over 432 grid-boxes. Lowest values of the AOD are found in the north-western part of Europe and highest values in central and southern Europe, both in satellite and ground-based measurements. This is consistent with the findings of *Wandinger et al.* [2004] (using lidar measurements), who found that AOD increase with increasing distance from the North Atlantic. However lower values are found at the Jungfraujoch ground-based station, reflecting the fact that this site is located in the free troposphere most of the year.

Spatial variations are represented correctly when the model is compared to AERONET (r=0.56) and even better if the area is restricted north of 46°N (r=0.94). The correlation coefficient between simulated and MODIS AOD (calculated for the region shown on Figure 5.10) is relatively low (0.34). We noted larger discrepancies between the model and MODIS AOD south of 46° and over France and eastern Europe, which may be due to the presence of dust and problems in the MODIS retrieval as discussed before [*Remer et al.*, 2005].

Figure 5.11 shows seasonal variations of simulated and observed AOD for the 19 AERONET and GAW stations. Values for MODIS are also represented with corresponding values for GEOS-Chem. Those monthly values are highly dependent on the sampling of the data (see red and orange dotted lines of Figure 5.11). The different observed data set provide a similar picture of seasonal variations, although large differences are seen in some cases. Differences in temporal sampling, as illustrated by the two model results (red line versus orange dashed line), can only explain part of the differences. One specific case is at the Jungfraujoch station, where higher AOD are found for MODIS than for both GAW and simulated values. The MODIS AOD, originally provided at 1°x1° resolution, were degraded to the 2°x2.5° model grid-box resolution; this could explain the difference seen between GAW and MODIS, and highlights the necessity of using observations at fine spatial resolution to provide a clear picture of the large variability in aerosol distributions. For this station, the GEOS-Chem AOD are similar to the GAW AOD, as the model was sampled only for the free troposphere, thus representing better the free tropospheric conditions observed at the Jungfraujoch.

Both the observed and simulated AOD tend to be higher in the south, which likely reflects an increased contribution of mineral dust from North Africa, as also noted by *Matthias et al.* [2004]. There is no clear signal in terms of seasonal variations, but

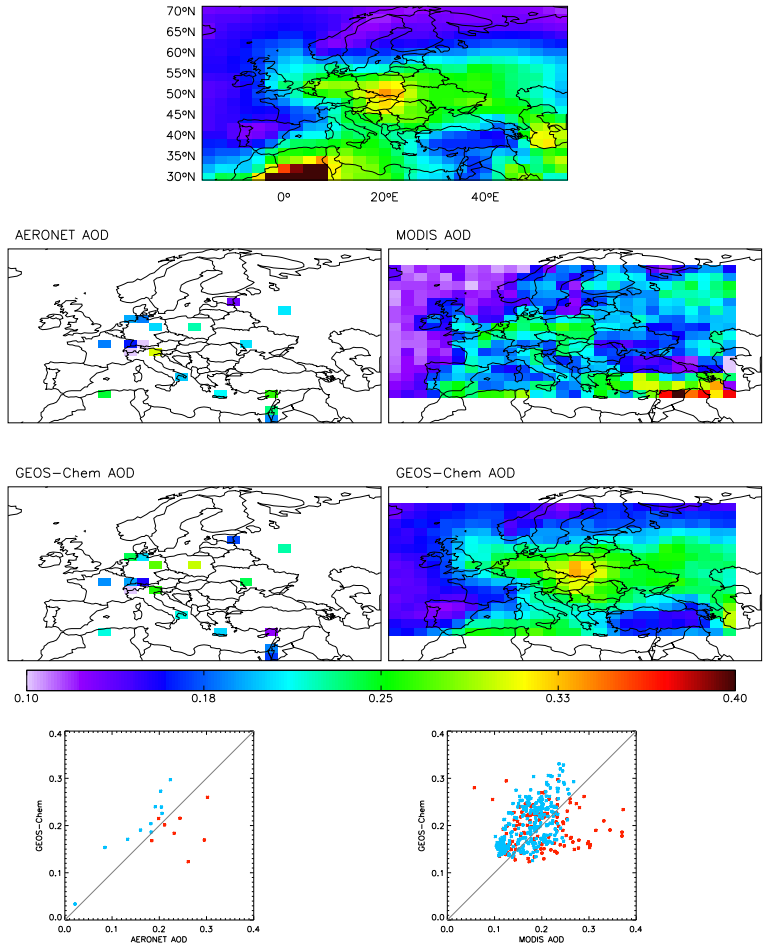

Figure 5.10: Annual value of AOD. First row: Simulated 2004 AOD from the surface up to the tropopause. Second row: Average of 2004 annual AOD for AERONET sites and retrieved with MODIS. Third row: Simulated 2004 annual AOD sample in the same way as AERONET sites and in the same way as MODIS. Fourth row: Scatterplot of simulated versus observed AOD at AERONET sites and retrieved AOD from MODIS with regression line. The blue and red dots correspond to the stations located north and south of 46°N, respectively.

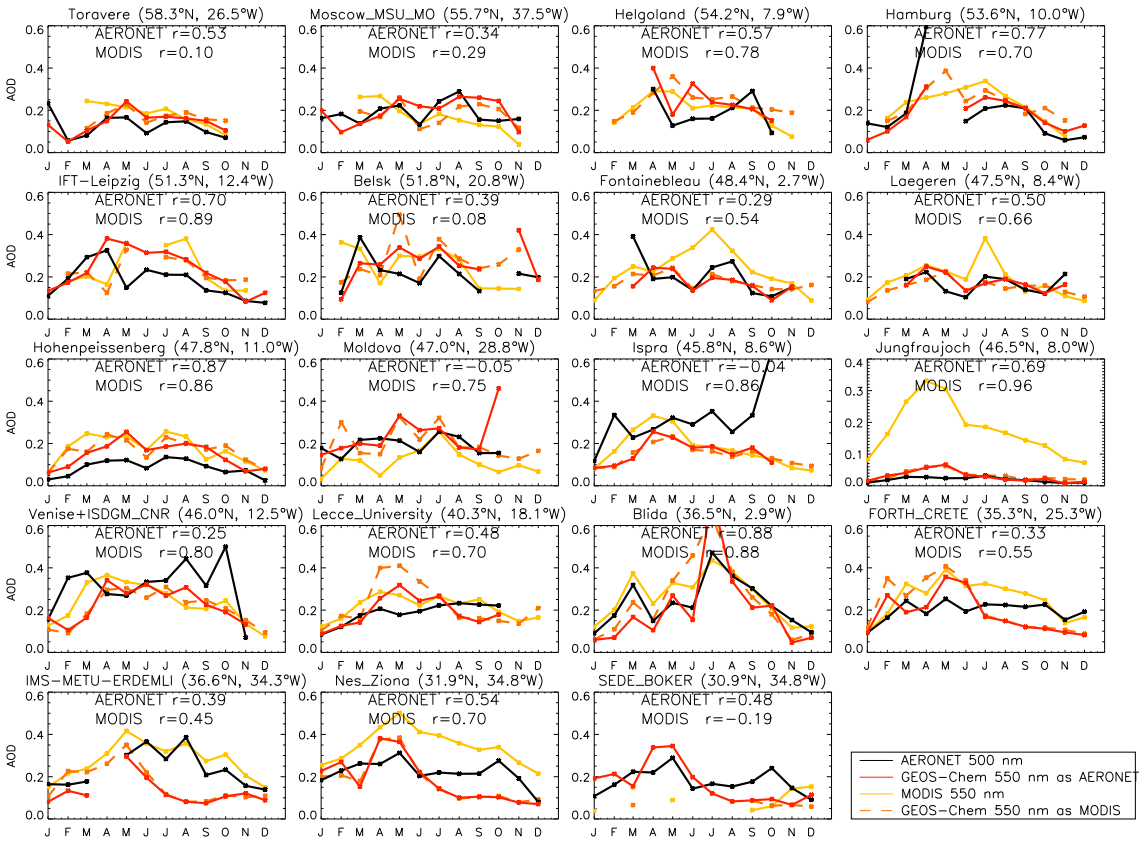

Figure 5.11: Comparison between simulated and observed monthly AOD at AERONET stations. Black line: AERONET AOD at 500 nm; Red line: GEOS-Chem AOD at 550 nm sampled with the same temporal frequency as AERONET; Yellow line : MODIS at 550nm; Orange dashed line: GEOS-Chem AOD at 550 nm sampled with the same temporal frequency than MODIS. The latitude and longitude coordinates indicated at the top of each graph correspond to the coordinate at the center of the model grid-box. Correlation coefficients r between model monthly mean and AERONET AOD and mode monthly mean and MODIS AOD are also indicated in each graph.

AOD are in general lower in winter, which is consistent with the lidar measurements presented in *Matthias et al.* [2004]. *Wandinger et al.* [2004] also indicated smaller AOD in winter than in summer (by 10–30%). This likely reflects a combination of different processes, including enhanced scavenging in wintertime, enhanced ammonia emissions in summertime, enhanced dust transport in springtime, and enhanced summertime biogenic emissions (and thus SOA formation). In fact, the main contributors to AOD are the sulfate-nitrate-ammonium aerosols in the northern stations, which drive the seasonal cycle while the southern stations are more influenced by dust, which then drive the seasonal cycle (see Figure 5.17).

5.3.4 Particulate Matter

We further evaluate aerosol concentrations with PM measurements available from air quality networks. $PM_{2.5}$ concentrations in the model are calculated as the sum of sulfate, nitrate, ammonium, BC, OC, fine mineral dust (diameter from 0.2 to 2 μm) and fine sea-salt (diameter ranging from 0.2 to 1 μm). PM_{10} includes $PM_{2.5}$ plus coarse mineral dust (diameter from 2 to 12 μm). We choose not to include the sea-salt coarse fraction with a diameter ranging from 1 to 20 μm. PM measurements are available from the Airbase network for 2004 and from the EMEP network from 2000 to 2003. PM_{10} ($PM_{2.5}$) concentrations are measured in several stations distributed over 25 (13) different 2°x2.5° grid-boxes of the model for EMEP and over 93 (27) different 2°x2.5° grid-boxes for Airbase. For comparison to EMEP data set, we show the simulated monthly and annual mean. For comparison with Airbase data set, simulated monthly and annual mean are constructed using only the days for which data are available. The first part of this section compares simulated annual and monthly means PM with observed PM_{10} and $PM_{2.5}$ from EMEP and Airbase, and the second part examines the PM distribution over continental Europe in term of individual components.

Comparison to $PM_{2.5}$ and PM_{10} observations

Figure 5.12 compares annual mean of simulated and observed PM concentrations from EMEP and Airbase and Table 5.6 presents statistic results. Lower PM_{10} values are found in Northern Europe and maximal values are found in Southern Europe (Spain and Balkan Peninsula). Note that over Spain, the PM_{10} observations provided by Airbase are quite different from those provided by EMEP. According to *Buijsman and de Leeuw* [2004], the quality of the data from the networks may be questionable, and it could be dangerous to compare the observations from different sites which do not use the same equipment. These differences between the two networks may also indicate regional features which are not well captured by the model, even though we selected data only from the background and rural sites. Despite the differences between the two networks, one can see that the model only capture poorly the observed spatial variability of the PM_{10} concentrations (r= 0.32 and 0.44 for EMEP and Airbase, respectively). In particular, the model largely overestimates concentrations observed over western and central Europe and fails to reproduce enhanced concentrations over southern Europe.

From the few available observations, the spatial distribution in $PM_{2.5}$ concentrations appears to be slightly different: higher concentrations are found in central Europe, which seems to be represented relatively well by the model (r=0.7 and 0.85 for EMEP and Airbase, respectively).

	r	Mean obs	Mean model	Bias (%)	Absolute bias (%)	RMS_c
PM_{10} EMEP	0.32	18.32	22.51	4.20 (32%)	6.60 (42%)	6.90
PM_{10} Airbase	0.44	20.97	21.39	0.42 (14%)	6.18 (31%)	8.02
$PM_{2.5}$ EMEP	0.85	11.35	10.29	-1.06 (-1%)	2.64 (21%)	3.38
$PM_{2.5}$ Airbase	0.70	13.13	13.80	0.67 (10%)	2.63 (20%)	3.50

Table 5.6: Statistical quantities between observed (through Airbase and EMEP networks) and simulated annual PM_{10} and $PM_{2.5}$ concentrations.

We now examine the seasonal variations in some of the Airbase stations, by choosing stations which are in the same grid-box than the AERONET stations (Section 5.3.3). Figure 5.13 shows seasonal variations for these 13 selected PM_{10} individual stations (see white dots on the first row of Figure 5.12 for the location of each station). The model actually shows higher seasonal variations than the observed values. According to the model, dust and sulfate-nitrate-ammonium aerosols are the main contributors to PM_{10} concentrations. Seasonal variations in the simulated values are driven by dust concentrations. In particular, the model simulates PM_{10} peaks in winter in southern Europe and in summer north of 46°N which are not seen in the observations. Such different behaviors between the two regions may reflect, for example, differences in precipitations for the two regions. Some dust plumes may also leave North Africa following a north-easterly path over the Atlantic ocean before entering continental Europe at higher altitudes.

Seasonal variations of $PM_{2.5}$ concentrations at individual stations (corresponding to the stations present in the same grid-box than AERONET stations) are shown in Figure 5.14 (see white dots on the first row of Figure 5.12 for the location of each station). The seasonal variation is relatively well represented (correlation coefficient averaged for all stations of 0.58) and is mainly driven by sulfate-nitrate-ammonium aerosols. Sulfate-nitrate-ammonium aerosols account for the main part of $PM_{2.5}$ concentrations. The remaining part is due to dust and POM (in summer).

Retrieval of particulate matter concentrations from satellite

Previous works have explored the possibility of using AOD observed from space to estimate the surface PM concentrations. This could compensate the lack of $PM_{2.5}$ measurements, and provide a cost-effective way for monitoring $PM_{2.5}$ pollution. *Wang and Christopher* [2003] have found a strong relationship between $PM_{2.5}$ concentrations and MODIS AOD retrieval in Alabama (U.S.). *Liu et al.* [2004] developed a simple approach to retrieve $PM_{2.5}$ from AOD provided by satellite by applying local scaling factors from a global three-dimensional model and suggested the following relationship:

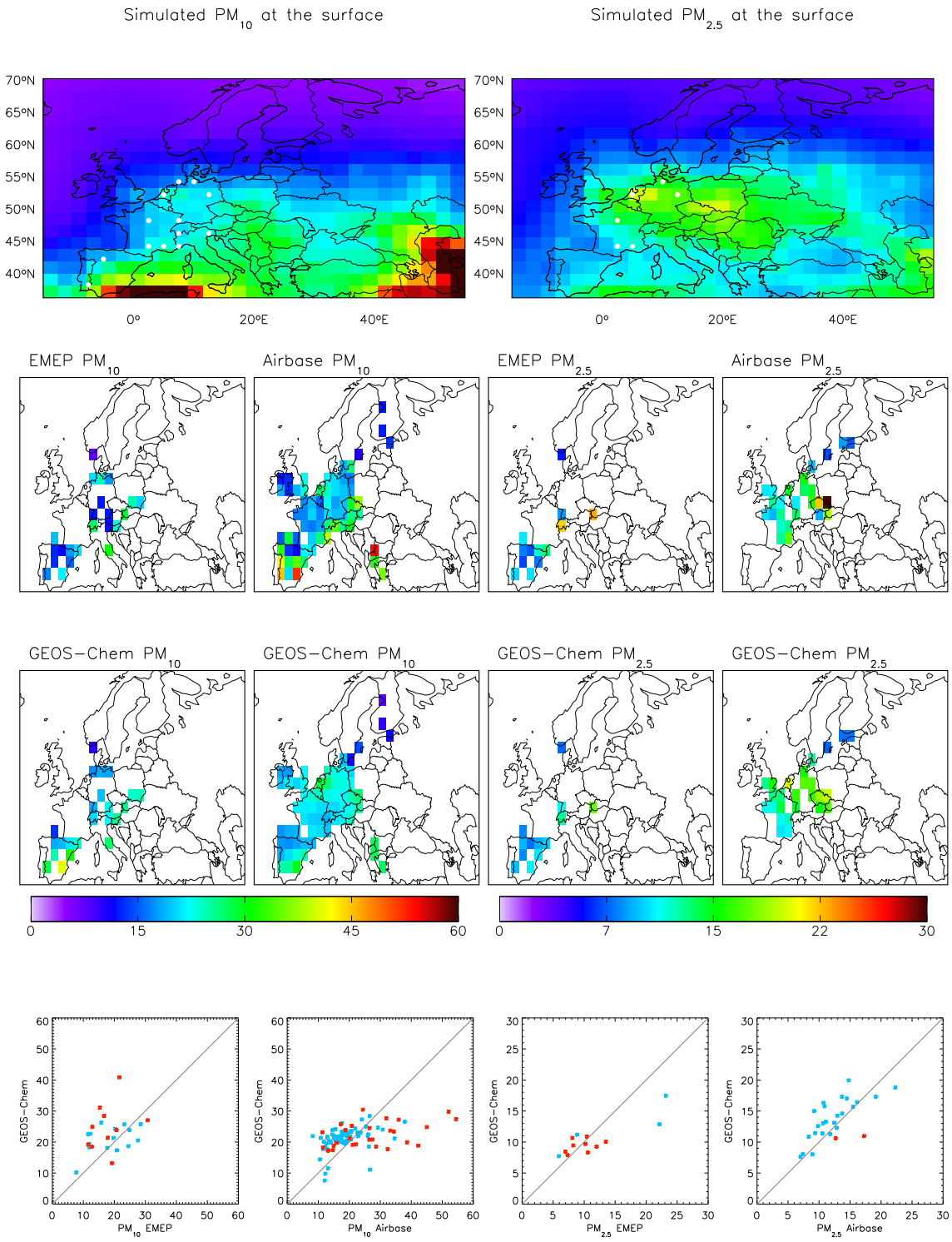

Figure 5.12: Annual value of PM_{10} and $PM_{2.5}$ concentrations ($\mu g/m^3$). First row: Simulated 2004 annual concentrations at the surface. Second row: Average of 2000–2003 annual concentrations for EMEP sites and 2004 annual concentrations for Airbase sites. Third row: Simulated 2004 annual concentrations for EMEP and Airbase sites. Fourth row: Scatterplot of simulated versus observed concentrations at EMEP and Airbase sites with regression line. The blue and red dots correspond to the stations located north and south of 46°N, respectively.

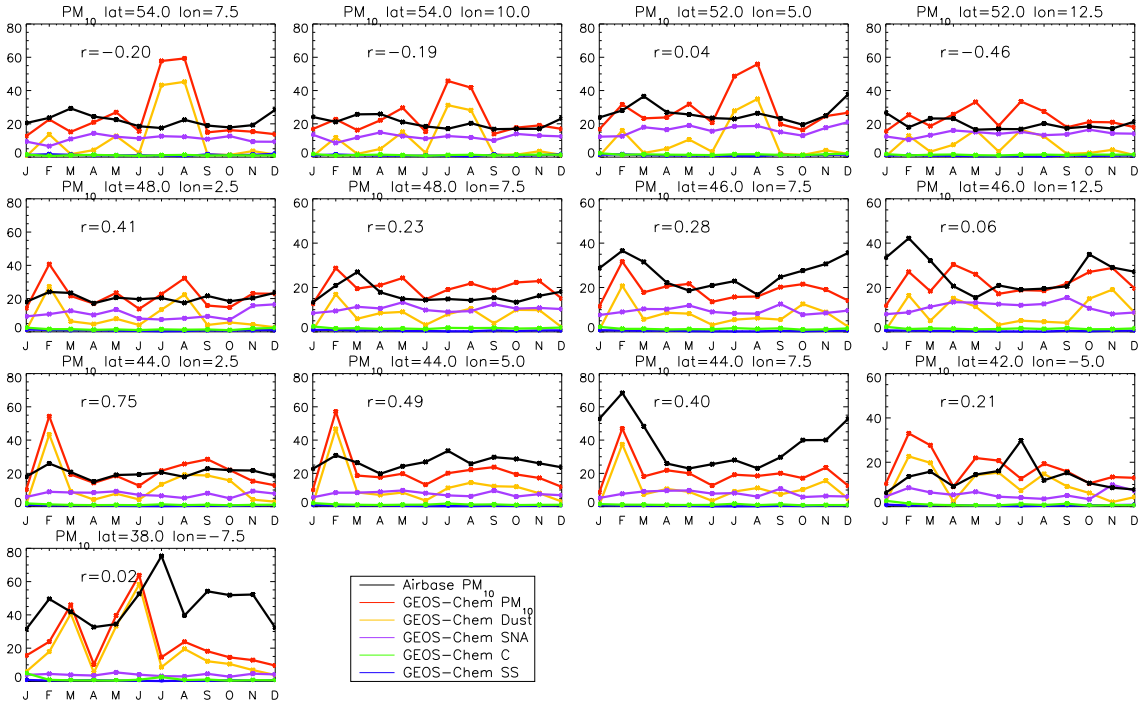

Figure 5.13: Comparison between simulated (red line) and observed (black line) monthly PM_{10} concentrations at some Airbase stations ($\mu g/m^3$). Simulated contribution of each compound to PM_{10} is also presented: dust (yellow line), sea-salt (blue line), carbonaceous compounds (green line) and sulfate-nitrate-ammonium compounds (purple line). Correlation coefficient r between monthly simulated and observed value is also indicated in each graph.

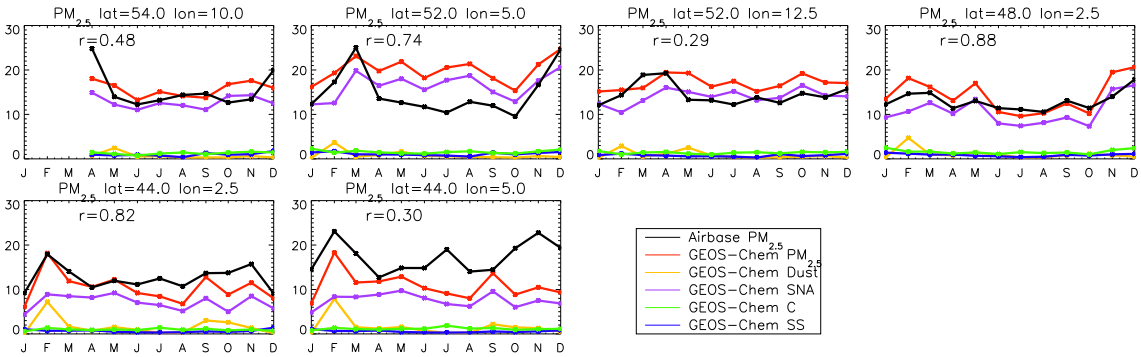

Figure 5.14: Comparison between simulated (red line) and observed (black line) monthly mean $PM_{2.5}$ concentrations at some Airbase stations ($\mu g/m^3$). Simulated contribution of each compound to $PM_{2.5}$ is also presented: dust (yellow line), sea-salt (blue line), carbonaceous compounds (green line) and sulfate-nitrate-ammonium compounds (purple line). The latitude and longitude coordinates indicated at the top of each graph is the coordinate at the center of the model grid-box. Correlation coefficient r between monthly simulated and observed value is also indicated in each graph.

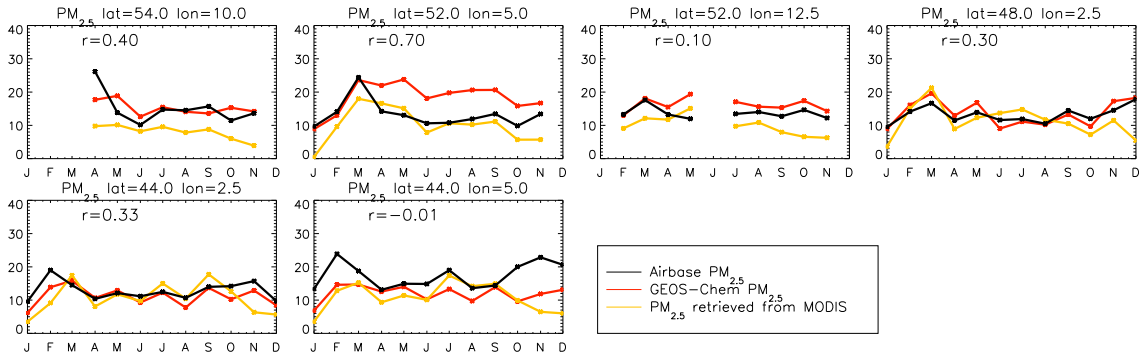

Figure 5.15: Comparison between simulated monthly $PM_{2.5}$ concentrations (red line), $PM_{2.5}$ retrieved from MODIS AOD (yellow line) and observed value (black line) selected at some Airbase stations ($\mu g/m^3$).

estimated surface $PM_{2.5}$ concentrations = simulated surface $PM_{2.5}$ concentrations / simulated AOD $\times$ observed AOD

Following that method, *Liu et al.* [2004] found a correlation coefficient of 0.81 between retrieved AOD from the Multi-angle Imaging SpectroRadiometer (MISR) space borne instrument and $PM_{2.5}$ measurements from the U.S. EPA. More recently, *van Donkelaar et al.* [2006b] investigated this method using AOD retrieved from both MODIS and MISR space borne instruments over North Canada and the U.S. and evaluated the method using AERONET AOD. In their study, spatial variations were better represented when using AOD retrieved from MODIS than from MISR. Over southern Europe, the problem might be a little bit more complicated as dust (whose a large part is not included in $PM_{2.5}$) is more important than in the U.S.. However, as further discussed in section 5.3.5 dust contribute similarly to $PM_{2.5}$ and AOD over continental Europe.

We apply this method to MODIS AOD using the GEOS-Chem model. Figures 5.15 and 5.16 compare $PM_{2.5}$ estimated from MODIS AOD (including the fine mode) to Airbase $PM_{2.5}$ observations and $PM_{2.5}$ simulated with GEOS-Chem. The correlation coefficient between MODIS-derived $PM_{2.5}$ concentrations and Airbase $PM_{2.5}$ concentrations ranges from 0.5 to 0.7 in summer. This diagram also shows that at all seasons, $PM_{2.5}$ retrieved from MODIS are better than the simulated values.

5.3.5 Aerosol characterization over Europe

Figure 5.17 summarizes our findings in terms of individual contributions of different types of aerosols to the aerosol loads (in terms of AOD and mass) over continental Europe.

On average over continental Europe, AOD show a maximum of 0.4 in May, which coincides with a maximum in sulfate-nitrate-ammonium and dust contributions (around 0.2 each). Sulfate-nitrate-ammonium aerosols and dust contribute annually to 65% and 21%, respectively to the total AOD. Carbonaceous compounds contribute to 8% (40%

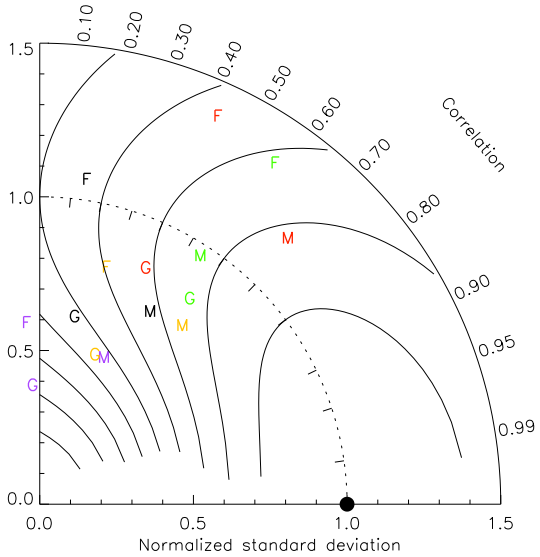

Figure 5.16: Taylor diagram for $PM_{2.5}$ concentrations. Observed $PM_{2.5}$ at Airbase stations are used for reference (27 model grid-box). The black dot is used as the reference to which simulated or derived from MODIS $PM_{2.5}$ concentrations are compared. (G): $PM_{2.5}$ simulated with GEOS-Chem; (M): $PM_{2.5}$ estimated from MODIS AOD; (F) $PM_{2.5}$ estimated from MODIS fine mode AOD. Statistical quantities presented are annual average (black), winter average (purple), spring average (green), summer average (red) and fall average (yellow).

BC and 60% POM) and sea-salt to 6%.

PM_{10} concentrations range between 10 and 30 $\mu g/m^3$ (Figure 5.17). The annual PM_{10} concentrations are about 20.0 $\mu g/m^3$, which correspond to the new limitation levels recently defined by *WHO* [2005] relative to human health for annual PM_{10} (20 $\mu g/m^3$). Mineral dust is the single most important contributors. The percentage of sulfate-ammonium-nitrate aerosols (35%) is in agreement with the findings of *Putaud et al.* [2004] who reported a measured contribution of those aerosols to PM_{10} of 32% at 11 natural and rural background sites. However, for the same sites, *Putaud et al.* [2004] reported a lower fraction of dust (10%) than the one we simulated (55%) as well as a higher fraction of carbonaceous aerosols (BC 6% and POM 16%) than the ones simulated (BC 1.5% and POM 5.6%). Measurements taken during the EMEP BC/OC campaign which took place at 14 European sites from the 1^{st} July 2002 to the 1^{st} July 2003 [*EMEP*, 2004] indicated similar results than those of *Putaud et al.* [2004], with BC and POM contributions to PM_{10} ranging from 1 to 5% and from 13 to 45%, respectively. Figure 5.17 also shows that the contribution of sulfate-ammonium-nitrate aerosols to the aerosol load is larger north of 46°N while dust largely dominates in southern Europe. Those high PM_{10} concentrations in the south are in agreement with the results of *Rodriguez et al.* [2002], who reported PM_{10} measurements ranging from 40 to 60 $\mu g/m^3$ at rural sites over eastern Spain in the summer 2000. Based on meteorological analysis and of TOMS-spectrometer satellite observations, the authors associate those events to outbreaks of African dust.

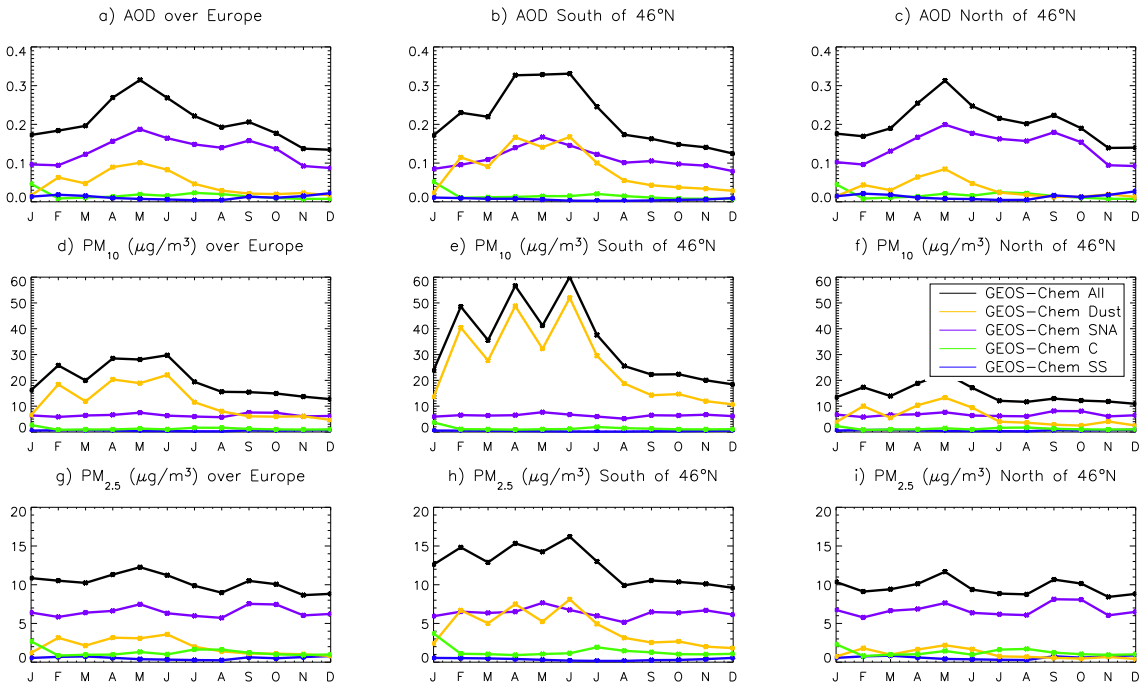

Figure 5.17: Timeseries of simulated monthly AOD, PM_{10} and $PM_{2.5}$ concentrations in $\mu g/m^3$ (black line) over continental Europe (left panel), continental Europe South of 46°N (middle panel) and continental Europe North of 46°N (right panel). Each aerosol chemical contribution is also represented: dust (yellow line), sea-salt (blue line), carbonaceous compounds (green line) and sulfate-nitrate-ammonium compounds (purple line).

$PM_{2.5}$ concentrations range between 10 and 15 $\mu g/m^3$. Average on a annual basis, $PM_{2.5}$ concentrations is of 10.3 $\mu g/m^3$, which is above the new limitation levels define by *WHO* [2005] relative to human health for annual $PM_{2.5}$ (10 $\mu g/m^3$). As already seen for individual stations, sulfate nitrate and ammonium concentrations contribute more than half to $PM_{2.5}$ concentrations all year round and is about 6 $\mu g/m^3$ (64% divided into 1/2 sulfate, 1/4 ammonium, 1/4 nitrate). Carbonaceous compounds contribute to $PM_{2.5}$ for 12% (2/3 of POM and 1/3 of black carbon) and sea-salt for 5%. $PM_{2.5}$ concentrations increase in southern Europe due to dust concentrations that reach a broad maximum in spring (15 $\mu g/m^3$). In northern Europe, the dust contribution does not exceed 10%. *Putaud et al.* [2004] in the mentioned above 11 natural and rural background sites, found a lower fraction of dust (7 versus 19%) and sulfate-nitrate-ammonium (44 versus 63%) and a higher fraction of carbonaceous aerosol (30 vs. 13%) to $PM_{2.5}$ than the ones simulated.

5.3.6 Summary of the evaluation

Simulated sulfate and ammonium concentrations are overestimated over Europe, and this is likely due to too low deposition as well as too high emissions of SO_2 and NH_3. As nitrate depends primarily on the sulfate and ammonium concentrations, simulated nitrate is slightly overestimated. Simulated POM concentrations are clearly underestimated over Europe, which most probably reflects a missing source of SOA. Using the DEAD scheme with a scaling to the *Laurent* [2005]'s emissions improved our simulation of mineral dust over Europe, but the contribution of dust may still be too high. Compensation between the different aerosol chemical species leads to a relatively good representation of the spatial and temporal variation of PM loads and AOD over Europe.

The model reproduces relatively well the SO_x concentrations observed in the continental outflow of U.S but underestimates POM concentrations in both the outflow and over the Azores.

5.4 Long-range transport of aerosols over the North Atlantic

5.4.1 Seasonal variations of aerosol loads over the North Atlantic and entering Europe

In this section we examine the transport of aerosols over the North Atlantic ocean and the aerosol fluxes entering Europe (Figure 5.18 and Figure 5.19). Discussions in the previous chapters of this thesis have indicated that pollution transport may occur all year round. This is mostly associated with front passages in spring, fall, and winter, and some extent summer with convection being an additional pathway for non-soluble compounds.

Figure 5.18 shows seasonal mean of simulated and MODIS AOD over the North Atlantic. One should note that model results are presented as seasonal mean while MODIS outputs are averaged over a season but depend of the local time overpass of the satellite and of the availability of the data. Thus, in this section, we only use satellite observations in a qualitative way to examine seasonal variations. Figure 5.19 shows the fluxes of North American anthropogenic and biomass burning aerosols (as the sum of sulfate, nitrate, ammonium and carbonaceous compounds) and of dust which enter Europe over the course of the year 2004. North American O_3 and CO fluxes are also reported here to be used as a reference and to differentiate between transport pathways associated with trace gases and aerosols.

AOD retrieved by MODIS are higher over the North Atlantic during spring and summer to some extent, as well as fine mode MODIS AOD, indicating the presence of aerosols of anthropogenic origin. Sources of anthropogenic aerosols in the model do not present a large seasonal variation, except for the NH_3 emissions, which are more important in summer. Therefore the aerosol loads over the North Atlantic pictured in Figure 5.18 reflect a seasonal variation in transport pathways and decreased scavenging in spring and summer. The maximal outflow from North America is located at lower latitudes in spring (30–40°N) than in summer (40–50°N). GEOS-Chem clearly reproduces an enhanced aerosol loading in spring, as well as a shift in latitude for the maximal North American outflow from spring to summer. The observed latitudinal shift of North American outflow between spring and summer is explained by (i) the presence of high latitude biomass burning sources and outflow in summer and (ii) the meteorological features, especially the stronger northwest winds along the U.S. west coast in summer.

The seasonal variation of the North American aerosol fluxes reaching Europe follows that of the AOD seen over the Atlantic. Biomass burning aerosols fluxes are confined during the fire season (June to September). North American aerosol anthropogenic fluxes reach Europe at lower altitude than North American O_3. Highest aerosol fluxes are typically found in the altitude range of 2 to 4 km. This probably reflects the stronger scavenging (compared to that of CO and O_3) occurring to aerosols during export from the boundary layer. Aerosols due to North American biomass burning reach Europe at higher altitude than that due to North American anthropogenic sources because biomass burning emissions are directly emitted into the free troposphere, and thus are not scavenged during export out off the boundary layer. Highest North American biomass burning aerosols fluxes reach Europe between 4 and 6 km of altitude according to the model. Dust fluxes are strong from January to August, as already seen in the aerosol distribution over Europe. Dust fluxes enter the European south border all-year round from 1 to 10 km of altitude, as well as the European east border from the surface up to 4 km of altitude, due to direct transport through the Mediterranean basin. A fraction of the dust fluxes enter also Europe through its west side in the altitude range 2–10 km, especially in spring, leaving the horn of North Africa and following a north-easterly path over the Atlantic ocean before entering continental Europe (50–60°N).

In terms of chemical composition (not shown), sulfate is the major component of North American anthropogenic aerosols entering Europe, as SO_2 partly escapes

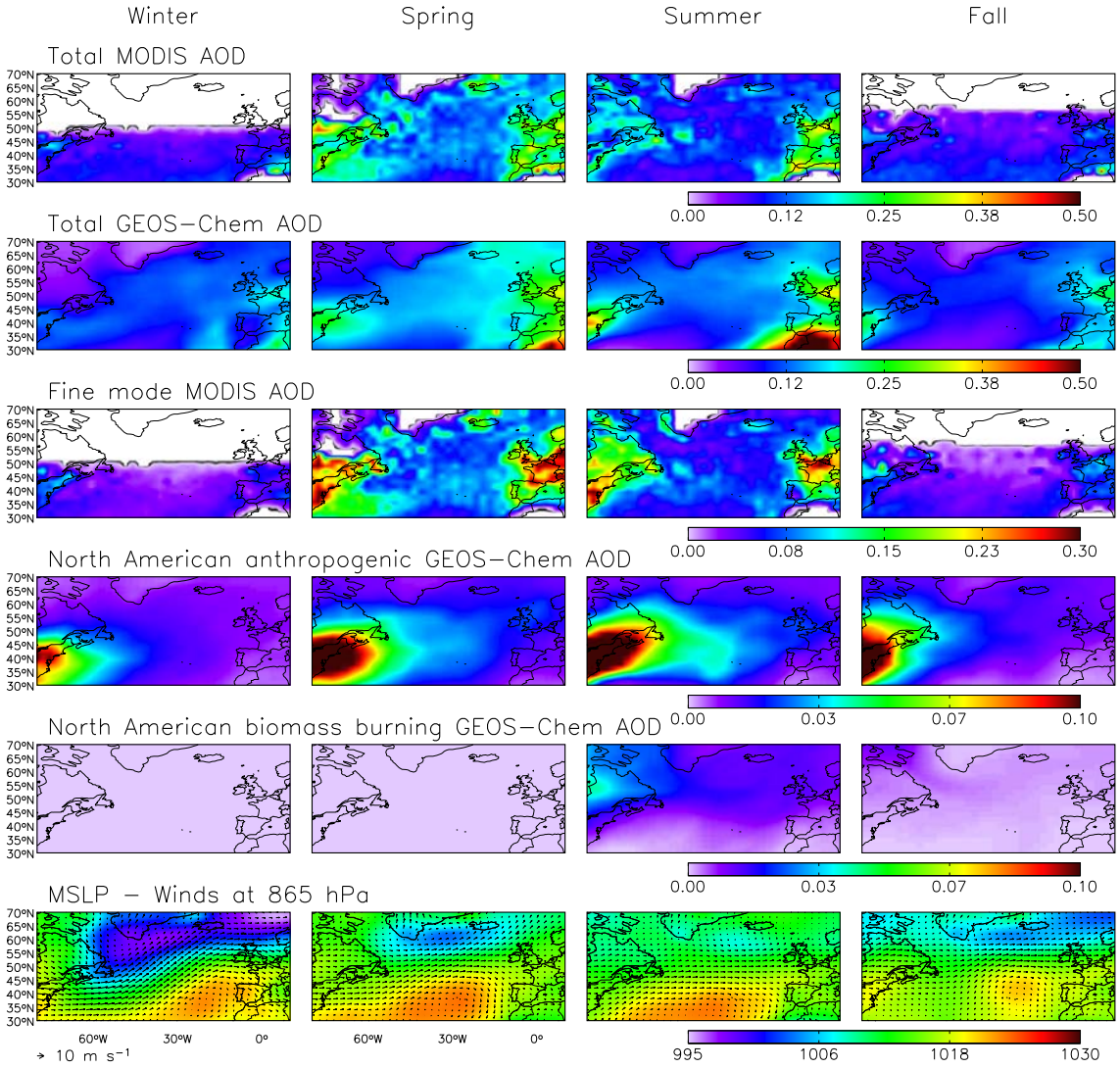

Figure 5.18: First to fourth row: Seasonal variation of AOD at 550 nm over the North Atlantic in 2004. Mean gridded values (2°x2.5°) are shown for MODIS, GEOS-Chem, MODIS fine mode and the North Anthropogenic anthropogenic and biomass burning component of the aerosol in GEOS-Chem. Fiveth row: Seasonal variation of mean sea level pressure (MSLP) and winds at 865 hPa. Color scales are saturated at the maximum value indicated in the legend.

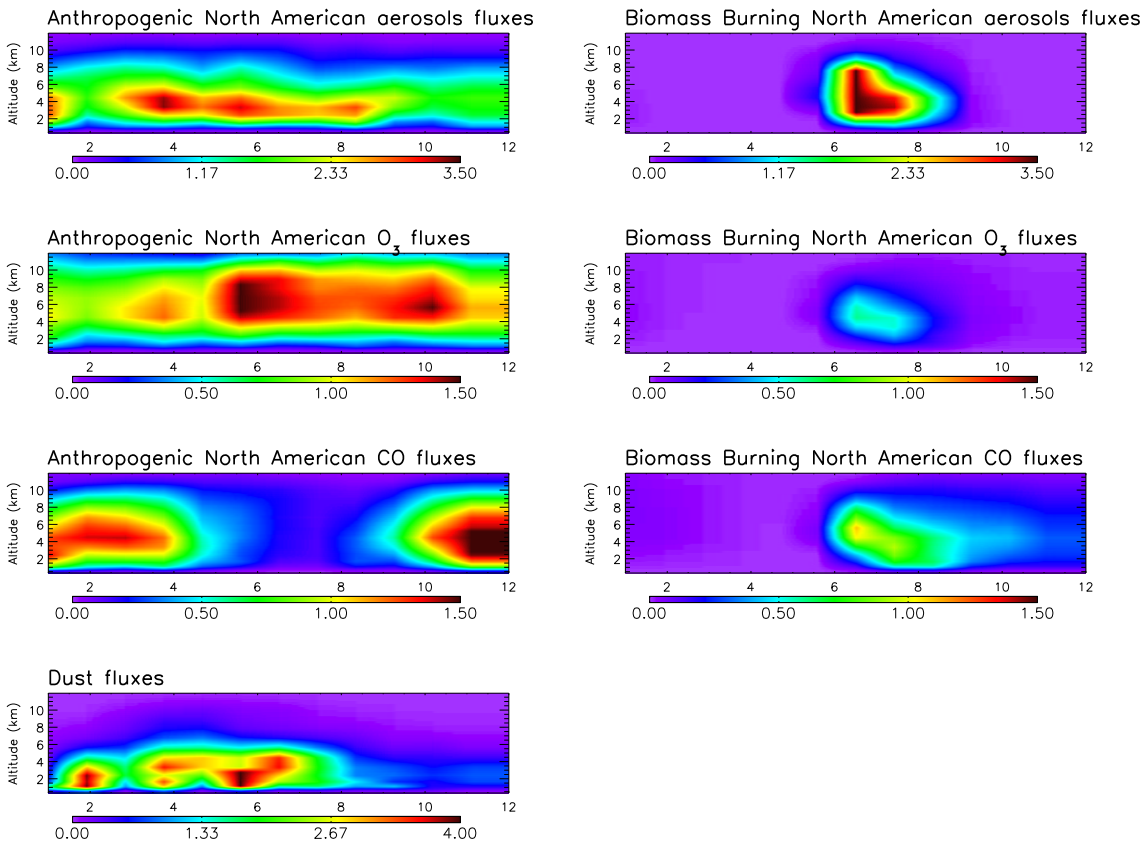

Figure 5.19: Monthly timeseries of North American anthropogenic and biomass burning fluxes of aerosols (sum of sulfate, nitrate, ammonium and carbonaceous compounds), O_3 and CO entering the west, north and south sides of Europe (coordinate of the European box: 36°N–72°N, 12.5°W–57.5°W). Units are in 10^{13} kg.cm^{-2}.s^{-1} for aerosols and 10^{11} kg.cm^{-2}.s^{-1} for O_3 and CO. Color scales are saturated at the maximum value indicated in the legend.

scavenging during lifting [*Mari et al.*, 2000; *Park et al.*, 2004] and could be potentially converted to sulfate during transport. However, during drier seasons (i.e. in summer), ammonium and nitrate (to a lesser extent) fluxes also enter Europe. Major component of North American aerosol biomass burning sources is OC with a small contribution of nitrate (SO_2 emissions by fires are small, and thus nitrate aerosols are quickly formed).

5.4.2 Case studies of long-range transported aerosols

This section examines three individual cases of long- and medium-range transport of aerosols. The first case illustrates an episode of biomass burning originating from Alaska recorded during the ICARTT Lagrangian experiment. Different matching methods were used to identify five main Lagrangian cases, linking three flights or more across the Atlantic [*Methven et al.*, 2006]. The first episode investigated here corresponds to one of these matches. It is examined through MODIS observations, trace gase, aerosol concentrations and optical depth sampled by the different aircrafts, lidar observations at Leipzig and GEOS-Chem outputs. The second episode discussed here corresponds also to a Lagrangian experiment seen during ICARTT. It originates from the New-York/Boston area and thus shows an anthropogenic signature. The model results are compared to MODIS observations, trace gase, aerosol concentrations and optical depth sampled by the different aircrafts. Finally, the third case depicts a strong transport of dust originating over the Saharan region in spring 2004. We evaluated this episode with AOD from MODIS and AERONET, as well as with PM_{10} concentrations measured by Airbase over a five day period. The processes involved in the export and subsequent transport of aerosols over the North Atlantic are not examined in great detail here, but we use these three cases to illustrate the model capabilities to reproduce qualitatively the load of long-range transported aerosols over Europe.

North American biomass burning outflow

According to the Lagrangian matches, a North American biomass burning plume was sampled on the 18^{th} of July near the Eastern North American coast by the DC-8, in the mid-Atlantic on the 20^{th} of July by the BAE146 and over western Europe on the 23^{rd} of July by the Falcon. Figure 5.20 shows daily maps of MODIS AOD in the fine mode, simulated AOD in the fine mode (i.e. the sum of sulfate, nitrate, ammonium, carbonaceous aerosols and sea-salt from the fine mode) and simulated AOD due to North American biomass burning sources from the 18^{th} to the 23^{rd} of July. Figure 5.21 shows observed and simulated vertical profiles obtained during the flights taken by the three different planes during which the biomass burning plume was sampled and we also consider the flight of the Falcon on 22^{nd} of July. Despite the lack of data in MODIS due to presence of clouds especially important during lifting events, the huge AOD plume coming from western Canada and arriving over the North Atlantic between 50–60°N is clearly visible. GEOS-Chem reproduces these features and attributed them to biomass burning.

On July 18, the DC-8 sampled high CO concentrations (higher than 300 ppbv)

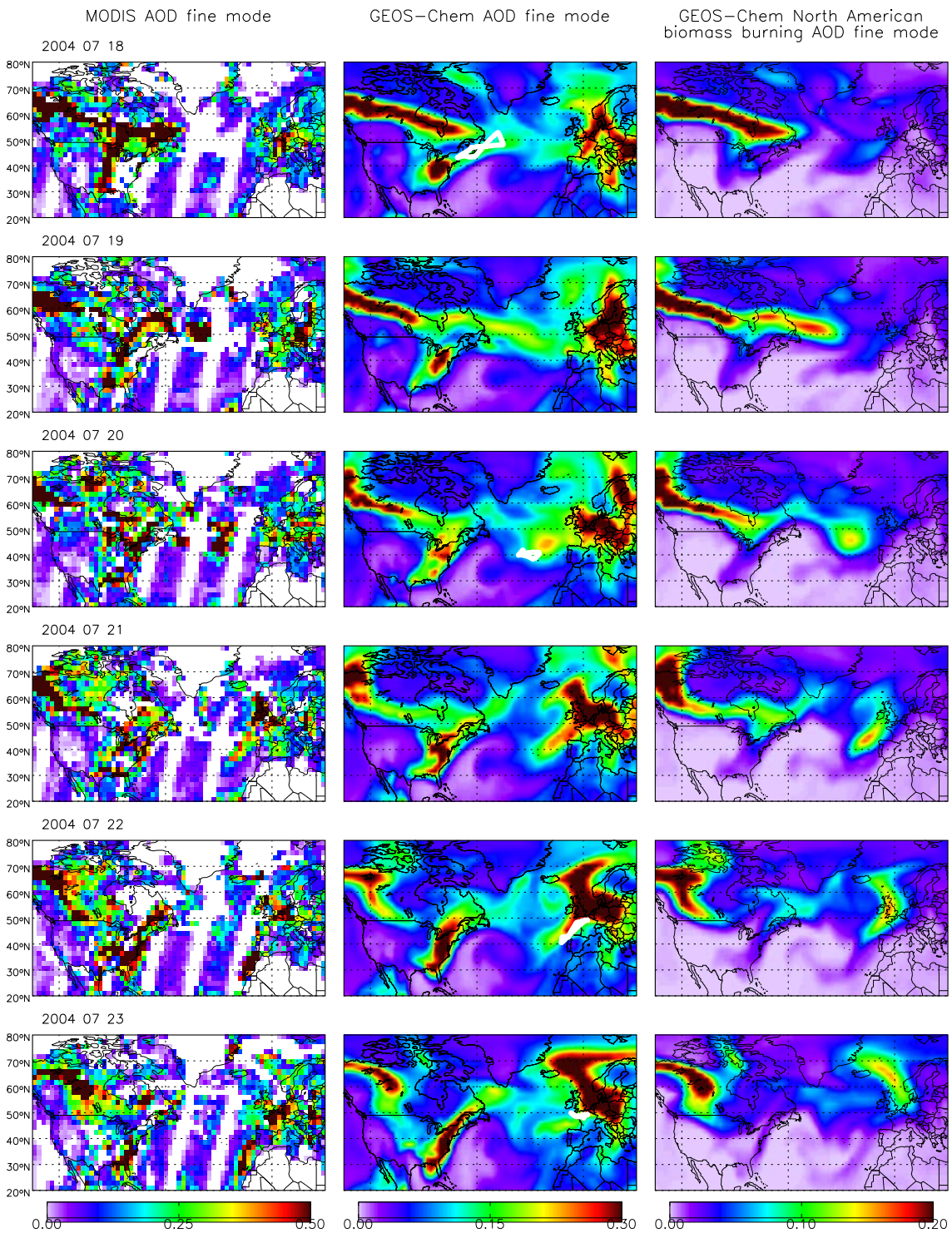

Figure 5.20: Transatlantic biomass burning event from the 18^{th} to the 23^{rd} of July 2004. First column: daily MODIS fine mode AOD; Second and third column: simulated fine mode AOD and North American biomass burning fine mode AOD. Color scales are saturated at maximum values. Flight tracks of the Lagragian experiment are indicated in white.

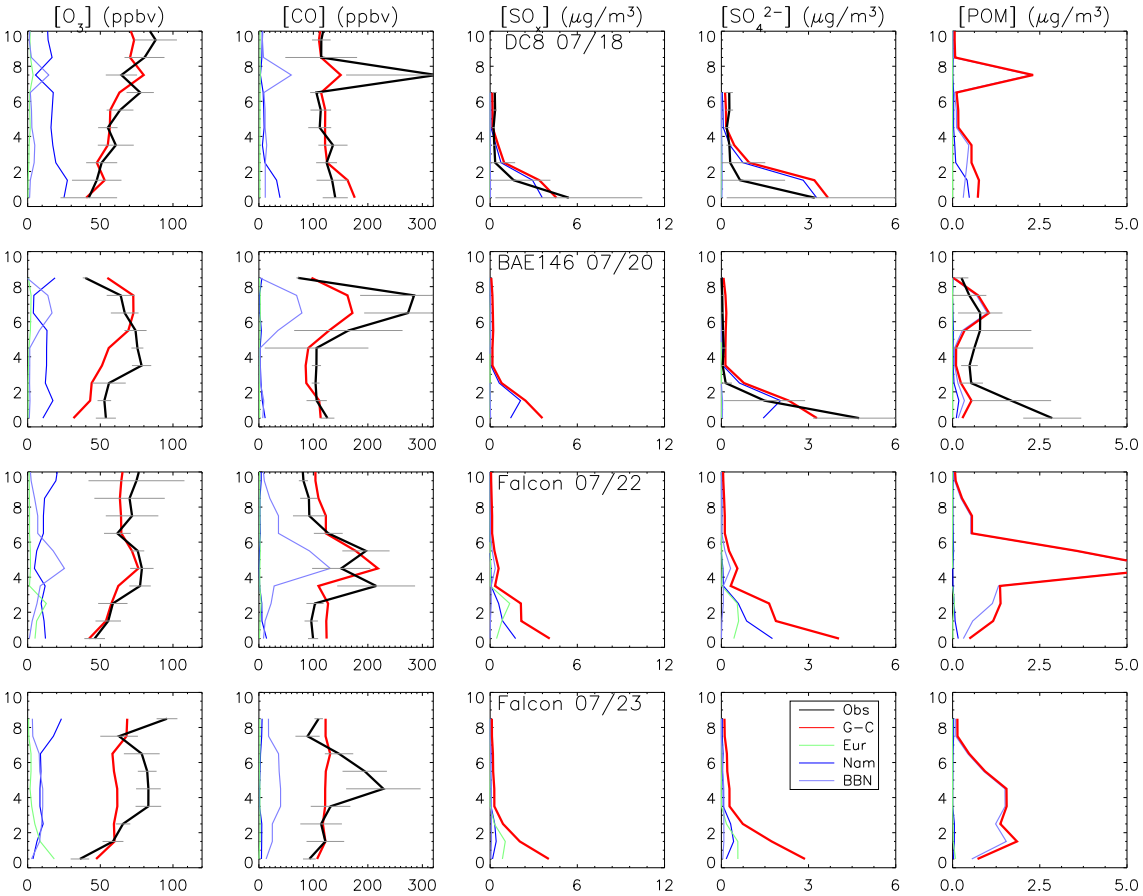

Figure 5.21: Observed (black line) vertical profiles of the ten-second median of O_3, CO, SO_x (defined as the sum of SO_2 and sulfate aerosol), SO_4^{2-} and POM binned over 1 km of altitude for individual flights of ICARTT campaign involved in the Lagrangian biomass burning plume experiment. Measurements of OC are transformed into organic matter by using an organic carbon factor of 1.4. GEOS-Chem results (red line) are sampled along the flight tracks at the time and location of the flights. Results of sensitivity tests are also shown (see legend). The horizontal bars show the observed standard deviations which reflect the variability found over the course of the flights. OC observations are not available for the DC-8. SO_x observations are not available for the BAE-146. SO_x, SO_4^{2-} and OC observations are not available for the Falcon.

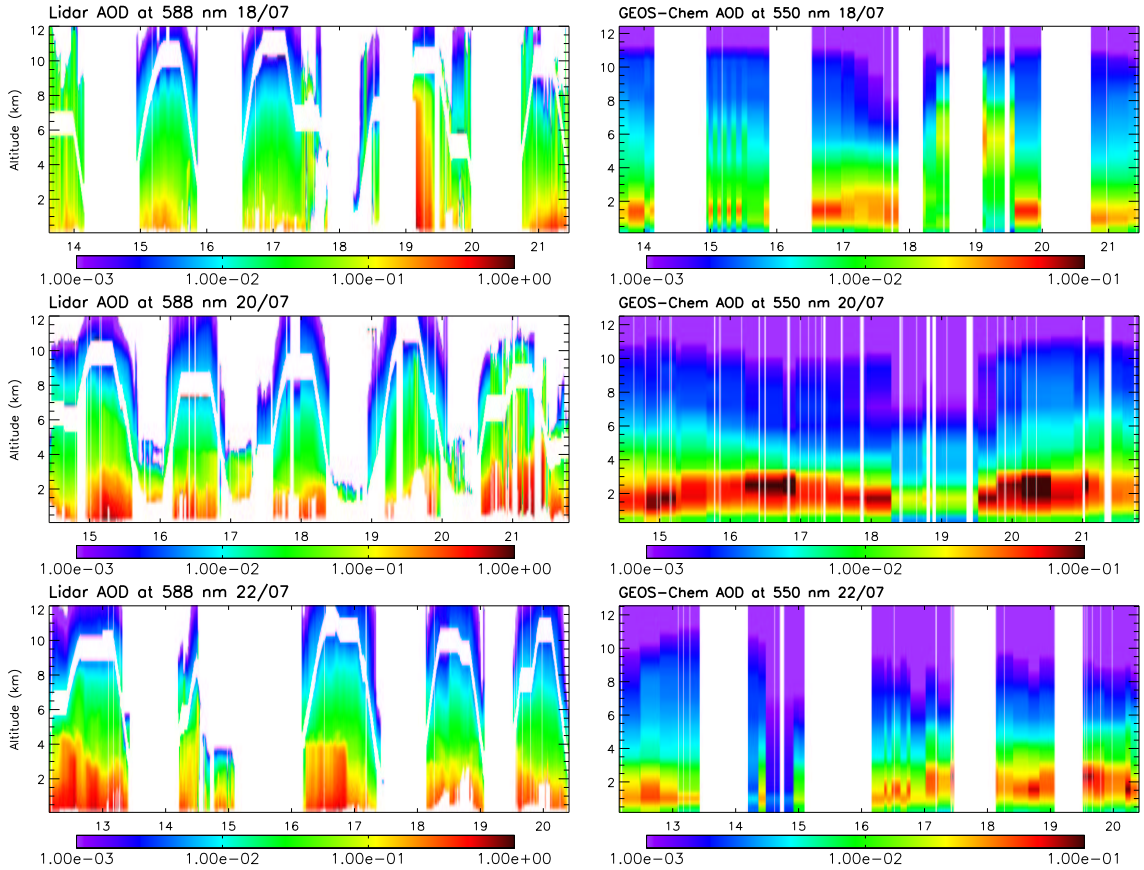

Figure 5.22: Timeseries of AOD as a function of altitude, along the flight track of the DC-8 on the 18^{th}, 20^{th} and 22^{nd} of July 2004. X axis is the hours (UTC). First column: AOD measured with the DC-8 lidar. Second column: AOD simulated with GEOS-Chem. Note that the scales are different.

between 6 and 9 km of altitude. This CO peak is reproduced by the model and attributed to biomass burning, although it is too low in the model. At the same altitude, the model simulates a peak in OC concentrations. Figure 5.22 also shows the AOD measured with the lidar on-board of the DC-8 and simulated by GEOS-Chem. AOD are higher in the first two kilometers, reflecting anthropogenic outflow. Around 7 pm, high AOD are measured throughout the column and GEOS-Chem also finds enhancement in AOD at high altitude at the same time, and attributes those to biomass burning sources. However, the model dramatically underestimates observed AOD (by a factor 5). This could reflect too low biomass burning emissions for that event, too high scavenging in the export processes, but this is also clearly linked to dilution in the coarse model grid.

From the 19^{th} to the 20^{th} of July, MODIS sampled high AOD values over the North Atlantic, which are well reproduced by the model (in particular the highest value around -20°W). On the 20^{th}, the BAE146 also sampled this plume and found CO around 290 ppbv and POM around 1 $\mu g/m^3$ between 6 and 8 km of altitude. These enhancements are reproduced by the model.

On the 21^{st}, high AOD values are recorded by MODIS and simulated by the model

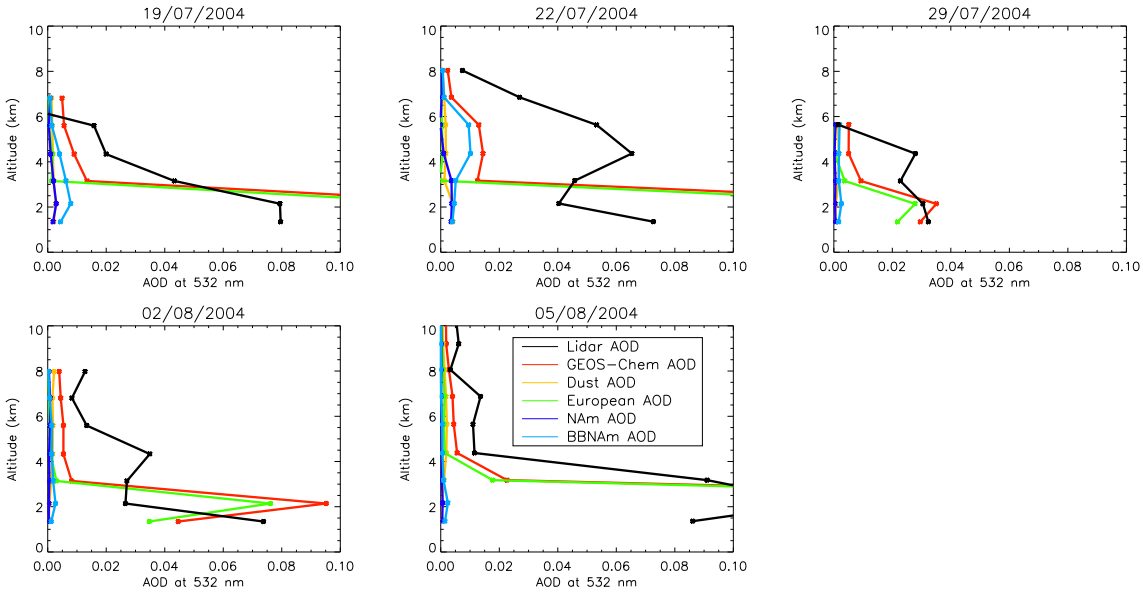

Figure 5.23: Vertical profiles of AOD retrieved from measurements of the extinction coefficient at 532 nm by the Leipzig lidar (black). Corresponding GEOS-Chem AOD simulated at Leipzig (red). Results of sensitivity tests are also shown (see legend). NAm stands for North American anthropogenic contribution and BBNAm for North American biomass burning contribution.

over the UK and western Europe. The plume moved northward will penetrating Europe on the following days. Note that high AOD values sampled on that day by MODIS on the western part of Spain are not well reproduced by the model. These high levels may be attributed to anthropogenic North American sources associated with a plume travelling from the 15^{th} to the 22^{nd} of July (case one in the Lagrangian matches described by *Methven et al.* [2006], which we do not describe here) or to dust present in the fine mode which is not accounted for in the model.

The Falcon flights of the 22^{nd} and 23^{rd} of July measured CO values higher than 200 ppbv between 3 and 6 km of altitude. These values are again underestimated by the model, and the model misses the highest value of the 23^{rd}. The model simulates OC concentrations as high as 5 $\mu g/m^3$ on the 22^{nd}. Lidar measurements at Leipzig on the 22^{nd} of July show enhanced AOD at the altitude range of 3 to 7 km in comparison to other days during the summer 2004 (Figure 5.23). Although the model underestimates the enhanced AOD at these altitudes, it indicates that they are linked to the biomass burning plume.

North American anthropogenic outflow

Figure 5.24 shows the progression of the anthropogenic North American plume (so called the New-York/Boston plume) as seen by the MODIS AOD in the fine mode as well as by the model. From the 20^{th} to the 22^{nd} of July, the DC-8 and P3 aircrafts sampled high CO outflow in the lower troposphere up to 200 ppbv, well captured by the model (Figure 5.25). This outflow is associated with high sulfate and SO_x enhancement up to 1.5 km. The model underestimates the sulfate and SO_x outflow for that event. As a consequence, AOD in the boundary layer over the eastern coast of U.S. are also underestimated compared to lidar DC-8 measurements (Figure 5.22). On the 23^{rd} and 24^{th} of July, MODIS recorded high AOD in the fine mode over the North Atlantic ocean, illustrating the New-York/Boston plume that leaves the east coast between 50 and 60°N. This signal is well seen in the model. The low-level plume reached the U.K. on the 25^{th} of July and was intercepted by the Falcon at about 1.5 to 3.5 km. The plume then penetrated Europe on the following days. Unfortunately, no aerosol observations are available to further evaluate the model simulation of the plume over Europe. However, the underestimate of the simulated aerosol concentrations and optical depth in the North American outflow indicates that the model probably underestimates the impact of North American anthropogenic aerosol concentrations over Europe.

Dust event in March 2004

North African dust outbreaks are frequently observed over the Mediterranean sea. They are generally transported by southerly winds generated by cyclones located over south Atlas [*Moulin et al.*, 1998]. During spring, typical events cross the Mediterranean sea between Libya and Egypt [*Alpert and Ziv*, 1989] and may not directly impact western and central Europe. In mid-March 2004, however, a high pressure system located over the Mediterranean sea favored transport of dust through Spain for a few days (Figure 5.26). Loaded dust air mass, originating from Niger and Chad were trapped by the northwestwards winds, turning clockwise around the high pressure system of the Mediterranean basin on the 14^{th} of March. On the 15^{th}, another dust-loaded air mass originating from Algeria begins to cross the Mediterranean sea up to eastern Spain. On the 16^{th}, the first air mass mixes with the second one and together they continue their way across Spain. They turn anticyclonically over Europe and pass over France, Germany and Czech Republic on the 18^{th}. MODIS confirms this episode by registering enhanced AOD in the coarse mode (e.g. above the mean level of March) in Spain on the 16^{th} and 17^{th} of July (but lower than GEOS-Chem). On the 18^{th}, despite the lack of data over Europe mainly due to cloud coverage, MODIS acquired relatively high value of AOD over Spain, eastern France and southern Germany. The progression of the dust plume over Europe during those 5 days is confirmed by individual ground-based observations of PM_{10} measurements reported by AERONET and Airbase (Figure 5.27). Higher AOD sampled at 440 nm are reported over Spain and South of France from the 16^{th} to the 17^{th}, conjointly with higher PM_{10} Airbase measurements. On the 17^{th} and the 18^{th} high PM_{10} concentrations are measured over France, Germany and Czech Republic. Although this kind of event is rare in spring, as usually most of the dust

escapes North Africa either through its west coast (around Senegal and Mauritania) or through Libya and Egypt [*Moulin et al.*, 1998], it has a strong impact over Europe.

Conclusion

In conclusion, it appears that GEOS-Chem is capable to capture qualitatively the transport of the plume but that it tends to underestimate the outflow of biomass burning sources as well as its influence over Europe. Similarly, it is likely that the model underestimates the impact of North American anthropogenic aerosol concentrations over Europe. The dust event examined here appears to be relatively well reproduced, both in terms of transport pathways and impact over Europe.

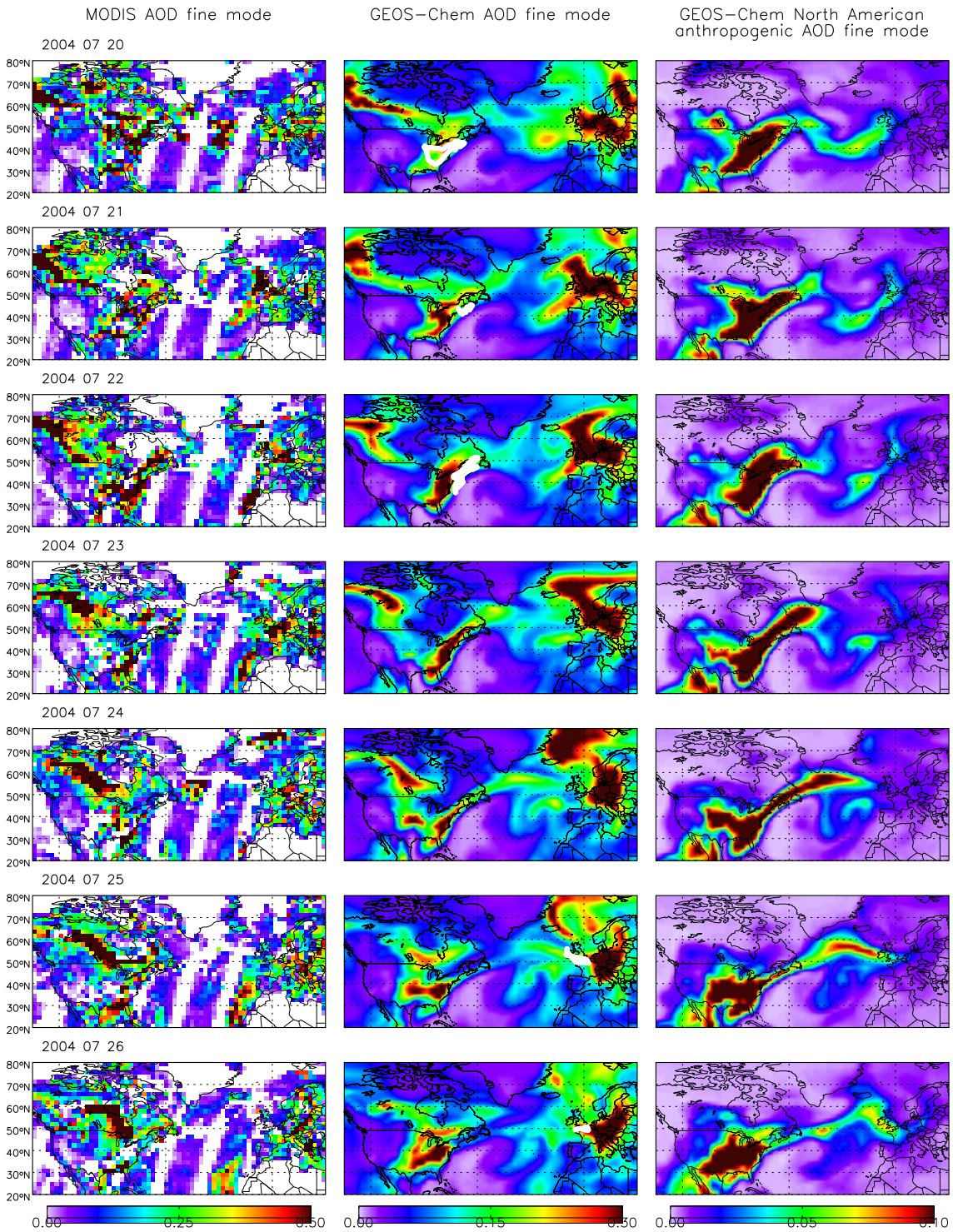

Figure 5.24: Transatlantic anthropogenic event from the 20^{th} to the 26^{th} of July 2004. MODIS fine mode AOD (first column), simulated fine mode AOD (second column) and North American anthropogenic fine mode AOD (third column). Color scales are saturated at maximum values. On the middle panels, flight tracks involved in the Lagrangian experiment are indicated in white.

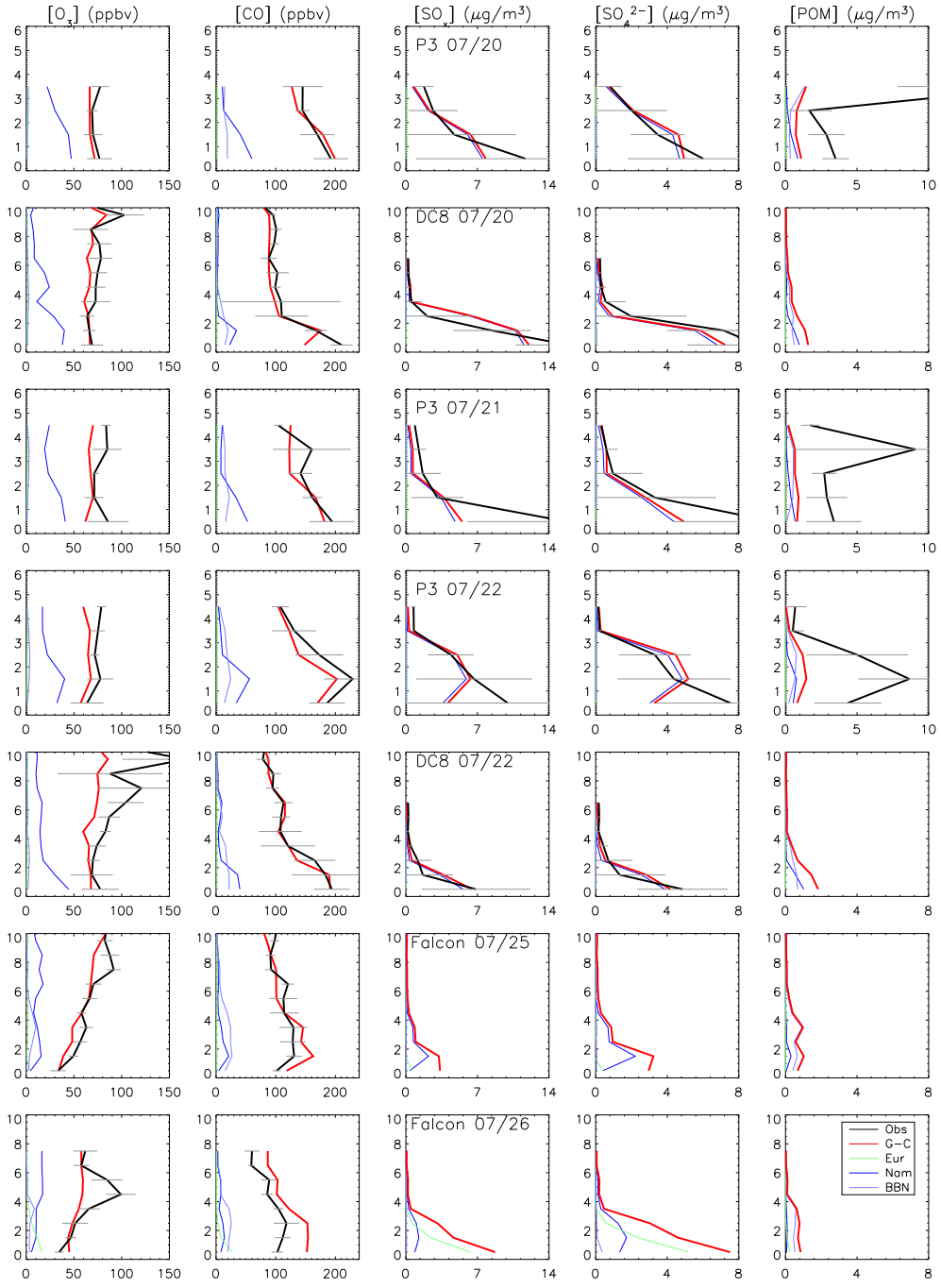

Figure 5.25: Observed (black line) vertical profiles of the ten seconds median of O_3, CO, SO_x (defined as the sum of SO_2 and sulfate aerosol), SO_4^{2-} and POM binned over 1 km of altitude for individual flights of ICARTT involved in the Lagrangian New-York Boston plume experiment. For the P3, only the water soluble part for the organic carbon is measured (and simulated as well). Measurements of OC are transformed into organic matter by using an organic carbon factor of 1.4. GEOS-Chem results (red line) are sampled along the flight tracks at the time and location of the flights. Results of sensitivity tests are also shown (see legend). The horizontal bars show the observed standard deviations which reflect the variability found over the course of the flights. OC observations are not available for the DC-8. SO_x observations are not available for the BAE-146. SO_x, SO_4^{2-} and OC observations are not available for the Falcon.

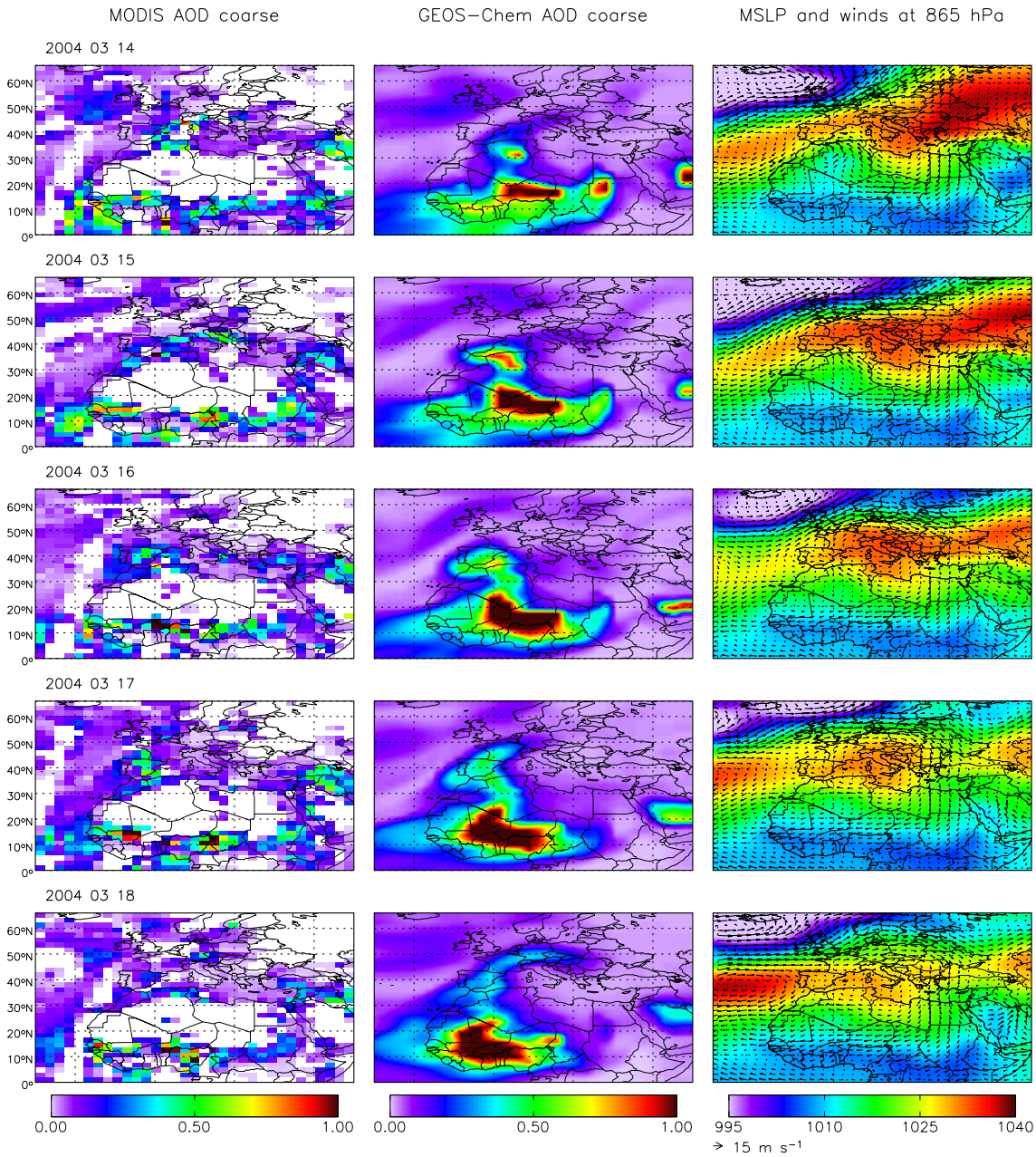

Figure 5.26: Dust event from the 14^{th} to the 18^{th} of March 2004 reaching central Europe analyzed through MODIS coarse AOD (550 nm)(first column), GEOS-Chem coarse AOD (500 nm)(second column). Third column: Daily model winds at 865 hPa and mean seal level pressure.

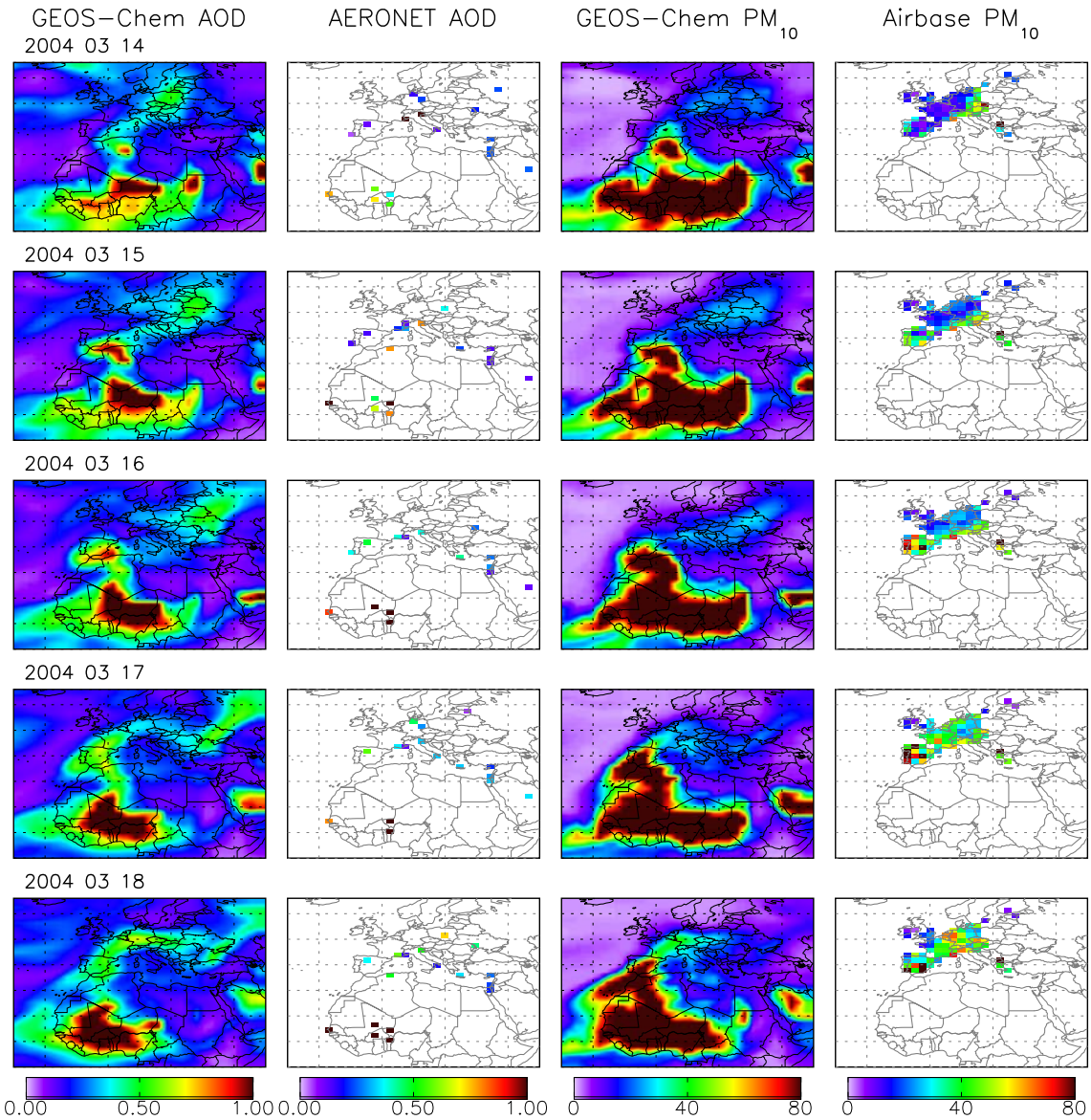

Figure 5.27: Dust event from the 14^{th} to the 18^{th} of March 2004 reaching central Europe analyzed through GEOS-Chem AOD (400 nm) (first column), AERONET AOD (440 nm) (second column) and through GEOS-Chem (third column) and Airbase (fourth column) PM_{10} concentrations ($\mu g/m^3$).

5.5 Relative contribution of local sources versus long-transport to the aerosol burden over Europe

The objective of that section is to quantify the relative contribution of the local sources versus the long and medium-range transported aerosols to the continental European loads of aerosol at the surface (e.g. impact on air quality) and AOD (e.g. impact on climate) on a seasonal basis.

5.5.1 Seasonal variations of aerosol loads over the North Atlantic and entering Europe

Figure 5.28 shows the seasonal variations of surface $PM_{2.5}$ and AOD integrated over continental Europe as a function of their origins. Different components are pictured, including anthropogenic sources from Europe and from North America, biomass burning from North America, dust (mainly from Sahara) and sea-salt. The remaining contributions (in black on these graphs) include natural sources (POM produced from biogenic emissions, ammonium produced from soils and oceans, sulfate produced from volcanoes, oceans and soil) and anthropogenic and biomass burning aerosols from Asia and other countries not mentioned previously. As expected, the model indicates that the main sources of $PM_{2.5}$ and AOD are local pollution. European source contribute between 55 and 68% for $PM_{2.5}$ with a minimum in summer and a maximum in fall. The contribution of European sources to AOD is smaller and range between 40 and 58% with a maximum in fall and a minimum in winter. Vertical profiles (not shown) of $PM_{2.5}$ and AOD indicate that the European pollution is strongly confined in the 2–3 lowest kilometers (especially in winter). The North American contribution reaches a maximum in the 2–5 km range. Dust is found between 3 and 7 km, especially in spring and summer.

As mentioned before, the second largest contribution to the aerosol budget comes from dust. It contributes to between 10 and 25% to $PM_{2.5}$ and from 12 to 30% to AOD. The third contribution to the aerosol budget is from the remaining origin. North American anthropogenic sources contribute to $PM_{2.5}$ from 1.7% to 2.8% and to AOD from 4 to 4.5%. We find a larger contribution of North American source to AOD in spring than in summer, but the opposite for $PM_{2.5}$ because in spring, North American emissions are transported at a broader altitude range. Finally, biomass burning from North America contributes only in summer (2.4% to $PM_{2.5}$ and of 3% to AOD). Note that southern Europe receives a larger contribution of the long-range transported emissions compared to northern Europe.

North American anthropogenic sources contribute to sulfate-ammonium-nitrate concentrations up to 4.2% and to carbonaceous compounds up to 1.9% in summer. Surface concentrations of sulfate-ammonium-nitrate from North American origin reach about 0.25 $\mu g/m^3$ in spring and summer, which is similar to the findings of *Park et al.*

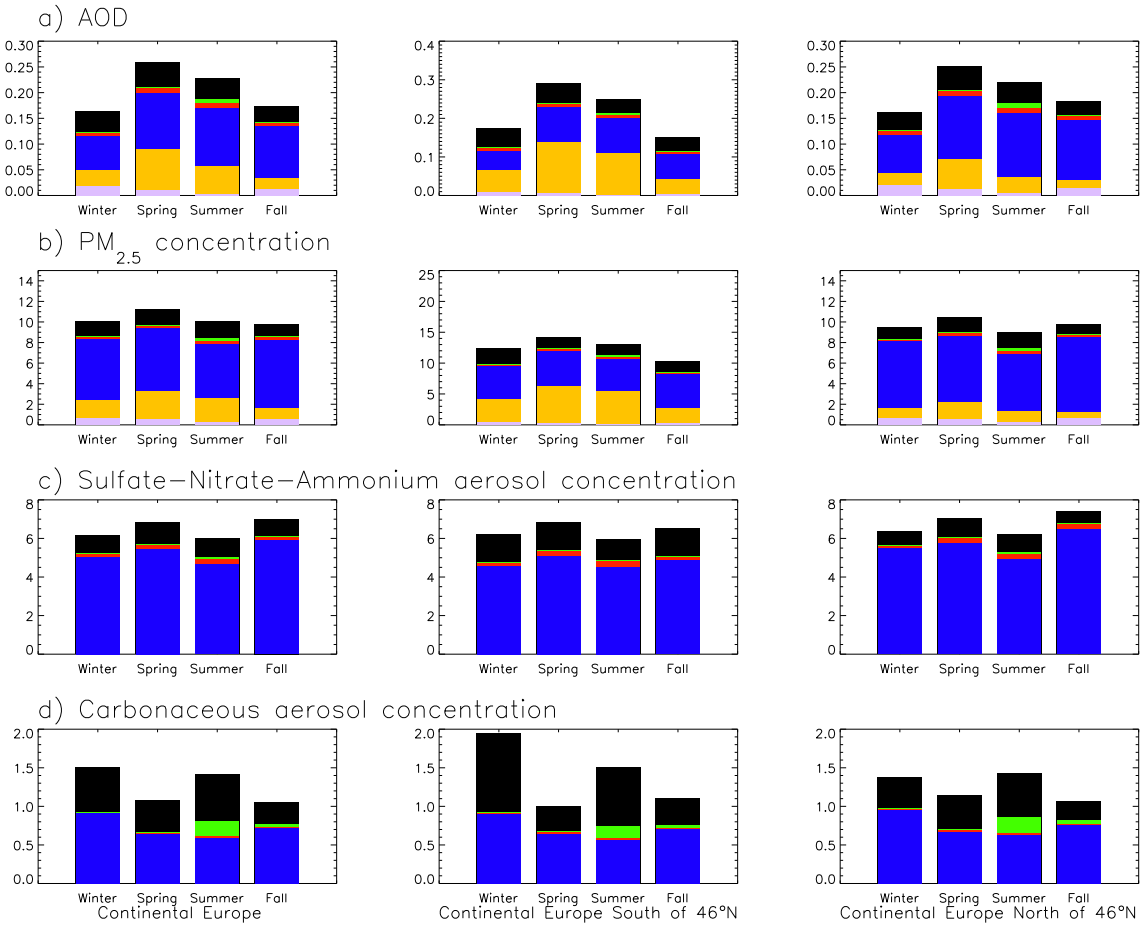

Figure 5.28: Seasonal variation of (a) AOD (b) $PM_{2.5}$ concentrations, (c) sulfate-nitrate-ammonium concentrations and (d) carbonaceous aerosol concentrations over continental Europe (first columns), continental Europe South of 46°N (second column) and continental Europe North of 46°N (third column) in black. Different contributions are superimposed over the black bar, including sea-salt (purple), dust (yellow), European anthropogenic sources (blue), North American anthropogenic sources (red), and North American biomass burning sources (green). Units for concentrations are in $\mu g/m^3$.

[2004] for the enhancement over the U.S. due to Asian sources. *Heald et al.* [2006] reported an enhancement of sulfate from Asian anthropogenic sources over the Northwest U.S. of 0.16 $\mu g/m^3$ in spring. Europe appears thus to be at least as impacted as Western U.S by upwind sources, as we found a contribution of 0.21 $\mu g/m^3$ of sulfate averaging over continental Europe in spring. North American biomass burning sources contribute up to 13% to carbonaceous aerosols concentrations in summer, and result in an enhancement of 0.19 $\mu g/m^3$ in average at the surface.

Note however that OC concentrations appear to be underestimated in the continental outflow of North American, as discussed in section 5.3. This indicates that the North American anthropogenic and biomass burning aerosol contribution may be underestimated by the model.

5.5.2 Maximal contribution of polluted events to the aerosol budget in spring and summer 2004

This section examines the impact of individual meduim- and long-range transport events on the European aerosol budget. Figures 5.5.2 and 5.5.2 show the daily enhancement associated with different sources (European anthropogenic, North American anthropogenic and biomass burning, dust) as a function of the simulated AOD, and $PM_{2.5}$, sulfate and OC concentrations for spring and summer 2004.

Both in spring and in summer, although on average European anthropogenic sources contribute the most to AOD and $PM_{2.5}$ concentrations over Europe, the highest values of AOD and $PM_{2.5}$ concentrations recorded by the model are attributed to dust. Taken individually, European anthropogenic contribution and dust contribution both exceed the *WHO*[2005] daily standard of 10 $\mu g/m^3$ and the U.S. EPA $PM_{2.5}$ daily standard of 65 $\mu g/m^3$ in a large number of cases. Highest dust contribution is restricted to southern Europe. However, in spring dust contributes up to 120 $\mu g/m^3$ North of 46°. The dust episode investigated in section 5.4.2 is not among the strongest as it contributes to AOD up to 0.9 and to $PM_{2.5}$ up to 14 $\mu g/m^3$ on the 15^{th} of March 2004 in Spain.

In spring, North American anthropogenic sources contribute up to 7 $\mu g/m^3$ to the $PM_{2.5}$ concentrations and to 0.16 to AOD. In summer, some of the days with AOD from North American anthropogenic sources higher than 0.08 correspond to the polluted episode investigated in section 5.4.2 (25, 26 and 28^{th} of July 2004). This event is less visible in the $PM_{2.5}$ concentrations for which maximal $PM_{2.5}$ values of 2.75 $\mu g/m^3$ are recorded. This event contributes also up to 2 $\mu g/m^3$ to sulfate concentrations but contributions as high as 3 $\mu g/m^3$ are seen in spring and summer.

One should note that maximal North American anthropogenic contribution is associated with low local pollution or low dust-loaded air masses, reflecting the transport of maritime air masses over Europe. In such relatively "clean" air masses, North American anthropogenic sources contribute to 85% and 55% to sulfate concentrations in spring and summer, respectively. Moreover, when sulfate concentrations alone are in the daily $PM_{2.5}$ limit reported by *WHO* [2005] of 10 $\mu g/m^3$ range, North American anthropogenic impact is relatively important (0–3 $\mu g/m^3$).

North American biomass burning sources contribute up to 1.4 $\mu g/m^3$ to $PM_{2.5}$ and up to 0.17 to AOD in summer over Europe (5.5.2). The North American biomass burning plumes have a larger impact on AOD than North American anthropogenic plumes for that summer. The highest value of AOD of North American biomass burning origin is recorded for the episode investigated in section 5.4.2. However, as the plume was transported at relatively high altitude (4–6 km), it does not appear in surface $PM_{2.5}$ or OC concentrations. Again, maximal North American biomass burning contribution is associated with low contribution from European anthropogenic or dust sources. On those days, OC from North American biomass burning contributes up to 78% to the total OC concentrations.

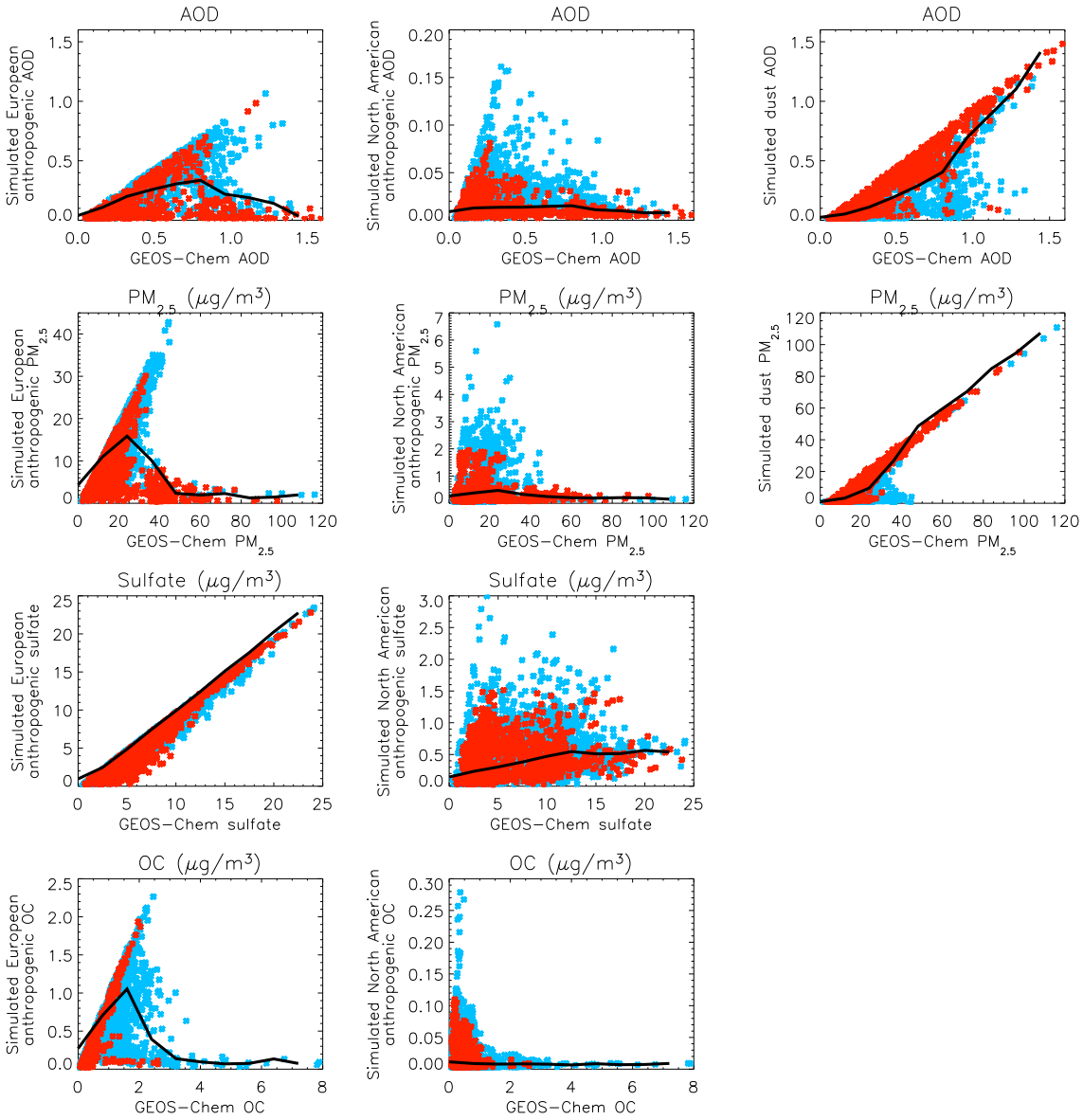

Figure 5.29: Simulated daily enhancement of AOD (first row), $PM_{2.5}$ (second row), sulfate (third row) and OC (fourth row) concentrations over continental Europe (36°N–60°N, 12°W–46°W) for springtime due to European anthropogenic emissions (first column), North American anthropogenic emissions (second column) and dust emissions (third column). These enhancements are plotted as a function of simulated AOD and $PM_{2.5}$, sulfate and OC concentrations. Blue dots are grid-boxes located North of 46°N and red dots South of 46°N. The black line is a locally weighted regression.

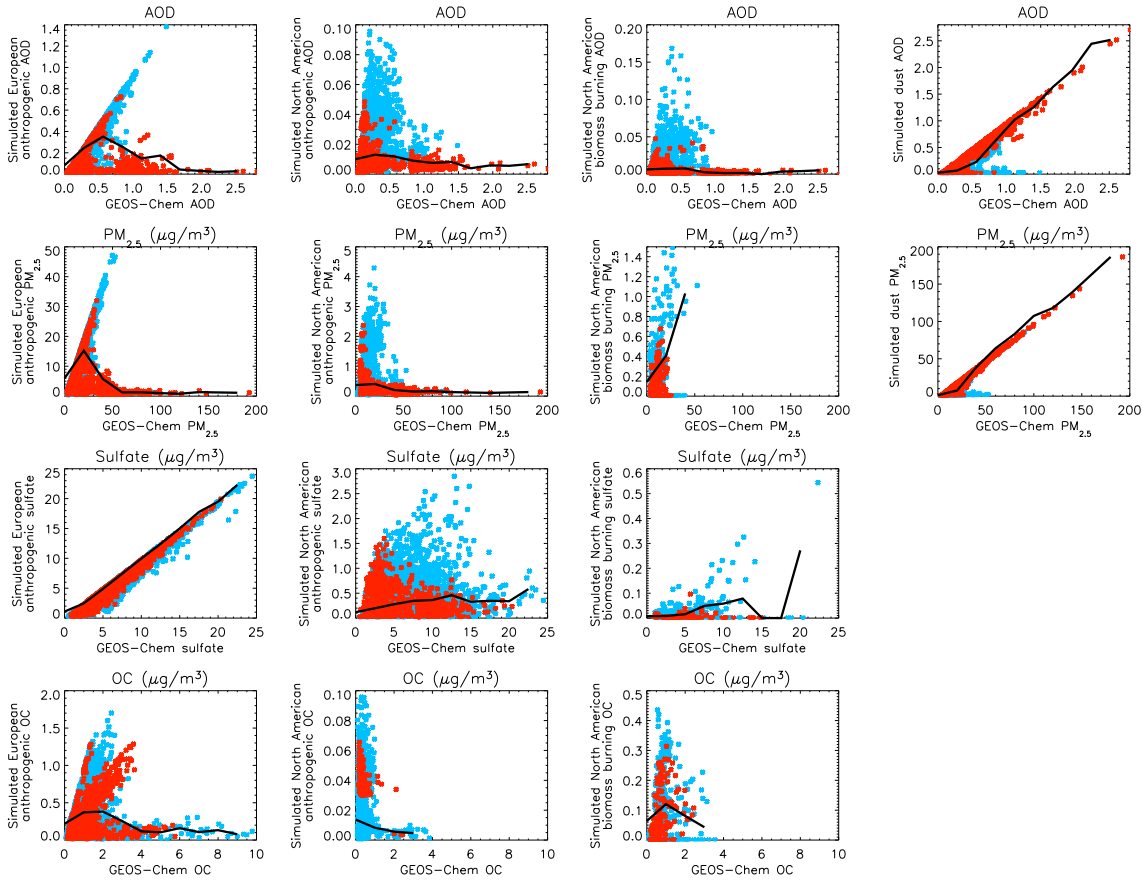

Figure 5.30: Simulated daily enhancement of AOD (first row), $PM_{2.5}$ (second row), sulfate (third row) and OC (fourth row) concentrations over continental Europe (36°N–60°N, 12°W–46°W) for summertime due to European anthropogenic emissions (first column), North American anthropogenic emissions (second column), North American biomass burning emissions (third column) and dust emissions (fourth column). These enhancements are plotted as a function of simulated AOD and $PM_{2.5}$, sulfate and OC concentrations. Blue dots are grid-boxes located North of 46°N and red dots South of 46°N. The black line is a locally weighted regression.

5.6 Summary and conclusions

We used a global chemical transport model to estimate an aerosol budget for continental Europe and to quantify the contribution of local sources versus that of long-range transported sources to AOD and surface $PM_{2.5}$ concentrations. The first part of this chapter consists in a thorough evaluation of aerosol distributions over Europe as simulated by the global model GEOS-Chem. The seasonal variations in aerosol loads over the Atlantic and entering Europe are then discussed. We investigated two episodes of trans-Atlantic transport of aerosols and their impacts over Europe using aircraft observations, MODIS AOD satellite, and lidar measurements obtained in the frame of the ICARTT campaign. Networks of AOD and PM_{10} measurements developed over Europe conjointly with AOD from MODIS satellite allowed us to investigate the impact of dust emissions for a specifically strong episode. Finally, we examine the impact of long and medium-range transport to the aerosols burden and AOD over Europe.

Simulated sulfate, nitrate and ammonium concentrations are overestimated over Europe. That could be associated with too low deposition fluxes and too high NH_3 and SO_2 emissions. POM concentrations are underestimated over Europe, which may reflect too low surface OC emissions and missing SOA sources. Scaling the dust emissions obtained with the DEAD scheme to the ones of *Laurent* [2005] strongly reduces the model bias in AOD (and PM concentrations, not shown) over both Europe and North Africa. Overall, both PM concentrations and AOD appear to be correctly represented over Europe when compared to PM measurements provided by air quality networks, and to AERONET and MODIS AOD. This may however result, to some extent, from compensating errors associated with individual aerosol species.

In term of PM_{10}, dust is the main constituent of the aerosol load over continental Europe. The main component of $PM_{2.5}$ and AOD is sulfate, ammonium and nitrate. However fine dust contribution, especially in southern Europe could be as high as that of sulfate-ammonium-nitrate. Annual $PM_{2.5}$ concentrations averaged over continental Europe are slightly above the new limitation levels defined by *WHO* [2005] relative to human health (10 $\mu g/m^3$). The relative contributions of individual species to total AOD and $PM_{2.5}$ concentrations are relatively similar, which makes possible the retrieval of aerosol $PM_{2.5}$ concentrations from satellite observations such as MODIS AOD. That could compensate the lack of $PM_{2.5}$ measurements over Europe.

The model is able to reproduce specific trans-Atlantic episodes as seen during the ICARTT campaign with a good timing and spatial resolution. However, comparison with measurements of aerosol concentrations and lidar AOD taken during individual flights indicate that simulated aerosol concentrations in such episodes are underestimated, especially for POM and to a lesser extent SO_x. The simulated impact of episodic transport over Europe in this study is thus a lower limit. We also showed that the model reproduces well a strong dust event occurring in mid-March 2004.

Seasonal variations of transport over the North Atlantic and of fluxes entering Europe of aerosol of anthropogenic North American origin occur all year round but present a maximum in spring (and to a lesser extent summer), reflecting seasonal

variations in transport pathway and a lower scavenging efficiency. Those fluxes (mainly under the form of sulfate) enter Europe at lower altitude than O_3 fluxes, preferentially at 2–4 km of altitude, which reflects stronger scavenging for aerosols. Note that, in addition, for O_3, additional sources (e.g. NO_x from lightning) are available directly in the free troposphere (see Chapter 3). Transport of biomass burning aerosol from North America (mainly under the form of OC) are restricted to summer, during the strong fire period of North American and Canadian forests of 2004. As the simulated biomass burning sources are directly injected in the free troposphere, biomass burning aerosol enter Europe up to 9 km of altitude. Because of the different location of North American anthropogenic and biomass burning sources, as well as the different meteorological features, maximum North American outflow is found at higher latitude in summer (40–50°N) than in spring (30–40°N). Dust fluxes enter Europe preferentially from January to August, following the seasonal cycle of dust emissions. After direct transport over the Mediterranean basin, dust fluxes enter Europe through its south and east borders. They also enter Europe through its western side, especially in spring after export of the North African horn.

Over Europe, local pollution is the main source to $PM_{2.5}$ and AOD. Annually, European sources contribute by 58 and 48% to the surface $PM_{2.5}$ and AOD, respectively. In winter, European emissions are more confined at lower altitude. Dust emissions contribute to the aerosol budget with a maximum in spring, between 3 and 7 km of altitude. Annually, dust contributes to around 20% to both surface $PM_{2.5}$ and AOD. North American anthropogenic sources (preferentially under the form of sulfate) contribute in spring and summer, while biomass burning North American contribution (mainly OC) is restricted to summer. Average on a year, anthropogenic North American contribute to 2.2 and 4.2% to surface $PM_{2.5}$ and AOD, while North American biomass burning contribution is less than 1%.

As polluted outflow from North America, as well as dust events over Europe are highly episodic [e.g., *Li et al.*, 2005; *Moulin et al.*, 1998], we also investigate the impact of individual episodes on the European aerosol budget. We find that North American anthropogenic sources contribute up to 3 $\mu g/m^3$ to sulfate surface concentrations over continental Europe both in spring and summer. North American biomass burning sources contribute to OC surface concentrations up to 0.45 $\mu g/m^3$ but have a stronger impact on AOD than North American anthropogenic sources as the plumes are traveling at higher altitude. The maximal simulated AOD values from North American biomass burning origin over continental Europe was recorded during the episode investigated in detail in the frame of the ICARTT project. Those polluted North American episodes are in general associated with low contribution from European anthropogenic or dust sources. However, a non negligible part of sulfate from North American anthropogenic origin (0–3 $\mu g/m^3$) impacts Europe when total sulfate concentrations are in the 10–15 $\mu g/m^3$ range. Finally, the highest value of $PM_{2.5}$ or AOD simulated over continental Europe are entirely due to dust emissions, which can reach and even exceed the contribution of local sources, especially North of 46°N.

Trans-Atlantic transport has only little influence on the European aerosol budget on average but individual events can have a substantial impact, especially during the

summer 2004, which was recorded as one of the strongest fire season over Alaska and Canada. Such events may increase with climate change and associated global warming [*Conny and Slater*, 2002].

The distribution of PM_{10} and $PM_{2.5}$ over Europe is driven, to some extent, by dust import from Sahara and Middle-East. Southern Europe is more impacted than Northern Europe. Air quality standard should be established in such ways that the geographic distribution of the natural contribution to aerosol loads is accounted for. The establishment of such standards should be based on both experimental observations and modelling studies. At the moment, the observations of individual aerosol components (that are needed to evaluate the fundamental processes in models) are lacking.

Acknowledgements

The GEOS-CHEM model is managed by the Atmospheric Chemistry Modeling Group at Harvard University with support from the NASA Atmospheric Chemistry Modeling and Analysis Program. I would like to thank the EMEP and Airbase teams for providing aerosol data over Europe. I am grateful to the ICARTT, ITOP and ADRIEX teams (especially J. Crosier) for their efforts during and after the campaigns. I am very grateful to S. Turquety and R. Hudman for helping me with emission inventories in the GEOS-Chem model, to D. Fairlie and B. Laurent for helpful discussions on the dust simulations, to R. Park for interactions on the GEOS-Chem aerosol simulations, and to A. van Donkelaar and R. Martin for their help with the isoprene sensitivity tests. I wish to thank the MODIS team for the aerosol product and S. Generoso for helping me in the treatment of the data. I gratefully acknowledge the AERONET principal investigators and their staff for establishing and maintaining the sites used in this investigation. Finally, I thank E. Browell and I. Mattis for their work on the lidar data.

References

Alexander, B., R. J. Park, D. J. Jacob, Q. B. Li, R. M. Yantosca, J. Savarino, C. C. W. Lee, M. H. Thiemens (2005), Sulfate formation in sea-salt aerosols: Constraints from oxygen isotopes, *J. Geophys. Res.*, *110*, D10307, doi:10.1029/2004JD005659.

Alpert, P., and B. Ziv (1989), The Sharav cyclone: observations and some theoretical considerations, *J. Geophys. Res.*, *94*, 18,495–18,514.

Amiridis, V., D. S. Balis, S. Kazadzis, A. Bais, E. Giannakaki, A. Papayannis, C. Zerefos (2005), Four-year aerosol observations with a Raman lidar at Thessaloniki, Greece, in the framework of European Aerosol Research Lidar Network (EARLINET), *J. Geophys. Res.*, *110*, D21203, doi:10.1029/2005JD006190.

Andreae, M. O., and P. Merlet (2001), Emission of trace gases and aerosols from biomass burning, *Global Biogeochem. Cycles*, *15*(4), 955–966.

Angström, A. (1964), The parameters of atmospheric turbidity, *Tellus*, *16*, 64–75.

Ansari, A. S., and S. N. Pandis (1998), Response of inorganic PM to precursor concentrations, *Environ. Sci. Technol.*, *32*, 2706–2714.

Auvray, M., and I. Bey (2005), Long-range transport to Europe: Seasonal variations and implications for the European ozone budget, *J. Geophys. Res.*, *110*, D11303, doi:10.1029/2004JD005503.

Auvray, M., I. Bey, E. Llull, M. G. Schultz, and S. Rast (2006), A model investigation of the impact of long-range transport on tropospheric ozone chemical tendencies, submitted to *J. Geophys. Res.*

Barkan, J., P. Alpert, H. Kutiel, P. Kishcha (2005), Synoptics of dust transportation days from Africa toward Italy and central Europe, *J. Geophys. Res.*, *110*, D07208, doi:10.1029/2004JD005222.

Benkovitz, C. M., M. T. Scholtz, J. Pacyna, L. Tarrasòn, J. Dignon, E. C. Voldner, P. A. Spiro, J. A. Logan, and T. E. Graedel (1996), Global gridded inventories of anthropogenic emissions of sulfur and nitrogen, *J. Geophys. Res.*, *101*, 29239–29254.

Bertschi, I. T., D. A. Jaffe, L. Jaeglé, H. U. Price, J. B. Dennison (2004), PHOBEA/ITCT 2002 airborne observations of transpacific transport of ozone, CO, volatile organic compounds, and aerosols to the northeast Pacific: Impacts of Asian anthropogenic and Siberian boreal fire emissions, *J. Geophys. Res.*, *109*, D23S12, doi:10.1029/2003JD004328.

Bey, I., D. J. Jacob, R. M. Yantosca, J. A. Logan, B. D. Field, A. M. Fiore, Q. Li, H. Y. Liu, L. J. Mickley, M. G. Schultz (2001), Global modeling of tropospheric chemistry with assimilated meteorology: Model description and evaluation, *J. Geophys. Res.*, *106*(D19), 23073-23096, 10.1029/2001JD000807.

Bond, T. C., D. G. Streets, K. F. Yarber, S. M. Nelson, J.-H. Woo, Z. Klimont (2004), A technology-based global inventory of black and organic carbon emissions from combustion, *J. Geophys. Res.*, *109*, D14203, doi:10.1029/2003JD003697.

Buijsman, E., and F. de Leeuw (2004), Correction factors and PM_{10} measurements in Airbase, *ETC/ACC Technical paper 2004/4*, Netherland. (Available at http://air-climate.eionet.eu.int/docs/meetings/041122_9th_EIONET_AQ_WS/05d_PM10_corr_factors_in_AirBase_Nov2004-TempDraft.pdf)

Callot, Y., Marticorena, B., Bergametti, G., 2000. Geomorphologic approach for modelling the surface features of arid environments in a model of dust emissions: Application to the Sahara desert, *Geodinamica Acta*, *13*, 245–270.

Cakmur, R. V., R. L. Miller, O. Torres (2004), Incorporating the effect of small-scale circulations upon dust emission in an atmospheric general circulation model, *J. Geophys. Res.*, *109*, D07201, doi:10.1029/2003JD004067.

Carmichael, G. R., et al. (2003), Regional-scale chemical transport modeling in support of the analysis of observations obtained during the TRACE-P experiment, *J. Geophys. Res.*, *108*(D21), 8823, doi:10.1029/2002JD003117.

Chatenet, B., Marticorena, B., Gomes, L., Bergametti, G. (1996), Assessing the microped size distributions of desert soils erodible by wind, *Sedimentology*, *43*, 901–911.

Chin, M., P. Ginoux, S. Kinne, O. Torres, B. Holben, B. N. Duncan, R. V. Martin, J. A. Logan, A. Higurashi, and T. Nakajima (2002), Tropospheric aerosol optical thickness from the GOCART model and comparisons with satellite and sunphotometer measurements, *J. Atmos. Sci.*, *59*, 461–483.

Chin, M., R. B. Rood, S.-J. Lin, J.-F. Müller, A. M. Thompson (2000), Atmospheric sulfur cycle simulated in the global model GOCART: Model description and global properties, *J. Geophys. Res.*, *105*(D20), 24671–24688, 10.1029/2000JD900384.

Chung, S. H., and J. H. Seinfeld (2002), Global distribution and climate forcing of carbonaceous aerosols, *J. Geophys. Res.*, *107*(D19), 4407, doi:10.1029/2001JD001397.

Claeys, M., W. Wang, A. C. Ion, I. Kourtchev, A. Gelencsér and W. Maenhaut (2004a), Formation of secondary organic aerosols from isoprene and its gas-phase oxidation products through reaction with hydrogen peroxide, *Atmos. Environ.*, *38*, 4093–4098.

Claeys, M. et al. (2004b), Formation of secondary organic aerosols through photooxidation of isoprene, *Science*, *303*, 1173–1176.

Clarke, A. D., et al. (2004), Size distributions and mixtures of dust and black carbon aerosol in Asian outflow: Physiochemistry and optical properties, *J. Geophys. Res.*, *109*, D15S09, doi:10.1029/2003JD004378.

Colarco, P. R., M. R. Schoeberl, B. G. Doddridge, L. T. Marufu, O. Torres, E. J. Welton (2004), Transport of smoke from Canadian forest fires to the surface near Washington, D.C.: Injection height, entrainment, and optical properties, *J. Geophys. Res.*, *109*, D06203, doi:10.1029/2003JD004248.

Conny, J. M., and J. F. Slater (2002), Black carbon and organic carbon in aerosol particles from crown fires in the Canadian boreal forest, *J. Geophys. Res.*, *107* (D11), doi:10.1029/2001JD001528.

Cooke, W. F., C. Liousse, H. Cachier, J. Feichter (1999), Construction of a $1^\circ \times 1^\circ$ fossil fuel emission data set for carbonaceous aerosol and implementation and radiative impact in the ECHAM4 model, *J. Geophys. Res.*, *104*(D18), 22137-22162, 10.1029/1999JD900187.

d'Almeida, G. A., 1986. A model for Saharan dust transport, *J. Clim. Appl. Meteorol.*, *25*, 903–916.

Damoah, R., N. Spichtinger, C. Forster, P. James, I. Mattis, U. Wandinger, S. Beirle, T. Wagner, A. Stohl (2004), Around the world in 17 days - hemispheric-scale transport of forest fire smoke from Russia in May 2003, *Atmos. Chem. Phys.*, *4*, 1311–1321.

Darmenova, K., I. N. Sokolik, A. Darmenov (2005), Characterization of east Asian dust outbreaks in the spring of 2001 using ground-based and satellite data, *J. Geophys. Res.*, *110*, D02204, doi:10.1029/2004JD004842.

Dentener, F. et al. (2006), Nitrogen and sulfur deposition on regional and global scales: a multi-model evaluation, *Global Change Biol.*, in press.

Deuzé, J. L., et al. (2001), Remote sensing of aerosols over land surfaces from POLDER-ADEOS-1 polarized measurements, *J. Geophys. Res.*, *106*(D5), 4913–4926, 10.1029/2000JD900364.

Duncan, B. N., R. V. Martin, A. C. Staudt, R. Yevich, and J. A. Logan (2003), Interannual and seasonal variability of biomass burning emissions constrained by satellite observations, *J. Geophys. Res.*, *108* (D2), 4100, doi:10.1029/2002JD002378.

Edney, E. O., T. E. Kleindienst, M. Jaoui, M. Lewandowski, J. H. Offenberg, W. Wang and M. Claeys (2005), Formation of 2-methyl tetrols and 2-methylglyceric acid in secondary organic aerosol from laboratory irradiated isoprene/NO_x/SO_2/air mixtures and their detection in ambient $PM_{2.5}$ samples collected in the eastern United State, *Atmos. Environ.*, *39*, 5281–5289.

Edwards, D. P., et al. (2004), Observations of carbon monoxide and aerosols from the Terra satellite: Northern Hemisphere variability, *J. Geophys. Res.*, *109*, D24202, doi:10.1029/2004JD004727.

EMEP (2004), Transboundray particulate matter in Europe, *status Report 4/2004*, 92pp. (Available at http://www.nilu.no/projects/ccc/reports/emep4-2004.pdf)

Fairlie, T. D., D. J. Jacob, and R. J. Park (2006), The impact of transpacific transport of mineral dust in the United States, submitted to *Atmos. Environ.*

Forster, C., et al. (2001), Transport of boreal forest fire emissions from Canada to Europe, *J. Geophys. Res.*, *106*(D19), 22887–22906, 10.1029/2001JD900115.

Fromm, M., J. Alfred, K. Hoppel, J. Hornstein, R. Bevilacqua, E. Shettle, R. Servranckx, Z. Li, and B. Stocks (2000), Observations of boreal forest fire smoke in the stratosphere by POAM III, SAGE II, and lidar in 1998, *Geophys. Res. Lett.*, *27*, 1407–1410.

Fromm, M., R. Bevilacqua, R. Servranckx, J. Rosen, J. P. Thayer, J. Herman, and D. Larko (2005), Pyro-cumulonimbus injection of smoke to the stratosphere: Observations and impact of the super blowup in northwestern Canada on 3–4 August 1998, *J. Geophys. Res.*, *110*, D08205, doi:10.1029/2004JD005350.

Ginoux, P., M. Chin, I. Tegen, J. M. Prospero, B. Holben, O. Dubovik, S.-J. Lin (2001), Sources and distributions of dust aerosols simulated with the GOCART model, *J. Geophys. Res.*, *106*(D17), 20255–20274, 10.1029/2000JD000053.

Gonzalez, C. R., J. P. Veefkind, G. de Leeuw (2000), Aerosol optical depth over Europe in August 1997 derived from ATSR-2 data, *Geophys. Res. Lett.*, *27*(7), 955–956, 10.1029/1999GL010962.

Gonzalez, C. R., M. Schaap, G. de Leeuw, P.J.H. Builtjes and M. van Loon (2003), Spatial variation of aerosol properties over Europe derived from satellite observations and comparison with model calculations, *Atmos. Chem. Phys.*, *3*, 521–533.

Grousset, F., P. Ginoux, A. Bory, and P. Biscaye (2003), Case study of a Chinese dust plume reaching the French Alps, *Geophys. Res. Lett.*, *30* (6), 1277, doi:10.1029/2002GL016833.

Guenther, A., et al. (1995), A global model of natural volatile organic compound emissions, *J. Geophys. Res.*, *100*(D5), 8873–8892, 10.1029/94JD02950.

Guerova, G., I. Bey, J.-L. Attié, R. V. Martin, J. Cui, and M. Sprenger (2006), Impact of transatlantic transport episodes on summertime ozone in Europe, *Atmos. Chem. Phys.*, *6*, 2057–2072.

Heald, C. L., D. J. Jacob, R. J. Park, L. M. Russell, B. J. Huebert, J. H. Seinfeld, H. Liao, R. J. Weber (2005), A large organic aerosol source in the free troposphere missing from current models, *Geophys. Res. Lett.*, *32*, L18809, doi:10.1029/2005GL023831.

Heald, C. L., D. J. Jacob, R. J. Park, B. Alexander, T. D. Fairlie, R. M. Yantosca, D. A. Chu (2006), Transpacific transport of Asian anthropogenic aerosols and its impact on surface air quality in the United States, *J. Geophys. Res.*, in press.

Hjellbrekke, A.-G. (2005), Data Report 2003 Acidifying and eutrophying compounds, *EMEP/CCC-Report 3/2005*.

Holben, B. N., et al. (1998), AERONET - A federated instrument network and data archive for aerosol characterization, *Rem. Sens. Environ.*, *66*, 1–16.

Hsu, N. C., J. R. Herman, J. F. Gleason, O. Torres, C. J. Seftor (1999), Satellite detection of smoke aerosols over a snow/ice surface by TOMS, *Geophys. Res. Lett.*, *26*(8), 1165–1168, 10.1029/1999GL900155.

Huebert, B. J., C. A. Phillips, L. Zhuang, E. Kjellström, H. Rodhe, J. Feichter, C. Land (2001), Long-term measurements of free-tropospheric sulfate at Mauna Loa: Comparison with global model simulations, *J. Geophys. Res.*, *106*(D6), 5479–5492, 10.1029/2000JD900627.

Husar, R. B., et al. (2001), Asian dust events of April 1998, *J. Geophys. Res.*, *106*(D16), 18317–18330, 10.1029/2000JD900788.

Jacob, D. J. (2000), Heterogeneous chemistry and tropospheric ozone, *Atmos. Environ.*, *34*, 2131–2159.

Jaffe, D., I. McKendry, T. Anderson, and H. Price (2003), Six new episodes of trans-Pacific transport of air pollutants, *Atmos. Environ.*, *37*, 391–404.

Kaufman, Y. J., O. Boucher, D. Tanré, M. Chin, L. A. Remer, T. Takemura (2005), Aerosol anthropogenic component estimated from satellite data, *Geophys. Res. Lett.*, *32*, L17804, doi:10.1029/2005GL023125.

Laurent, B. (2005), Simulation des aérosols désertiques à l'échelle continentale : Analyse climatologique des émissions du nord de l'Asie et du nord de l'Afrique, Ph.D., pp.225, Université Paris 12, Paris, France.

Laurent, B., B. Marticorena, G. Bergametti, P. Chazette, F. Maignan, C. Schmechtig (2005), Simulation of the mineral dust emission frequencies from desert areas of China and Mongolia using an aerodynamic roughness length map derived from the POLDER/ADEOS 1 surface products, *J. Geophys. Res.*, *110*, D18S04, doi:10.1029/2004JD005013.

Li, Q. B., D. J. Jacob, J. W. Munger, R. M. Yantosca, D. D. Parrish (2004), Export of NO_y from the North American boundary layer: Reconciling aircraft observations and global model budgets, *J. Geophys. Res.*, *109*, D02313, doi:10.1029/2003JD004086.

Li, Q. B., D. J. Jacob, R. Park, Y. Wang, C. L. Heald, R. Hudman, R. M. Yantosca, R. V. Martin, M. Evans (2005), North American pollution outflow and the trapping of convectively lifted pollution by upper-level anticyclone, *J. Geophys. Res.*, *110*, D10301, doi:10.1029/2004JD005039.

Liu, H., D. J. Jacob, I. Bey, R. M. Yantosca (2001), Constraints from 210Pb and 7Be on wet deposition and transport in a global three-dimensional chemical tracer model driven by assimilated meteorological fields, *J. Geophys. Res.*, *106*(D11), 12109–12128, 10.1029/2000JD900839.

Liu, Y., R. J. Park, D. J. Jacob, Q. Li, V. Kilaru, J. A. Sarnat (2004), Mapping annual mean ground-level $PM_{2.5}$ concentrations using Multiangle Imaging Spectroradiometer aerosol optical thickness over the contiguous United States, *J. Geophys. Res.*, *109*, D22206, doi:10.1029/2004JD005025.

Luo, C., N. M. Mahowald, J. del Corral (2003), Sensitivity study of meteorological parameters on mineral aerosol mobilization, transport, and distribution, *J. Geophys. Res.*, *108* (D15), 4447, doi:10.1029/2003JD003483.

Mari, C., D. J. Jacob, P. Bechtold (2000), Transport and scavenging of soluble gases in a deep convective cloud, *J. Geophys. Res.*, *105*(D17), 22255–22268, 10.1029/2000JD900211.

Marticorena, B., G. Bergametti (1995), Modeling the atmospheric dust cycle: 1. Design of a soil-derived dust emission scheme, *J. Geophys. Res.*, *100*(D8), 16415–16430, 10.1029/95JD00690.

Marticorena, B., G. Bergametti (1996), Two-year simulations of seasonal and interannual changes of the Saharan dust emissions, *Geophys. Res. Lett.*, *23*(15), 1921–1924, 10.1029/96GL01432.

Marticorena, B., P. Chazette, G. Bergametti, F. Dulac, Legrand, M. (2004), Mapping the aerodynamic roughness length of desert surfaces from the POLDER/ADEOS bi-directional reflectance product, *Int. J. Remote Sensing*, *25*, 3, 603–626.

Martin, R. V., et al. (2002a), An improved retrieval of tropospheric nitrogen dioxide from GOME, *J. Geophys. Res.*, *107* (D20), 4437, doi:10.1029/2001JD001027.

Martin, R. V., et al. (2002b), Interpretation of TOMS observations of tropical tropospheric ozone with a global model and in situ observations, *J. Geophys. Res.*, *107* (D18), 4351, doi:10.1029/2001JD001480.

Martin, R. V., D. J. Jacob, R. M. Yantosca, M. Chin, and P. Ginoux (2003), Global and regional decreases in tropospheric oxidants from photochemical effects of aerosols, *J. Geophys. Res.*, *108*(D3), 4097, doi:10.1029/2002JD002622.

Matsunaga, S. N. , C. Wiedinmyer, A. B. Guenther, J. J. Orlando, T. Karl, D. W. Toohey, J. P. Greenberg, Y. Kajii (2005), Isoprene oxidation products are a significant atmospheric aerosol component, *Atm. Chem. Phys. Discuss.*, *5*, 11143–11156.

Matthias, V., et al. (2004), Vertical aerosol distribution over Europe: Statistical analysis of Raman lidar data from 10 European Aerosol Research Lidar Network (EARLINET) stations, *J. Geophys. Res.*, *109*, D18201, doi:10.1029/2004JD004638.

Mattis, I., A. Ansmann, D. Müller, U. Wandinger, and D. Althausen (2002), Dual-wavelength Raman lidar observations of the extinction-to-backscatter ratio of Saharan dust, *Geophys. Res. Lett.*, *29* (9), doi:10.1029/2002GL014721.

Mattis, I., A. Ansmann, U. Wandinger, D. Müller (2003), Unexpectedly high aerosol load in the free troposphere over central Europe in spring/summer 2003, *Geophys. Res. Lett.*, *30*(22), 2178, doi:10.1029/2003GL018442.

Mattis, I., A. Ansmann, D. Müller, U. Wandinger, D. Althausen (2004), Multiyear aerosol observations with dual-wavelength Raman lidar in the framework of EARLINET, *J. Geophys. Res.*, *109*, D13203, doi:10.1029/2004JD004600.

McKendry, I. G., J. P. Hacker, R. Stull, S. Sakiyama, D. Mignacca, K. Reid (2001), Long-range transport of Asian dust to the Lower Fraser Valley, British Columbia, Canada, *J. Geophys. Res.*, *106*(D16), 18361–18370, 10.1029/2000JD900359.

Methven, J., et al. (2006), Establishing Lagrangian connections between observations within air masses crossing the Atlantic during the ICARTT experiment, submitted to *J. Geophys. Res.*

Millet, D.B., et al. (2006), Chemical characteristics of North American surface-layer outflow: Insights from Chebogue Point, submitted to *J. Geophys. Res.*

Moulin, C., et al. (1998), Satellite climatology of African dust transport in the Mediterranean atmosphere, *J. Geophys. Res.*, *103*(D11), 13137–13144, 10.1029/98JD00171.

Müller, D., I. Mattis, U. Wandinger, A. Ansmann, D. Althausen, A. Stohl (2005), Raman lidar observations of aged Siberian and Canadian forest fire smoke in the free troposphere over Germany in 2003: Microphysical particle characterization, *J. Geophys. Res.*, *110*, D17201, doi:10.1029/2004JD005756.

Park, R. J., D. J. Jacob, M. Chin, R. V. Martin (2003), Sources of carbonaceous aerosols over the United States and implications for natural visibility, *J. Geophys. Res.*, *108* (D12), 4355, doi:10.1029/2002JD003190.

Park, R. J., D. J. Jacob, B. D. Field, R. M. Yantosca, M. Chin (2004), Natural and transboundary pollution influences on sulfate-nitrate-ammonium aerosols in the United States: Implications for policy, *J. Geophys. Res.*, *109*, D15204, doi:10.1029/2003JD004473.

Park, R. J., et al. (2005), Export efficiency of black carbon aerosol in continental outflow: Global implications, *J. Geophys. Res.*, *110*, D11205, doi:10.1029/2004JD005432.

Park, R. J., D. J. Jacob, N. Kumar, and R. M. Yantosca (2006), Regional visibility statistics in the United States: Natural and transboundary pollution influences, and implications for the Regional Haze Rule, *Atmos. Environ.*, in press.

Parrish, D. D. (2006), Critical evaluation of US on-road vehicle emission inventories, *Atmos. Environ.*, 40, 2288–2300.

Price, H. U., D. A. Jaffe, P. V. Doskey, I. McKendry, T. L. Anderson (2003), Vertical profiles of O_3, aerosols, CO and NMHCs in the Northeast Pacific during the TRACE-P and ACE-ASIA experiments, *J. Geophys. Res.*, *108* (D20), 8799, doi:10.1029/2002JD002930.

Prospero, J. M., P. Ginoux, O. Torres, S. E. Nicholson, T. E. Gill (2002) Environmental characterization of global sources of atmospheric soil dust identified with the Nimbus 7 Total Ozone Mapping Spectrometer (TOMS) absorbing aerosol product, *Rev. Geophys.*, *40*, 1, 1–31.

Prospero, J. M., D. L. Savoie, and R. Arimoto (2003), Long-term record of nss-sulfate and nitrate in aerosols on Midway Island, 1981–2000: Evidence of increased (now decreasing?) anthropogenic emissions from Asia, *J. Geophys. Res.*, *108* (D1), 4019, doi:10.1029/2001JD001524.

Putaud, J. P. et al. (2004), A European aerosol phenomenology-1: physical characteristics of particulate matter at kerbside, urban, rural and background sites in Europe, *Atmos. Environ.*, *38*, 2579–2595.

Quinn, P. K., T. S. Bates (2003), North American, Asian, and Indian haze: Similar regional impacts on climate?, *Geophys. Res. Lett.*, *30* (11), 1555, doi:10.1029/2003GL016934.

Remer, L. A., et al., (2005) The MODIS Aerosol Algorithm, Products and Validation, *Journal of the Atmospheric Sciences*, *Special Section. Vol 62*, 947–973.

Rodriguez, S., X. Querol X, A. Alastuey and E. Mantilla (2002), Origin of high summer PM_{10} and TSP concentrations at rural sites in Eastern Spain, *Atmos. Environ.*, *36*, 3101–3112.

Schaap, M., et al. (2004), Anthropogenic black carbon and fine aerosol distribution over Europe, *J. Geophys. Res.*, *109*, D18207, doi:10.1029/2003JD004330.

Seinfeld, J. and S. Pandis (1998), *Atmospheric chemistry and physics*, John Wiley and Sons, Inc., New York.

Taylor, K. E. (2001), Summarizing multiple aspects of model performance in a single diagram, *J. Geophys. Res.*, *106*(D7), 7183–7192, 10.1029/2000JD900719.

Technical working group on particles (1997), Ambient air pollution by particulate matter, *Particles position paper*, European commission, Europe. (Available at http://europa.eu.int/comm/environment/air/pdf/pp_pm.pdf)

Turpin, B. J., H. J. Lim (2001), Species contributions to $PM_{2.5}$ mass concentrations: Revisiting common assumptions for estimating organic mass, *Aerosol Science and Tech.*, *35* (1), 602–610.

Turquety, S., et al. (2006), Inventory of boreal fire emissions for North America in 2004: the importance of peat burning and pyro-convective injection, submitted to *J. Geophys. Res.*

van Dingenen, R. et al. (2004), A European aerosol phenomenology-1: physical characteristics of particulate matter at kerbside, urban, rural and background sites in Europe, *Atmos. Environ.*, *38*, 2561–2577.

van Donkelaar, A., R. V. Martin, R. J. Park, C. L. Heald, T.-M. Fu, H. Liao, and A. Guenther (2006a), Model evidence for a significant source of secondary organic aerosol from isoprene, submitted to *Geophys. Res. Lett.*

van Donkelaar, A., R. V. Martin, and R. J. Park (2006b), Estimating ground-level $PM_{2.5}$ with aerosol optical depth determined from satellite remote sensing, submitted to *J. Geophys. Res.*

Vestreng, V. and H. Klein (2002), Emission data reported to UNECE/EMEP: Quality insurance and trend analysis & Presentation of WebDab, *MSC-W Status Report 2002*, 101pp., Norwegian Meteorological Institute, Oslo, Norway. (Available at http://www.emep.int/publ/reports/2002/mscw_note_1_2002.pdf)

Vestreng, V., K. Breivik, M. Adams, A. Wagner, J. Goodwin, O. Rozovskaya, J. M. Pacyna (2005), Emission Data reported to LRTAP Convention and NEC Directive. Initial review for HMs and POPs, *MSC-W Technical Report 1/05*, 131pp. (Available at http://www.emep.int/publ/reports/2005/emep_technical_1_2005.pdf)

Wandinger, U. et al. (2002), Optical and microphysical characterization of biomass-burning and industrial-pollution aerosols from multiwavelength lidar and aircraft measurements, *J. Geophys. Res.*, *107* (D21), doi:10.1029/2000JD000202.

Wandinger, U., et al. (2004), Air mass modification over Europe: EARLINET aerosol observations from Wales to Belarus, *J. Geophys. Res.*, *109*, D24205, doi:10.1029/2004JD005142.

Wang, J., S. A. Christopher (2003), Intercomparison between satellite-derived aerosol optical thickness and $PM_{2.5}$ mass: Implications for air quality studies, *Geophys. Res. Lett.*, *30* (21), 2095, doi:10.1029/2003GL018174.

Wesely, M.L. (1989), Parameterization of surface resistances to gaseous dry deposition in regional-scale numerical-models, *Atmos. Env.*, *23*, 1293–304.

WHO (2005), WHO air quality guidelines global update 2005, *EUR/05/5046029*, pp.30, World Health organisation, Bonn, Germany. (Available at http://www.euro.who.int/Document/E87950.pdf)

Wild, O., X. Zhu, and M. J. Prather (2000), Fast-J: Accurate simulation of in- and below-cloud photolysis in tropospheric chemistry models, *J. Atmos. Chem.*, *37*, 245–282.

Wilkening, K. E., L. A. Barrie, and M. Engle (2000), Trans-Pacific air pollution, *Science*, *290*, 65–67.

Zender, C. S., H. Bian, D. Newman (2003), Mineral Dust Entrainment and Deposition (DEAD) model: Description and 1990s dust climatology, *J. Geophys. Res.*, *108* (D14), 4416, doi:10.1029/2002JD002775.

Zhang, L., S. Gong, J. Padro, L. Barrie (2001), A size-segregated particle dry deposition scheme for an atmosopheric aerosol module, *Atmos. Env.*, *35*, 549–60.

Zoltai, S. C., L. A. Morrissey, G. P. Livingston, and W. J. de Groot (1998), Effects of fire on carbon cycling in North American boreal peatlands, *Env. Rev.*, *6*, 13–24.

Chapter 6

Conclusions and Outlook

The main objective of this thesis was to investigate in a quantitative manner the respective contribution of local sources and of long-range transported sources to tropospheric ozone (O_3) and aerosol burdens over continental Europe. In particular, I examined:

- the impact of continental outflow on the O_3 chemical tendencies over oceanic regions (Chapter 3);
- the seasonal variations of long-range transported sources from North America and Asia into Europe and the impact of these sources on the O_3 background over Europe, including the role of changing emissions over the past decades (Chapter 4);
- the aerosol load over Europe and the contribution of long and medium-range sources including anthropogenic and biomass burning pollution from North America and mineral dust from North Africa, using, among others, observations provided by the International Consortium for Atmospheric Research on Transport and Transformation (ICARTT) experiment (Chapter 5).

This is achieved by means of global model of chemistry and transport simulations constrained by a large suite of experimental datasets including ground-based and space-born measurements and in-situ aircraft observations. In Chapter 3, I used two global models (namely the GEOS-Chem and MOZECH models) in order to enhance the robustness of the results presented in this study, and also to provide some quantification of the uncertainties associated with model results. In the present chapter, I answer the different scientific questions posed in the introduction (Chapter 1), as well as discuss different shortcomings and future works related to each of those questions.

How well global models represent the processes associated with long-range transport?

A large portion of the work was first devoted to the evaluation of the models to test if our current knowledge with respect to emission, chemistry, transport and deposition processes is adequate to represent correctly O_3 chemical tendencies and concentrations as well as aerosol concentrations and optical properties on a global scale and more specifically over the North Atlantic/Europe area.

The profiles of O_3 chemical terms simulated by the two global models were evaluated with observationally-constrained box model results for the Atlantic [*Reeves et al.*, 2002] and Pacific [*Davis et al.*, 1996; 2003] regions (Chapter 3). Regional and seasonal variations of O_3 chemical terms are relatively well reproduced in general. In particular, the GEOS-Chem model reproduces the positive net O_3 production calculated with box models throughout the tropospheric column in spring over the Pacific associated with strong Asian anthropogenic and biomass burning outflow.

Simulated distributions of O_3 and its precursors (mainly CO and NO_x) in the North American outflow (Chapter 5), the mid-Atlantic ocean (Chapter 3) and over Europe (Chapter 4) were also evaluated. Simulated vertical profiles of O_3 precursors by GEOS-Chem reproduce in general the observed shape and magnitude, in the North American outflow, in the mid-Atlantic area and over Europe. At the surface of Europe, seasonal cycles of CO and NO_2 are well reproduced by GEOS-Chem and the CO simulation improved (to fall within 20 ppbv of the observations) when implementing a new European Monitoring and Evaluation Program (EMEP) inventory for European anthropogenic sources [*Vestreng and Klein*, 2002].

This good representation of the seasonal and regional features of O_3 precursors as well as O_3 chemical terms results in an overall satisfying representation of O_3 in the different regions examined. In particular, the O_3 seasonal cycle over Europe is in general well represented by GEOS-Chem except that the model overestimates concentrations by up to 10 ppbv at the surface in summer and that the seasonal cycle is a little bit too flat in the upper troposphere. Photochemical episodes in summer are also well captured at the surface of Europe (Chapter 4). Finally the model captures successfully a number of observed long-range transport of O_3 from North America in terms of timing, extent and magnitude of the plume, with the exception that in general maximum concentrations are underestimated which likely reflect the rather coarse grid used in global models.

Aerosol evaluation is less successful in general (Chapter 5). The evaluation is made difficult because only little observations are available. In particular, observations of individual aerosol components are missing and the instruments used to measure particulate matter (PM) over the European countries are too different to provide a homogeneous dataset. Nevertheless, the available observations allowed us to point out some issues in the GEOS-Chem aerosol simulations:

- Sulfate aerosol concentrations are overestimated (by nearly a factor 2) over Europe. Ammonium concentrations also appear to be overestimated. Some of this overestimate in aerosol concentrations seems to be related to too low deposition

fluxes and too high precursor emissions.

- Using "state-of-the-art" dust emission schemes in our global model did not allow us to obtain a satisfying dust simulation over North Africa and Europe. This can only be achieved by scaling our simulated emissions to those estimated by *Laurent* [2005] who used specific database for soil sizes and textures and satellite-derived roughness lengths as well as meteorological winds at a much lower horizontal resolution than that usually used in global models (i.e. 0.25°x0.25°).

- The particulate organic matter (POM) concentrations are also likely underestimated in our model. This could reflect a missing secondary organic aerosol (SOA) source from biogenic compounds or from other compounds.

Compensating errors between the different contributions of various components result in a correct simulation of particulate matter of diameter smaller than 10 μm (PM_{10}) and 2.5 μm ($PM_{2.5}$) concentrations, as well as aerosol optical depth (AOD) in terms of both spatial and seasonal variations (absolute bias in the order of 35% for PM_{10} and 20–25% for $PM_{2.5}$ and AOD).

We also examined the aerosol concentrations in North American outflow and found that the model reproduces well the occurrence of polluted events of North American biomass burning and anthropogenic origin, but tends to underestimate the concentrations observed during those events. Despite these (relative) deficiencies, the model provides anyway insights about the contribution of long-range transport on the O_3 and aerosol loads over Europe.

What are the processes controlling O_3 production over the Atlantic during long-range transport episodes?

Over the oceanic areas downwind of source regions, the net O_3 photochemical production is enhanced compared to the background environment at almost all seasons with a maximum in the boundary layer of 2 to 6 ppbv/day. In the two models, the apparent agreement in the enhancement of the net O_3 production in the plumes reflects the effect of compensating processes: in MOZECH, the enhancement of the net O_3 production in the plumes mainly results from enhanced NO_x concentrations and thus enhanced O_3 production rates; while in GEOS-Chem, this mainly results from a decrease in water vapour and temperature, and thus a decrease in the O_3 loss rates. This is likely associated with different emission schemes used in the two models (including NO_x from lightning) as well as different water vapour concentration fields with respect to the transport processes.

In this work, we did not manage to establish which model best represents the O_3 production and loss rates and their perturbation by continental outflow. More investigation is needed concerning the representation of water vapour with respect to plume location in the two models. In addition, we did not examine the different role of anthropogenic vs. biomass burning plumes on the background environment. These

two issues could be examined with observations gathered during the ICARTT aircraft campaign. This Lagrangian experiment could (1) provide profiles of water vapour in several plumes travelling across the North Atlantic and (2) allow us to differentiate between anthropogenic and biomass burning plumes. Finally, the O_3 production terms obtained by the global models could be compared to the ones calculated with Lagrangian chemical box models such as those developed by *Real et al.* [2006].

What are the processes controlling O_3 and aerosol transport over the Atlantic during long-range transport episodes?

The seasonal variation of O_3 long-range transport from North America is driven by seasonality of winds and photochemical production (i.e. maximum in summer), while aerosol long-range transport is driven by seasonality of winds and scavenging processes (i.e. maximum in spring).

North American pollution is lifted in the free troposphere during frontal passages over the east North American coast (with a minimum in summer) or during deep convection (for non-soluble species only) over central and south eastern U.S. in summer. North American pollution can be transported in low-level flows, but this is only an efficient pathway for O_3 when the O_3 loss rates are at a minimum in the boundary layer (i.e. in spring). Aerosols are transported at lower altitudes than O_3 as, in the model, they are scavenged before reaching high altitudes. The flow of pollution is driven by the position and strength of the Azores high and Icelandic low and thus reaches Europe at lower latitudes in summer. However, because of intense biomass burning in the summer 2004 in the Alaska-Canada area (at higher latitudes than the anthropogenic pollution), long-range transported aerosols reach Europe at higher latitudes.

Aerosol optical depth (AOD) and concentrations of sulfate and of POM gathered during ICARTT during North American outflow episodes showed that the model tends to underestimate severely this export. This might be related to too strong scavenging. To look into more detail this issue, as proposed by several studies [e.g., *Park et al.*, 2005; *Petzold et al.*, 2006], we could examine the export efficiency of individual soluble species (like sulfate or POM) with reference to the CO inert combustion tracer in the outflow over the North Atlantic a few days downwind from the point of emissions both in the model and in the observations. The potential problem in the representation of water vapour with respect to export processes mentioned previously is also critical for aerosol scavenging. Again data provided by the ICARTT campaign could allow to better constrain the model. Finally, further work is needed to examine the processes that contribute to penetration of free tropospheric polluted air in the boundary layer over Europe.

What are the O_3 and aerosol European budgets? How these budgets are influenced by long-range transport on a monthly and seasonal mean? How do specific long-range transport events influence the European troposphere?

Besides receiving O_3 and aerosol from North American sources, Europe could also be affected by other remote sources. For example, O_3 produced from Asian anthropogenic sources impact Europe to a lesser extent all year round through transport by westerly winds. During the summer period, Asia affects more substantially Europe with a polluted flow transported by the monsoon winds directly into the Mediterranean basin. In addition a high O_3 contribution from lightning NO_x emissions associated with convection during the monsoon season increase O_3 over the Mediterranean area. Another example of long-range transport is dust from the Saharan region. This thesis illustrates a dust episode penetrating far into western and central Europe.

North American and Asian anthropogenic pollution contribute substantially to the annual O_3 burden (integrated over the whole tropospheric column) over Europe, accounting for 11% and 8%, respectively while the European contribution only accounts for 9%. At the surface, North American and Asian anthropogenic contributions are at a maximum in spring up to 7.5 ppbv over western, northern Europe and at the north of the Mediterranean basin. Only little contribution from North American anthropogenic origin is found for highest O_3 polluted events as such polluted episodes are preferentially experimented during stable high-pressure period.

European sources contribute by 58% and 48% to the surface $PM_{2.5}$ and column AOD over Europe. The second main aerosol source is the mineral dust which represent in average 20% of the surface $PM_{2.5}$ and AOD. This high dust load is more important for southern Europe and increases strongly the aerosol levels in this region. According to the model, the highest aerosol concentrations are related to dust outbreaks. In summer, North American aerosol anthropogenic and biomass burning emissions represent between 2 to 5% of the surface $PM_{2.5}$ and AOD. However, during specific episodes, sulfate from North America anthropogenic origin contribute up to 55–85% of surface sulfate over Europe; and OC from biomass burning origin contribute up to 78% of surface OC over Europe.

The main shortcoming of the O_3 burden issue lies in the non-linearity of O_3 photochemistry. Although in Chapter 4 we found that the effect of non-linearity is relatively small, that could be due to compensating effect between the different feedbacks resulting from decrease of both NO_x and CO anthropogenic emissions (see section 2.1.2 of Chapter 2). Different methods could be tested to evaluate the impact of this non-linearity on the relative contribution of a given geopolitical region. For example, we could use simulation with perturbed emissions (e.g., by increasing both NO_x and CO anthropogenic emissions by 10%) and then multiplying the difference between our standard simulation and this simulation by a factor of 10. The difference between the results presented in this thesis and the results obtained with this method could give us an error bar on the role of the different contribution to the O_3 budget. In addition, an important feature which is missing in our discussion of the European O_3 budget is the role of biomass burning from boreal forests.

Aerosol budget over Europe is very sensitive to the set of emissions used. Substantial uncertainties remain in anthropogenic emissions like NO_x, SO_x, NH_3 and PM (including resuspended dust). Using the new set of emissions provided by EMEP [*Vestreng et al.*, 2005] could be a first step to improve the model emissions. Natural emissions like dust and biogenic compounds are also important processes, leading to important O_3 and aerosol levels. Evaluation of the model in Chapter 5 has shown that dust emissions are currently overestimated in the Sahara region. The representation of on-line dust emissions could be improved by implementing map of roughness length as well as appropriate soil characterization, following *Laurent* [2005]'s methodology. Recently, *Guenther et al.* [2006] produced a new inventory emission for biogenic compounds which should be implemented in the model. Our knowledge with respect to SOA formation is also limited, but only few observations over Europe are available for POM. The investigation of long-range transport could also be extended to biogenic compounds, which impact heavily O_3 over the south-eastern U.S. in summer.

The role of Asian aerosol emissions on the European aerosol budget should be quantify. The INDOEX campaign showed the presence of high BC concentrations over South Asia. Although most of the aerosols are soluble and then efficiently scavenged during the monsoon, BC that are mainly assumed to be hydrophobic when they are emitted from primary sources, have the potential to be lifted to the upper troposphere in deep convective clouds and then to be transported over long distances.

Finally, nesting models from the global to the local scale could provide a more precise quantification of pollution episodes at a given area, as well as the contribution of local versus long-range transported sources. Using a finer resolution would also probably enhance the capabilities of the model in terms of dust events. However, a finer resolution will only be useful if the previous mentioned processes (emissions, transport and deposition) are described accurately at a smaller scale. Further observations at the appropriate scale are thus needed, among those satellites could offer good opportunities.

How changes in O_3 precursors emissions contribute to changes in background and total O_3 over Europe?

The role of change in O_3 precursor emissions for the last two decades (1980–1997) is investigated in Chapter 4. Surface O_3 concentrations decrease in summer because of the decrease in local emissions; surface O_3 concentrations increase in winter due to both a decrease in local NO_x emissions (and thus enhanced O_3 concentrations due to less O_3 titration by NO_x) and an increase in Asian contribution. At higher altitude, the compensation between reduction of local sources and increase of foreign contribution is clearly demonstrated for the free troposphere, as O_3 concentrations increase all year round despite the European O_3 precursors regulation. However, this work further highlights the need of international treaties regulating the emissions.

The main shortcoming of this issue is that we did not investigate the variation of other factors in the change of the O_3 budget. Such factors could include change in the meteorology as well as change in natural processes like lightning and biogenic emissions

or stratospheric-tropospheric exchange. Next step could be to examine the impact of long-range transport into Europe in future times, to better link climate change and air quality issues.

References

Davis, D. D., et al. (1996), Assessment of ozone photochemistry in the western North Pacific as inferred from PEM-West A observations during the fall 1991, *J. Geophys. Res.*, 101(D1), 2111–2134, 10.1029/95JD02755.

Davis D. D., et al. (2003), An assessment of western North Pacific ozone photochemistry based on springtime observations from NASA's PEM-West B (1994) and TRACE-P (2001) field studies, *J. Geophys. Res.*, *108* (D21), 8829, doi:10.1029/2002JD003232.

Guenther, A., T. Karl, P. Harley, C. Wiedinmyer, P.I. Palmer, and C. Geron (2006), The Model of Emissions of Gases and Aerosols from Nature (MEGAN) Estimates of global Isoprene Emissions, *Atm. Chem. Phys. Discuss.*, *6*, 107–173.

Laurent B. (2005), Simulation des aérosols désertiques à l'échelle continentale : Analyse climatologique des émissions du nord de l'Asie et du nord de l'Afrique, Ph.D., pp.225, Université Paris 12, Paris, France.

Park, R. J., et al. (2005), Export efficiency of black carbon aerosol in continental outflow: Global implications, *J. Geophys. Res.*, *110*, D11205, doi:10.1029/2004JD005432.

Petzold, A., et al. (2006), Perturbation of European free troposphere aerosol by North American forest fire plumes during the ICARTT-ITOP Experiment in Summer 2004, submitted to *J. Geophys. Res.*.

Real, E., et al. (2006), Processes influencing ozone levels in Alaskan forest fires plumes during long-range transport over the North Atlantic, submitted to *J. Geophys. Res.*.

Reeves C. E., et al. (2002), Potential for photochemical ozone formation in the troposphere over the North Atlantic as derived from aircraft observations during ACSOE, *J. Geophys. Res.*, *107* (D23), 4707, doi:10.1029/2002JD002415.

Vestreng, V. and H. Klein (2002), Emission data reported to UNECE/EMEP: Quality insurance and trend analysis & Presentation of WebDab, *MSC-W Status Report 2002*, 101pp., Norwegian Meteorological Institute, Oslo, Norway. (Available at http://www.emep.int/publ/reports/2002/mscw_note_1_2002.pdf)

Vestreng V., K. Breivik, M. Adams, A. Wagner, J. Goodwin, O. Rozovskaya, J. M. Pacyna (2005), Emission Data reported to LRTAP Convention and NEC Directive. Initial review for HMs and POPs, *MSC-W Technical Report 1/05*, 131pp. (Available at http://www.emep.int/publ/reports/2005/emep_technical_1_2005.pdf)

Marion Auvray
Born on October, 1979 in Melun, France
French citizenship

Curriculum Vitae

Education

2002 – 2006 Ph.D., Laboratoire de la Pollution Atmosphérique, LMCA, EPFL. Advisor: Isabelle Bey (EPFL)

2001 – 2002 Master degree (D.E.A.) in Atmospheric Pollution Chemistry and Environmental Physics, University of Paris VII, France. Advisors: Gilles Bergametti & Béatrice Marticorena (LISA)

1999 – 2003 Engineering diploma at the Engineering School of Water and Environment of Strasbourg (ENGEES), France.

1997 – 1999 Two years of preparatory courses (Classe Préparatoire aux grandes écoles) at Lycée François I^{er}, France.

1997 French baccalaureat in science.

Publications

Auvray M., I. Bey, E. Llull, M. G. Schultz, and S. Rast (2006), A model investigation of tropospheric ozone chemical tendencies in long-range transported pollution plumes, submitted to *J. Geophys. Res.*

Li, Y., J. Staehelin, M. Auvray, I. Bey, and M. Schultz (2005), Comparison between numerical simulations of two 3-D global models (GEOS-CHEM and MOZART) with ozone observations at Jungfraujoch (Switzerland) and ozone sondes from Payerne, submitted *to Atmos. Env.*

Barret, B., S. Turquety, D. Hurtmans, C. Clerbaux, J. Hadji-Lazaro, I. Bey, M. Auvray, P.-F. Coheur, Global carbon monoxide vertical distributions from spaceborne high-resolution FTIR nadir measurements, *Atmos. Chem. Phys.*, *5*, 2901–2914.

Auvray, M., and I. Bey, Long-Range Transport to Europe: Seasonal Variations and Implications for the European Ozone Budget, *J. Geophys. Res.*, *110*, D11303, doi:10.1029/2004JD005503.

Lausanne, Switzerland, April 2006